FLORIDA INTERNATIONAL UNIVERSITY

Miami, Florida

EPOXY GLASS FIBER REINFORCED PLASTIC DOWEL SPLICE FOR PRESTRESSED PRECAST CONCRETE PILE

A dissertation submitted in partial fulfillment of

the requirements for the degree of

DOCTOR OF PHILOSOPHY

in

CIVIL ENGINEERING

by

Saman Farhangdoust

2021

To: Dean John L. Volakis
College of Engineering and Computing

This dissertation, written by Saman Farhangdoust, and entitled Epoxy Glass Fiber Reinforced Plastic Dowel Splice for Prestressed Precast Concrete Pile, having been approved in respect to style and intellectual content, is referred to you for judgment.

We have read this dissertation and recommend that it be approved.

_____
Arindam Gan Chowdhury

_____
David Garber

_____
Seung Jae Lee

_____
Pezhman Mardanpour

_____
Armin Mehrabi, Major Professor

Date of Defense: November 8, 2021

The dissertation of Saman Farhangdoust is approved.

_____
Dean John L. Volakis
College of Engineering and Computing

_____
Andrés G. Gil
Vice President for Research and Economic Development
and Dean of the University Graduate School

Florida International University, 2021

DEDICATION

To my parents and my supervisor for their continuous support and motivation

ACKNOWLEDGMENTS

First of all, I would like to thank God for his blessings to successfully complete my research work. Special thanks to my parents for backing me in this difficult journey and motivating me like fighting an uphill battle.

I would like to express my sincere gratitude to my major advisor Dr. Armin Mehrabi for the continuous support of my Ph.D. study and related research, for his patience, motivation, and immense knowledge. His guidance helped me in all the time of research and writing of this thesis. I could not have imagined having a better advisor and mentor for my Ph.D. study.

I greatly acknowledge the financial support from the Florida Department of Transportation to conduct this research. Particularly, the contributions of the project manager Steven Nolan and others at the State Structures Design Office are greatly appreciated. I also acknowledge the University Graduate School, Florida International University for providing support for this research in the form of Dissertation Year Fellowships (DYF).

I sincerely express my gratitude to all my committee members, Dr. Arindam Gan Chowdhury, Dr. David Garber, Dr. Seung Jae Lee, and Dr. Pezhman Mardanpour for their invaluable suggestions, comments, and support throughout all stages of my academic work which incented me to widen my research from various perspectives. Last but not the least, I would like to thank the staff at the department of civil and environmental engineering and the staff at the dean's office of college of engineering and computing who were always there to assist me during my stay at the university.

ABSTRACT OF THE DISSERTATION

EPOXY GLASS FIBER REINFORCED POLYMER DOWEL SPLICE FOR PRESTRESSED PRECAST CONCRETE PILE

by

Saman Farhangdoust

Florida International University, 2021

Miami, Florida

Professor Armin B. Mehrabi, Major Professor

Due to limitations in operation, shipping difficulties, and unforeseen soil conditions, it often happens that splicing of precast-prestressed concrete pile (PPCP) segments has to be performed at the construction site to achieve longer lengths. In order to splice PPCPs, Glass fiber reinforced polymer (GFRP), Carbon Fiber Reinforced Polymer (CFRP), and Stainless Steel (SS) dowels can be used as corrosion-resistant bars. In addition to their durability and superb mechanical performance, GFRP bars show cost advantage when compared to other corrosion-resistant materials. The objective of this study is to investigate the flexural behavior and effectiveness of the GFRP dowel and compare its performance to CFRP and conventional carbon steel dowels. In this research, a design procedure was developed using available design codes for FRP-reinforced concrete sections for epoxy GFRP dowel pile splices. In order to validate the design procedure and investigate the effectiveness of the GFRP dowels as well as to compare to dowels of other materials, 10 full-scale PPCP specimens of 18×18 in cross-section with a total length of 28 ft were fabricated and tested at the Florida Department of Transportation (FDOT) Structures Laboratory. For the PPCP specimens, three different materials of GFRP, CFRP, and traditional carbon steel were used as dowels in combination with

CFRP and steel prestressing strands for both drivable unforeseen and preplanned cases. The focus of this study was on the flexural performance at the splice. The experimental results show that the proposed design procedure underestimates the nominal moment capacities for GFRP dowel splices by an average of approximately 14% when compared to the test results. Furthermore, three distinctive failure types were observed in laboratory tests. As the first failure mode, unforeseen splice specimens failed by splitting and bond failure in the female segments due to short dowel lengths. In the second failure mode, specimens for which GFRP dowel was used in combination with piles using CFRP prestressing strands failed by flexural cracking and debonding in the male segment near the end of the GFRP dowel. This failure mode could be an indication of inadequate bond length for CFRP strands. Third failure mode dominating the remaining of the specimens was a classical flexural mode with the concrete crushing in the compression zone at splice section. To facilitate the design of pile splices with varying parameters and sizes for all types of materials and configurations, the design procedure was implemented in Mathcad to develop a stand-alone software tool. This tool provides the user with nominal and design flexural strengths, M-N interaction curves, and complete detailing of the splice zone. This research has developed new splice design and drawings for FRP dowel splices as part of the FDOT standard plans and construction specifications

TABLE OF CONTENTS

CHAPTER PAGE

LIST OF TABLES

FIGURE PAGE

LIST OF FIGURES

FIGURE PAGE

CHAPTER 1: INTRODUCTION

1.1 Problem Statement

Establishing bridge foundations where there is a top layer of weak soils normally requires application of deep foundations such as pile foundation. Driving precast-prestressed concrete pile (PPCP) is one of the practical options among various types of piles and installation methods. This option provides in many cases an economic and rapid alternative. For various reasons, it often happens that splicing of pile segments has to be performed at the site to achieve longer lengths. The shipping and transportation constraints may limit the length of PPCP segments that can be delivered to the bridge site. Also, when there is headroom limitation for pile driving, the length of pile segments may be smaller than the length required to establish adequate resistance. In such cases, splicing can be preplanned. Another reason that the pile segments would be less than the length required for resistance is the case of unpredictable soil resistance, which leads to unplanned splicing. Dowelling is one of the common splicing techniques in which holes are cast or drilled into the top of the lower pile to receive dowel rebars protruding out of the lower end of the upper pile [1]. Dowel rebars can be made of carbon steel, Stainless Steel (SS), Carbon Fiber Reinforced Polymer (CFRP), or Glass Fiber Reinforced Polymer (GFRP) bars.

Generally, traditional prestressed piles use carbon steel strands and bars which are prone to corrosion, especially when they are located in a marine environment. In such environment, alternating water levels and water splash and aerosols cause deposit,

migration and diffusion of salts and chloride ions into the pile that can accelerate corrosion [2-4]. In marine environments, many bridge foundations are exposed to saltwater and harsh marine environments which can cause expensive maintenance issues and shorten bridge life [5-6]. Conventional piles mostly deteriorate prematurely in such corrosive environments [7]. Corrosion in concrete piles also occurs in soils and groundwater where there are low pH levels, high level of chloride as well as sulfate. The consequence is a decrease in load-carrying capacities, and likely increase in settlement eventually resulting in the failure of superstructures [8]. Although deteriorated pile structures can be replaced or retrofitted, their maintenance will be costly and not reliable for their long-term serviceability. It has been estimated that repair and replacement of the conventional pile systems cost the United States more than $1 billion [9]. Therefore, high durability, low maintenance, and high safety are always top priorities for any bridge owner [10].

It is realized that GFRP, CFRP, and SS can be used as a corrosion resistant reinforcement. For prestressing strand in PPCPs, two types of CFRP and SS have shown great improvements in the resistance against corrosion. Despite occasional use of CFRP and SS for dowel splicing, their true behavior for pile splicing is not fully understood yet. In addition, no design procedure has been developed for GFRP dowel pile splice before. Therefore, more research needs to be performed to improve the effectiveness and reliability of the FRPs within structural components. As a part of the FDOT's sponsored research activities, this dissertation investigates the behavior of FRP dowels (e.g. CFRP and GFRP) for pile splicing, proposes a design procedure for epoxy GFRP dowel pile

splice, validates the procedure through testing, and develops a user-friendly software tools in Mathcad for future design modifications.

1.2 Research Objectives

The objective of this dissertation is to quantify the effectiveness of pile splices using corrosion-resistant materials of dowels (e.g. CFRP and GFRP) for PPCPs. The motivation of this dissertation is to develop a robust design procedure and implementing it in a programmable software tool to enable engineers to design dowel pile splices with a variety of materials, sizes, and configurations.

To achieve the objective of this research, a design procedure was developed for typical splice connection for an 18×18 in cross section PPCP with GFRP dowel bars to investigate the flexural resistance of pile splices. The design follows the respective AASHTO and ACI standards as well as the provisions of FDOT design specifications for both unforeseen and preplanned drivable splicing cases. In order to validate the design procedure, 10 full-scale PPCP specimens of 18×18 in cross-section with a total length of 28 ft are designed, fabricated, assembled and tested for different embedment depths and confinement at the FDOT Structures Research Center. For these specimens, three different materials for dowels; GFRP bars, CFRP strand, and traditional carbon-steel bars were used in combination with CFRP and steel prestressing strands for PPCPs. The focus of this study is on the flexural performance at the splice. After the experimental program, a user-friendly design tool are programmed in Mathcad software to allow engineers to develop the design procedure for other sizes of pile splices up to 30×30 in. The results of

this research will help removing the limitations on implementation of corrosion resistant piles where splicing is required.

1.3 Significance of Study

As per the 2021 Infrastructure Report Card by the American Society of Civil Engineers, the US infrastructure has received a grade of C-. Out of ~617,000 bridges in the USA, 42% of bridges are already more than 50 years old and 7.5% are structurally deficient [11-13]. In marine environments like the state of Florida, most of these bridge structures are prone to the negative effects of corrosion. The deterioration of reinforcing steel within the concrete by corrosion is one of the primary maintenance challenges and causes of failure for aging concrete structures. For example, in Florida alone, approximately 3600 coastal miles are constructed with aging sheet piles with an estimated $21B replacement cost and approximately one-third of the states' bridges are located in extremely aggressive environments [14-15].

To address these critical issues, FDOT have recognized the potential benefits that FRP provides for infrastructure as a corrosion-resistant reinforcement, and thus supported this dissertation to develop a practical design procedure for epoxy GFRP dowel pile splice as an economical and corrosion-resistant option for splicing PPCPs. This is the short-term impact of the dissertation. As the long-term impact, the findings of this research will be used fin the state specifications and design criteria to support the use of CFRP and GFRP bars and strands for major bridge components. This in turn will promote the use of

corrosion resistant piles and splices and therefore result in enhancing the resiliency and service life of transportation infrastructures.

1.4 Organization of Dissertation

Chapter 2 includes a comprehensive literature review on plies including wooden, steel, composite, precast prestressed concrete types and also on different types of pile splices with an emphasize on epoxy dowel pile splice. This chapter reviews previous investigations for all current pile splices. Chapter 3 provides a design procedure for the GFRP epoxy dowel pile splice and aims at recommending refinements to current designs. This chapter proposes detailed drawings for incorporation into the testing phase of the experimental program for both drivable unforeseen and preplanned pile splices. Chapter 4 develops construction drawings of the test specimens, detailed drawings depicting the design for loading and instrumentation to monitor and record the flexural response of pile splices, and detailed calculations predicting the capacity of pile splice test specimen. This chapter focuses on fabrication and laboratory test of 10 full-scale epoxy dowel splices using steel and corrosion resistance GFRP and CFRP as strands and dowels. The pile segments were fabricated and spliced at S&S Precast and tested at the FDOT Structures Laboratory. Chapter 5 investigates the test results and discusses experimental findings to develop a revised design procedure. Accordingly, in Chapter 6, the design procedure is programmed by Mathcad worksheet for all splice reinforcing materials that were tested in Chapter 4 to allow engineers for future design modifications. Chapter 7 provides the summary and conclusions, main contribution, and recommendations for future studies.

1.5 Major Contribution

The research performed for this dissertation has contributed to the body of the knowledge in several aspects:

- The effectiveness of GFRP dowels for PPCP splices was studied through analytical and experimental investigation.
- This research compares GFRP dowel splice performance to that of CFRP strand and conventional carbon steel bar dowels.
- A design procedure was developed for pile splices using different dowel materials of GFRP, CFRP, and Steel.
- The design procedure was experimentally validated by some laboratory tests.
- The design procedure was implemented in Mathcad software.
- This research has developed new splice design and drawings for FRP dowel splices as part of the FDOT standard drawings and has proposed refinement to the existing designs for CFRP and Steel dowel splices.

CHAPTER 2: LITERATURE REVIEW

2.1 Piles

A foundation transfers the gravity force of a building structure to earth. We have two types of foundation, shallow and deep. Pile is a deep foundation that is hammered into soft soils where any building structures need to be build. Piles are divided into two main groups of driven and cast in-place piles. Driven piles may be made of wood, steel, concrete, or various types of composite materials. This chapter of the dissertation presents a comprehensive literature review on different types of precast piles and pile splices with an emphasize on epoxy dowel pile splices for PPCPs.

2.1.1 Wooden Piles

Wooden piles in coastal waters are prone to damages caused by marine borer activity (Figure 1). Teredo, Bankia, and Limnoria have been recognized as the three most destructive borers who enter the wood as a larva or go through outside edges of the timber piles and follow the grain, tunneling deeper making the wood as holed as Swiss cheese [16]. There are some solutions for preventing their attacks such as using creosote and arsenate for pressure treatment of wood, or the use of wood composites including timber piling encased in fiberglass, and extruded mixtures of wood cutting and polymers. However, these options do not stop borers from attacking the wood completely. Therefore, fabricating more reliable piles is needed, especially in the splash zone

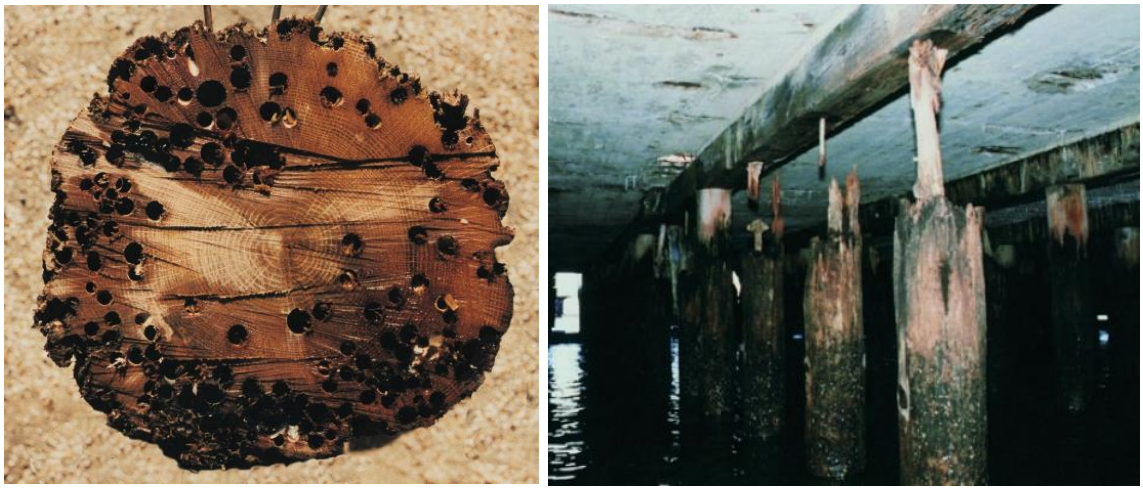

Figure 1: Tunneling in a timber pile caused by Teredo and Bankia (Left), untreated timber piles attacked by Limnoria (Right) [16]

2.1.2 Steel Piles

Steel piles are among cost-effective deep foundations. Their applications have been limited due to their vulnerability to corrosion (Figure 2). Two main destructive salts are sodium and calcium chlorides causing corrosion of the steel piles, especially in industrial and marine environments [16]. In regular soils, the rate of corrosion is around 0.03 mm per year which increases to 1.2 mm per year in the splash zone [17]. Coatings containing heavy metals can prolong the service life and enhance the lifecycle performance of the steel piles, but these treatments may be harmful to the environment. Therefore, there is a need for alternative materials for pile fabrication which are resistant to corrosion.

Figure 2: An example of corroded steel H pile supporting a harbor pier [16]

2.1.3 Composite Piles

Composite piles (plastic-and-steel type) were used for the first time as replacements for timber fender piles at the Port of Los Angeles in the United States in the late 1980s [18]. In 1987, the use of the first composite pile prototype consisting of recycled plastic was reported [19]. Table 1, shows a list of some pile projects, their manufacturer and applications in which composite piles have been utilized [20]. Some of the popular composite pile products available in the market today, include: steel pipe core piles, reinforced plastic matrix piles, concrete-filled FRP pipe piles, plastic lumber piles, and fiberglass pultruded piles [16 and 20]. Figure 3 shows the available commercialized types of composite piles.

Table 1: Selective projects using composite piles [20]

Site	Year	Application	Pile Manufacturer	Pile Type	Source
Port of Los Angeles, CA	1987	Fender piles	Plastic Pilings, Inc.	Steel pipe with thick plastic shell	Heinz (1993), Hoy (1995)
	1991–5	Fender piles	Plastic Pilings, Inc.; Seaward International, Inc.; Hammer's Plastic Recycling	Plastic piling with steel core	
Port of NJ, Newark, NJ	1991	Fender piles	Plastic Pilings, Inc.	Steel pipe with thick plastic shell	Hoy (1995)
Naval Station Roosevelt Roads, Puerto Rico	1991	Trial fender piles	Plastic Pilings, Inc.	Steel pipe with thick plastic shell	Hoy (1995)
Port of Grays Harbor, Aberdeen, WA	1992–3	Fender piles	Plastic Pilings, Inc.	Steel pipe with thick plastic shell	Hoy (1995) www.plasticpilings.com
Port of Seattle, WA	1993	Fender piles	Plastic Pilings, Inc.	Steel pipe with thick plastic shell	Hoy (1995) www.plasticpilings.com
Port of Oakland, CA	1993	Fender piles	Plastic Pilings, Inc.	Steel pipe with thick plastic shell	Hoy (1995) www.plasticpilings.com
Pearl Harbor, HI	1994	Fender piles	Plastic Pilings, Inc.	Steel pipe with thick plastic shell	Hoy (1995) www.plasticpilings.com
Port of NY/NJ	1994	Fender piles	Seaward International, Inc.	Recycled plastic with fiberglass reinforcing	Hoy (1995)
			Creative Pultrusions, Inc.	Ultra high molecular weight polyethylene	
Pier Bravo, NAS North Island, San Diego, CA	1995	Fender piles	Plastic Pilings, Inc.	Recycled plastic reinforced with welded steel rebar cage	Tetra Tech EM, Inc. (1999)
Delaware Bay, DE	1996	Fender piles	Hardcore Composites	Fiberglass shell filled with concrete	Phair (1997) www.hardcorecomposite.com
Port of New Orleans, LA	1996	Fender piles	Seaward International, Inc.	Recycled plastic with fiberglass reinforcing	Eustis Engineering Co, Inc. (1996)
Pier 16—Naval Amphibious Base Coronado, San Diego, CA	1996	Fender piles	Plastic Pilings, Inc.	Recycled plastic reinforced with welded steel rebar cage	Tetra Tech EM, Inc. (1999)
US Navy EMR Facility Pier Ingleside, TX	1997	Pier piles	Lancaster Composites	FRP shell with concrete core	Stapleman (1997)
Pier 23, Norfolk, VA	1997	Fender piles	Lancaster Composites	FRP shell with concrete core	Lancaster (2000) www.lancastercomposite.com

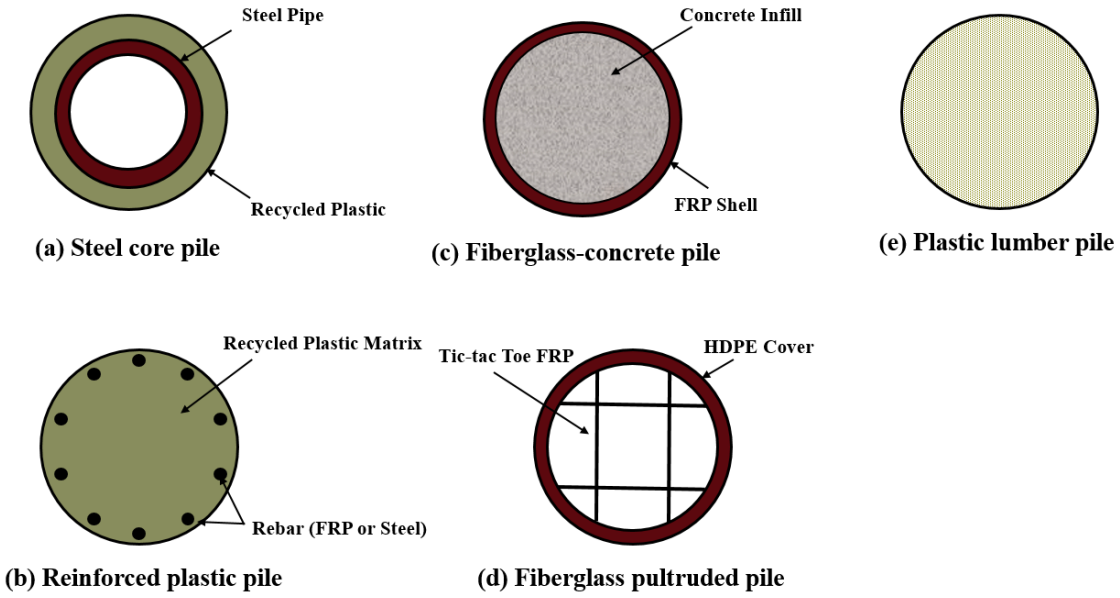

Figure 3: Available commercial composite piles

Steel pipe core piles, reinforced plastic matrix piles, concrete-filled FRP pipe piles have been recognized by [21] to be better suited for load-bearing applications among other types of piles. FRP composites have been used not only as internal reinforcements in

concrete piles [22], but also as external reinforcement and protective sheathing. Three FRP-type of piles comprised of internal FRP-reinforced piles (concrete piles with FRP reinforcement), external FRP-enclosed piles (steel pipe piles enclosed by recycled plastic, concrete piles enclosed by FRP shell, and timber piles enclosed by FRP shell), and FRP structural piles (FRP pultruded shapes and fiberglass-reinforced recycled plastic piles) have been studied by Hun et al. [23]. The elastic modulus of FRP varies from about 20% to 80% of the modulus of mild steel and depends directly on the properties and the volume fraction of fibers and matrix. New design methods for piles using FRP have been examined by Han et al. [23] for vertical and lateral loads considering buckling and load-displacement responses. Low section stiffness and high ratios of linear elastic to shear modulus are some other important characteristics of FRP piles which cause more significant nonlinear load-deformation behavior than conventional piles under vertical and lateral loads [23]. A test pile program was conducted by Pando et al. [20] to evaluate the axial and lateral load behavior of the composite piles compared with that of prestressed concrete piles. Laboratory tests were performed on three different piles with a length of about 18 m (59.0 ft) (Figure 4):

- A conventional, 610-mm (23.8 in) square, prestressed concrete pile,
- A 622-mm (24.3 in) diameter composite pile made of an FRP shell filled with concrete reinforced with steel bars,
- A 592-mm (23.1 in) diameter composite pile made of a polyethylene plastic matrix reinforced with steel bars.

The following conclusions were made as a result of Pando's report:

- The prestressed concrete pile and the FRP pile have the same axial stiffness which was about 2.5 times more than the axial stiffness of the plastic pile.
- Over a working range of bending moments, the flexural stiffness increased in order from the plastic pile to the FRP pile to the prestressed concrete pile.
- The axial load capacities for the concrete pile, the FRP pile, and the plastic pile were found to be 3,090, 2,260, and 2,130 kN (695, 508, and 479 kip), respectively.
- The average unit shaft resistances for the prestressed concrete pile, the FRP pile, and the plastic pile were 61.8, 46.9, and 48.9 kPa (8.96, 6.80, and 7.09 psi), respectively.
- The corresponding unit toe resistances for the prestressed concrete pile, the FRP pile, and the plastic pile were 1,854, 2,564, and 2,339 kPa (268.8, 371.8, and 339.2 psi), respectively.
- From the static lateral load test results, they found that the prestressed concrete pile and the FRP pile have the same load-deflection response which was much smaller than the plastic pile at the same lateral loads.

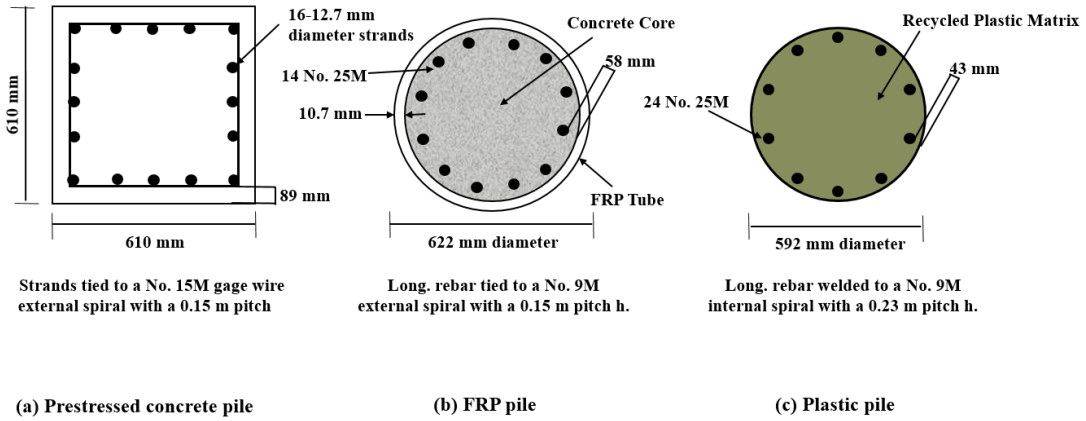

Figure 4: Cross section details of the three types of piles tested by Pando et al. [20]

2.1.4 Precast Prestressed Concrete Piles

One of the options for establishing pile foundation is the use of PPCP (Figure 5). PPCP is a concrete prism element with prestressed strands providing initial compressive stress and transverse tie or spiral providing for confinement and shear resistance. Conventional PPCP uses concrete of various strengths and high-strength steel strands. It normally offers an adaptable, economical pile foundation with reasonable corrosion resistance provided by concrete cover that is less prone to cracking because of compressive stress introduced by prestressing. However, in marine environments, in time, corrosion damages the strands and reduces the load carrying capacity of the piles. Alternative corrosion resistant material can be used for strands and ties to address this shortcoming.

© https://www.gimrock.com/FoundationWork.html

Figure 5: Prestressed-Precast Concrete Piles in marine environment

2.1.4.1 Conventional Steel Presteressed Strand

Conventional steel strands are normally made of seven wires (six wires spun around a king wire) of high-strength, low relaxation steel with various nominal diameters, most commonly 0.5 and 0.6 in diameter. As an example, Figure 6 shows pile details which are commonly used by the Virginia Department of Transportation (VDOT) bridge projects [20]. The prestressed concrete cross section is a 508-mm (20 in) square pile with a length of about 13.1 m (43 ft). As shown in Figure 6, this prestressed pile contains a total of fourteen, 12.7-mm (0.5 in) diameter, 7-wire strands of 1861 MPa (270 ksi) ultimate strength, pretensioned to produce a prestress level of 5.6 MPa (0.809 ksi) based on VDOT standards.

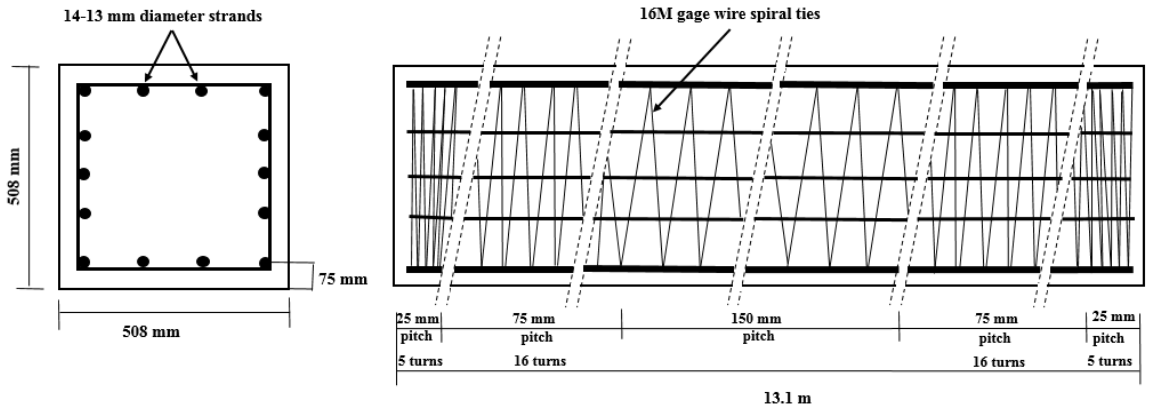

Figure 6: Details of prestressed concrete pile used in VDOT (Pando et al. 2006)

Florida Department of Transportation includes standard details for its precast prestressed square piles with conventional steel in FDOT Standard Drawings Index Series 455 (2018). Figure 7 shows these details for an 18x18 in square piles.

PPCP provides in many cases an economical alternative to other pile foundation types. However, traditional prestressed piles are susceptible to corrosion of the carbon-steel strands especially in marine environments. In such environments, alternating water levels and water splash promote deposit and migration of chlorides into the pile and provides a condition for accelerating corrosion. Florida Department of Transportation (FDOT) has implemented programs for utilization of alternative prestressing strand material that are corrosion resistant.

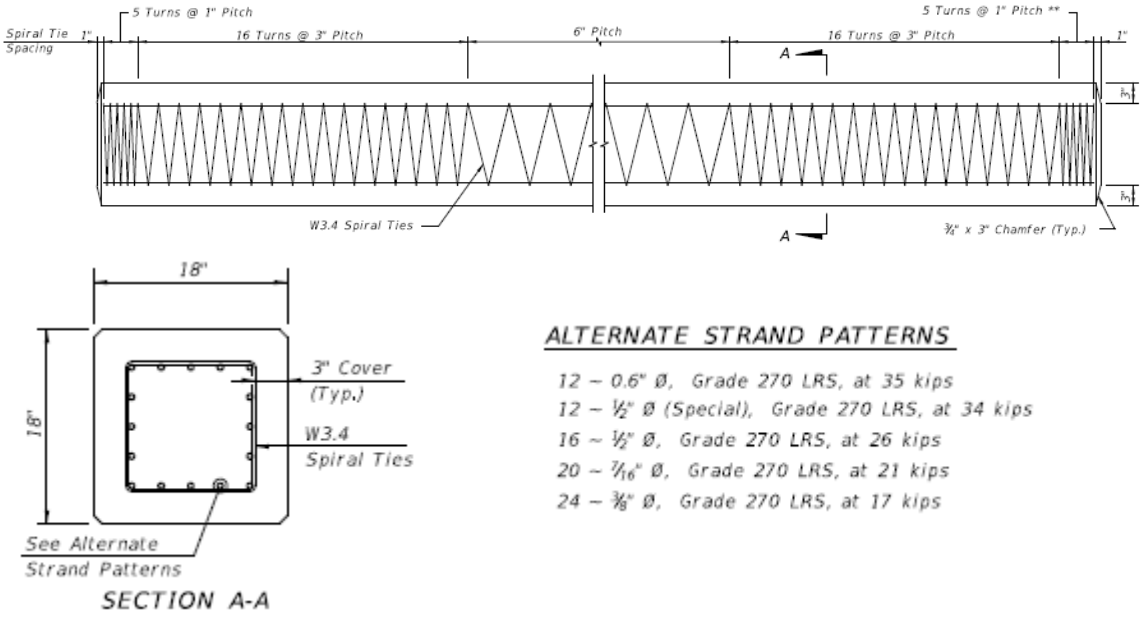

Figure 7: FDOT standard prestressed-precast concrete pile (FDOT Standard Drawings Index Series 455, 2018)

2.1.4.2 Fiber Reinforced Plastic (FRP) Presteressed Strand

In Florida, many bridge foundations are exposed to salt water and harsh marine environments which can cause expensive maintenance issues and shorten bridge life. Conventional piles mostly deteriorate prematurely in such corrosive environments. Corrosion in concrete piles also occurs in soils and groundwater where there are low pH

levels, high level of chloride as well as sulfate. The consequence is a decrease in load-carrying capacities, and likely increase in settlement eventually resulting in the failure of superstructures [23]. Although deteriorated pile structures can be replaced or retrofitted, their maintenance will be costly and not reliable for their long-term serviceability [24]. It has been estimated that repair and replacement of the conventional pile systems cost the United States more than $1 billion annually (according to the estimate at the time of investigation) [25]. Therefore, high durability, low maintenance, and high safety are always top priorities for any bridge owner. Fiber reinforced plastic (FRP) is a thermally and electrically nonconductive, lightweight, and high corrosion-resistant material [23]. Hence, they can offer a superior alternative material to conventional materials (e.g., steel) for driven pile construction. FRP is an anisotropic material with an excellent strength parallel to the direction of the fibers. This property of the FRP has a considerable effect on shear strength, dowel action, and bond performance. Although the weight of FRP is almost one-quarter of steel, its tensile strength is almost three times greater than conventional steel materials [23]. FRP is manufactured from two main parts of fibers and matrix resin The former part provides strength and stiffness and can be made of Glass, Basalt, Carbon, or Aramid. The matrix of FRP protects and transfers stresses between fibers and can be made by Polyester, Epoxy, Vinyl Ester, and Urethane. The most popular combinations of FRP are (Busel 2016):

- Glass/Vinylester (or epoxy)
- Glass/Polyurethane
- Basalt/Epoxy
- Carbon/Vinylester (or epoxy)

There have been several investigations on the application and performance of PPCP using alternative prestressing strand material. CFRP and its variant Carbon Fiber Composite Cable (CFCC) is one of the materials that has shown great promise for replacing normal prestressing strands. The use of Carbon Fiber Reinforced Polymers (CRFP) for strands, longitudinal (when needed) and transverse reinforcement in the precast concrete piles have shown great improvements in resistance against corrosion [24, 26, and 27]. ACI-440-04 covers an extensive review of the background, material properties and design recommendation for the use of these materials and other FRPs. Driving and installation of piles made with CFRP have been performed without any major damage to the pile despite the hard condition and high stress level. Some challenges in production were noted and modifications recommended including use of wood versus steel cap, care in installation and handling, lower stress rate, avoiding the use of regular vibrator, and strong QC. Grace [28] used CFRP for post-tensioning tendons and reinforcing bars for the first time in the superstructure of the Bridge Street Bridge in Southfield, MI. Although this application was not for piles, the study monitored the performance for long periods of time and demonstrated in general suitability of CFRP for use as prestressing/post-tensioning applications.

FRP can be manufactured using carbon (CFRP), glass (GFRP), or aramid (AFRP) fibers. Carbon fiber composite cables (CFCC) is a type of CFRP that has been used for prestressing and post-tensioning. In CFCC, wires containing carbon fibers of polyacrylonitrile and epoxy resin are twisted and wrapped with synthetic yarns to cover the fibers from ultraviolet radiation and mechanical abrasion [24]. CFCC has shown high

bond strength to concrete (about twice of that of steel), its relaxation is less than steel, and can be coiled in its twisted wire form. However, CFCC is more expensive than steel, has low impact resistance, and it is not as ductile as its steel counterpart [24]. According to the recorded data from pull-out tests, the bond strength of CFCC to concrete is 967 psi (6.67 MPa) which is more than twice that of steel.

CFCC has a longitudinal coefficient of expansion of 0.34 × 10-6/°F which is 1⁄20 of that for the steel. CFCC has a light weight with less relaxation of the strands compared to steel which makes it easy to handle. Roddenberry et al. [24 and 29] tested PPCP using CFCC of various lengths to investigate the flexural strength, transfer length, development length, and drivability (Figure 8).

Figure 8: Flexural testing of PPCP with CFCC [29]

They concluded that the development length of the tested CFCC strands is less than 72.0 in and therefore less than the AASHTO LRFD specifications prediction of 123 in (3120 mm) for steel strands (using CFCC's value for guaranteed ultimate tensile strength), and

flexural strength higher than anticipated. Figure 9 shows the side view and cross-section of the 24 in square piles and made by CFCC spiral transverse reinforcement.

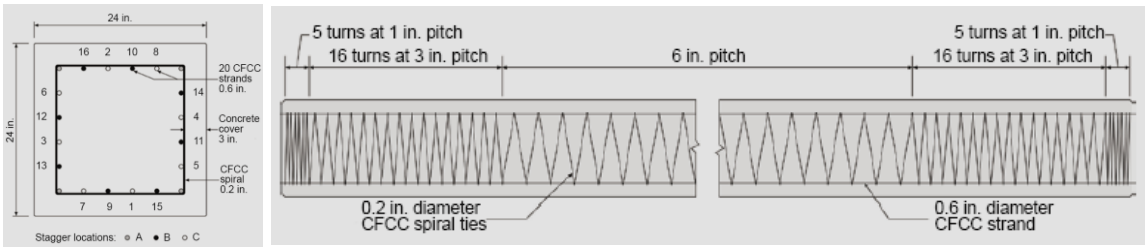

Figure 9: Cross-section (Top)and side view (Bottom)of the piles made by CFCC [24]

Florida Department of Transportation includes standard details for its precast prestressed square piles using CFRP strands and ties in FDOT Standard Drawings Index Series 455 (2018). Figure 10 shows these details for an 18x18 in square piles.

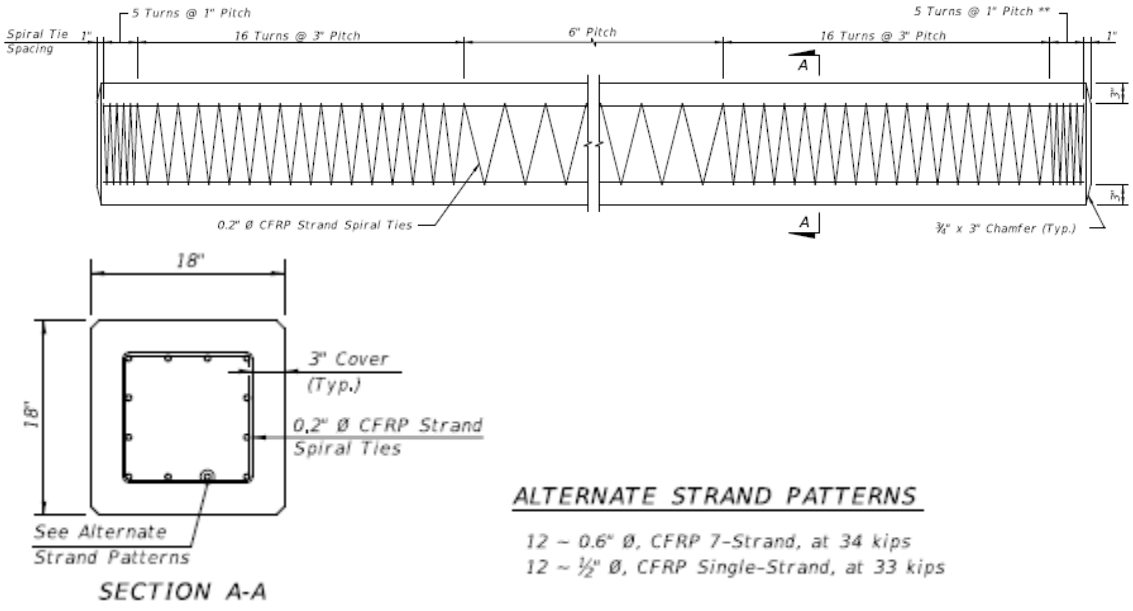

Figure 10: Details of prestressed concrete pile using CFRP strands and ties (FDOT Standard Drawings Index Series 455, 2018)

2.1.4.3 High Strength Stainless Steel (HSSS) Presteressed Strand

PPCP using SS strands and spirals have also been studied as another alternative to carbon steel strand piles. Mullins et al. [26] tested three types of stainless steel material that are available in strand form and compared their corrosion resistance and structural performance to conventional carbon steel prestressing strand. They showed that the use of SS strands had no adverse effect on transfer length, while it improves significantly the corrosion resistance (Figure 11).

Figure 11: PPCP with Stainless Steel Strand and Spiral [26]

From metallurgy perspective, stainless steel material is recognized as an iron – carbon alloy with a minimum of 11.5 wt% chromium content [30]. Stainless steel material is superior to conventional carbon steel due to their higher corrosion resistance property. Therefore, the stainless steel provides a better lifecycle performance for prestressed strands for piles as it relates to corrosion. To produce high strength stainless steel

(HSSS), manufacturers use cold working or similar process to increase the strength of the stainless steel [26].

FDOT includes standard details for its precast prestressed square piles using HSSS strands and SS ties in FDOT Standard Drawings Index Series 455,2018 [31]. Figure 12 shows these details for an 18x18 in square piles.

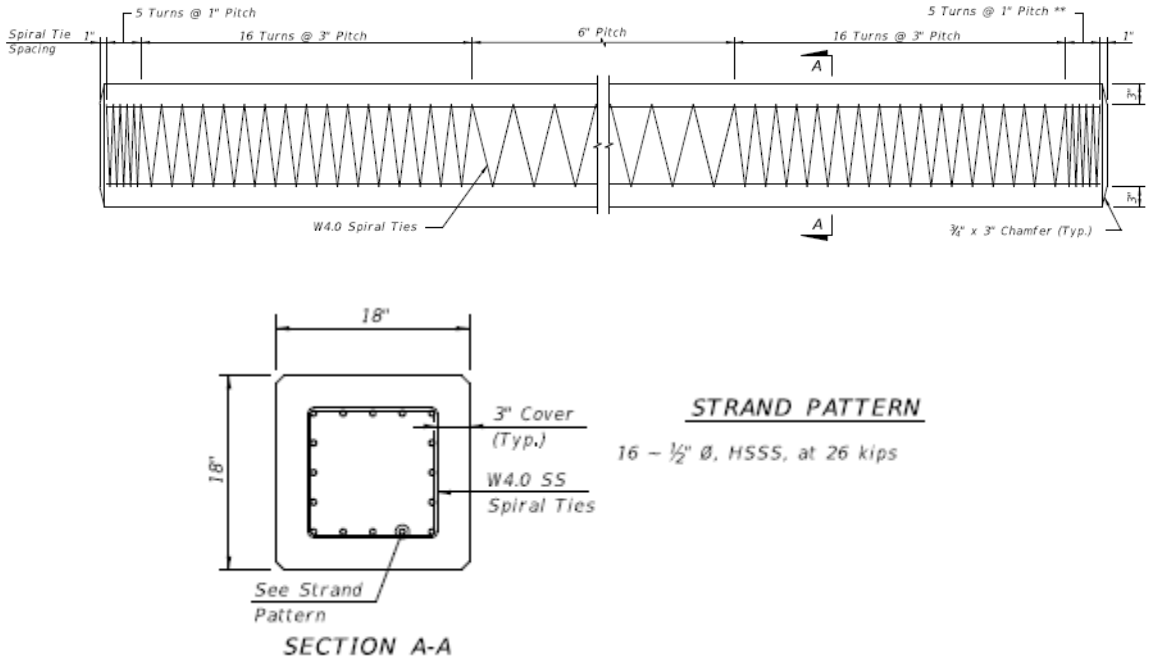

Figure 12: Details of prestressed concrete pile using HSSS strands and SS ties [31]

The conventional prestressing steel has been compared with strands made of HSSS by Nürnberger [32]. The comparison in Figure 13 illustrates that the HSSS strands have a better fatigue performance than conventional carbon steel strands (considered in their study) under various exposure conditions. Paul et al. [33] demonstrated through testing that transfer and development length for HSSS-2205 prestressing strands are considerably

smaller than that predicted by AASHTO LRFD, the flexural and shear strengths of piles using SS were greater than that predicted by both ACI-318 and AASHTO LRFD, and the stress loss was smaller than that predicted by AASHTO LRFD refined method. Prestress losses and transfer lengths were not affected by pile driving and extraction.

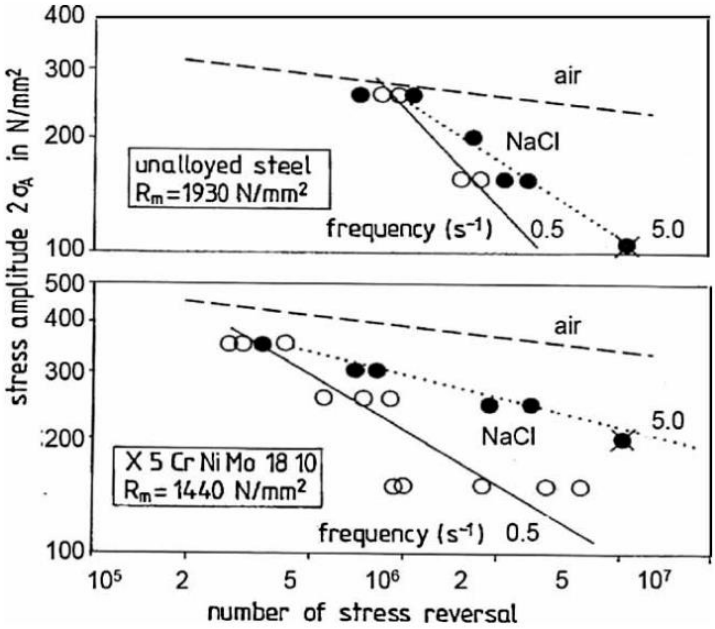

Figure 13: Results of comparing HSSS strands with conventional cold-drawn prestressing steel strand [32]

2.2 Piles Splice

PPCPs often require splicing for one or more of the following reasons:

- Shipping and transportation length limits,
- Limited headroom that will force planned splicing,
- Unplanned splicing when the required capacity is not achieved with the piles existing lengths.

There are various means for establishing bearing-type splices as illustrated in Figure 14 including wedge, pinned, welded end plates, sleeve, connecting ring, mechanical and finally dowel splices. While more variation of splice types and alternatives are available [34], this project makes specific focus on the dowel-type splicing using epoxy in accordance with FDOT Specification 926 Type AB.

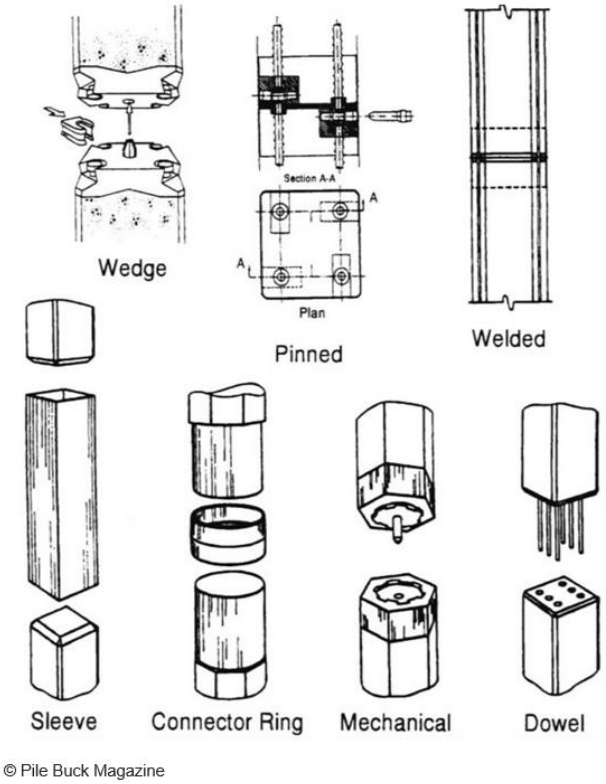

Figure 14: Various types of pile splicing

One of the earlier works conducted to investigate the existing methods for concrete pile splices is by Bruce and Hebert [35-36]. They categorized pile splices as follows:

- Welded Splices
- Bolted Splices
- Mechanical Locking Splices

- Connector Ring Splices
- Wedge Splices
- Sleeve Splices
- Dowel Splices

Driving conditions, a required concrete strength for piles, head and tip design practices, and requirements for an ideal splice were all investigated by Liu [37]. A combination of sleeve and wedge was used for splicing octagonal piles in Seattle by Alley [38]. Table 2 shows a summary of twenty types of pile splices from all over the world in terms of size range, field time for splicing, approximate cost of splice, availability, construction usage, structural integrity, and structural performance [35-36].

It is of importance to note that the information in the Table 2 mostly has been gathered from general correspondence with manufacturers or designers of the splice. Regarding the strengths provided for each of the pile splices, the presented data is dependent on suitable procedures in establishing the splice and close quality control. Data on the strength of the pile splices has been obtained from the experimental tests conducted by Bruce and Hebert, experiences and tests conducted by others, and the theoretical and analytical investigations [35-36].

Table 2: Summary data on different pile splices [35-36]

Name of Splice	Type	Origin	Approximate Size Range, in. (cm)	Approximate Field Time, min.	Strength		
					Percent Compressive	Percent Tensile	Percent Flexural Cracking
Marier	Mechanical	Canada	10-13 (25-33)	30	100*	100*	100*
Herkules	Mechanical	Sweden	10-20 (25-51)	20	100**	100**	100**
ABB	Mechanical	Sweden	10-12 (25-30)	20	100**	100**	100**
NCS	Welded	Japan	12-47 (30-119)	60	100**	100**	100**
Tokyu	Welded	Japan	12-47 (30-119)	60	100**	100**	100**
Raymond Cylinder	Welded	USA	36-54 (91-137)	90	100**	100**	100**
Bolognesi-Moretto	Welded	Argentina	Varied	60	100*	55*	100*
Japanese Bolted	Bolted	Japan	Varied	30	100**	90**	90**
Brunsplice	Connector ring	USA	12-14 (30-36)	20	100**	20*	50*
Anderson	Sleeve	USA	Varied	20	100*	0*	100*
Fuentes	Welded sleeve	Puerto Rico	10-12 (25-30)	30	100**	100*	100*
Hamilton Form	Sleeve	USA	Varied	90	100*	75**	100**
Cement Dowel	Dowel	USA	Varied	45	100**	40**	65**
Macalloy	Post-tensioned	England	Varied	120	100*	100*	100*
Mouton	Combination	USA	10-14 (25-36)	20	100*	40*	100*
Raymond Wedge	Welded wedge	USA	Varied	40	100*	100*	100*
Thorburn	---	Scotland	No information available on this splice				
Pile Coupler	Connector ring	USA	12-54 (30-137)	20	100**	100**	100**
Nilsson	Mechanical	Sweden	Varied	20	100*	100*	100*
Wennstrom	Wedge	Sweden	Varied	20	100*	100*	100*
Pogonowski	Mechanical	USA	Varied	20	100*	100*	100*

*and ** based on data furnished by proponent

*Calculated **Observed

2.2.1 Epoxy Dowel Splice

Recently, there has been growing interest in splicing PPCPs using dowel-type splice as a desired and economical splicing type in providing sufficient flexural resistance [39]. In the dowel-type splice, holes are cast or drilled into the top of the lower pile to receive dowel rebars protruding out of the lower end of the upper pile (Figure 15). Dowel rebars can be made of carbon steel, SS, CFRP, or GFRP bars. The author found no inspection report of damages at pile splice. However, the vulnerability of piles to corrosive environment is expected to affect also the pile splices. Implementation of corrosion resistant dowels for splicing piles, along with the use of corrosion-resistant strands in the

pile, can increase the durability of pile splices and accordingly enhance the piles service life.

In the lower section of the piles at splice location, the dowel bars usually need to cover a sufficient anchorage length [41]. Based on drawings by Transport Roads and Maritime Services of New South Wales [42], at the joint location, a splice sleeve may need to be used that is made of hot-dip galvanized steel (Figure 15). And, the lower edge of the splice sleeves needs to be sealed against pile. Alternatively, plywood pieces can be used to build a dam around the lower pile segment to contain the epoxy.

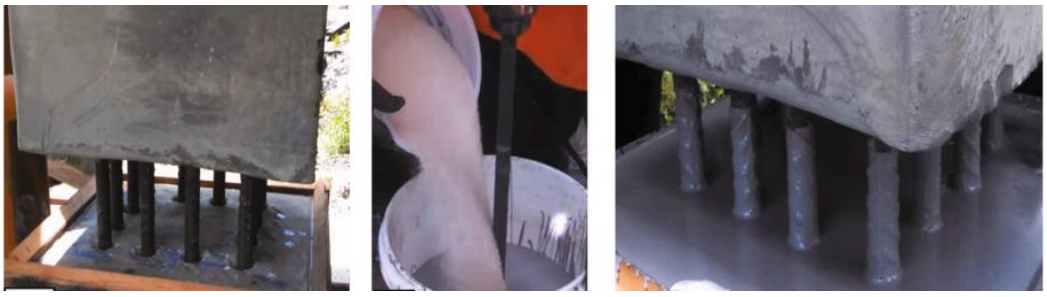

Figure 15: An example of dowel-type splice for PPCPs [40]

According to drawings by Transport Roads and Maritime Services of New South Wales [42], dowels can be made of steel reinforcing bars, grade D500 to AS/NZS 4671. Apart from the conventional splicing dowels, SS, CFRP, and GFRP bars are other alternatives for dowels. FDOT Standard Drawings Index Series 455 [31] include details and designs for conventional steel, CRFP and SS dowels (455-102), but does not cover GFRP dowel application. Following describes some of the features of dowel splice details prescribed in these drawings for 18x18 in square drivable prestressed precast concrete pile.

For a conventional dowel splice in 18x18 in pile, 8 No. 10 dowel bars are used. Three bars are used on each face spaced 3 ½ in center to center at an edge distance of 5 ½ in on center from the sides of the pile section. These dowels are cast in the upper pile segment (pile extension) for a length of 10’-6”. For unforeseen splice detail, dowels extension is projected out of the top segment (pile extension) only by 2’-6”, whereas for preplanned splice detail, this extension length is 4’. For the case of preplanned splices, a set of 8~No. 9 bars, 10’-6” long are cast in the lower pile segment as auxiliary reinforcement. Spiral ties of W3.4 is used along the pile segments in accordance with the standard requirements of the PPCPs with smaller 1” pitch for 5 turns followed by 3” pitch for 16 turns and 6” pitch afterwards from both ends. For CFRP and SS dowel types, the FDOT Standard Drawings Series 455 details for SS dowels are identical to the conventional splices with SS dowel bars replacing the conventional bars at the same size and lengths. However, for CFRP dowel splices, 9~No. 6 CFRP bars are used as dowels, 3 on each side and one at the center, with the same spacing and edge distance as the conventional dowels. Also, the length cast in the upper pile segment is shorter for CFRP at 4’-6” for both unforeseen and preplanned splices. Dowel bar extension length from the upper segment for CFRP dowels is the same as conventional dowel for unforeseen splices (2’-6”) and is slightly (6”) longer than conventional dowel for preplanned splices at 4’-6”. According to these drawings, auxiliary bars are not used in the lower pile segment for the case of CFRP dowel splices in CRFP prestressed pile option. Spiral ties of 0.2” diameter CFRP strand are used for piles with CFRP detail with the same spacing and pitches as conventional piles.

Dowels made of carbon-steel reinforcing bars have low durability and high maintenance cost because of high potential of degradation due to corrosion. Therefore, taking advantage of corrosion resistant materials for dowels (SS, CFRP) in pile construction has attracted attention of researchers and manufacturers as a practical alternative. Although the cost of using these advanced materials for foundation is greater than conventional carbon-steel, it is a relatively small percentage of the overall cost of the bridge. In this study, the use of GFRP dowel bars as replacement for SS and CFRP dowels for epoxy splice for prestressed precast concrete piles will be investigated. One of the major goals in this study is to investigate the performance of the different types of dowel bars for splicing PPCPs. The conventional carbon-steel reinforcing bars are corroded when chloride ions penetrate through concrete (and contaminations present in the material) and form electrochemical reactions resulting in corrosion inside the pile which induce high tensile stresses in the surrounding concrete causing cracking and spalling, and therefore higher exposure. Apart from chlorides, the variation of temperature, freezing and thawing are other sources for degrading the concrete [16]. GFRP bars are expected to provide a more economic option to other corrosion-resistant dowel materials.

Different types of resin and cement can be used as filler and bonding material to connect the two segments of pile at the splice. In precast prestressed concrete pile splice, epoxy is commonly used to fill the interface and sockets of the lower segment so that the dowel bars of the upper segment can be fully enveloped with the epoxy. The curing time for the epoxy can be accelerated with heating methods such as enclosing the joint with a steam jacket [41]. Moreover, dowel splice using cement filler like Florok Plasticized Cement,

manufactured by the Chargar Corporation of Hamden, Connecticut, has been studied by Bruce and Hebert [35-36]. CONCRESIVE® 1420 (currently known as MasterEmaco ADH® 1420) as a general-purpose gel epoxy adhesive has been used in prestressed concrete piles spliced with steel pipes investigated by Canner [43]. The investigation found, for the splice mating surface, CONCRESIVE® 1420 seemed to be the best product because of its high strength and ability to seal the mating surface, initially. However, in the field test, the plan for using CONCRESIVE® 1420 general purpose gel epoxy adhesive changed because the product was inconveniently supplied in two-part tubes with a mixing gun to apply it. The proper and more convenient way to apply the epoxy is to be able to mix them in larger containers and pour large volumes quickly to avoid setting of the epoxy before completion of the process. FDOT is frequently faced with the same problem of short setting time of epoxy adhesive in epoxy dowel splice projects [43]. It is also realized that some cement and resin materials that are very effective in anchoring dowels may require an excessive setting time, and vice versa. This motivates consideration of other filler material for establishing effective dowel anchorage within an acceptable setting and hardening time frame.

Among epoxy products available in the market, SEALBOND PILE SPLICING EPOXY (458-PE) is a two-component fast setting epoxy designed primarily for bonding concrete piles [44]. The cured resin provides high compressive and flexural strength to the joint when used with fine aggregates as filler. EPIWELD® 580 [45] is another epoxy product that has been used as filler for pile splices mixed with sandblasting sand 16-40.

With reference to the literature review carried out by Bruce and Hebert [35-36], it has been concluded that a cement-dowel splice (using Florok Plasticized Cement manufactured by Chargar Corporation of Hamden, Connecticut) is effective and acceptable for splicing PPCPs. This plasticized cement is a fast-setting material allowing pile driving to resume within 15 minutes. Figure 16 shows the details and fabrication of the pile splices used by Bruce and Hebert [35-36] in accordance with Louisiana Department of Highways specifications.

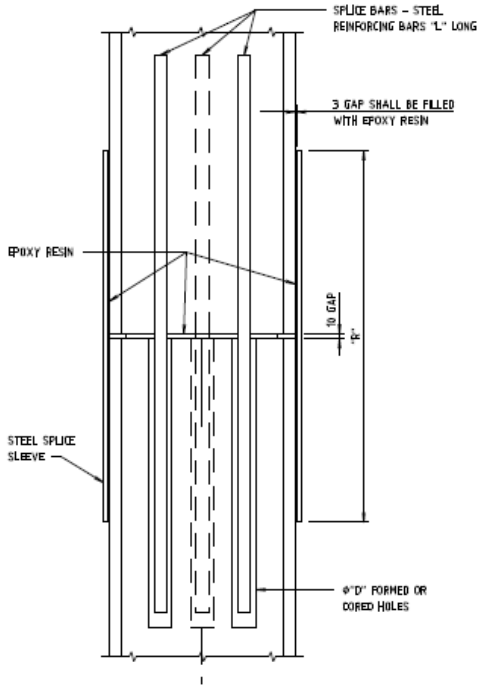

Figure 16: Galvanized sleeve at splice location [35-36]

Bruce and Hebert selected cement-dowel splice for an actual test to evaluate the performance of the pile splice under field conditions and the structural capacity of the splice. For the experimental test, six prestressed concrete specimens grouped in two series of "A" and "B," were fabricated by them. Series A and B were comprised of three

14 in piles, and of three 24 in piles, respectively. All of the pile splices were manufactured in square shape. Table 3 shows the arrangement for section and length of each pile splice.

Table 3: Size information for six tested pile splices [35-36]

Pile	Size Square Pile		Length					
			Bottom Section		Top Section		Total	
	in.	cm.	ft.	m.	ft.	m.	ft.	m.
A-1	14	35.6	45	13.7	15	4.6	60	18.3
A-2	14	35.6	45	13.7	15	4.6	60	18.3
A-3	14	35.6	40	12.2	38	11.6	78	23.8
B-1	24	61.0	45	13.7	35	10.7	80	24.4
B-2	24	61.0	45	13.7	35	10.7	80	24.4
B-3	24	61.0	40	12.2	20	6.1	60	18.3

For the field tests, firstly, the bottom sections of piles were driven and seated firmly in the soil. Then, the top sections were spliced to the bottom sections. Tensile capacity for Pile A-1 and flexural capacity for the remaining five piles were tested, respectively. Un-spliced pile specimens were used as control cases in the experimental evaluation, and the loads-deflections data was recorded for both spliced and un-spliced sections in the tests to failure. Bruce and Hebert [35-36] stated there was no visible damage to the pile splices throughout all of the driving operations, and results of the tensile and flexure tests were considered to be favorable. They mentioned that the pile splice number A-1 withstood a tensile pull of 60 tons up to bond failure between two sections of the pile where the dowels of the top section pulled out of the bottom section. Apart from that, the splice

withstood tensile forces and ultimate moments comparable to 40 percent of the cracking tensile load and 65 to 100 percent of the flexural cracking moments of the un-spliced pile, respectively. As it is shown in Figure 17, load-deflection measurements also were carried out by Bruce and Hebert [35-36] to conclude that the spliced sections for cement-dowel pile splice are more flexible than the un-spliced sections.

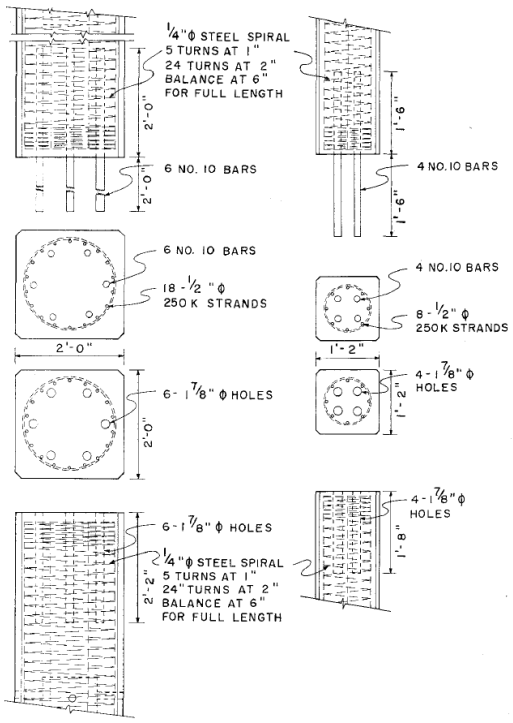

Figure 17: Details of cement-dowel splice [35-36]

Figure 18 shows the details of the tests on epoxy pile splice performed by Navaratnarajah [41]. In this figure, the parameters of L, HT, HY, and MS are the length of pile varied 9m -18m, high tension, high yield, mild steel (all dimensions in mm), respectively. The piles were prestressed with 16 ×7 mm diameter high-tensile (strength) wires arranged in a 300 mm diameter circular pattern. The secondary reinforcement was comprised of 6 mm

diameter mild steel spirals at a pitch of 150 mm. In addition, for reinforcing at the pile ends, 4×20 mm mild steel bars were used extending, in length, 900 mm into the pile with closer spacing of the secondary reinforcement spirals at a pitch of 25 mm over 300 mm from the end. At the joining sections, the upper section used four 25 mm high yield deformed bars 1.2 m long as dowels, and the other section used four holes with 32 mm diameter corrugated sheaths to receive the dowels. The holes were deeper than the length of dowels for better fit.

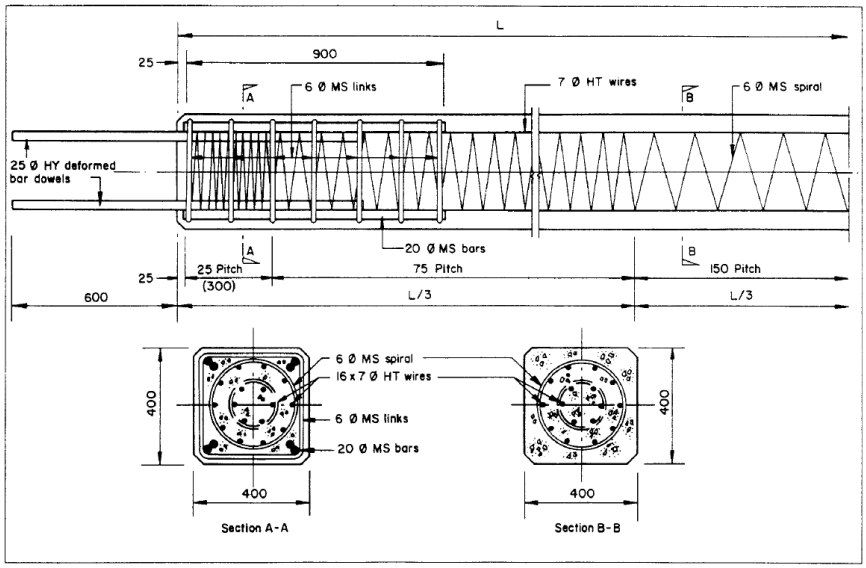

Figure 18: Details of test piles [41]

For establishing the pile splice, the bottom segment of the pile was held in a vertical position and the top segment including dowels projecting at the tip was positioned over the holes in the bottom segment. The detail of this epoxy dowel splice is shown in Figure 19. The sockets were filled with a proprietary brand two-part epoxy.

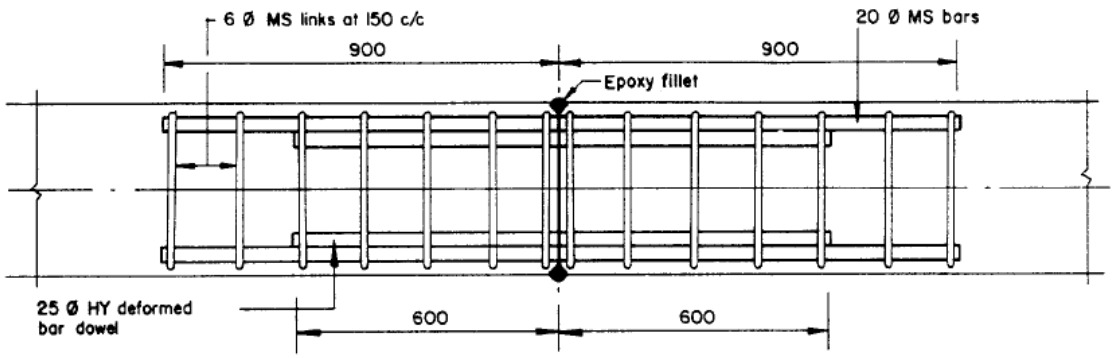

Figure 19: Details of epoxy splice [41]

Figure 20 shows experimental set-up used by Navaratnarajah's for the epoxy dowel spliced prestressed precast pile. The pile was supported on a rocker and roller support at the two ends, respectively, over a span of 5.4 m. A steel spreader beam was used to apply the loads in increments of 1000 kg. For measuring the deflection of the pile, a steel indicator was vertically fixed to the center of the span so that observations can be made with a telescope focused on the indicator. Five dial gauges (Dl, D2, D3, D4 and Ds) were also set against the bottom of the pile at 900 mm intervals to record the deflected shape of the pile at different loading steps.

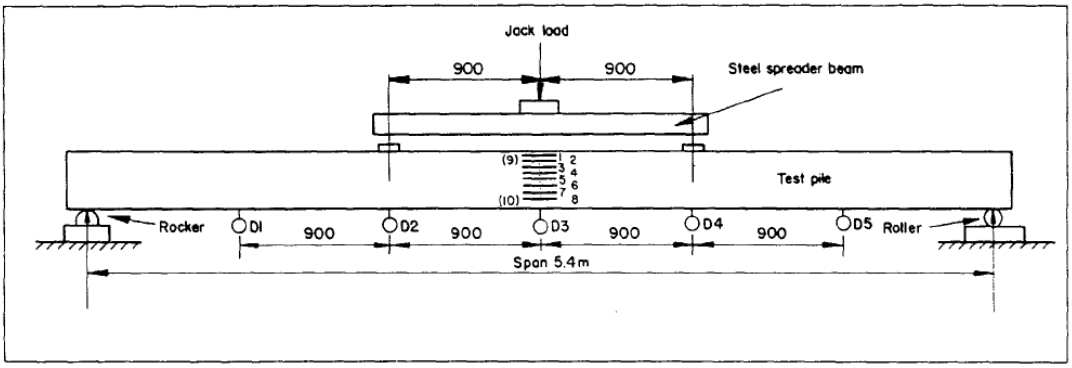

Figure 20: Experimental set-up [41]

In the experimental test, the first crack was noticed outside the joint and the maximum size of crack was recorded to be 4.0 mm (Figure 21). According to Navaratnarajah, the epoxy dowel splice pile failed as a result of the pull-out of the dowel bar due to local shear effects at the location of termination of the dowel rebars.

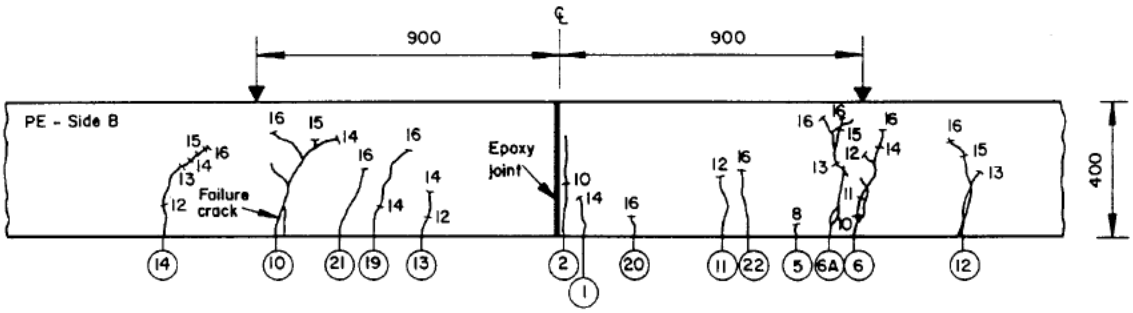

Figure 21: Cracking pattern in the epoxy-jointed pile [41]

The flexural behavior of an epoxy dowel splice for PPCP with a 400 ×400 mm cross-section and concrete strength of 45 N/mm^2 at 28 days was compared with the performance of an un-spliced pile and welded- joint pile. Figure 22 shows the load-deflection of three tested specimens at the center of the span or at the location of the splice. The results show that the pile using the epoxy joint failed at a higher ultimate load compared to the unjointed pile. This investigation also proved that the stiffness of the pile with epoxy joint was comparable to un-spliced pile and higher than the welded type.

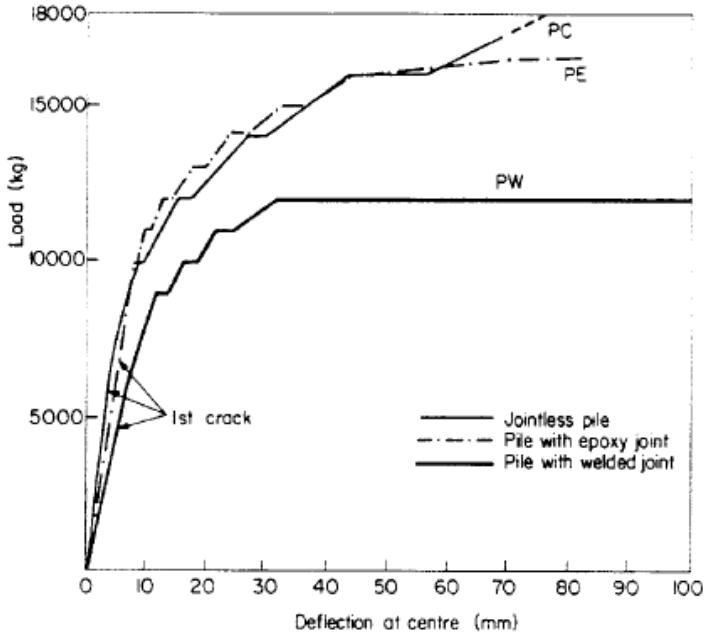

Figure 22: Load/deflection characteristics at the span center of the epoxy-jointed pile [41]

CHAPTER 3: DEVELOPMENT OF DESIGN PROCEDURE

In this Chapter, a design procedure for pile splice using GFRP dowels applicable to 18x18 in square piles is developed. A combination of applicable codes and standards as identified below are used to develop this design. It is realized that GFRP dowels can be used for piles that include corrosion-resistant reinforcement including CFRP and SS strands. In prestressed precast concrete piles, tensile stresses are readily resisted by the precompression from prestressing. The focus of this study will be on designing for flexural resistance and checking for other load effects.

Design and construction of the piles will follow the FDOT Structures Manual Volumes 1 (SDG) and 4 (FRPG) [46], FDOT Standard Specification for Road and Bridge Construction [47], and FDOT Standard Plans Index Series 455 [48]. The FRPG references both the 2018 AASHTO Design Guide Specifications for GFRP-Reinforced Concrete Bridges (AASHTO-GFRP2) [49] and Concrete Bridge Beams Prestressed with CFRP Systems (AASHTO-CFRP1) [50]. FDOT Standard Specification for Road and Bridge Construction Section 932 specifies the minimum mechanical properties for both GFRP and CFRP reinforcing, with equivalent limits to ASTM D7957-17 for GFRP reinforcing, but with some enhanced testing criteria for sustained load performance [47].

There may be several causes for pile bending. As an instance. Lateral forces from ground motions, impact of vessels and vehicles, and thermal expansion of bridge create bending for piles and plie splices. FDOT Spec. Section 933 specifies the minimum mechanical

properties for FRP prestressing strands, while Section 455 requires that pile splices develop the following capacities:

- Axial Compressive Strength:(Pile Cross sectional area)×(28-day concrete strength)=1944kips
- Axial Tensile Strength: (Pile cross sectional area)×900 psi (6205.3 kPa) = 291.6 kips
- Flexural Strength (Table 4) = 245 kip.ft

Table 4: Flexural Capacities Limits (from FDOT Spec. Section 455.7)

Pile Size (ines)	Bending Strength (kip-feet)
18	245
24	325
20	600
30	950

A reliable design procedure to calculate flexural capacity of piles at their splices is essential for designers and structural engineers designing the bridge foundation. In this Chapter, a design procedure was developed for flexural strength of pile splices using different dowel materials of GFRP, CFRP, and Steel. Axial compression is resisted by the concrete/epoxy in cross section and is not a concern in the case of splices. Furthermore, the required axial tension should not pose an issue since normally dowels are capable of transferring tension, including forces developed during driving, from one segment to the other.

3.1 Design Moment Strength

Design and detailing of piles were assumed to follow the FDOT Standard Plans Index No. 455-001 to 018. For the design of pile splice using GFRP Dowels, following assumptions were also made:

- It is assumed that epoxy does not reduce the bond strength of GFRP with concrete. In other words, the bond behavior of GFRP bar with epoxy adhesive is assumed to be the same as GFRP bar embedded directly in concrete,
- A linear relationship for tensile stress-strain for GFRP dowels all the way to rupture,
- The maximum compressive strain in the concrete (strain at crushing) is assumed to be 0.3%
- The most common type of GFRP uses E-glass fiber, but enhanced E-CR (Corrosion Resistant) glass fiber is mandated by FDOT Section 932 and ASTM D7957-17 for internal concrete reinforcing, and assumed for use in splice.
- For the case of pure axial compression, for calculation of the resistance, the gross cross-sectional area of the concrete is conservatively used and contribution of dowel bars are ignored.
- The material and mechanical properties comply with the mechanical properties of FRP reinforcing bars in accordance with Specifications Section 932 for the design of structural concrete [47]. Additionally, improved mechanical properties under consideration by ASTM D30 Committee will be evaluated to highlight the potential for improved performance.
- First trial design was adopted based on dowel consisting of GFRP #10 bars. The design is checked for other sizes if applicable. The main goal is to develop a design

that is optimized taking account the economy, higher bending strength, and simplicity. The latter would be satisfied especially if a design similar to conventional splices can be used.

- Splice is designed for pure flexure and checked for other combined load effects.

3.1.1 Cross-section physical and mechanical parameters

According to the FDOT Standard Plans Index Series 455-001 and 455-018 [48], the clear cover for tie is 3 in (76.2 mm) (Figure 23). Pile cross section including the dowels will be as shown in Figure 24 adopted from FDOT Standard Plans Index Series 455-018 and 455-118 [48]. Assuming #10 GFRP dowel bars following the pattern in the standard drawings, the clear cover (Eq. 1) and Spacing (Center to center) are 4.865 in (123.5 mm) and 3.3 in (83.82 mm), respectively.

$$\text{Clear cover} = \text{FDOT Effective Cover} - 1/2 \times \text{bar dia \#10} \quad (1)$$

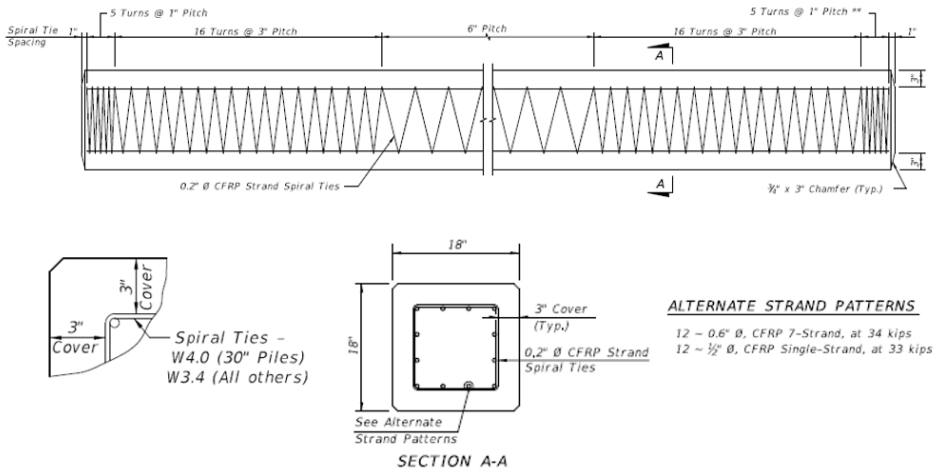

Figure 23: The typical cover of FDOT pre-design pile [48]

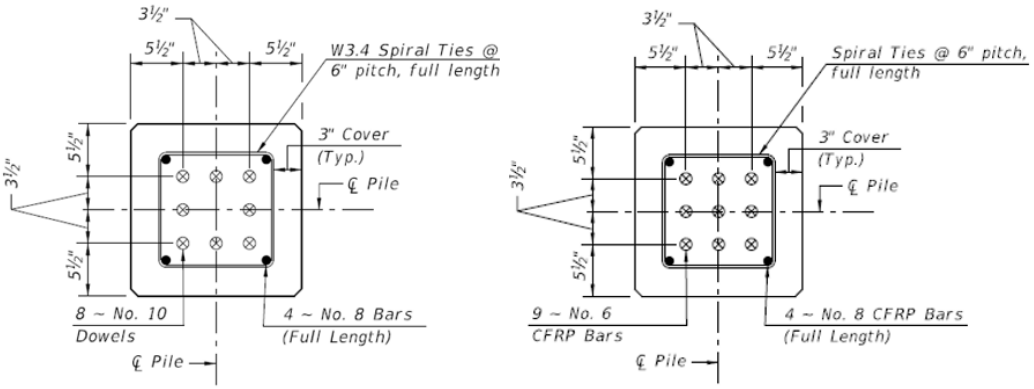

Figure 24: The pile cross section for steel bars (left) and CFRP bars (right) [48]

According to the FDOT Standard Specifications for Road and Bridge Construction (January 2020), section properties of FRP reinforcing bars shall meet the requirements in Table 5. Improved minimum mechanical properties are currently being considered by an ASTM D30 Committee working group for 20%-30% improved Modulus of Elasticity and Guaranteed Tensile Strength (GTS). For this Chapter, a higher modulus (E_f = 8,500 ksi) and GTS of 83 kips, 102.5 kips, 123 kips for #8, #9, and #10 bars, respectively, are also used reflecting the proposed (2021) improved properties.

Table 5: Sizes and tensile loads of FRP bars

Bar Size Designation	Nominal Bar Diameter (in)	Nominal Cross Sectional Area (in^2)	Measured Cross-Sectional Area (in^2)		Minimum Guaranteed Tensile Load (kips)	
			Minimum	Maximum	GFRP Bars	CFRP Bars
2	0.250	0.049	0.046	0.085	6.1	10.3
3	0.375	0.11	0.104	0.161	13.2	20.9
4	0.500	0.20	0.185	0.263	21.6	33.3
5	0.625	0.31	0.288	0.388	29.1	49.1
6	0.750	0.44	0.415	0.539	40.9	70.7
7	0.875	0.60	0.565	0.713	54.1	-
8	1.000	0.79	0.738	0.913	66.8	-
9	1.128	1.00	0.934	1.137	82.0	-
10	1.270	1.27	1.154	1.385	98.2	-

As per FDOT Standard Plans Index 455-001, the type of concrete for pile should be Class V (Special). According to the concrete classes and strength included in the FDOT Structures Manual Volume 1 [46], the minimum 28-day compressive strength (f'_c) is considered 6 (ksi) for concrete Class V (Special) (Table 6). The yield strength of steel (f_y), minimum ultimate tensile strength of strands, and other properties for section analysis are adopted from FDOT Standard Plans Index 455-000 series. GFRP bars are manufactured from two main parts of fibers and matrix resin The former part provides strength and stiffness, and the matrix of FRP protects and transfers stresses between fibers.

Table 6: FDOT concrete classes and strengths

Class II	3.4
Class II (Bridge Deck)	4.5
Class III	5.0
Class III (Seal)	3.0
Class IV	5.5
Class IV (Drilled Shaft)	4.0
Class V (Special)	6.0
Class V	6.5
Class VI	8.5

Many researchers have analyzed the mechanical and material properties of GFRP rebars in the past years [51-55]. Different types of GFRP bars have been summarized by Farhangdoust et al. [51] as shown in Figure 25.

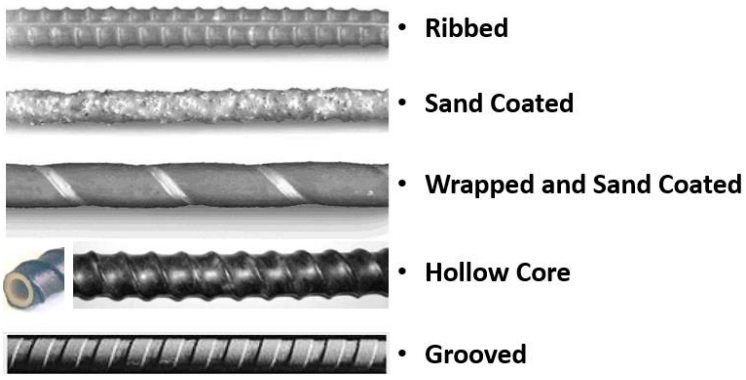

Figure 25: Different types of FRP [51]

E-glass fiber is considered the most common type used in GFRP for composite reinforcement having favorable electrical insulating properties, low susceptibility to moisture, and at the same time, high mechanical properties [56-57]. Recently, the durability benefits of E-CR (Corrosion Resistant) glass fibers has been recognized and mandated for internal concrete reinforcing bars under ASTM D7957-17. S-glass fibers provide for higher strength but are associated with higher costs. Figure 26 shows the stress-strain difference between FRPs and steel.

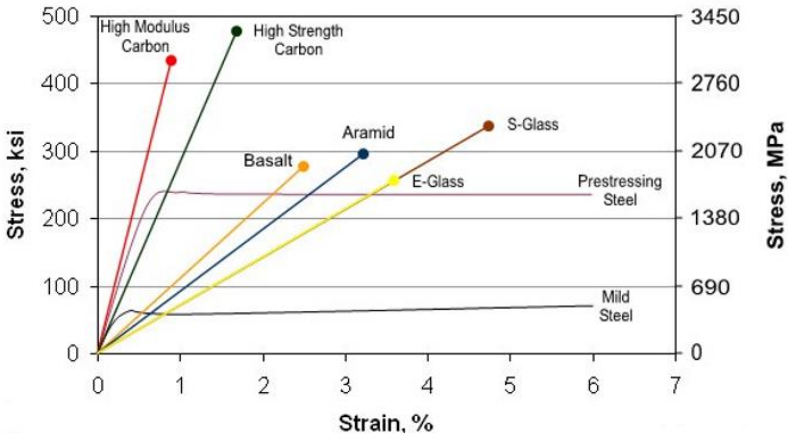

Figure 26: The stress–strain curves of FRPs and steel [51]

As it is shown in this figure, FRP material shows a linear elastic behavior all the way to rupture. Moreover, the GFRP has a lower strain and higher ultimate strength compared to steel. In the following sections, the resistance of the pile splice with GFRP dowels will be first calculated using the current (2020) GFRP properties for different arrangement of bars and sizes. Then, for each case, the pure flexural resistance that is the basis for the design of splice in this Chapter will also be calculated using the proposed (2021) GFRP properties.

3.1.2 Section Analysis of a Pile Splice using 8-GFRP Bars # 10 as Dowels

As it was mentioned earlier, as first trial (consistent with steel dowel design), 8-GFRP bar #10 is considered as dowels in the pile splice section. The cross-sectional area and minimum guaranteed (nominal) tensile load are selected from Table 5 per FDOT requirement to be 1.27 sq.in and 98.2 kips. The guaranteed tensile strength, f_{fu}^{*} , therefore is calculated to be 77.56 ksi. Design tensile strength of FRP, defined as the guaranteed tensile strength multiplied by the environmental reduction factor, $f_{fu} = C_E f_{fu}^{*}$. The C_E is the environmental reduction factor selected here to be 0.7 because pile structure is exposed to earth [58]. Therefore, $f_{fu} = 54.29\ ksi$. The Modulus of Elasticity, E_f , is adopted from ACI 440.1R.15 (Table 7.2.1) to be 6,500 ksi [58]. Accordingly, the design rupture strain (ε_{fu}) is calculated to be 0.0083. A section analysis by hand calculation was carried out to check the flexural resistance (Table 4) in accordance with ACI 440.1R-15 [58]. The analysis was performed to obtain:

A. Axial compression strength,
B. Axial tension strength,

C. Balanced failure point,

D. Pure flexural moment strength.

3.1.2.1 Balanced Failure

At the balanced failure point, concrete crushing and FRP rupture are assumed to occur simultaneously (Figure 27). At the balanced failure mode, the concrete reaches its ultimate in compression and the FRP bars in the farthest layer reaches the design rupture strain at the same time. The distance of the center of each of the three dowel layers to the upper edge of the section is calculated as:

d_1 = 5.5 in (139.7 mm) (2)

d_2 = 9 in (228.6 mm) (3)

d_3 = 12.5 in (317.5 mm) (4)

The position of the neutral axis C is calculated using the equation below 3.3 (84 mm).

$$\frac{0.003}{C} = \frac{0.0083}{d_3 - C} \quad (5)$$

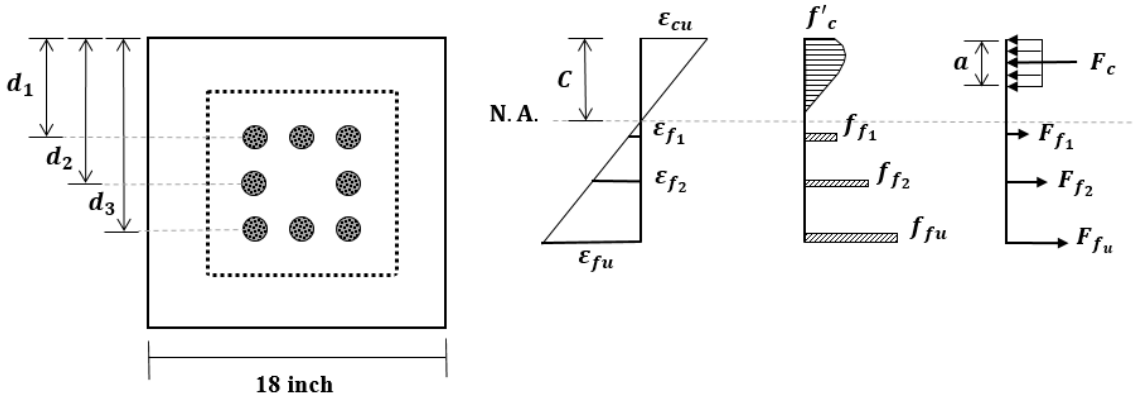

Figure 27: Strain and tress distribution at the balanced failure mode

Accordingly, based on the strain and stress conditions for balanced failure mode displayed in Figure 27, the compressive force of concrete and tension force of GRFP dowels were calculated by:

$$F_c = \alpha * f'_c * \beta * C * b = 0.85 * 6 * 0.75 * 3.3 * 18 = 227.42 \text{ kips} \quad (6)$$

$$f_{f_1} = [\varepsilon_{f_1}] * E_f = \left[\left(\frac{5.5-3.3}{3.3}\right) * 0.003\right] * 6500 = 12.96 \text{ ksi} < f_{fu} \quad (7)$$

$$F_{f_1} = f_{f_1} * A_{G1} = 12.96 * 3.81 = 49.25 \text{ kips} \quad \text{Tension} \quad (8)$$

$$f_{f_2} = [\varepsilon_{f_2}] * E_f = \left[\left(\frac{9-3.3}{3.3}\right) * 0.003\right] * 6500 = 33.62 \text{ ksi} < f_{fu} \quad (9)$$

$$F_{f_2} = f_{f_2} * A_{G2} = 33.62 * 2.54 = 85.16 \text{ kips} \quad \text{Tension} \quad (10)$$

$$F_{f_3} = F_{f_u} = f_{fu} * A_{G1} = 54.11 * 3.81 = 206.22 \text{ kips} \quad \text{Tension} \quad (11)$$

As a result, the force and moment of the balanced point due to the strain compatibility and force equilibrium are calculated as follows:

$$\begin{cases} P_n = 227.42 - (206.22 + 85.16 + 49.25) = -113.21 \text{ kips} \\ M_n = -172.405 + 1765.13 + 721.77 = 2314.49 \text{ k.in} = 192.874 \text{ k.ft} \end{cases} \quad (12)$$

3.1.2.2 Axial Compression Strength

The pure compression point is the second design parameter that needs to be calculated for analyzing the M-N interaction of FRP- based pile splice. According to the Figure 28, the strain of GFRP dowels ε_f cannot exceed the maximum compressive strain in the concrete (0.003). Therefore, the total compression force will be: $F_{Totol} = (N * \varepsilon_f * E_{fc} * A_G) + (\alpha * f'_c * [(a * b) - N * A_G])$, but is conservatively taken as the resistance of the gross section of concrete area: $\alpha * f'_c * a * b = 1652.4$ kips.

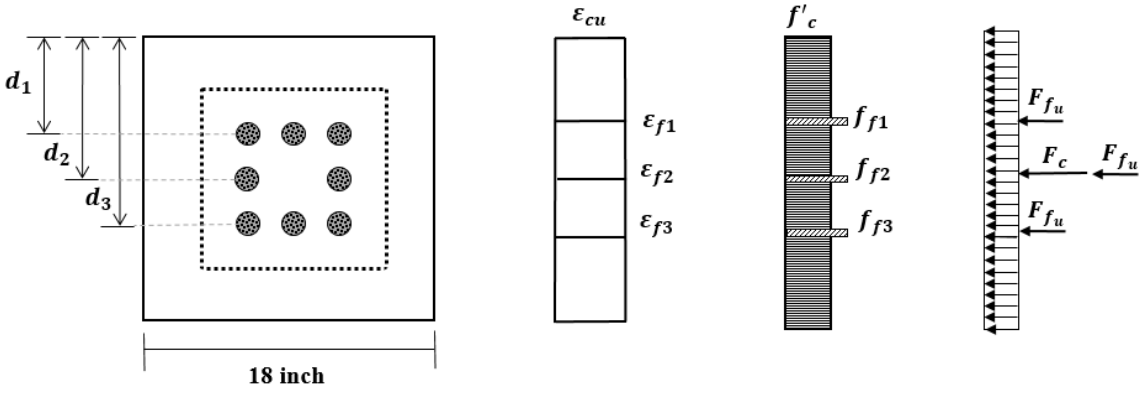

Figure 28: Strain and stress distribution at the pure compression mode (theoretical)

3.1.2.3 Axial Tension Strength

According to Figure 29, concrete does not contribute to tensile strength, therefore, axial tensile strength will include the tensile strength of all eight dowels at design tensile strength, f_{fu}. Therefore, the total compression force will be:

$$\mathrm{F_{Totol}} = \left(\mathrm{N} * f_{fu} * \mathrm{A_G}\right) = (8 * 54.29 * 1.27) \ = -549.92 \text{ kips} \quad (13)$$

Axial tensile strength is greater than required nominal strength of 291 kips.

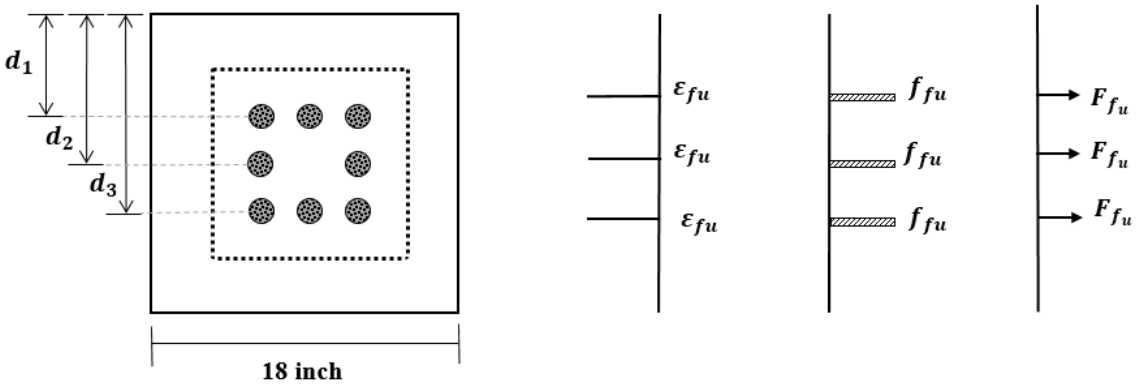

Figure 29: Strain and stress distribution at the pure tension mode

3.1.2.4 Pure Flexural Moment Strength

The pure flexural moment strength (no axial force) is governed by concrete crushing. At this mode of failure, the strain compatibility and force equilibrium is assumed for the pile splice section shown in Figure 30.

$$\mathrm{F_c} = \alpha * \ \mathrm{f'_c} * \beta * \mathrm{b} * \mathrm{C} = 0.85 * 6 * 0.75 * 18 * \mathrm{C} \quad (14a)$$

$$F_{f_1} = [\varepsilon_{f_1}] * E_f * A_{G1} = \left[\left(\frac{5.5-C}{C}\right) * 0.003\right] * 6500 * 3.8 \quad (15a)$$

$$F_{f_2} = [\varepsilon_{f_2}] * E_f * A_{G2} = \left[\left(\frac{9-C}{C}\right) * 0.003\right] * 6500 * 2.53 \quad (16a)$$

$$F_{f_3} = [\varepsilon_{f_3}] * E_f * A_{G3} = \left[\left(\frac{12.5-C}{C}\right) * 0.003\right] * 6500 * 3.8 \quad (17a)$$

As it was discussed earlier, the pure flexural moment strength is also calculated for the proposed (2021) improved GFRP rebar properties:

$$F_c = \alpha * f'_c * \beta * b * C = 0.85 * 6 * 0.75 * 18 * C \quad (14b)$$

$$F_{f_1} = [\varepsilon_{f_1}] * E_f * A_{G1} = \left[\left(\frac{5.5-C}{C}\right) * 0.003\right] * 8500 * 3.8 \quad (15b)$$

$$F_{f_2} = [\varepsilon_{f_2}] * E_f * A_{G2} = \left[\left(\frac{9-C}{C}\right) * 0.003\right] * 8500 * 2.53 \quad (16b)$$

$$F_{f_3} = [\varepsilon_{f_3}] * E_f * A_{G3} = \left[\left(\frac{12.5-C}{C}\right) * 0.003\right] * 8500 * 3.8 \quad (17b)$$

After simplification, the following set of equations for forces in concrete and dowel layers are calculated based on the depth to the neutral axis C:

Current (2020) GFRP properties

$$\begin{cases} F_c = 68.85 * C \\ F_{f_1} = 74.1\left(\frac{5.5-C}{C}\right) \\ F_{f_2} = 49.4\left(\frac{9-C}{C}\right) \\ F_{f_3} = 74.1\left(\frac{12.5-C}{C}\right) \end{cases}$$

(18a)

Proposed (2021) GFRP properties

$$\begin{cases} F_c = 68.85 * C \\ F_{f_1} = 96.85\left(\frac{5.5-C}{C}\right) \\ F_{f_2} = 64.57\left(\frac{9-C}{C}\right) \\ F_{f_3} = 96.85\left(\frac{12.5-C}{C}\right) \end{cases}$$

(18b)

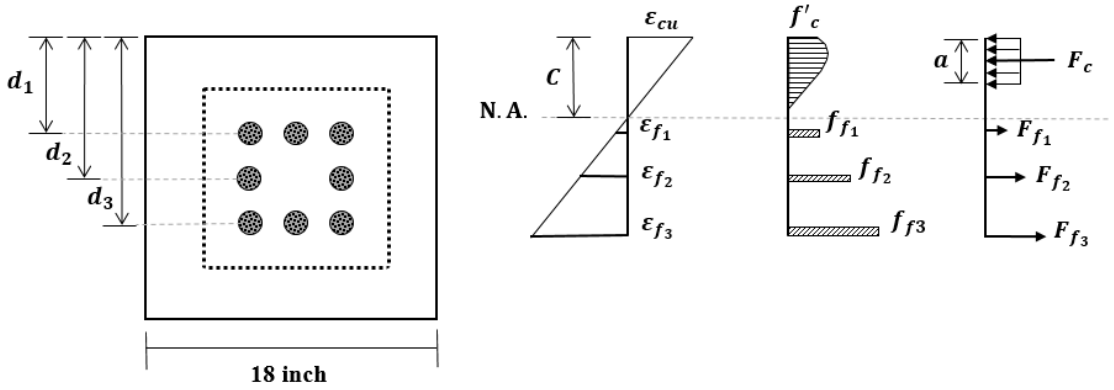

Figure 30: Strain and stress distribution at the concrete crushing failure mode

At the pure flexure point, $F_c = \sum F_{fi}$. As a result, the value of C for current and proposed ones, respectively, were found 3.84 in (97.5 mm) and 4.23 in (107.4 mm) as the depth to the neutral axis. Because the neutral axis is above all the FRP bars, all the dowel levels are in tension. Accordingly, the moment resistance of pile splice section and stress of three level GFRP dowels will be as by calculation 19a. For the proposed improved GFRP rebar properties, the moment resistance is also shown in calculation 19b:

Current (2020) GFRP properties (19a)

$$\begin{cases} f_{f_1} = -8.4 \text{ ksi} \\ f_{f_2} = -26.1 \text{ ksi} \\ f_{f_3} = -43.9 \text{ ksi} \\ M_{n\#10} = \sum F_i * Y_i = 2472.9 \text{ k} - \text{in} = 206.1 \text{ k} - \text{ft} \end{cases}$$

Proposed (2021) GFRP properties (19b)

$$\begin{cases} f_{f_1} = -7.6 \text{ksi} \\ f_{f_2} = -28.7 \text{ ksi} \\ f_{f_3} = -49.8 \text{ ksi} \\ M_{n\#10} = \sum F_i * Y_i = 2720.2 \text{ k} - \text{in} = 226.7 \text{ k} - \text{ft} \end{cases}$$

According to the above, the nominal moment resistance, M_n , was calculated to be 206.1 kip.ft and 226.7 kip.ft for 8-GFRP #10 dowels based on the current and proposed GFRP properties, respectively. This result shows this pile splice with 8-GFRP #10 dowels is able to develop 84% and 92 % required moment resistance (Table 4), respectively, based

on the current and proposed GFRP properties. The stress in the farthest bars is less than the design strength of the GFRP, therefore, the section fails with concrete crushing that is a desirable mode. The pure flexural strength of 18x18 in pile splice using 9 #6 CFRP dowels is also calculated to be 207.7 kip.ft that closely compares to splice using 8 #10 GFRP dowels. Comparison using the design moment resistance will be carried out later in this Chapter.

3.1.3 Section Analysis of a Pile Splice Using 8-GFRP Bars #8 as Dowel

Because the maximum stress in the GFRP dowel bar is less than the maximum strength specified for GFRP, it is only prudent to try a smaller size of GFRP bar. Therefore, a set of 8-GFRP #8 bars in three layers, with the same arrangement as the #10s was also examined for the pile splice. For the selected product, the cross-sectional area and minimum guaranteed (nominal) tensile load are selected from Table 5 per FDOT requirement to be 0.785 in^2 and 66.8 kips. For the GFRP dowels based on the current (2020) properties, the guaranteed tensile strength, f_{fu}^* , therefore is calculated to be 85.09 ksi. Design tensile strength of FRP, defined as the guaranteed tensile strength multiplied by the environmental reduction factor, $f_{fu} = C_E f_{fu}^*$.

The C_E is the environmental reduction factor selected here to be 0.7 because pile structure is exposed to earth [49 and 58]. Therefore, $f_{fu} = 59.56\ ksi$. The Modulus of Elasticity, E_f , is adopted from FDOT Spec 932-/ASTM D7957-17 to be 6500 ksi. A section analysis for the pure flexural bending strength was carried out in accordance with AASHTO-GFRP2 [49] to check the moment resistance of pile splice using #8 GFRP

bars. The failure is assumed to occur with crushing of concrete. The strain compatibility for the pile splice section is as shown in Figure 30.

$$F_c = \alpha * f'_c * \beta * b * C = 0.85 * 6 * 0.75 * 18 * C \quad (20a)$$

$$F_{f_1} = [\varepsilon_{f_1}] * E_f * A_{G1} = \left[\left(\frac{5.5-C}{C}\right) * 0.003\right] * 6500 * 2.35 \quad (21a)$$

$$F_{f_2} = [\varepsilon_{f_2}] * E_f * A_{G2} = \left[\left(\frac{9-C}{C}\right) * 0.003\right] * 6500 * 1.57 \quad (22a)$$

$$F_{f_3} = [\varepsilon_{f_3}] * E_f * A_{G3} = \left[\left(\frac{12.5-C}{C}\right) * 0.003\right] * 6500 * 2.35 \quad (23a)$$

Similar calculations for the proposed (2021) improved GFRP rebar properties show:

$$F_c = \alpha * f'_c * \beta * b * C = 0.85 * 6 * 0.75 * 18 * C \quad (20b)$$

$$F_{f_1} = [\varepsilon_{f_1}] * E_f * A_{G1} = \left[\left(\frac{5.5-C}{C}\right) * 0.003\right] * 8500 * 2.35 \quad (21b)$$

$$F_{f_2} = [\varepsilon_{f_2}] * E_f * A_{G2} = \left[\left(\frac{9-C}{C}\right) * 0.003\right] * 8500 * 1.57 \quad (22b)$$

$$F_{f_3} = [\varepsilon_{f_3}] * E_f * A_{G3} = \left[\left(\frac{12.5-C}{C}\right) * 0.003\right] * 8500 * 2.35 \quad (23b)$$

After simplification, section forces of the pile splice is calculated based on the depth to the neutral axis C:

Current (2020) GFRP properties (24a)

$$\begin{cases} F_c = 68.85 * C \\ F_{f_1} = 45.92\left(\frac{5.5-C}{C}\right) \\ F_{f_2} = 30.61\left(\frac{9-C}{C}\right) \\ F_{f_3} = 45.92\left(\frac{12.5-C}{C}\right) \end{cases}$$

Proposed (2021) GFRP properties (24b)

$$\begin{cases} F_c = 68.85 * C \\ F_{f_1} = 60.05\left(\frac{5.5-C}{C}\right) \\ F_{f_2} = 40.03\left(\frac{9-C}{C}\right) \\ F_{f_3} = 60.05\left(\frac{12.5-C}{C}\right) \end{cases}$$

To investigate the pure flexural point, $F_c = \sum F_{fi}$ should be considered as the force equilibrium equition. As a result, the depth to the neutral axis C for current and proposed properties, respectively, were found to be 3.20 in (81.3 mm) and 3.55 in (90.2 mm). Accordingly, the moment of pile splice section and stress of three level GFRP dowels will be:

Current (2020) GFRP properties (25a)

$$\begin{cases} f_{f_1} = -13.92 \text{ ksi} \\ f_{f_2} = -35.18 \text{ ksi} \\ f_{f_3} = -56.45 \text{ ksi} \\ M_{n\#8} = \sum F_i * Y_i = 2073.3 \text{ k} - \text{in} = 172.7 \text{ k} - \text{ft} \end{cases}$$

Proposed (2021) GFRP properties (25b)

$$\begin{cases} f_{f_1} = -13.92 \text{ ksi} \\ f_{f_2} = -39 \text{ ksi} \\ f_{f_3} = -64.09 \text{ ksi} \\ M_{n\#8} = \sum F_i * Y_i = 2291.3 \text{ k} - \text{in} = 190.9 \text{ k} - \text{ft} \end{cases}$$

The nominal moment resistance for the pile section using 8-GFRP #8 bars in three layers, M_n, was calculated to be 172.7 kip.ft and 190.9 kip.ft based on the current and proposed GFRP properties, respectively. This result shows the pile splice with 8-GFRP #8 dowels is able to develop 70% and 78% of the required moment resistance (Table 4), respectively, based on the current and proposed GFRP properties.

The stress in the farthest bars is less than the design strength of the GFRP (but closer than that of 8-#10 bars), therefore, the section fails with concrete crushing. Comparison using the design moment resistance will be carried out later in this Chapter.

3.1.4 Section Analysis of a Pile Splice using 9-GFRP Bars #10 as Dowels

As the next trial, 9-GFRP bars #10 is selected as a replacement for CFRP dowels in FDOT Standard Plans Index Series 455-118 [48]. For the GFRP bars, the cross-sectional area and minimum guaranteed (nominal) tensile load are selected from Table 5 per FDOT requirement to be 1.27 in2 and 98.2 kips. The design tensile strength of FRP, f_{fu} is 54.29 ksi. The Modulus of Elasticity, E_f , is also adopted from FDOT Spec 932-3/ASTM D7957-17 to be 6500 ksi. As the pure flexural moment resistance (no axial force) is governed by concrete crushing, the failure is assumed to occur with crushing of concrete. At this mode of failure, the strain compatibility and force equilibrium is assumed for the pile splice section shown in Figure 31.

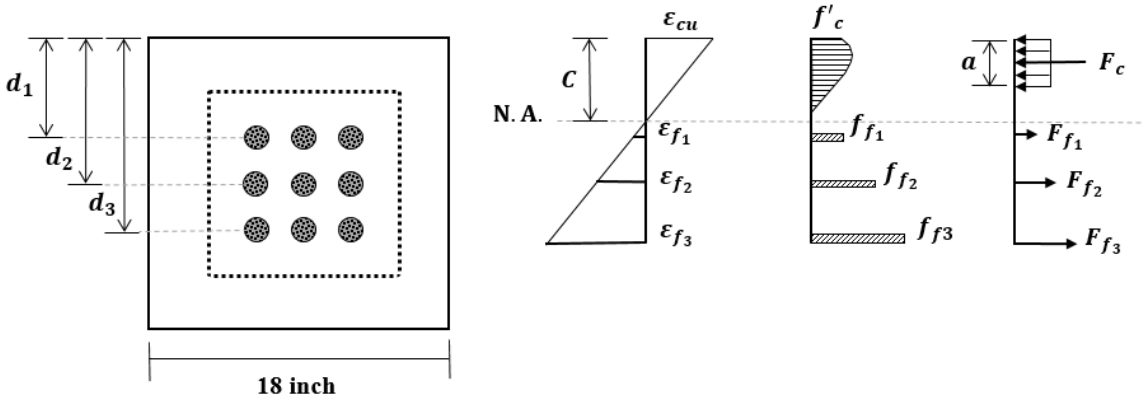

Figure 31: Strain and stress distribution at the concrete crushing failure mode

A section analysis for the pure flexural bending strength was carried out in accordance with AASHTO-GFRP2 [49] to check the moment strength resistance of pile splice using 9-GFRP dowels #10:

$$F_c = \alpha * f'_c * \beta * b * C = 0.85 * 6 * 0.75 * 18 * C \quad (26a)$$

$$F_{f_1} = [\varepsilon_{f_1}] * E_f * A_{G1} = \left[\left(\frac{5.5-C}{C}\right) * 0.003\right] * 6500 * 3.8 \quad (27a)$$

$$F_{f_2} = [\varepsilon_{f_2}] * E_f * A_{G2} = \left[\left(\frac{9-C}{C}\right) * 0.003\right] * 6500 * 3.8 \quad (28a)$$

$$F_{f_3} = [\varepsilon_{f_3}] * E_f * A_{G3} = \left[\left(\frac{12.5-C}{C}\right) * 0.003\right] * 6500 * 3.8 \quad (29a)$$

Similar calculations for the proposed improved GFRP rebar properties show:

$$F_c = \alpha * f'_c * \beta * b * C = 0.85 * 6 * 0.75 * 18 * C \quad (26b)$$

$$F_{f_1} = [\varepsilon_{f_1}] * E_f * A_{G1} = \left[\left(\frac{5.5-C}{C}\right) * 0.003\right] * 8500 * 3.8 \quad (27b)$$

$$F_{f_2} = [\varepsilon_{f_2}] * E_f * A_{G2} = \left[\left(\frac{9-C}{C}\right) * 0.003\right] * 8500 * 3.8 \quad (28b)$$

$$F_{f_3} = [\varepsilon_{f_3}] * E_f * A_{G3} = \left[\left(\frac{12.5-C}{C}\right) * 0.003\right] * 8500 * 3.8 \quad (29b)$$

After simplification, the following set of equations for forces in concrete and dowel layers are calculated based on the depth to the neutral axis C, for both material options:

Current (2020) GFRP properties (30a)

$$\begin{cases} F_c = 68.85 * C \\ F_{f_1} = 74.1\left(\frac{5.5-C}{C}\right) \\ F_{f_2} = 74.1\left(\frac{9-C}{C}\right) \\ F_{f_3} = 74.1\left(\frac{12.5-C}{C}\right) \end{cases}$$

Proposed (2021) GFRP properties (30b)

$$\begin{cases} F_c = 68.85 * C \\ F_{f_1} = 96.86\left(\frac{5.5-C}{C}\right) \\ F_{f_2} = 96.86\left(\frac{9-C}{C}\right) \\ F_{f_3} = 96.85\left(\frac{12.5-C}{C}\right) \end{cases}$$

At the pure flexure point, $F_c = \sum F_{fi}$. As a result, the value of C for the current and proposed ones, respectively, were calculated to be 4.01 in (101.8 mm) and 4.40 in (111.76 mm) as the depth to the neutral axis. Because the neutral axis is above all the FRP bars, all the dowel levels are in tension. Accordingly, the moment of pile splice section and stress of three level GFRP dowels will be:

Current (2020) GFRP properties (31a)

$$\begin{cases} f_{f_1} = -7.23 \text{ ksi} \\ f_{f_2} = -24.24 \text{ ksi} \\ f_{f_3} = -41.25 \text{ ksi} \\ M_{n\#10} = \sum F_i * Y_i = 2522.8 \text{ k.in} = 210.2 \text{ k.ft} \end{cases}$$

Proposed (2021) GFRP properties (31b)

$$\begin{cases} f_{f_1} = -6.34 \text{ ksi} \\ f_{f_2} = -26.61 \text{ ksi} \\ f_{f_3} = -46.87 \text{ ksi} \\ M_{n\#10} = \sum F_i * Y_i = 2767 \text{ k.in} = 230.6 \text{ k.ft} \end{cases}$$

According to the above, the nominal moment resistance, M_n, for the pile section using 9-GFRP #10 bars in three layers was calculated to be 210.2 kip.ft and 230.6 kip.ft based on the current and proposed GFRP properties, respectively. This result shows the pile splice with 9-GFRP #10 dowels is able to develop 86% and 94% of the required moment resistance (Table 4), respectively, based on the current and proposed GFRP properties. A comparison between splice with 8 #10 and 9 #10 bars indicates that addition of one bar

increases the nominal flexural resistance only by 2 percent. Comparison using the design moment resistance will be carried out later in this Chapter.

3.1.5 Section Analysis of a Pile Splice Using 9-GFRP Bars #8 as Dowel

Because the maximum stress in the GFRP dowel bar is less than the maximum strength specified for GFRP, it is only prudent to try a smaller size of GFRP bar. Therefore, a set of 9-GFRP #8 bars in three layers was also examined for the pile splice.

For this case study, the cross-sectional area and minimum guaranteed (nominal) tensile load are selected from Table 5 per FDOT requirement to be 0.785 in^2 and 66.8 kips. The design tensile strength of FRP, f_{fu} is 59.56 ksi. The Modulus of Elasticity, E_f , is also adopted from AASHTO-GFRP2 [49] to be 6500 ksi. A section analysis for the pure flexural bending strength was carried out in accordance with AASHTO-GFRP2 [49] to check the moment strength resistance of pile splice using 9-GFRP dowels of #8. The failure is assumed to occur with crushing of concrete. The strain compatibility for the pile splice section is as shown in Figure 31.

$$F_c = \alpha * f'_c * \beta * b * C = 0.85 * 6 * 0.75 * 18 * C \quad (32a)$$

$$F_{f_1} = [\varepsilon_{f_1}] * E_f * A_{G1} = \left[\left(\frac{5.5-C}{C}\right) * 0.003\right] * 6500 * 2.35 \quad (33a)$$

$$F_{f_2} = [\varepsilon_{f_2}] * E_f * A_{G2} = \left[\left(\frac{9-C}{C}\right) * 0.003\right] * 6500 * 2.35 \quad (34a)$$

$$F_{f_3} = [\varepsilon_{f_3}] * E_f * A_{G3} = \left[\left(\frac{12.5-C}{C}\right) * 0.003\right] * 6500 * 2.35 \quad (35a)$$

Similar calculations for the proposed improved GFRP rebar properties show:

$$F_c = \alpha * f'_c * \beta * b * C = 0.85 * 6 * 0.75 * 18 * C \quad (32b)$$

$$F_{f_1} = [\varepsilon_{f_1}] * E_f * A_{G1} = \left[\left(\frac{5.5-C}{C}\right) * 0.003\right] * 8500 * 2.35 \quad (33b)$$

$$F_{f_2} = [\varepsilon_{f_2}] * E_f * A_{G2} = \left[\left(\frac{9-C}{C}\right) * 0.003\right] * 8500 * 2.35 \quad (34b)$$

$$F_{f_3} = [\varepsilon_{f_3}] * E_f * A_{G3} = \left[\left(\frac{12.5-C}{C}\right) * 0.003\right] * 8500 * 2.35 \quad (35b)$$

After simplification, section forces of the pile splice is calculated based on the depth to the neutral axis C:

Current (2020) GFRP properties (36a)

$$\begin{cases} F_c = 68.85 * C \\ F_{f_1} = 45.92\left(\frac{5.5-C}{C}\right) \\ F_{f_2} = 45.92\left(\frac{9-C}{C}\right) \\ F_{f_3} = 45.92\left(\frac{12.5-C}{C}\right) \end{cases}$$

Proposed (2021) GFRP properties (36b)

$$\begin{cases} F_c = 68.85 * C \\ F_{f_1} = 45.92\left(\frac{5.5-C}{C}\right) \\ F_{f_2} = 45.92\left(\frac{9-C}{C}\right) \\ F_{f_3} = 45.92\left(\frac{12.5-C}{C}\right) \end{cases}$$

To investigate the pure flexural point, $F_c = \sum F_{fi}$ should be considered as the force equilibrium equation. As a result, the depth to the neutral axis C for the current and proposed ones, respectively, were calculated to be 3.36 in (85.34 mm) and 3.71 in (94.23 mm) which shows all the dowel levels are in tension mode as we expected. Accordingly, the moment of pile splice section and stress of three level GFRP dowels will be:

Current (2020) GFRP properties (37a) Proposed (2021) GFRP properties (37b)

$$\begin{cases} f_{f_1} = -12.42 \text{ ksi} \\ f_{f_2} = -32.74 \text{ ksi} \\ f_{f_3} = -53.05 \text{ ksi} \\ M_{n\#8} = \sum F_i * Y_i = 2125.23 \text{ k.in} = 177.1 \text{ k.ft} \end{cases} \quad \begin{cases} f_{f_1} = -12.22 \text{ ksi} \\ f_{f_2} = -36.23 \text{ ksi} \\ f_{f_3} = -60.24 \text{ ksi} \\ M_{n\#8} = \sum F_i * Y_i = 2342.6 \text{ k.in} = 195.2 \text{ k.ft} \end{cases}$$

The nominal moment resistance, M_n, for the pile section using 9-GFRP #8 bars in three layerswas calculated to be 177.1 kip.ft and 195.2 kip.ft based on the current and proposed GFRP properties, respectively. This result shows the pile splice with 9-GFRP #8 dowels is able to develop 72% and 80% of the required moment resistance (Table 4), respectively, based on the current and proposed GFRP properties. A comparison between splice with 8-#8 and 9-#8 bars indicates that addition of one bar increases the nominal flexural resistance only by 2 percent. Comparison using the design moment resistance will be carried out later in this Chapter.

3.1.6 Resistance Factor

According to ACI 440.1R-15 [58] and AASHO-GFRP2 [49], the design flexural strength of an FRP-reinforced section dependents on whether it is controlled by concrete crushing or FRP rupture. This can be determined by comparing the FRP reinforcement ratio, ρ_f, to the balanced reinforcement ratio ρ_{fb}. Accordingly, there are three possible failures for pile splice:

- Balanced failure condition (concrete crushing and FRP rupture occurs at the same time)
- Failure governed by concrete crushing (concrete crushing occurs before FRP rupture)
- Failure governed by FRP rupture (FRP rupture occurs before concrete crushing)

According to ACI 440.1R-15 [58], for a single-layer GFRP tension reinforcement, balanced reinforcement ratio can be calculated using the equations below:

$$\rho_{fb} = \left(\alpha_1 \beta_1 \frac{f'_c}{f_{fu}}\right)\left(\frac{E_f \varepsilon_{cu}}{E_f \varepsilon_{cu} + f_{fu}}\right) \quad (38)$$

$$\rho_f = \frac{A_f}{bd} \quad (39)$$

Where A_f refers to the area of three bars in the single layer reinforcement farthest from compression zone. It is structurally advantageous for a concrete section reinforced with FRP that concrete crushes first, i.e., FRP reinforcement ratios is larger than the balanced ratio. In AASHTO-GFRP2 [49], the balanced reinforcement is expressed in terms of strain and defined as Compression-Controlled or Tensioned-Controlled with a Transition zone due expected variations in material properties. If the reinforcement ratios are equal to balanced reinforcement ratio, the failure is balanced. If $\rho_f \geq \rho_{fb}$, then the failure will be initiated by crushing of concrete, and the nominal moment strength will be calculated for the case of single-layer tension reinforcement by:

$$M_n = A_f f_f \left(1 - 0.59 \frac{\rho_f f_f}{f'_c}\right) d^2 \quad (40)$$

However, if $\rho_f < \rho_{fb}$, then the flexural failure will be governed by rupture of FRP bar, and the nominal moment strength for the case of single-layer reinforcement will be calculated by:

$$M_n = A_f f_{fu}\left(d - \frac{\beta_1 C_b}{2}\right) \quad (41)$$

As it is shown in Figure 32, according to the Sec. 2.5.5.2 of the AASHTO-GFRP2 [49], for the case of single-layer GFRP tension reinforcement, the resistance factor can be calculated by (42). The tensioned-controlled resistance factor is slightly less conservative than the ACI 440.1R-15 [58] strength reduction factor, based on more recent comparative reliability analysis:

$$\phi = \text{Resistance Factor} \begin{cases} 0.55 & \text{for } \varepsilon_{ft} = \varepsilon_{fd}\ (Tension - Controlled) \\ 0.75 & \text{for } \varepsilon_{ft} \le 0.80\varepsilon_{fd}\ (Compression - Controlled) \\ 1.55 - \frac{\varepsilon_{ft}}{\varepsilon_{fd}} & \text{For } 0.80\varepsilon_{fd} < \varepsilon_{ft} < \varepsilon_{fd}\ (Transition) \end{cases} \quad (42)$$

Where the $\varepsilon_{fd} = C_E \varepsilon_{fu}$ is design rupture strain and ε_{fu} is guaranteed rupture strain from AASHTO. It should be noted that different terminology has been used by ACI 440.1R-15 [58] and AASHTO-GFRP2 [49]to describe the design rupture strain and guaranteed rupture strain To clarify, the ε_{fd} and ε_{fu} used by AASHTO [49] correspond to ε_{fu} and ε_{fu}^{*} used by ACI 440.1R-15 [58], respectively.

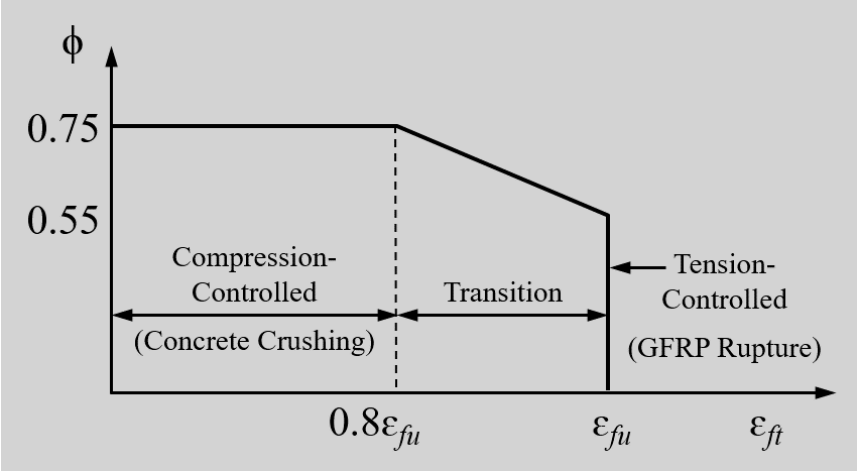

Figure 32: Strength Limit State resistance factor [49]

Table 7 shows the strength resistance factor, ϕ, corresponding to #8 and #10 bars for two different number of bars at pure flexural moment based on conditions set by Eq. 42.

Table 7: The resistance factor for current (2020) GFRP properties

Design	Number of Bars	ε_t	ε_{fd}	$\varepsilon_t/\varepsilon_{fd}$	ϕ
With GFRP Dowel #10	**8**	**0.00675**	**0.00835**	**0.80**	**0.75**
	9	**0.00635**	**0.00835**	**0.76**	**0.75**
With GFRP Dowel #8	**8**	**0.00868**	**0.00916**	**0.95**	**0.60**
	9	**0.00816**	**0.00916**	**0.89**	**0.66**

When using the current (2020) GFRP properties, the ratio of $\varepsilon_t/\varepsilon_{fd}$, for #10 bars is 0.80 for 8 number of bars and 0.76 for 9 number of bars. Therefore, for both cases, the strength resistance factor, ϕ , for pure bending of a pile splice for Sections using #10 bars can be taken as 0.75. Similarly, for #8 bars, the ratio of $\varepsilon_t/\varepsilon_{fd}$ for 8 and 9 number of

bars, respectively, are 0.95 and 0.89. Therefore, the strength resistance factor, ϕ , for pure bending for a pile splice using #8 bars is calculated as 0.60 and 0.66, respectively for 8 and 9 number of bars..

For the proposed (2021) GFRP properties, the strength resistance factor, ϕ, corresponding to #8 and #10 bars for 8 and 9 number of bars at pure flexural moment is calculated and shown in Table 8.

Table 8: The resistance factor for proposed (2021) GFRP properties

Design	Number of Bars	ε_t	ε_{fd}	$\varepsilon_t/\varepsilon_{fd}$	ϕ
With GFRP Dowel #10	**8**	**0.00586**	**0.008**	**0.73**	**0.75**
	9	**0.00551**	**0.008**	**0.69**	**0.75**
With GFRP Dowel #8	**8**	**0.00754**	**0.00871**	**0.86**	**0.68**
	9	**0.00709**	**0.00871**	**0.81**	**0.74**

3.1.6.1 Design Moment Strength for the Case of 8-GFRP Dowels

For a pile splice using three layers of 8-GFRP bars # 10, based on the calculated resistance factor, the failure will be governed by concrete crushing, and the resistance factor ϕ will be 0.75. Hence, the factored flexural moment will be:

$$\mathrm{M_{u\#10}} = \phi \mathrm{M_{n\#10}} = \begin{cases} Current\ (2020): 0.75 * 206.1 \ = 154.57\ \mathrm{K-ft} \\ Proposed\ (2021): 0.75 * 226.7 \ = 170.02\ \mathrm{K-ft} \end{cases} \quad (43)$$

In the same manner, for a pile splice using three layers of 8-GFRP # 8 bars, the design flexural moment will be:

$$M_{u\#8} = \phi M_{n\#8} = \begin{cases} Current\ (2020): 0.60 * 172.7 = 103.62\ K-ft \\ Proposed\ (2021): 0.68 * 190.9 = 129.81\ K-ft \end{cases} \quad (44)$$

3.1.6.2 Design Moment Strength for the Case of 9-GFRP Dowels

For a pile splice using three layers of GFRP # 10 bars, based on the modified resistance factor, the failure will be governed by concrete crushing, and the resistance factor ϕ will be 0.75. Therefore, the factored flexural resistance will be:

$$M_{u\#10} = \phi M_{n\#10} = \begin{cases} Current\ (2020): 0.75 * 210.2 = 157.65\ K-ft \\ Proposed\ (2021): 0.75 * 230.6 = 172.95\ K-ft \end{cases} \quad (45)$$

In the same manner, for a pile splice using three layers of GFRP # 8 bars, the design flexural moment will be:

$$M_{u\#8} = \phi M_{n\#8} = \begin{cases} Current\ (2020): 0.66 * 177.1 = 116.89\ K-ft \\ Proposed\ (2021): 0.74 * 195.2 = 144.45\ K-ft \end{cases} \quad (46)$$

As it shown in Tables 9 and 10, comparing two cases of #8 and #10 bars, the use of both 8 and 9-GFRP #10 bars can provide a better design for pile splice because it provides for significantly higher resistance and more importantly, the design with #10 bars are more consistent with conventional design used by FDOT (Figure 24). It is realized that the splice design moment strength provided by GFRP #10 bars is lower than that required by

Standard Specification for Road and Bridge Construction [47], however, it is believed that the use of larger diameter bars as well as the use of larger number of dowels on each side of the section are not practical and will create spacing and installation issues.

Table 9: Comparison between bending moment strength and required moment strength for GFRP dowels of different sizes (current 2020 specifications)

Design	Nominal Moment Strength (kip.ft)	Design Moment Strength (kip.ft)	FDOT Required Moment Resistance (kip.ft)	Ratio of Nominal Moment Strength to Required (Nominal)	Ratio of Design Moment Strength to Required (Design)
With 8-GFRP Dowel #10	206.1	154.57	**245**	**84%**	**63%**
With 8-GFRP Dowel #8	172.7	103.62	**245**	**70%**	**42%**
With 9-GFRP Dowel #10	210.2	157.65	**245**	**86%**	**64%**
With 9-GFRP Dowel #8	177.1	116.89	**245**	**72%**	**48%**

Table 10: Comparison between bending moment strength and required moment strength for GFRP dowels of different sizes (proposed 2021 specifications)

Design	Nominal Moment Strength (kip.ft)	Design Moment Strength (kip.ft)	FDOT Required Moment Resistance (kip.ft)	Ratio of Nominal Moment Strength to Required (Nominal)	Ratio of Design Moment Strength to Required (Design)
With 8-GFRP Dowel #10	226.7	170.02	**245**	**92%**	**69%**
With 8-GFRP Dowel #8	190.9	129.81	**245**	**78%**	**53%**
With 9-GFRP Dowel #10	230.6	172.95	**245**	**94%**	**71%**
With 9-GFRP Dowel #8	195.2	144.45	**245**	**80%**	**59%**

For the current (2020) GFRP properties- The results show that 8-GFRP #10 bars in three layers can develop 84% and 63% of the required moment resistance (Table 4) when using the nominal moment resistance and design moment resistance, respectively. Moreover, these results show a pile splice with 9-GFRP #10 bars in three layers can develop 86% and 64% of the required moment resistance (Table 4) when using the nominal moment resistance and design moment resistance, respectively.

For the proposed (2021) GFRP properties- The results show that 8-GFRP #10 bars in three layers can develop 92% and 69% of the required moment resistance (Table 4) when using the nominal moment resistance and design moment resistance, respectively. Moreover, these results show a pile splice with 9-GFRP #10 bars in three layers can develop 94% and 71% of the required moment resistance (Table 4) when using the nominal moment resistance and design moment resistance, respectively.

It should also be noted that the capacities calculated using the available design codes have proven to result in extremely conservative estimation. This is verified later in this dissertation with the section analysis using Response 2000 and experimental program. From this point on, the splice design configuration using 8-#10 bars will be used for detailing and other considerations. This configuration provides the consistency of design with steel counterpart as well as near maximum strength (only up to 2 percent lower than 9-#10).

3.2 Detailing for Pre-Planned Pile Splice

Similar to the design of existing pile splice details reflected in the FDOT Standard Plan Index 455-102 [48], the detailing of the pile splice using GFRP dowel bars will require calculation of two lengths; one is the development length of strand used inside the pile segments, and the other is lap splice length for GFRP bar dowel. The strand development length needs to be defined since for developing the full resistance of the pile beyond the splice section in the upper segment, the GRFP dowel will need to extend and overlap along that length with the strand. The lap splice length for dowel needs to be determined since for the splice to develop its full resistance, the dowel shall be inserted in the lower pile segment with that length to splice with the auxiliary bar already embedded in the lower pile segment. Lap splice length in turn is calculated based on the development length of GFRP bar in concrete. Development length in general depends on confinement, bar surface roughness and shape, embedment length, type of concrete, concrete compressive strength. Development length for strand and lap splice length for GFRP bar is calculated in the following sections.

3.2.1 Strand – Development Length

3.2.1.1 Steel Strand

Although GFRP dowels are not intended to be used with conventional steel reinforced piles, for completeness as well as to use for Stainless-Steel reinforcing case, development and lap splice lengths are calculated for conventional steel. ACI 318R-14 [59] and AASHTO LRFD Bridge Design-8th Edition [60] were used to calculate the development length and lap splice of steel strands in pile. The specified jacking force in FDOT

Standard Plans for steel strand of 0.6 in diameter is 35 kips, which gives an initial stress in the strand of 161.3 ksi (35 kips / 0.217 in2). Fifteen (15) percent loss is assumed to determine the effective stress in the prestressing strands [61].

ACI 318R-14

Based on section of 25.4.8.1 of the ACI 318R-14 [59], the development for pretensioned seven wire strands of pile in tension was calculated by:

$$l_d = \left(\frac{f_{se}}{3}\right) d_b + \left(\frac{f_{ps} - f_{se}}{1}\right) d_b \quad (47)$$

Where

- f_{se} (the effective stress in prestressing reinforcement) = 85% f_{pi} = 137.1 ksi (assuming 15% loss) [61]
- f_{pi} (jacking stress or initial stress) = 161.3 ksi
- f_{pu} (Minimum guaranteed ultimate strength) = 270 ksi [61]
- f_{ps} (stress in strand at flexural failure of beam)= $f_{pu}\left(1 - \frac{\gamma_p \rho_p f_{pu}}{\beta_1 f'_c}\right) = 270\left(1 - \frac{0.28*0.0032*270}{0.75*6}\right)$ =255.4 ksi

In which,

- $\rho_p = \frac{A_{ps}}{b d_p} = \frac{0.86}{18*(14.5)}$=0.0032
- $d_p = 18 - 0.3\,(\text{half of strand dia.}) - 0.2(\text{spiral dia.}) - 3(\text{clear cover}) = 14.5$

- $A_{\rho s} = 4 * 0.217\ (\text{strand area}) = 0.86$
- $\gamma_p = 0.28$ (typical low relaxation strand)
- $\beta_1 = 0.85 - \left(0.05 * (f_c' - 4)\right) = 0.75$

Accordingly, development length is calculated to be 98.4 in For 0.5 in-diameter strands used in 18x18 in piles for 16-0.5 in strand configuration, this development length is calculated to be 80.25 in Normally, the larger of these two development lengths is used in the design. However, since GFRP dowels will be used only with 16-0.5 in HSSS strand configuration in the pile (FDOT Standard Plans Index 455-118), the 80.25 in (6' 9") development length will be used for GFRP splice design in HSSS pile option.

AASHTO

Based on section 5.9.4.3.2 of AASHTO LRFD Bridge Design-8th Edition [60], the development length of pretensioning strand is calculated by:

$$l_d \geq k\left(f_{ps} - \frac{2}{3} f_{pe}\right) d_b \qquad (48)$$

Where

- k is1 for piling with a depth smaller than 24 is (in old version of AASHTO this factor was 1.6),
- f_{ps} (stress in strand at flexural failure of beam)
- f_{pe} (the effective stress in prestressing reinforcement) = f_{se} above

$$l_d \geq 1\left(255.4 - \frac{2}{3}137.1\right)0.6 = 98.4 \text{ in} \quad (49)$$

Development length for steel strand from the both ACI and AASHTO Specification are identical.

3.2.1.2 HSSS Strand

Paul et al. [65] demonstrated through testing that transfer and development length for HSSS-2205 prestressing strands are considerably smaller than that predicted by AASHTO LRFD, the flexural and shear strengths of piles using SS were greater than predicted by both ACI-318 and AASHTO LRFD, and the stress loss was smaller than that predicted by AASHTO LRFD refined method. These properties were not affected after installation and extraction. Also, Mullins et al. [66] demonstrated that transfer and development lengths of HSSS strands are not longer than comparable conventional carbon steel strands. Accordingly, the development length of HSSS strand will be considered to be the same as the conventional steel strand.

3.2.1.3 CFRP Strand

The development length for the CFRP strands can be calculated for CFRP strands in tension through both from AASHTO-CFRP1 [50] and ACI 440.4R-04 [63].

ACI 440.4R-04: According to Section 6-2 of the ACI 440.4R-04 [63] with unit conversion coefficients, the recommended equation for development length can be calculated using Eq. (50):

$$L_d = L_t + L_{fb} \tag{50}$$

In which L_t and L_{fb} were calculated by $L_t = \frac{(f_{pe})d_b}{\alpha_t(f'_c)^{0.67}}$ and $L_{fb} = \frac{(f_{\rho u} - f_{pe})d_b}{\alpha_{fb}(f'_c)^{0.67}}$

Where:

f'_c= Concrete strength at time of loading

$f_{\rho u}$= Ultimate tensile strength of the CFCC

f_{pe}= Effective prestressing stress

α_{fb}= Factor for the flexural bond length of FRP tendon

α_t= Factor for the transfer length of FRP tendon

As a result, the development length of prestressing strand of pile in tension will be calculated by:

$$L_d = \frac{(f_{pe})d_b}{\alpha_t(f'_c)^{0.67}} + \frac{(f_{\rho u} - f_{pe})d_b}{\alpha_{fb}(f'_c)^{0.67}} \tag{51}$$

It has been observed that there are some idiosyncrasies with these development length equations when the strand is not pretensioned to near the maximum permitted transfer limits, which is sometime the case for FDOT square piles where 1000 psi residual

compression is the controlling design condition. Figure 33 shows the available Commercial CFRP prestressing tendons under the brand names of Carbon Fiber Composite Cable (CFCC) by Tokyo Rope (Japan) [67].

Designation (Configuration diameter) 呼 称		Diameter 直 径 (mm)	Effective cross sectional area 有効断面積 (mm²)	Guaranteed capacity 保証破断荷重 (kN)	Nominal mass density* 単位長さ質量 (g/m)	Tensile elastic modulus* 弾性係数 (kN/mm²)
●	U 5.0φ	5.0	15.2	38	30	167
	1×7 7.5φ	7.5	31.1	76	60	155
	1×7 10.5φ	10.5	57.8	141	111	155
	1×7 12.5φ	12.5	76.0	184	145	155
	1×7 15.2φ	15.2	115.6	270	221	155
	1×7 17.2φ	17.2	151.1	350	289	155
	1×19 20.5φ	20.5	206.2	316	410	137
	1×19 25.5φ	25.5	304.7	467	606	137
	1×19 28.5φ	28.5	401.0	594	777	137
	1×37 35.5φ	35.5	591.2	841	1,185	127
	1×37 40.0φ	40.0	798.7	1,200	1,529	145

Figure 33: CFCC standard specification [67]

Figure 34 shows recently published updates to the CFCC minimum specifications.

Shape of cross section	Standard specification of CFCC									
	Designation	Diameter	Effective cross sectional area		Guaranteed capacity		Nominal mass density		Tensile elastic modulus	
		inch	mm^2	in^2	kN	kip	g/m	lb/ft	kN/mm^2	ksi
○	CFCC U 5.0 φ	0.20	15.9	0.025	40.4	9.1	30	0.020	167	24,221
	CFCC 1×7 7.9 φ	0.31	31.1	0.048	79.3	17.8	60	0.040	155	22,481
	CFCC 1×7 10.8 φ	0.43	57.8	0.090	147.2	33.1	112	0.075	155	22,481
	CFCC 1×7 12.5 φ	0.49	75.6	0.117	192.5	43.3	146	0.098	155	22,481
	CFCC 1×7 15.2 φ	0.60	115.6	0.179	294.4	66.2	223	0.150	155	22,481
	CFCC 1×7 17.2 φ	0.68	151.1	0.234	385.0	86.6	292	0.196	155	22,481

Figure 34: CFCC standard specification [62]

The development length analysis was carried out for CFRP strand pattern shown in FDOT Standard Plans 2020 (455-118) for 0.6 in diameter strand. As it is shown in Figure 23, the pile uses 12-0.6 in diameter CFRP strands. According to Section 933 of the FDOT

Standard Specification for Road and Bridge Construction [60], the nominal cross sectional area of the CFRP 0.6 in diameter strand is considered to be 0.179 ines (Table 11).

The specified jacking force in FDOT Standard Plans for CFCC strand of 0.6 in diameter is 34 kips, which gives an initial stress in the strand of 189.9 ksi (34 k/0.179 in^2). Fifteen (15) percent loss is assumed to determine the effective stress in the prestressing strands [61].

Table 11: Different sizes and loads of current CFRP prestressing strands and bars [64]

Typical Sizes and Loads of CFRP Prestressing Strands and Bars				
Type	Nominal Diameter (in)	Nominal Cross Sectional Area (in^2)	Nominal Ultimate Load (Pu) (kips)	Nominal Ultimate Tensile Stress (ksi)
Single Strand-5.0mm Ø	0.20	0.025	9.1	364
7-Strand-7.9mm Ø	0.31	0.048	17.8	370
7-Strand-10.8mm Ø	0.43	0.090	33.1	367
Single Strand-9.5mm Ø	0.38	0.110	35.0	318
7-Strand-12.5mm Ø	0.49	0.117	43.3	370
Single Strand-12.7 mm Ø	0.50	0.196	59.0	301
7-Strand-15.2mm Ø	0.60	0.179	66.2	369
7-Strand-17.2mm Ø	0.68	0.234	86.6	370

All required information for development length calculations are:

- f'_c= 6 ksi,
- $f_{\rho u}$= 341 ksi [61],
- f_{pi}=189.9 ksi
- f_{pe}= 161.5 ksi (assuming loss of 15%) [61],
- α_{fb}= 14.8 (in-pound units) for CFCC [63],
- α_t= 25.3 (in-pound units) for CFCC [63].

As a result, the development length of the CFRP strand will be:

$$L_d = \frac{161500 * 0.6}{25.3 * (6000)^{0.67}} + \frac{(341000 - 161500) * 0.6}{14.8 * (6000)^{0.67}} = 11.6 + 22.0 = 33.6" \quad (52)$$

AASHTO-CFRP1: According to AASHTO-CFRP1, the equation below can be used for calculation of development length in which the development length is equal to the transfer length+ the flexural bond length.

$$L_d = \frac{(f_{pbt})d_b}{\alpha_t (f'_{ci})^{0.67}} + \frac{(f_{\rho u} - f_{pe})d_b}{\alpha_d (f'_c)^{0.67}} \quad (53)$$

- f'_{ci}= 4 ksi,
- f'_c= 6 ksi,
- $f_{\rho u}$= 341 ksi [61], *(note that this is now 369 ksi in the 2021 FDOT Spec),*
- f_{pi}=f_{pbt}=189.9 ksi,

- f_{pe}= 161.5 ksi (assuming loss of 15% from initial prestressing) [61],
- α_d= 1.48,
- α_t= 1.1

As a result, the development length of the CFRP strand will be:

$$L_d = \frac{189.9 * 0.6}{1.1 * (4)^{0.67}} + \frac{(341 - 161.5) * 0.6}{1.48 * (6)^{0.67}} = 40.9 + 21.9 = 62.8"$$

According to AASHTO and ACI, alternatively, transfer length can be estimated as $50d_b$ for prestressing CFRP cables. Therefore:

$$L_d = 50(0.6) + \frac{(341-161.5)*0.6}{1.48*(6)^{0.67}} = 30 + 21.9 = 51.9" \quad (54)$$

The calculations above results in three different development lengths for CFRP strands, 33.5" (ACI 440.4R), 62.8" (AASHTO CFRP1), and 51.9" (Alternative estimate). There have been several investigations on determining the development length for CFCC strands. Table 12 summarizes the results of some of these investigations [29]. According to these results, the development length of CFCC can be in the range of 29 to 49 in A consistent value for development length of CFCC cannot be established from the available literature, and experimental evaluation is needed to derive such. For the time being, for a preplanned splice using CFCC strand and GFRP dowel, the dowel length inside the lower pile segment will be taken consistent with the current design of FDOT (Index 455-102) that is 54 in without the use of auxiliary bars in the lower segment.

Table 12: Development length predictions

Reference	Predicted Length (in)
Roddenberry et al. [19]	< 72
Mahmoud and Rizkalla [68]	29
Grace [69]	49
Calculated in this Chapter using ACI 440.4R-04 [63]	33.6

3.2.2 Development and Lap Splice Lengths for Conventional Steel (and Stainless Steel)

As indicated in the overall objectives and research approach, in this project, various combinations of material types for dowels and prestressing strands are to be evaluated. This includes conventional steel, stainless steel, and CFRP strands, and steel, stainless steel, CFRP and GFRP dowels. In this section, development and lap splice lengths for conventional steel is examined. These will be also applicable to the case of stainless steel strands and dowels. ACI 318R-14 and AASHTO LRFD Bridge Design-8th Edition were used to calculate the development length and lap splice of steel dowels in pile splice.

3.2.2.1 ACI

Based on Section 25.4.2.3.9 of ACI 318R-14 [59], for deformed steel bars or wires, the development length in tension shall be calculated by Eq. (55):

$$l_d = \left(\frac{3}{4d} \frac{f_y}{\lambda \sqrt{f'_c}} \frac{\psi_f \psi_e \psi_s}{\left(\frac{c_b + k_{tr}}{d_b} \right)} \right) d_b \qquad (55)$$

In which, ψ_t, λ, ψ_e, ψ_s respectively are casting position, material, epoxy, and size factors which were calculated by:

$$\psi_t = 1 \text{ (Less than 12 in of fresh concrete placed below horizontal bar)} \quad (56)$$

$$\psi_e = 1 \text{ (No Epoxy coating on bar)} \quad (57)$$

$$\lambda = 1 \text{ (Normal weigth concrete)} \quad (58)$$

$$\psi_s = 1 \text{ (Bar size is larger than \#7)} \quad (59)$$

For the confinement term $\left(\frac{c_b+k_{tr}}{d_b}\right)$, k_{tr}, c_b, and d_b were calculated by:

$$k_{tr} = 40 * \frac{A_{tr}}{SR} = 40 * \frac{0.207^2 * \pi * \frac{1}{4}}{3*1} = 0.45 \quad (60)$$

$$c_b = 1.75 \text{ (Half of spacing)} \quad (61)$$

$$d_b = 1.27 \text{ (Diameter size for bar \#10)} \quad (62)$$

As a result, the development length for steel bar in tension, l_d, will be 42.65 in (1.08 m). The lap splice length of deformed bar in tension was calculated based on Section 25.5.2.1 of ACI 318-14 [59]. To develop yielding in the bars, $\frac{A_{s,provided}}{A_{s,required}} = 1$, and the splice type will be in the class B. Accordingly, using Eq. (63) the lap splice, l_{st}, is calculated to be 55.44" (1.4 m).

$$l_{st} = 1.3 * l_d = 1.3 * 42.65 = 55.44" \quad (63)$$

3.2.2.2 AASHTO

Based on Section 5.10.8.2.1a-1 of AASHTO LRFD Bridge Design-8th Edition [60], for deformed steel bars, the development length in tension shall be calculated by:

$$l_d = l_{db}\left(\frac{\lambda_{rl}*\lambda_{cf}*\lambda_{rc}*\lambda_{er}}{\lambda}\right) \quad (64)$$

In which, ψ_t, λ, ψ_e, ψ_s respectively are casting position, material, epoxy, and size factors which were calculated by:

$$l_{db} = 2.4 d_b \frac{f_y}{\sqrt{f'_c}} = 74.7" \quad (65)$$

$$\lambda_{rl} = 1 \text{ (Reinforcement location)} \quad (66)$$

$$\lambda_{cf} = 1 \text{ (Coating factor)} \quad (67)$$

$$\lambda_{rc} = \frac{d_b}{(40\frac{A_{tr}}{Sn})+C_b} = \frac{1.27}{(40\frac{(\pi*0.207^2)/4}{3*1})+1.75} = 0.58 \text{ (Reinforcent confinement factor)} \quad (68)$$

$$\lambda_{er} = \frac{A_{s,required}}{A_{s,provided}} = 1 \text{ (Excess reinforcement factor)} \quad (69)$$

$$\lambda = 1 \text{ (Concrete density modification factor)} \quad (70)$$

As a result, the development length for steel bar in tension, l_d, will be 43.2" in (1.09 m):

$$l_d = 74.7\left(\frac{1*2*0.58*1}{1}\right) = 43.2 \quad (71)$$

The lap splice for deformed bar in tension was also calculated based on Section 5.10.8.4.3A of the AASHTO. The minimum length of lap splice in tension lap shall be as required for class A or B lap splice, but not less than 12 in At the old version of the AASHTO Specification, there was a Class C in which the lap splice calculated by $1.7l_d$, but at the new version of the AASHTO, it is changed to Class B in which the splice length is $1.3l_d$.

Therefore, the lap splice in tension is calculated to be 56.1 in (1.42m) by Eq. (72):

$$\text{lap splice} = 1.3 * \mathrm{l_d} = 1.3 * 43.3 = 56.1" \quad (72)$$

3.2.3 Development and Lap Splice Lengths for 8-GFRP #10 Bars

3.2.3.1 Calculation Assuming a Single layer of GFRP Dowel

The standard specification of AASHTO LRFD Bridge Design Guide Specifications for GFRP-Reinforced Concrete – 2nd Edition [49] was used to calculate the development length and lap splice of and GFRP Dowel in pile splice. This calculation is performed for GFRP with both current and proposed/improved properties. Based on Section 2.9.7.4.1-1 of the AASHTO, for deformed FRP bars, the development length in tension can be calculated using Eq. 73.

$$\mathrm{l_d} \geq \max\left\{ \frac{31.6\alpha\frac{f_{fr}}{\sqrt{f'_c}} - 340}{13.6 + \frac{c}{d_b}} d,\ 20 * d \right\} \quad (73)$$

Where f_{fr} = Minimum { f_f and f_{fd}} (74)

The GFRP stress at the time of concrete crushing (bending failure), f_f, is calculated by Eq. (75) assuming a single-layer reinforcement in tension.

$$f_f = \sqrt{\frac{(E_f\varepsilon_{cu})^2}{4} + \frac{0.85\beta_1 f'_c E_f \varepsilon_{cu}}{\rho_f}} - 0.5E_f\varepsilon_{cu} = \begin{cases} Current\ \ GFRP\ properties: = 57.40 \text{ ksi} \\ Proposed\ \ GFRP\ properties: = 64.28 \text{ ksi} \end{cases} \quad (75)$$

Where:

$$E_f = \begin{cases} 6500\ ksi\ \ for\ current\ properties \\ 8500\ ksi\ \ for\ improved\ properties \end{cases}$$

$\rho_f = \frac{A_f}{bd} = 0.0169$ (GFRP reinforcement ratio assuming single layer with 3 bars)

$A_f = 3.81 in^2$ (Assuming the area of 3 GFRP reinforcement)

$$\beta_1 = \max\left\{0.65; 0.85 - 0.05\left(\frac{f'_c}{1000} - 4\right)\right\} = 0.75$$

$\alpha = 1$ (Bar location modification factor)

C = 1.75 (Half of the center-to-center spacing of the bars being developed)

In addition, the maximum strength of GFRP bar, f_{fd} , is calculated by:

<u>Current (2020) GFRP properties</u>

$f_{fd} = C_E * f^*_{fu}$ = 54.29 (ksi)

(76-a)

<u>Proposed (2021) GFRP properties</u>

$f_{fd} = C_E * f^*_{fu}$ 67.79 (ksi)

(76-b)

In which, f_{fu} depends on the size and the type of GFRP bar (E-CR glass of #10 was picked for our calculations). The C_E is the environmental reduction factor selected here to be 0.7 because pile structure is exposed to earth. Therefore, according to Eq. 77 below, f_{fr} will be 54.29 ksi and 64.28 ksi for the current and the proposed GFRP properties, respectively.

Current (2020) GFRP properties (77a)

$$f_{fr} = \min \begin{cases} f_f = 54.40 \text{ ksi} \\ f_{fd} = 54.29 \text{ ksi} \end{cases}$$

Proposed (2021) GFRP properties (77b)

$$f_{fr} = \min \begin{cases} f_f = 64.28 \text{ ksi} \\ f_{fd} = 67.79 \text{ ksi} \end{cases}$$

As a result, the development length for GFRP bar at pile splice in tension, l_d, for the current and proposed GFRP properties will be, respectively, 30.55 in (0.77 m) and 41.48 in (1.05m) by:

$$\begin{cases} Current\ (2020)\ GFRP: l_d \geq \max\left\{\dfrac{31.6 * 1 * \dfrac{54.29}{\sqrt{6}} - 340}{13.6 + \dfrac{1.75}{1.27}} * 1.27,\quad 20 * 1.27\right\} = 30.55" \\ Proposed\ (2021)\ GFRP: l_d \geq \max\left\{\dfrac{31.6 * 1 * \dfrac{64.28}{\sqrt{6}} - 340}{13.6 + \dfrac{1.75}{1.27}} * 1.27,\quad 20 * 1.27\right\} = 41.48" \end{cases}$$

Accordingly, based on the Section 2.9.7.6 of the AASHTO-GFRP2 [49], the lap splice of GFRP deformed bar in tension is calculated to be 40 in (1.00 m) and 54 in (1.4 m), respectively, for the current and proposed GFRP properties using Eq. 78.

Current (2020) GFRP properties (78a)

$$\text{lap splice length} = 1.3 * l_d \cong 40 \text{ in}$$

Proposed (2021) GFRP properties (78b)

$$\text{lap splice length} = 1.3 * l_d \cong 54 \text{ in}$$

Consider: Given that the adhesive dowels are not touching the strands (non-contact splice), and the surrounding concrete is not interrupted, the use of a 1.3 factor may not be necessary and only the additional offset length (approximately 2 ines) need be added to the basic development length. Additionally, the high degree of confinement offered by the spiral reinforcing at 1 in and 3 in spacing near the head and tip of the pile provide enhanced bond development.

3.2.3.2 Calculation for Three layers of GFRP Dowel

The development length calculated in the previous section assumed one layer of reinforcement for calculating the stress level at bars. Since the splice is actually designed using three layers of GFRP dowels (Figure 24), and as such, the actual configuration needs to be considered in calculating the development length and lap splice for GFRP bars. To calculate the development length of GFRP bars, it is necessary to calculate the stress in GFRP at the point of bending failure of pile splice governed by concrete crushing. According to earlier calculation, the actual stress in GFRP and maximum moment strength at crushing of concrete are:

Current (2020) GFRP properties

$$\begin{cases} f_{f_1} = -8.4 \text{ ksi} \\ f_{f_2} = -26.1 \text{ ksi} \\ f_{f_3} = -43.9 \text{ ksi} \\ M_{n\#10} = \sum F_i * Y_i = 206.1 \text{ k} - \text{ft} \end{cases}$$

Proposed (2021) GFRP properties

$$\begin{cases} f_{f_1} = -7.6 \text{ ksi} \\ f_{f_2} = -28.7 \text{ ksi} \\ f_{f_3} = -49.8 \text{ ksi} \\ M_{n\#10} = \sum F_i * Y_i = 226.7 \text{k} - \text{ft} \end{cases}$$

Similar to the development length calculation for one-layer reinforcement in AASHTO, development length for the case of three layers of reinforcement is calculated by considering $f_f = f_{f3}$ (Eq. 79). Accordingly, f_{fr} is calculated to be 43.9 ksi and 49.8 ksi, respectively, for the current and proposed GFRP properties using Eq. 77.

Current (2020) GFRP properties

$$f_{fr} = \min \begin{cases} f_f = f_{f3} = 43.9 \text{ ksi} \\ f_{fd} = 54.29 \text{ ksi} \end{cases}$$

(79-a)

Proposed (2021) GFRP properties

$$f_{fr} = \min \begin{cases} f_f = f_{f3} = 49.8 \text{ ksi} \\ f_{fd} = 67.79 \text{ ksi} \end{cases}$$

(79-a)

Therefore, the development length for GFRP bars in tension, l_d, can be calculated to be $\text{Max}\{19.19", 25.4"\} = 25.4$ in (0.64 m) and $\text{Max}\{20.19", 25.4"\} = 25.4$ in (0.64 m) for the current and proposed GFRP properties, respectively. Accordingly, the lap splice of the deformed bar in tension for both current and proposed GFRP properties will be calculated to be 33.02 in (0.84 m).

Nevertheless, to be conservative and to allow the GFRP bars to develop their maximum strength, the lap splice length calculated based on developing full strength, i.e., 40 in for current and 54 in for proposed properties, is recommended for the design of pile splice using GFRP dowels. It should also be noted that often, it is expected that the concrete will develop strengths considerably higher than specified, therefore, allowing GFRP dowels to develop stresses larger than that calculated for pure bending assuming the nominal concrete strength.

3.2.4 Ultimate Bond Stress for 8-GFRP Dowel #10

The bond stress, τ, of the GFRP dowels (Figure 35) can be calculated according to Section 10.1 of the ACI 440.1R.15 [58], by :

$$l_e \pi d_b \tau = A_{f,bar} f_{fu} \tag{80}$$

Figure 35: Transfer of force through bond of the concrete and The GFRP dowels

The embedded length of the GFRP bar, l_e, is equal to the proposed development length for GFRP dowel in previous section. Embedded length and other properties were selected for GFRP bar #10. As a result, the bond stress is:

$$\tau = \frac{A_{f,bar} f_{fu}}{l_d \pi d_b} = \frac{1.27*54.11}{40*3.14*1.27} = \frac{53.8}{131.6} = 430.8 \text{ psi} \tag{81}$$

The ultimate bond stress for the GFRP #10 can be examined by experimental test data. It should be cautioned that the bond stress distribution along the bar is increasingly non-linear, the longer the development length, and so the bond stress is only a reference value rather than a design property.

3.2.5 Adhesive-Bonded Anchors and Dowels Systems

According to Section 1.6.2 of FDOT Structures Design Guidelines [46], the design tensile strength for adhesive anchor bond is calculated by:

$$\Phi N_c = \Phi_c \Psi_e \Psi_{gn} \Psi_m N_{bond} \quad (82)$$

Where:

$N_{bond} = \tau\pi d_b h_{ef} = 1.080 * 3.14 * 1.27 * 40 = 172.3\ k$

$A_{no} = (16d_b)^2 = 412.9$ (Figure 36)

$A_n = A_{gross} = 18^2 = 324$ (Figure 36)

$h_{ef} = l_d = 40$ in (Note: beyond 20d, this value is unconservative, per ACI 318-14 [59])

$\Phi_c = 0.85$

$\Psi_e = 0.70 + 0.30$ (Cover / 8d) = 0.86

$\Psi_{gn} = A_n / A_{no} = 324 / 412.9 = 0.78$

$\Psi_m = 2.5 /(1+ z / h_{ef}) = 1$

τ= 1.08 ksi nominal bond strength for general use products on the APL (Type V and Type HV), however FDOT specifications require the use of Epoxy Compound Type AB, due to constructability reasons.

Design Commentary: It is advised by the FDOT Structures Design Office engineers that both the anchor group factor (Ψ_{gn}) and eccentricity modification factor (Ψ_m) are only applicable to concrete breakout failure modes and do not appreciably affect the adhesive bond resistance.

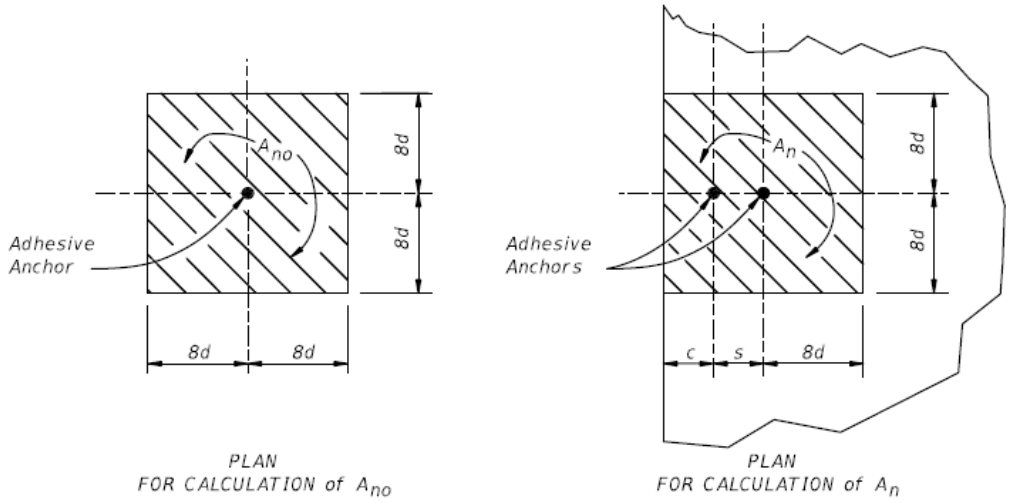

Figure 36: Effective tensile areas for adhesive anchors [46]

After substitution to the Eq. (82), $\Phi N_c = \Phi_c \Psi_e \Psi_{gn} \Psi_m N_{bond}$ = 98.2 k > 68.7 k . As a result, the design tensile strength for adhesive anchor bond is greater than the design tensile resistance of one GFRP bar, and therefore will allow the resistance to develop. Again, it should be cautioned that the bond stress distribution along the adhesive dowel bar is increasingly non-linear, the longer the development length [63]. As such, ACI 318-14 (Chapter 17) [59] advises that the linear bond stress model is not valid beyond 20 bar diameters. It is unknown whether this limit is applicable for GFRP dowel bars given that the tensile modulus of Elasticity is approximately on quarter of steel.

3.2.6 Detailing for Unforeseen Pile Splice

It is realized that the case of unforeseen splices imposes some limitations on the length of holes that can be drilled into the lower segment of the piles. In communication with FDOT, it was determined that a practical drilling length is limited to 30 in for the case of GFRP dowels however, this limitation does not affect the strength expected from the splice itself. As calculated in the previous sections, the development length of GFRP #10 bar in concrete is 25.4 in Accordingly, the splice section in the unforeseen case will be able to develop the maximum nominal pure moment resistance of 206.1 kip.ft (226.7 kip.ft for proposed/improved properties). However, it is realized that the moment resistance in the lower segment of the pile immediately below the splice section may be limited by the limited lap splice of the GRFP bars with the prestressing strands. Nevertheless, this limitation will be present regardless of what type of dowel is used in the splice, and such, this limitation needs to be expressed clearly for the designer to consider. For the case of stainless steel strands, this will definitely limit the moment resistance for the lower segment of the pile. On the other hand, according to the calculation performed in this Chapter, the development length for CFRP (CFCC) strand can be as low as 33.6 in, that is slightly bigger than the length of the hole to be drilled into the lower pile segment. Therefore, in the best scenario, when CFCC strand is used, the role of any auxiliary bar will be minimized. However, according to other sources, the development length of CFCC strand can be as high as 49 in according to Mahmoud and Rizkalla [68], Grace [69], and Roddenberry et al. [29]. A consistent value for development length of CFCC cannot be established from the available literature, and experimental evaluation is needed to derive such. To allow the maximum attainable

resistance for unforeseen splices, the length of holes to be drilled into the lower pile segment will be kept at its maximum practical length of 30 in, and the enhanced confinement provided by the tight spiral spacing at the head of the pile is anecdotally recognized.

3.3 M-N Interaction Diagrams for Piles and Pile Splices

In the following sections, analyses are performed to compare the moment-axial force interaction results for piles using steel strands and splices using steel and GFRP material. Hand calculation using AASHTO and ACI codes, and layer-by-layer analysis using Response 2000 program are included.

3.3.1 Steel Strands and Dowels

For pile splice using conventional steel dowels, the results of hand calculations for moment axial force interaction diagram based on nominal strengths before application of resistance factor were compared to the results of Response 2000 in the same graph (Figure 37). As it is shown in Figure 37, the moment and axial force values obtained by hand calculation for three points of balanced, tension-controlled, and pure flexural match with the results calculated by Response 2000. However, for pure axial tensile and compressive strength, Response 2000 provides higher resistances.

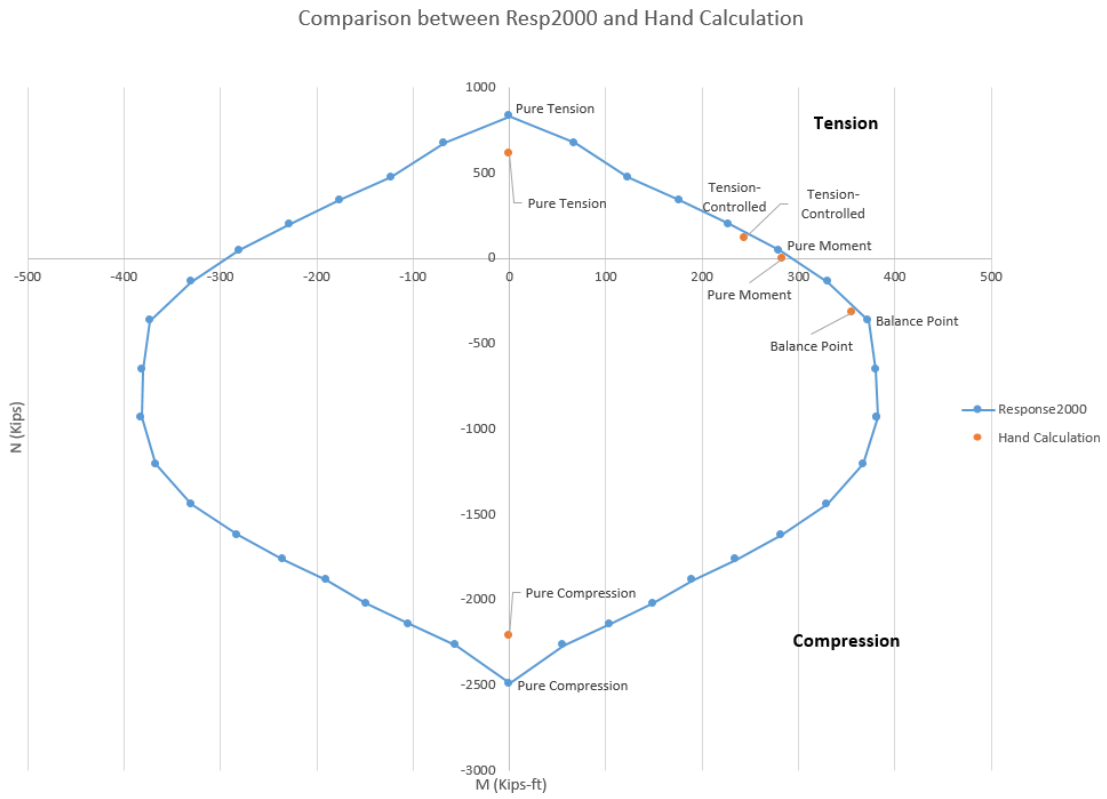

Figure 37: Comparison between results of hand calculation and Response 2000 for pile splice

To make this comparison for design strengths, application of resistance factors is required. Table 13 shows resistance factors calculated based on ACI 318 R-14 [59] and AASHTO LRFD Bridge Design-8th Edition [60].

Table 13: Resistance factors on AASHTO and ACI specifications

Resistance Factor	AASHT (Article 5.5.4.2.1)[60]	ACI (Sec. 21.2)[59]
Axial	0.75	0.65
Flexural	1.0	0.9

Table 14, summarizes the results for the pile and pile splice at pure axial compression, pure axial tension, pure flexural moment, and balanced points.

Table 14: Moment and force values for both pile and pile splice based on the different φ

Points	**without *φ*** Moment (kip.ft), Force (kips)		**ACI *φ*** Moment (kip.ft), Force (kips)		**AASHTO *φ*** Moment (kip.ft), Force (kips)	
	Pile	Pile Splice	Pile	Pile Splice	Pile	Pile Splice
Pure Axial Compression	-- 0, 1616	-- 0, 2488	**0.65** 0, 1050	**0.65** 0, 1617	**0.75** 0, 1212	**0.75** 0, 1866
Balanced Failure	-- 360, 463	-- 382, 931	**0.65** 234, 301	**0.65** 248, 605	**0.75** 270, 347	**0.75** 286, 698
Pure Flexural Moment	-- 306, 0	-- 293, 0	**0.76** 233, 0	**0.74** 217, 0	**0.86** 263, 0	**0.84** 246, 0
Pure Axial Tension	-- 0, 660	-- 0, 831	**0.9** 0, 594	**0.9** 0, 748	**1** 0, 660	**1** 0, 831

According to Table 14, the AASHTO resistance factors for pure tension, balanced condition, and pure compression were calculated to be 1.0, 0.75, and 0.75, respectively. The resistance factors at pure flexural point for pile and pile splice, respectively, were calculated to be 0.86 and 0.84 using a linear interpolation between two resistance factors of balanced and tension controlled points. Similarly, the ACI resistance factors for pure tension, balanced condition, and pure compression were calculated to be 0.9, 0.65, and 0.65, respectively.

The resistance factors at pure flexural point for pile and pile splice, respectively, were calculated to be 0.76 and 0.74 by using a linear interpolation between two resistance factors of balanced and tension controlled points. To check the calculated resistances for pile and splice against FDOT required resistances (Table 4), section analyses were carried out for a pile and pile splice using conventional steel strands utilizing Response 2000 (Figures 38 and 39).

Figure 38 shows a comparison between the nominal and design moment-axial load interaction diagrams obtained using Response 2000 for pile splice with steel dowels in accordance with resistance factors from ACI 318 R-14 [59] and AASHTO LRFD Bridge Design-8th Edition [60]. Interaction diagrams are shown in Figure 39 for an 18x18 in pile for nominal and design strengths.

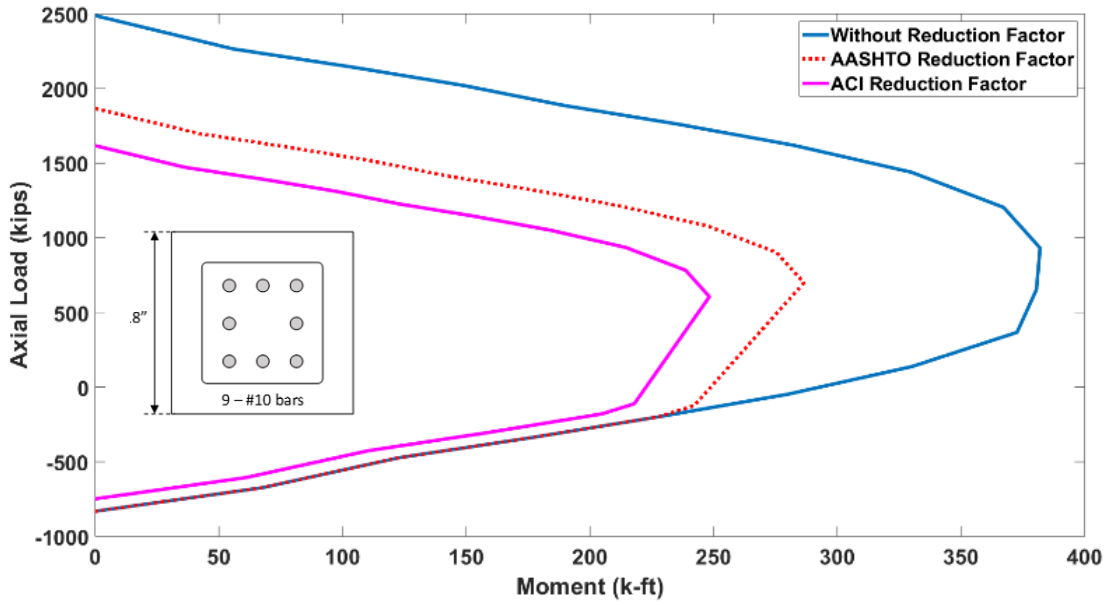

Figure 38: Comparison among M-N diagrams for pile splice using steel dowels

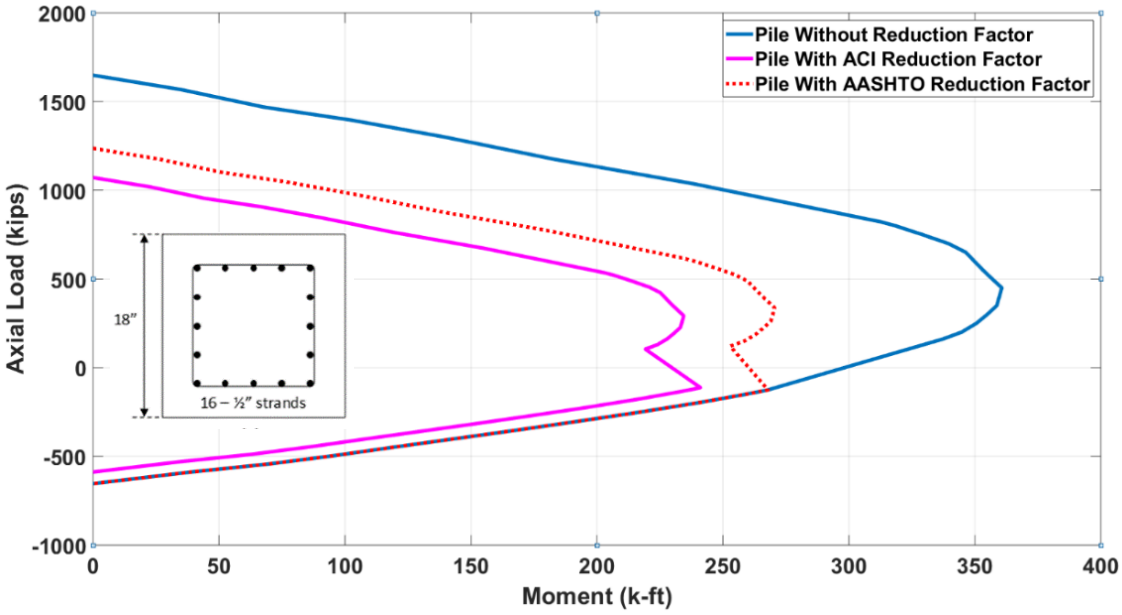

Figure 39: M-N diagrams for pile using steel strands

At pure flexural moment, the results show that the pile splices provide resistance slightly smaller than the pile itself. Moreover, these results also show that a pile splice with 8-steel #10 steel dowels can develop 100% and 91% of the required design moment resistance (Table 4 – 245 kip.ft) when using the AASHTO and ACI resistance factors, respectively.

Figure 40 provides a comparison between M-N diagrams for pile and pile splice separately for nominal and design strengths using the AASHTO and ACI resistance factors.

3.3.2 GFRP Dowels

Design moment-axial load interaction diagrams were calculated for pile splices using GFRP dowels of various size and configuration as discussed earlier. Hand calculations incorporated into Excel and MATLAB was employed to calculate and plot the M-N diagrams for these cases in Figure 41. Both current (2020) and proposed (2021) properties for GFRP dowels were considered.

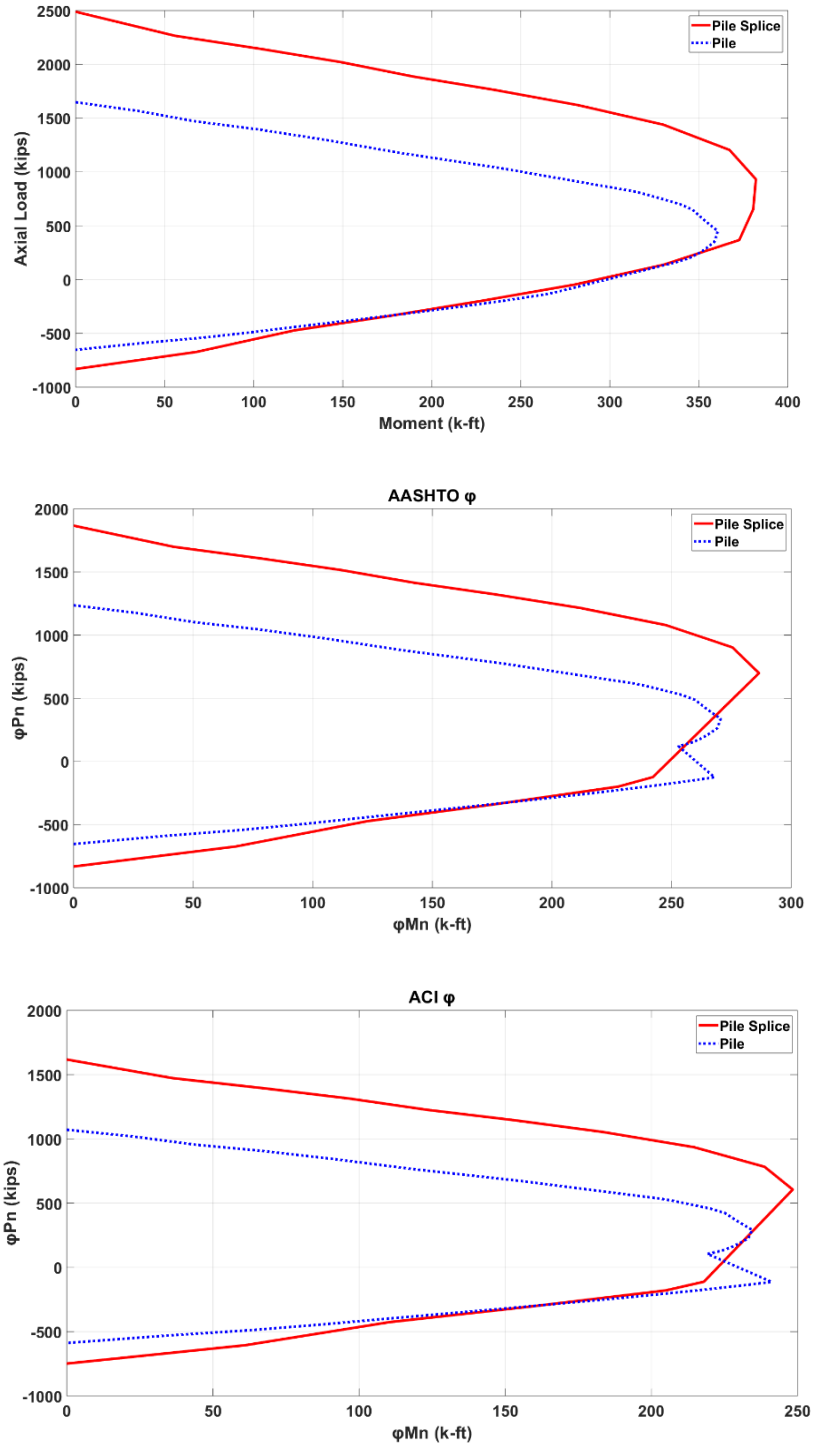

Figure 40: M-N interaction diagrams for pile and pile splice reinforced with steel (Top: nominal strengths, middle: AASHTO design, bottom: ACI design)

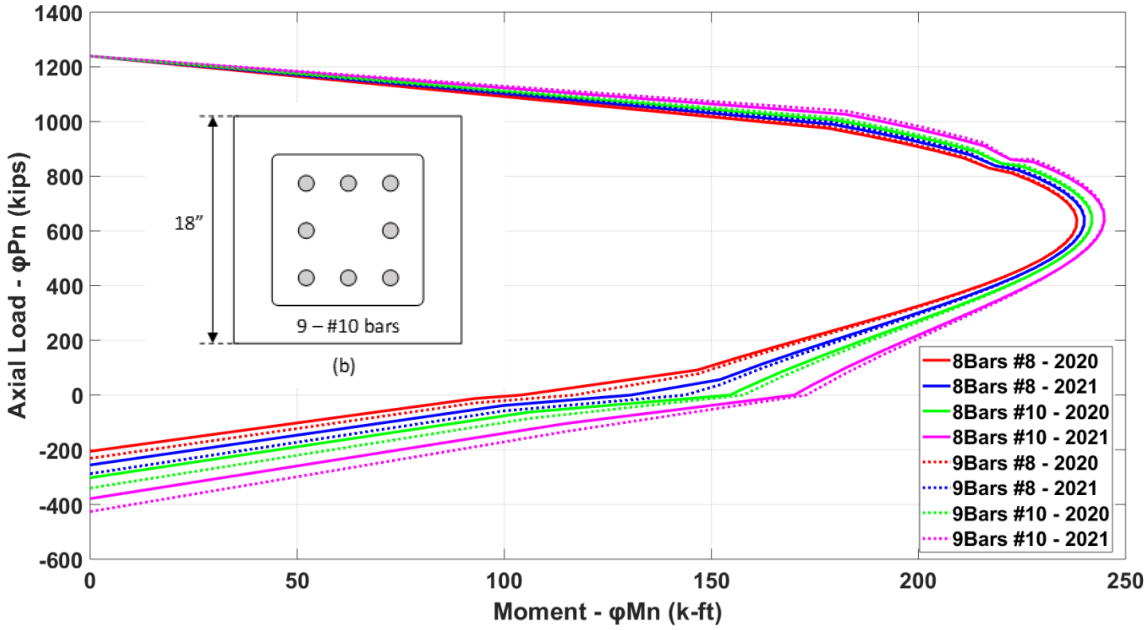

Figure 41: M-N interaction diagrams for all cases of the pile splice reinforced with GFRP

The use of improved GFRP dowel bar shows noticeable improvement in the resistances. Because of the dimension of holes required for encasing the dowels, the dowels are positioned 5 ½ in from the edge of the cross section. According to the spacing requirement for the design, two arrangements of 9 and 8 dowels were possible for the pile splice with the specific size of the dowel. As it is shown in Figure 41, using an additional dowel bar (e.g. 9 vs. 8) in the splice has negligible effect in increasing the resistance. The use of larger diameter dowel bars with the same configuration results in a significant improvement in the resistance.

3.3.2.1 M-N Interaction Diagrams for Pile Splice using 8-# 10 GFRP and Steel Dowels

In this section, design moment-axial force interaction diagrams (based on AASHTO resistance factors) are compared for two cases of pile splice using 8-#10 steel and GFRP dowels (based on current GFRP properties). As it is shown in Figure 42, the pile splice using the GFRP dowels with 155 (kip.ft) design moment resistance (at pure bending) can cover 63% of the design moment resistance of the steel pile splice using steel dowel with 246 (kip.ft).

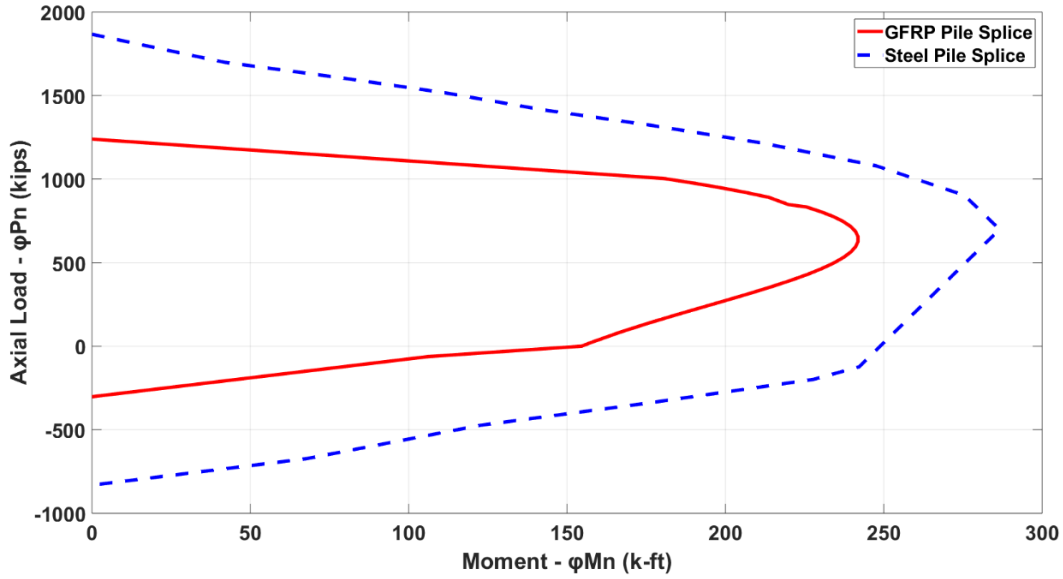

Figure 42: M-N interaction diagrams for pile splice reinforced with 8-bars #10 of steel and GFRP

3.3.2.2 M-N Interaction Diagrams for Pile using 8-# 10 GFRP and Pile with Steel Strand

Design moment-axial force interaction diagrams (based on AASHTO resistance factors) are compared for a pile using steel strands and GFRP dowels (based on current GFRP properties). As it is shown in Figure 43, the pile splice with 155 (kip.ft) design moment

resistance (at pure bending) can cover 59% of pile design moment resistance with 263 (kip.ft).

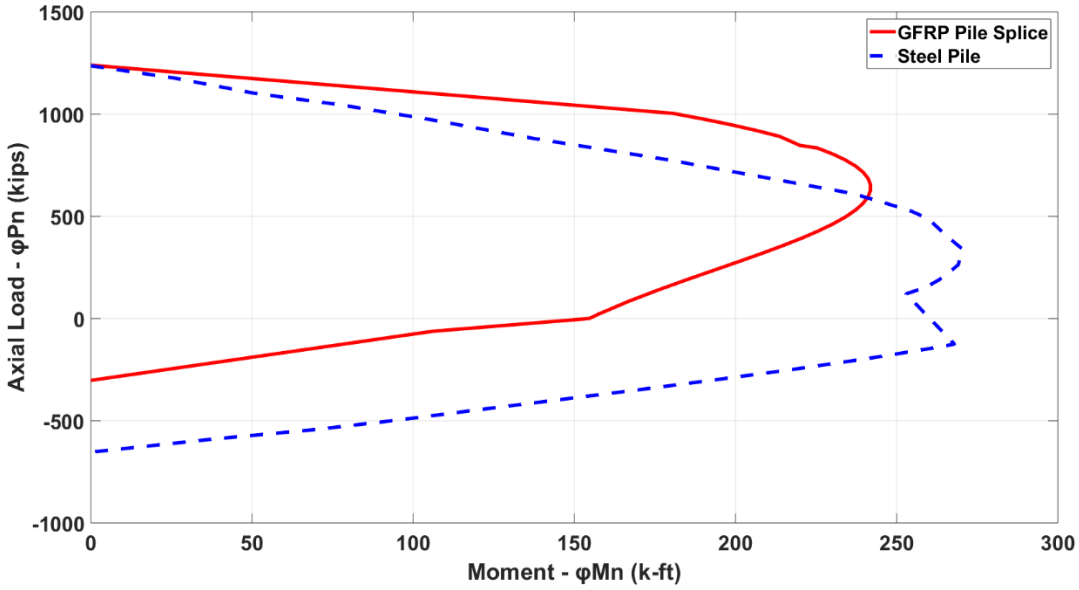

Figure 43: M-N interaction diagrams for pile splice reinforced with 8-bars #10 GFRP and steel strands pile

3.4 Proposed Design for Epoxy Dowel Splice using GFRP Bars

Based on the calculations for moment resistance and development and lap splice lengths presented above, Figures 44 and 45 shows the pile splice design with GFRP dowels with current properties.

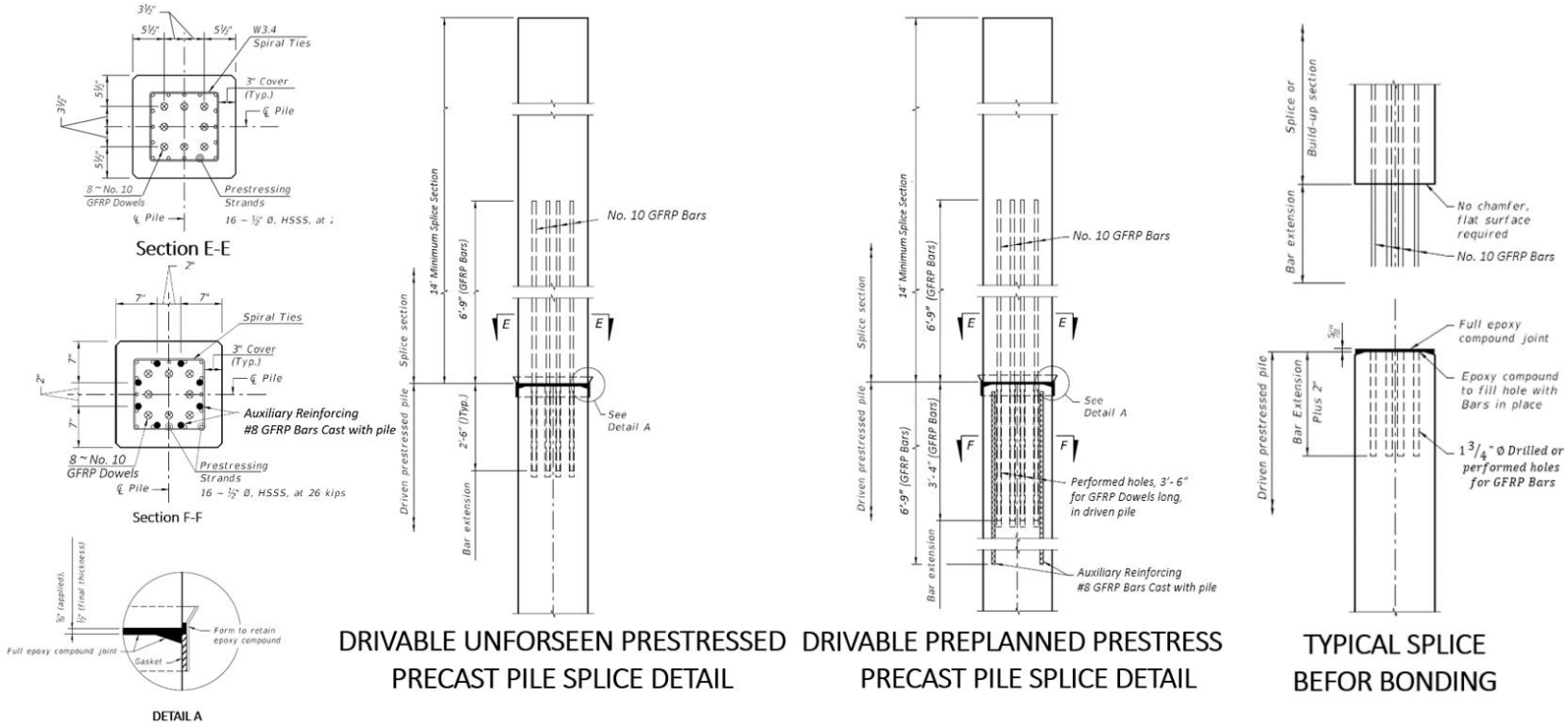

Figure 44: Development of Epoxy Dowel Pile Splice Design (SS Strands and GFRP Bars)

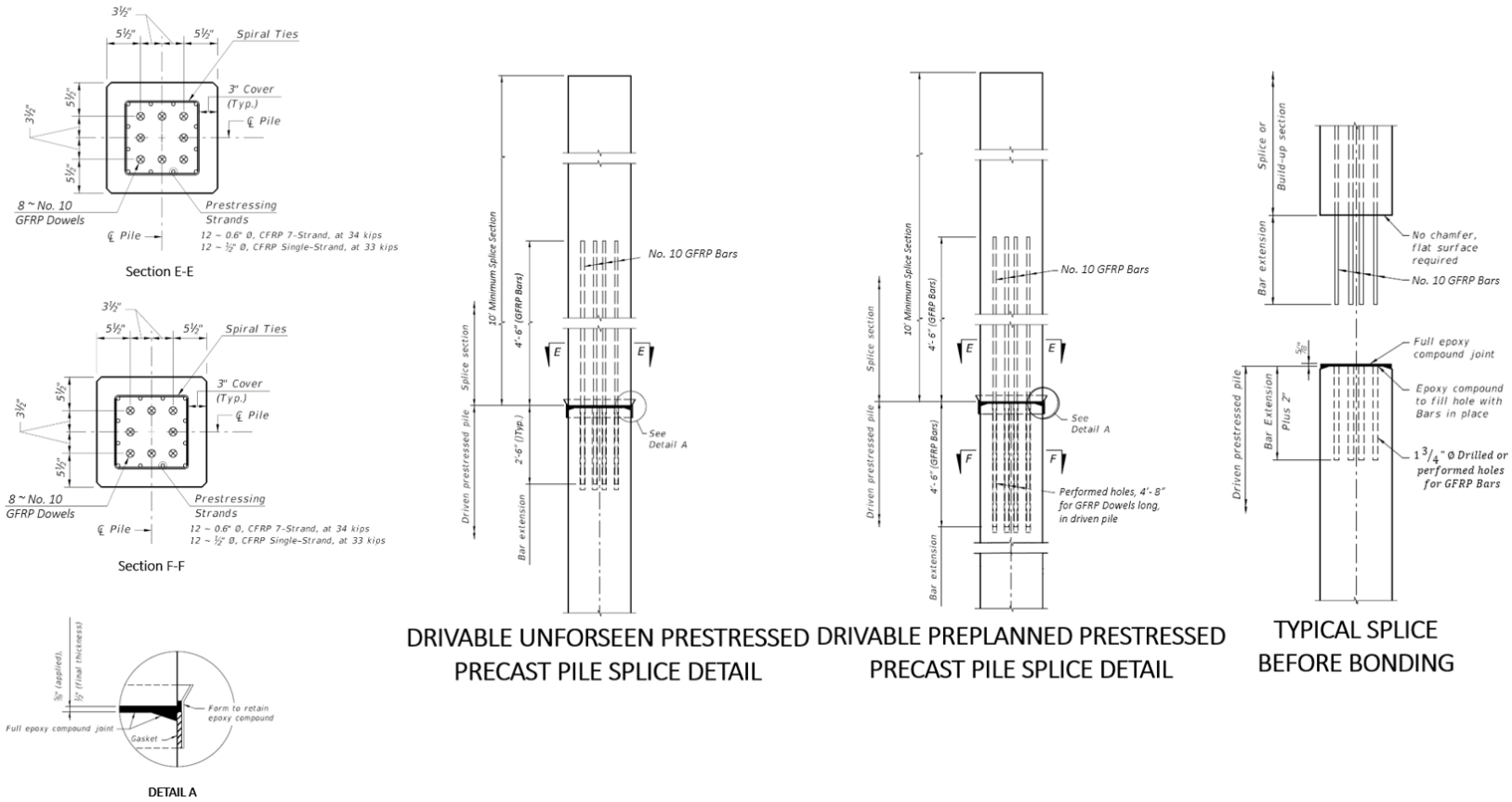

Figure 45: Development of Epoxy Dowel Pile Splice Design (CFRP Strands and GFRP Bars)

CHAPTER 4: TEST SPECIMENS, FABRICATION, AND TEST SETUP

The fabrication and laboratory test of epoxy dowel splices were developed for 10 precast prestressed concrete pile specimens for both drivable unforeseen and preplanned pile splices. Each test specimen was comprised of two segments (14ft + 14ft), with a total length of 28 ft. The testing is limited to piles of 18x18 in cross-section and focuses on the flexural resistance of pile splices.

4.1 Test Matrix

The original test matrix included the use of CFRP, SS, and GFRP dowel splices, as well as carbon steel dowels connecting pile segments of compatible material. As part of the investigation in Chapter 3, it became clear that the behavior of piles and splices using stainless steel (SS) material is expected to be similar to those using carbon steel material for strands and dowels. Accordingly, in coordination with the FDOT Project Manager (PM) and technical committee, the test matrix was modified by eliminating specimens using stainless steel material and adding to the number of specimens using GFRP dowels in combination with piles using CFRP and carbon steel strands.

Additional changes were applied because of constructability and precast plant operation limitations. Because of availability issues, the precast plant requested to use Concrete Class V with nominal compressive strength of 6,500 psi instead of project specified Class V (Special) with compressive strength of 6,000 psi. The change was approved by FDOT PM. For ease of operation, the precast plant also asked to change the number and size of

the steel strands in the pile segments from 16~0.5” to 12~0.6”. This was to have the same number and arrangement of strands for steel and CFRP strands so that they could be fabricated in the same casting bed. This request was evaluated by the research team and was approved. Accordingly, FIU team changed from 6’9” to 8’3” the strand development length and the dowel embedment length in the upper segment and for the auxiliary bar length in the lower segment.

Also, as a consequence, the specified jacking force of the individual strands for the piles using CFRP strands was increased from the specified 34 kips to 35 kips to be consistent with the current design of FDOT Standard Plans for the steel strand of 0.6” diameter. It is believed these changes will not affect negatively the purpose of this study, since the main purpose of the study is to investigate the behavior at the splice region and performance of the dowels. In addition, in consultation with Tokyo Rope USA (TRUSA)and communication with the FDOT Project Manager (PM) and technical committee, the (9) #6 CFRP dowel was changed to (9) 7-strand 19.3 mm diameter CFRP for the test specimens 9 and 10. These dowels have been reportedly used for splices in other investigations and have performed satisfactorily. The shop drawings prepared by S&S Precast containing all changes applied are shown in Appendix A. The updated test matrix shown in Table 15 was used for fabrication and flexural testing.

Table 15: Matrix of the test specimens

Dowel Type	Specimen	Strand Type	Splice for Drivable	Segment 1 Length-ft	Segment 2 Length-ft	Spliced Length- ft
GFRP	1	Steel SPindex-455-018	Unforeseen SP-455 [See Shop Drawings in App. A]	14	14	28
	2	CFRP SPindex 455-118	Unforeseen SP-455 [See Shop Drawings in App. A]	14	14	28
GFRP	3	Steel SPindex-455-018	Preplanned SP-455 [See Shop Drawings in App. A]	14	14	28
	4	Steel SPindex-455-018	Preplanned SP-455 [See Shop Drawings in App. A]	14	14	28
	5	CFRP SPindex 455-118	Preplanned SP-455 [See Shop Drawings in App. A]	14	14	28
	6	CFRP SPindex 455-118	Preplanned SP-455 [See Shop Drawings in App. A]	14	14	28
Steel	7	Steel SPindex-455-018	Preplanned SP-455-002 [See Shop Drawings in App. A]	14	14	28
	8	Steel SPindex-455-018	Preplanned SP-455-002 [See Shop Drawings in App. A]	14	14	28
CFRP	9	CFRP SPindex 455-118	Preplanned SP-455-102 [See Shop Drawings in App. A]	14	14	28
	10	CFRP SPindex 455-118	Preplanned SP-455-102 [See Shop Drawings in App. A]	14	14	28

4.2 Specimen Fabrication

Fabrication of the test specimens followed all relevant specifications within FDOT Standard Specifications [47], especially in the notes and specifications within FDOT Standard Drawings Index 455 with the exceptions noted above. The fabrication of the test specimens followed the shop drawings presented in Appendix A.

4.2.1 Forms and Preparations

Figure 46 shows the precast bed used for fabrication of the specimens. Wooden headers were used, along with a casting bed to construct the test specimens. Twelve holes were drilled in the headers to accommodate the CFRP and steel strands. According to the dowel arrangements, eight or nine holes were also drilled in the headers to accommodate the steel, CFRP, and GFRP dowels. In addition, spacing between wooden headers were used to allow for the embedment length required for the dowels of the “male” pile specimens (Figure 46, right photo).

Figure 46: Wooden headers arrangement in casting bed

As shown in Figure 47, the strands were delivered in spools. The strands were pulled from the spool along with the casting bed, while being fed through the headers. #10 steel dowels and strands were used for pile splices in accordance with the FDOT Standard Drawings Index 455-002 and 455-018.

Figure 47: Stand installation

Material properties of FRP dowel bars were expected to comply at minimum with the FDOT Specifications as shown in Table 16 below. Because of availability, the actual material used for FRP dowels varied from those in this table.

Table 16: Sizes and mechanical properties of FRP bars

Bar Size Designation	Nominal Bar Diameter (in)	Nominal Cross Sectional Area (in^2)	Measured Cross-Sectional Area (in^2)		Minimum Guaranteed Tensile Load (kips)	
			Minimum	Maximum	GFRP Bars	CFRP Bars
2	0.250	0.049	0.046	0.085	6.1	10.3
3	0.375	0.11	0.104	0.161	13.2	20.9
4	0.500	0.20	0.185	0.263	21.6	33.3
5	0.625	0.31	0.288	0.388	29.1	49.1
6	0.750	0.44	0.415	0.539	40.9	70.7
7	0.875	0.60	0.565	0.713	54.1	-
8	1.000	0.79	0.738	0.913	66.8	-
9	1.128	1.00	0.934	1.137	82.0	-
10	1.270	1.27	1.154	1.385	98.2	-

The exact material for the GFRP dowels were selected by the precast contractor (S&S Precast, Inc.) based on availability from V-Rod Material supplied by Pultral of Canada and communicated with the FDOT Project Manager to meet the requirements of ASTM D7957-17 and FDOT Standard Specification for Road and Bridge Construction [47] Section 932.

According to proposed Drawings in Chapter 3 of this dissertation, GFRP #10 and #8 bars were used as dowel and auxiliary bars, respectively (Figure 48) in accordance with the original design presented in Chapter 3.

Figure 48: The GFRP bars used for the construction

The modulus of elasticity and tensile strength of the GFRP bars reported by the supplier is included in the Table 17.

Table 17: The mechanical properties of the GFRP bars

Bar Size Designation	Minimum Tensile Module	Guaranteed Tensile Strength
8	7252 ksi	130.5 ksi
10	7252 ksi	116 ksi

The exact material for the CFRP strands and spirals were selected in consultation with TRUSA and communication with the FDOT project manager to meet the requirements of FDOT Standard Specification Section 933 (Figure 49). As stated earlier, the 7-strand 19.3mm ϕ strand material was used instead of #6 CFRP bar for dowels. The modulus of elasticity and guaranteed breaking load of the 7-strand 19.3mm ϕ strand are 21,756 ksi and 106.9kips, respectively.

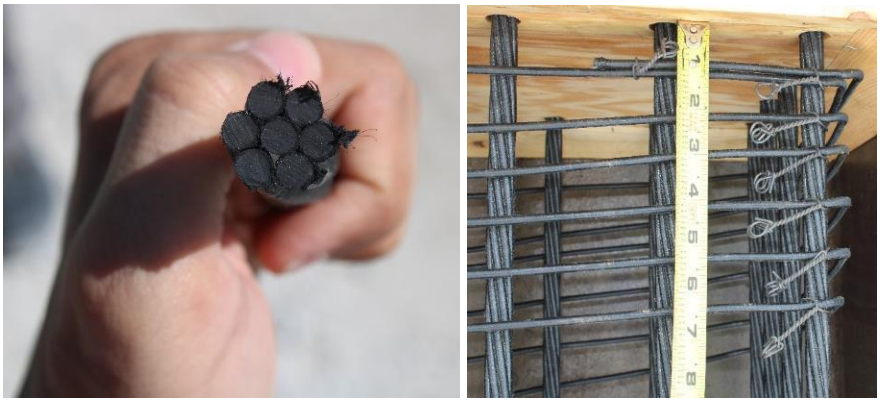

Figure 49: The CFRP strands and spirals used for the construction

According to FDOT Standard Drawings Index 455, the holes for the "female" pile specimens were cast using 2in galvanized pipes for the preplanned Specimens 3-8, and 1 ½in galvanized pipes for Specimens 9 and 10 (Figure 50) meeting the requirements of ASTM A653, Coating Designation G90, 26 gauge. The holes for "Unforeseen Splice" specimens (Specimens 1 and 2) were to be drilled with 1 ¾ in drill size. However, the contractor used 1 ¼ in PVC pipes to first cast the holes, and then drilled 1 ¾ in holes in the pipes to simulate field conditions.

Figure 50: The pipes used for the construction

As shown in Figure 51 (left), in accordance with Index 455-102, Note 4. “1” spiral tie pitch was considered to be continued to 4 ft below the head of the pile where the dowel holes are utilized. One full turn spiral was used to splice the spiral ties. Each wrap of the spiral strand was tied to a minimum of two corner strands. All CFRP and steel spirals were tied in their final position to strands with steel ties (Figure 51, upper right photo). According to the proposed drawings in Chapter 3 of this dissertation, all auxiliary bars were installed with a distance of 1in from the chamfer (Figure 51, lower right photo).

Figure 51: The spirals, strands and bars configuration

4.2.2 Stressing

For this fabrication, all specimens were constructed, along with the same casting bed. Accordingly, to splice the CFRP strands to steel strands, the TRUSA couplers were used following strict installation procedure prescribed by TRUSA (Figure 52). TRUSA engineer was present to train the precaster and inspect the procedure.

Figure 52: Coupling arrangement and installation by TRUSA

Figure 53 shows one of these special couplers in which the CFRP strand end installed with wedges and buffer materials was coupled to the steel strand end by twisting together the threaded ends of the sleeve and the coupler.

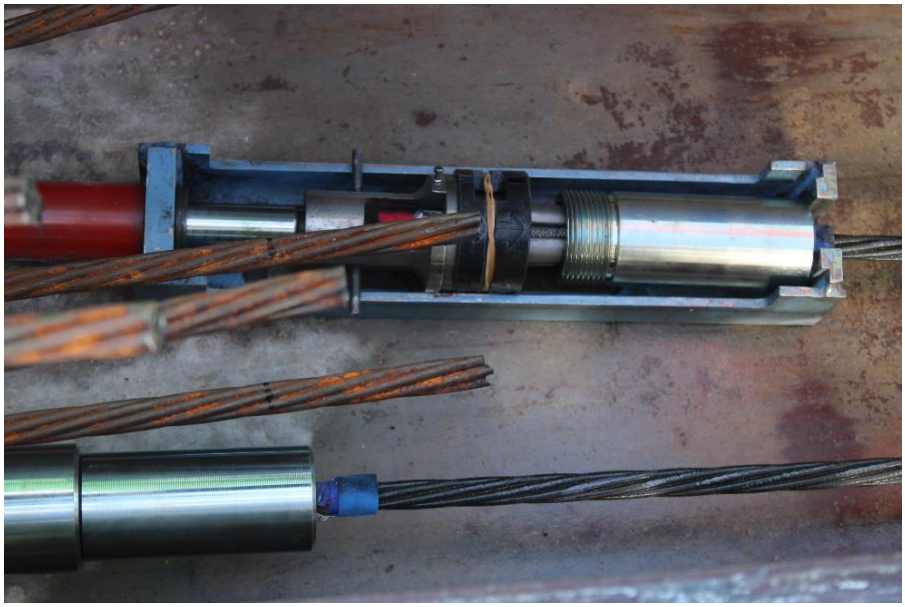

Figure 53: The steel strands (left) coupled with the CFRP stands (right)

As it was noted before, because of casting pile segments with steel and CFRP strands in the same bed, it was decided to apply the same tension force to each strand that is 35 kips. The calculated elongation corresponding to this tension force for CFRP and steel strands are shown in Table 18.

Table 18: Calculated elongations for steel and CFRP strands

Strand	Calculated Elongation		
	-5%	Target	+5%
CFRP elongation (in)	19.79	20.83	21.87
Steel elongation (in)	15.79	16.63	17.46
Total Elongation (in)	35.58	37.46	39.33

Table 19 shows the parameters used for calculation of total elongation for the CFRP strand based on TRUSA recommendations. The total elongation includes also an estimate of the wedges displacement in the CFRP anchoring device.

Table 19: Calculations for CFRP strand elongation

Symbol	Value	Unit	Description
ΔL_{CF}	19.020	in	Elongation of a CFRP
D_{WCF}	0.906	in	Insert displacement of the wedge into the sleeve while loading pre-stressing load
L_{CF}	283.000	ft	Length of CFRP
P	35.000	kips	Prestressing load
A_{CF}	0.217	sqin	Nominal effective area of CFRP
E_{CF}	2.88E+07	psi	Elastic modulus of CFRP
ΔL_{T-CF}	20.83	in	Total elongation of CFRP

The strand tensioning schedule/order is shown in Figure 54.

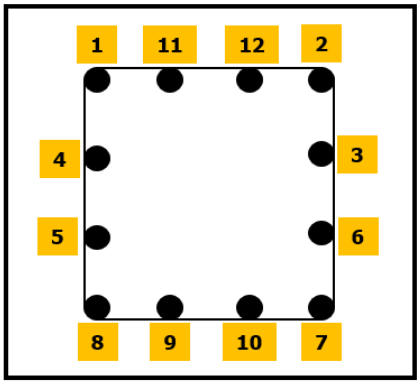

Figure 54: The stressing schedule

4.2.3 Concrete Casting

To cast all 10 piles, three truckloads of concrete were used. The top surface of the concrete was leveled to a smooth finish (Figure 55). Furthermore, cylindrical samples

were collected during the construction for future testing to determine the compressive strength of the concrete used for fabrication of the test specimens. Concrete pour for all specimens was carried out between 12:30 and 2pm on Friday, November 6, 2020. Temperature at the time of casting was in the range of 82°F to 88°F.

Figure 55: Casting concrete

4.2.4 Curing

The pile specimens were cured in the open field under ambient condition. The cylindrical samples to be used for compressive strength tests were moist cured per AASHTO R18 and ASTM C-31 specifications.

4.2.5 Cutting Strands – Strand Release

The strands were detensioned prior to removal of the forms and after the concrete cylinder tests indicated reaching the strength required for strand release per approved specifications. Detensioning was performed on Tuesday, November 10, 2020. The strand detensioning was performed per FDOT 450-11.3 by using a low-oxygen flame in

accordance with a pattern/order provided in Figure 56. The side forms were removed after strand detensioning on the same day.

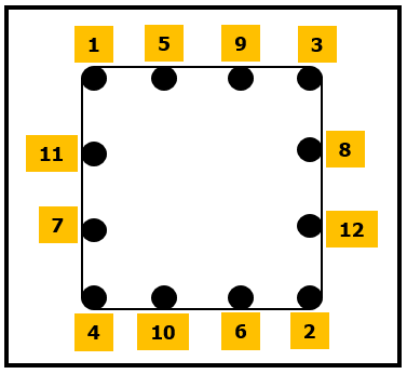

Figure 56: The detensioning schedule

Pile specimens were taken out from the casting bed on Tuesday (November 10, 2020) to be spliced after their concrete reached a minimum compressive strength of 80 percent of the nominal 28-day compressive strength.

4.3 Splicing

A total of 20- 14-ft-long prestressed precast pile segments with a 18x18 in cross-section were built at the S&S Precast, Inc. yard to be spliced based on the test matrix shown in Table 15. Figure 57 shows some of the prestressed precast pile segments.

4.3.1 Preparation

For the test specimens, holes are either cast or drilled into one end of the female pile segments to receive dowel rebars protruding out of the male pile segment. Specifically,

for the “Unforeseen Splice” specimens (Specimens 1 and 2), the holes were cast with 1 ¼ in PVC pipes, and then 1 ¾ in holes were drilled to simulate field conditions (Figure 58).

Before installation, concrete members receiving dowels were checked to be structurally sound and free of cracks in the vicinity of the holes. The interior surfaces of the holes were cleaned to be free of loose particles, oil, and other contaminants (Figure 59). For installation, all debris, oils, and any other deleterious material from dowels were first removed to avoid contamination of the adhesive bonding material. As shown in Figure 59, the pile segments were assembled in a vertical alignment to mimic the site condition. The precast contractor (S&S Precast, Inc.), established a setup to first keep the 10 female pile specimens in a vertical position. The male pile segments were then installed with the use of crane one by one. A proper lifting device and suitable locations were determined to keep the segments balanced at the splice location.

Figure 57: Pile specimens using steel (top), GFRP (middle), and CFRP (bottom) dowels

Figure 58: Drilling (top) and cleaning (bottom) the holes for Unforseen Splice specimens

Figure 59: Splice setup

To adequately fill the holes and cover the dowels with epoxy, a wooden framework was installed at the pile splice location before splicing (Figure 60).

Figure 60: Wooden framework used for splicing the pile specimens

4.3.2 Epoxy

In accordance with FDOT Standard Specification Sections 926 [47], epoxy was used to fill the interface and sockets of the lower segment (female pile) so that the dowel bars of the upper segment (male pile) could be fully enveloped with the epoxy. Type AB Epoxy-Pilgrim EM 5-2 compound was used to fill the holes and form the joint between pile sections. The final mixture of this epoxy contained the A (epoxy) + B (curing agent) and C (aggregate).

As shown in Figure 61, the kiln-dried 20-30 grade silica was used as the aggregate with the epoxy to increase its strength and reduce the potential shrinkage. In addition, some epoxy samples were collected for bond testing with concrete.

Figure 61: Epoxy mixture and sampling

The exact proportion of mixing sand with the epoxy and mixing process were determined in consultation with the FDOT project manager, the precast contractor (S&S Precast, Inc.) and the supplier (Pilgrim). Table 20 shows the details of the epoxy mixture used for the pile splicing. Two recommended ratios were used to make the final mixture by 1.5 to 1 volumes of silica to 1 volume of mixed epoxy. Because of the lower than expected temperature at the time of mixing (ranging from 61 to 77 F), the originally prescribed 1.5:1 (sand: epoxy) ratio resulted in low flowability. Therefore, it was decided to switch to 1:1 proportion. For splicing the pile specimens, different epoxy volumes were used for splicing based on the type of dowels.

Table 20: The ratio and volume of used Epoxy for the pile splicing

Pile Specimen Number	Mixture Ratio		Volume for one Round		Number of Rounds
	Epoxy	Sand	Epoxy	Sand	
1	1	1	2 gallons	2 gallons	~ 3
2	1	1	2 gallons	2 gallons	~ 3
3	1	1	2 gallons	2 gallons	~ 3
4	1	1	2 gallons	2 gallons	~ 3
5	1	1	2 gallons	2 gallons	~ 3
6	1	1.5	2 gallons	3 gallons	~ 3
7	1	1.5	2 gallons	3 gallons	~ 2
8	1	1	2 gallons	2 gallons	~ 2
9	1	1	2 gallons	2 gallons	~ 4
10	1	1	2 gallons	2 gallons	~ 4

4.3.3 Splicing

Piles were spliced with particular attention to the requirements and limitations due to ambient temperature and curing. As shown in Figure 62, adequate quantities of the epoxy were used to fill the drilled hole and the joint between segments at the splice to ensure no air voids. Table 21 shows the details and conditions of the pile splicing for all specimens.

Table 21: Detailed conditions at splicing time

Specimen Number	Splicing Date	Weather Conditions	Moving date	Weather Conditions	Days Curing	Dunnage type
1	Tue, Dec. 15, 2020	75°, wind 4.9 mph W, overcast	Sat, Dec 19,02020	75°, wind 7.5 mph ESE, sunny	4	wood, 4 points
2	Mon, Dec. 14, 2020	77°, wind 9.3 mph SSW, cloudy	Sat, Dec 19,02020	75°, wind 7.5 mph ESE, sunny	5	wood, 4 points
3	Tue, Dec. 8, 2020	61°, wind 11.8 mph NW, sunny	Wed, Dec. 16, 2020	81°, wind 10.5 mph S, sunny	8	wood, 4 points
4	Thu, Dec. 10, 2020	72°, wind 4.9 mph N, sunny	Sat, Dec 19,02020	75°, wind 7.5 mph ESE, sunny	9	wood, 4 points
5	Wed, Dec. 9, 2020	64°, wind 4.9 mph N, sunny	Fri, Dec 18, 2020	68°, wind 10.5 mph NE, clear	9	wood, 4 points
6	Wed, Dec. 2, 2020	70°, wind 11.8 mph NE, sunny	Wed, Dec. 16, 2020	81°, wind 10.5 mph S, sunny	14	wood, 4 points
7	Tue, Dec. 1, 2020	66°, wind 8.0 mph N, cloudy	Wed, Dec. 16, 2020	81°, wind 10.5 mph S, sunny	15	wood, 4 points
8	Sat, Dec. 12, 2020	79°, wind 6.2 mph SW, cloudy	Fri, Dec 18, 2020	68°, wind 10.5 mph NE, clear	6	wood, 4 points
9	Fri, Dec. 11, 2020	73°, wind 9.30 mph ENE, sunny	Sat, Dec 19,02020	75°, wind 7.5 mph ESE, sunny	8	wood, 4 points
10	Fri, Dec. 4, 2020	77°, wind 9.3 mph SE, sunny	Wed, Dec 16, 2020	81°, wind 10.5 mph S, sunny	12	wood, 4 points

Figure 62: Filling the holes by epoxy and assembling pile specimens

4.3.4 Storage and Shipping

The piles, once spliced, were left standing for a minimum of seven days for the epoxy to be fully cured, and then all spliced piles were lowered and placed on multiple supports, with two near the ends and two straddling the splice section in close proximity (Figure 63). The contractor used bridles, slings and other required handling equipment for supporting the splices during storage and shipment.

Figure 63: The spliced specimens

Nine cylindrical specimens for each batch of concrete were collected to determine the compressive strength at the time of flexural testing. The cylinders were tested at 28 days, and at the time of splice flexural testing. Cube samples of epoxy compound were also prepared and shipped to the laboratory for testing. Moreover, five 6 ft bars for each size and type of bars (steel and GFRP), as well as strand pieces for each size and type (steel and CFRP), were collected for tension testing.

4.4 Testing

As shown in Figure 64, the assembled test specimens were installed in the test setup with extreme caution to avoid damage to the splice section. This testing program focused on the global behavior and flexural capacity of the epoxy dowel splices. The test specimens were instrumented to capture the flexural behavior of the splice.

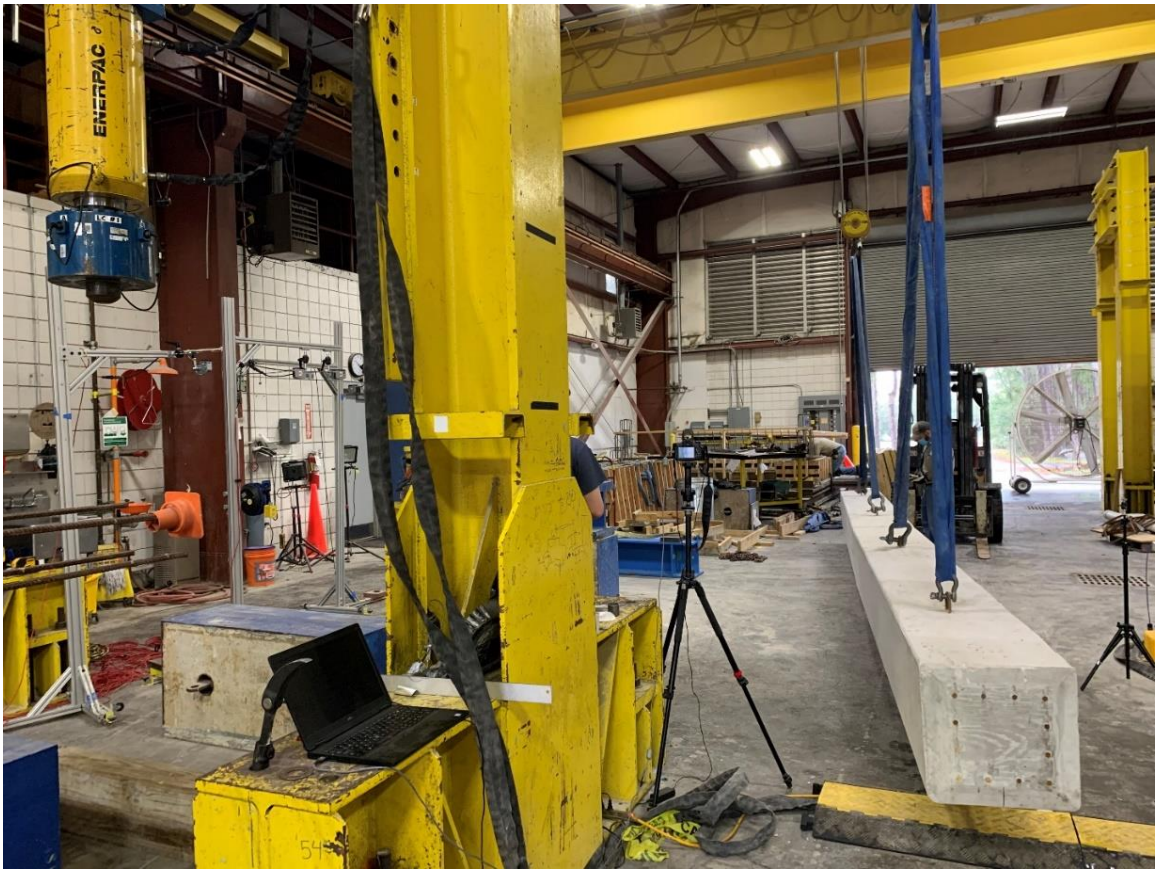

Figure 64: Test specimen installation

4.4.1 Instrumentation

Figures 65 and 66 show the schematic of the test setup and instrumentation from different views. The test setup and instrumentation with precise scale were also designed in

AutoCAD (Appendix B). The spliced specimens with a length of 28 ft were supported at the ends with the help of neoprene bearing pads, with the center of pads located 6in from the end of the specimen to produce a 27-ft overall bending span. A two-point loading scheme was used at an equal distance of 3'3" from the splice section. The distance between the loads was determined to be 6' 6" according to the spreader beam configuration available at the FDOT SRC laboratory.

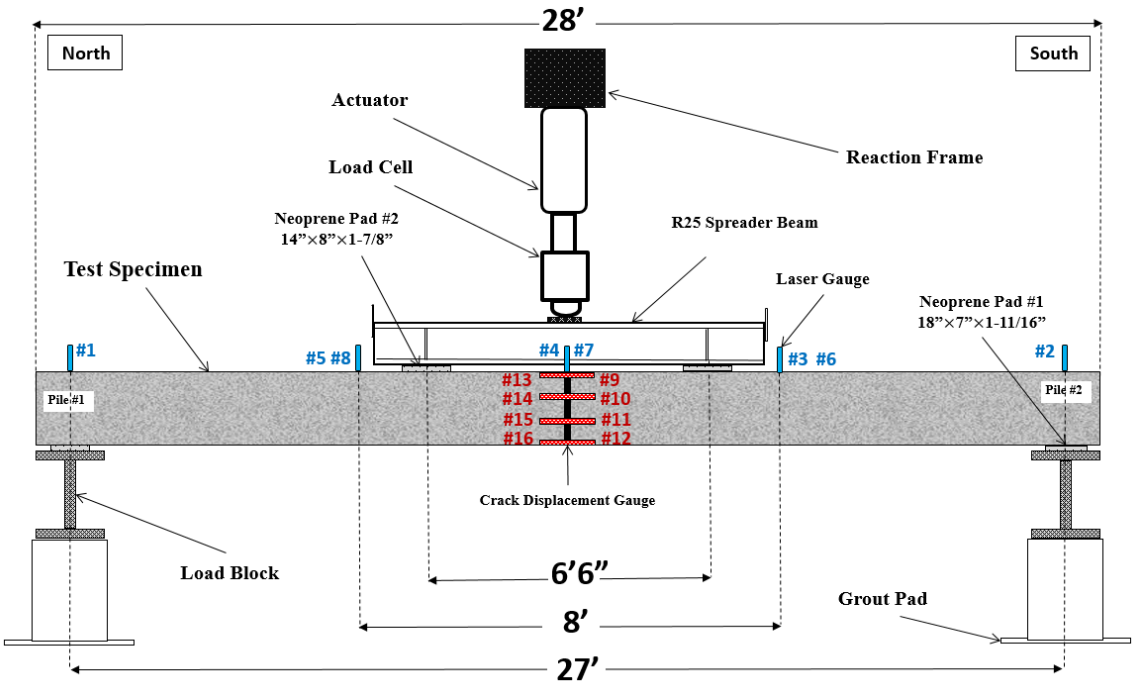

Figure 65: Instrumentation of the front view of test specimen

Eight crack displacement transducers (#9 through #16 in Fig. 21), four on each face of specimen. with equal distance (5in) were used to measure the potential crack development at the joint. Furthermore, six laser displacement sensors (#3 through #8 in Fig. 21) were installed on frames above the specimen and pointing to the top of the

specimen. Two of these sensors were installed on both sides of the splice section, and four (two on each side) with a distance of 4 ft from the splice section. Two laser displacement (#1 and #2 in Figure 66), one at each end of the specimen were also installed pointing to the top of the specimen immediately over the bearing pads to measure any displacement at the support locations. This arrangement of the laser transducers was used to obtain the deflected shape of the pile during its loading.

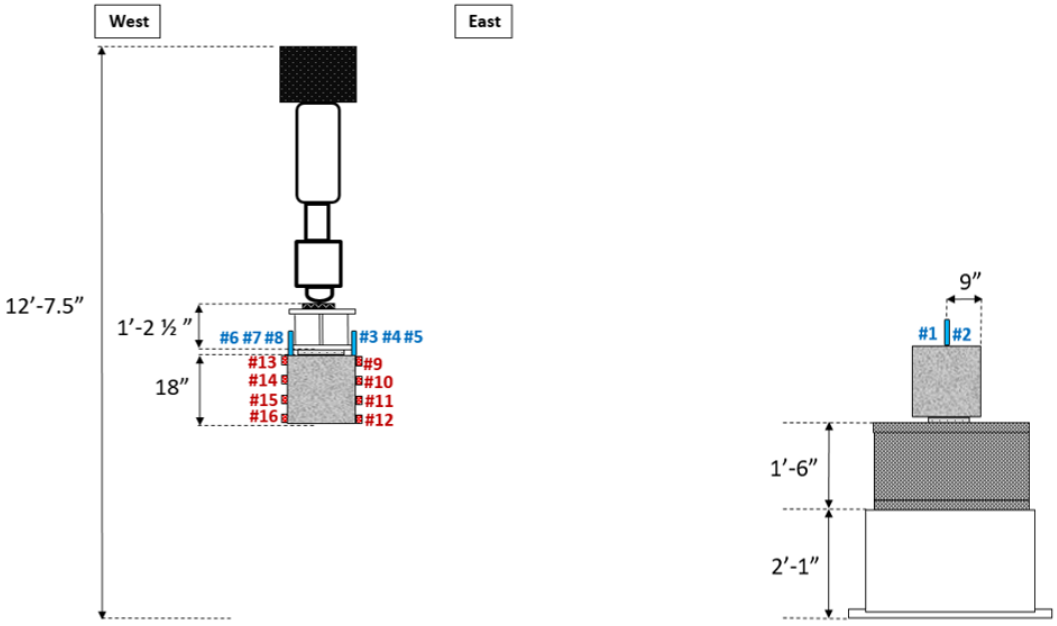

Figure 66: Instrumentation of the side view of test specimen at middle (left) and bottom (right) locations

4.4.2 Flexural Capacity of the Test Specimens

Figure 67 shows the moment diagram for a simply-supported beam with two-point loads, in which the maximum moment is expressed by Eq. (83).

$$M_{max} = \frac{P}{2} * a \tag{83}$$

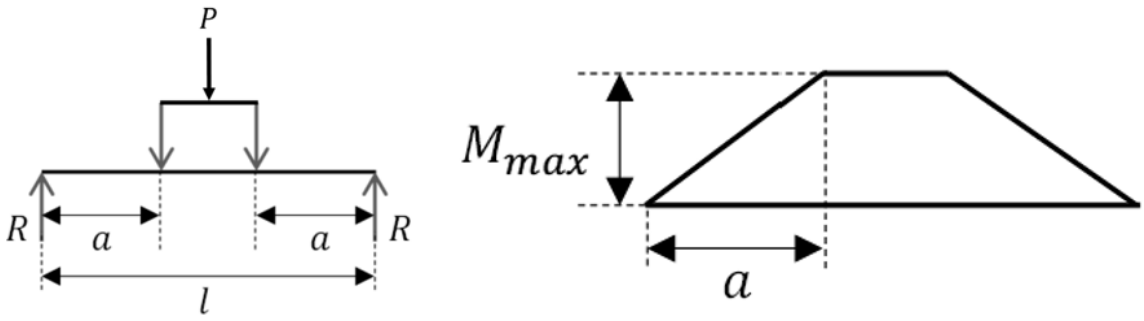

Figure 67: Moment diagram for two-point loading

The cracking moment was calculated to be 47.06 k-ft for an 18x18 in pile section. To calculate the cracking load, the self-weight moment of the system must be subtracted from the cracking moment. The moment corresponding to self-weight of the pile is shown below.

$$W_{sw} = 2.25 \times 145 \text{ lb/ft}^3 = 326.25 \text{ lb/ft} \tag{84}$$

$$M_{sw} = \frac{\left(326.25 \frac{\text{lb}}{\text{ft}}\right)(27)^2}{8} = 29.7 \text{ k-ft} \tag{85}$$

The weight of the spreader beam that is below the load cell needs to be also considered. The moment added from the weight of the spreader beam is shown below.

$$M_{sb} = \frac{\left(109 \frac{\text{lb}}{\text{ft}}\right)(8 \text{ ft})(10.25 \text{ ft})}{2} = 4.47 \text{ k-ft} \tag{86}$$

Adding this moment to the moment from the self-weight of the specimen results in a total dead-weight moment of 34.17. This moment must be added to the moment from loading measured by the load cell to obtain the total moment capacity from testing.

The cracking load, P_{cr}, corresponds to cracking moment, M_{cr}, of the splice section. Using Eq. 87, the total applied load corresponding to the cracking moment is estimated to be 3.38 kips.

$$P_{cr} = \frac{2(Mcr - Msw)}{a} = \frac{2\times(47.06-34.17)}{10.25} = 2.51 \text{ kips} \quad (87)$$

At the point of the cracking moment, the maximum tensile stress is considered to be f_t (Eq. 88).

$$f_t = 7.5\sqrt{f_c'} = \frac{7.5*\sqrt{6000}}{1000} = 0.581 \text{ ksi} \quad (88)$$

To estimate the Ultimate Load, the maximum moment resistance calculated in Chapter 3 of this dissertation was used. Maximum moment resistances (before application of the resistance factor) for various types of dowel material for 18x18 in piles splices are listed in Table 22. To calculate the estimated ultimate load, the self-weight of the system must be added to the moment from the applied load and set equal to the estimated moment resistance (Eq. 89).

$$P = \frac{2(Mn - Msw)}{a} \quad (89)$$

During the laboratory bending tests of the splice pile specimens, the average compressive strength of eighteen (18) cylindrical samples was obtained to be 7,336 psi. From section analysis of the test specimens, the nominal moment strength of the splice sections was calculated for both nominal concrete strength (6.5 ksi) and actual average concrete strength at the time of testing (7.3 ksi) using formulation developed in Chapter 3 and are included in Column 3 of Table 22. The ultimate loads corresponding to these moment capacities taking into account the self-weight were calculated and are shown in Column 4 of Table 22.

Table 22: Ultimate loads of the test specimens from section analysis

Dowel Material	Concrete Strength	Estimated Moment Resistance	Estimated Ultimate Load
GFRP	6.5 ksi	222.74 k-ft	36.79 kips
	7.3 ksi	233.26 k-ft	38.84 kips
CFRP	6.5 ksi	198.02 k-ft	31.97 kips
	7.3 ksi	207.2 k-ft	33.76 kips
Steel	6.5 ksi	305.1 k-ft	52.86 kips
	7.3 ksi	323.4 k-ft	56.43 kips

To have a better expectation from pile splice behavior in this laboratory test, the estimated deflections at failure were calculated for both steel- and FRP-based pile specimens (Table 23).

Table 23: Estimated deflection at failure of the test specimen

Dowel Material	Total Deflection		
Steel	Yield deflection=3.01 “	Plastic Load=0.158 “	Total= ~ 4“
FRP	Pre-crack Deflection=0.64“	Post-crack Deflection=4.92”	Total= ~ 6“

4.4.3 Loading Procedure

Three load levels were used as references during the flexural testing. The “Initial Loading” is a low-level loading that is used to set the test setup before taking initial readings of the instrumentation. The “Cracking Load” is a load level at which the first flexural cracking is expected to occur and the load-deflection curve deviates from the linear elastic (Figure 68). The “Ultimate Load” refers to the maximum load in flexural testing that corresponds to the Maximum Moment Resistance of the section.

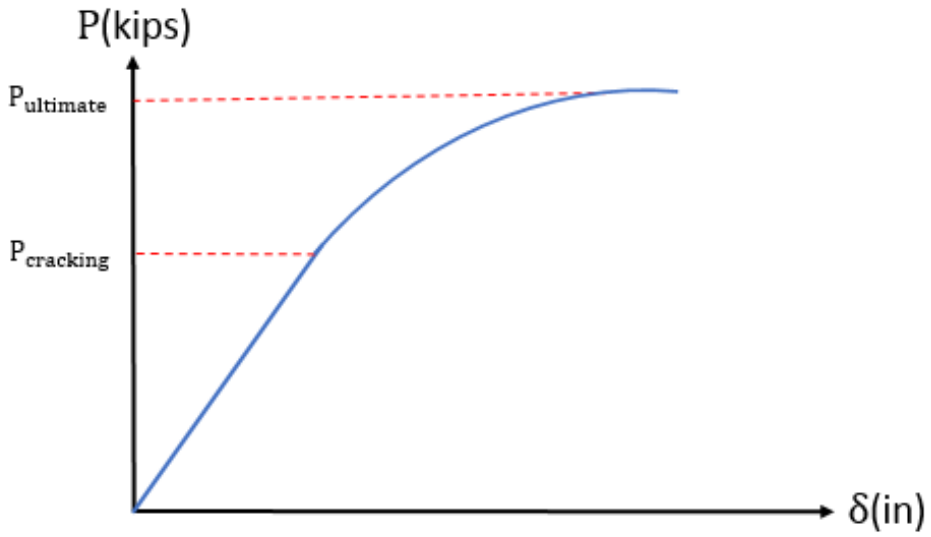

Figure 68: Schematic applied load against deflection in flexural testing

A 1-kip load was initially applied and removed to set the supports. Initial readings were taken at this interval. Then, the applied load was increased at stages with different load rates and intervals to investigate the cracking and failure load and deflection at pile splice, as shown in Tables 24 and 25. The specimens were inspected at each load interval, cracks were mapped and photos were taken.

Table 24: Loading details for test specimens using GFRP and CFRP Dowels (Specimens 1, 2, 3, 4, 5, 6, 9, and 10)

Steps	Start Load	End Load	Load Rate
Initial Loading	0 kips	1 kips	150 lbs/s
Initial Loading	1 kips	0 kips	150 lbs/s
1	0 kips	5 kips	150 lbs/s
2	5 kips	10 kips	100 lbs/s
3	10 kips	20 kips (Gauge Removal)	100 lbs/s
4	20 kips	Failure Load	100 lbs/s

Table 25: Loading details for test specimens using Steel Dowel (Specimens 7 and 8)

Steps	Start Load	End Load	Load Rate
Initial Loading	0 kips	1 kips	150 lbs/s
Initial Loading	1 kips	0 kips	150 lbs/s
1	0 kips	5 kips	150 lbs/s
2	5 kips	10 kips	100 lbs/s
3	10 kips	20 kips	100 lbs/s
4	20 kips	30 kips (Gauge Removal)	100 lbs/s
5	30 kips	Failure Load	100 lbs/s

CHAPTER 5: TEST RESULTS AND DISSCUSION

This chapter presents the results that were obtained from the experimental test performed at the FDOT structures lab based on the proposed experimental program. The main purpose of this experimental program was to determine the flexural strength of different pile splices. Another purpose was to determine the development length of the proposed FRP dowels. Figure 69 shows the test setup with a spliced pile specimen. The equipment type and instrumentation arrangement were set based on discussions with the FDOT Project Manager (PM), equipment availability at the FDOT structures lab, and prior similar test setups.

Figure 69: The test setup

As shown in Figure 70, for each specimen, an inspection sheet was filled out in detail, and the specimens were photographed.

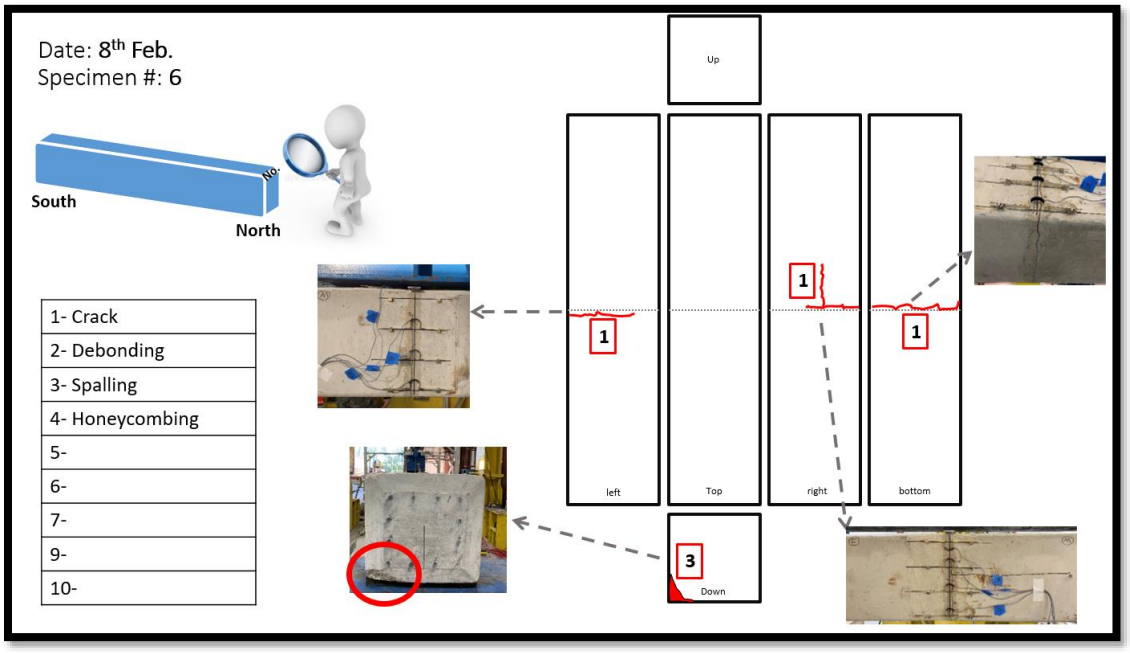

Figure 70: An example of the inspection sheet

5.1 Laboratory Tests

The experimental program was scheduled to test about one pile per day during a two-week time period. Before the experimental test, all pile specimens were inspected for cracks, debonding, and spalling caused by shipping. Data from instrumentations were collected at an acceptable frequency, e.g., 10 per second, and stored in a data acquisition system. According to the loading procedure, the test was paused at each loading interval to inspect the specimen for cracks, openings and other events. The cracks and openings were traced and marked with an identifying designation. Photographs were taken at the end of each pause.

The entire test process was videotaped. After the completion of each test, the data was processed to obtain plots for:

- **Load-displacement**: In this plot, deflection is the average of readings from Gauges #4 and #7 (at mid span), minus the average of readings from Gauges #1 and #2 (at two ends) (Figure 65). The load is the reading from the load cell.

- **Load-deflection profile**: The average of readings from Gauges #3 and #6, #4 and #7, and #5 and #8, minus the average of readings from Gauges #1 and #2, provides the deflection profile of the specimen.

- **Crack-opening profile**: In this plot, the crack opening over the section depth of the pile splice is the average of readings from Gauges #9 and #13, #10 and #14, #11 and #15, and #12 and #16 (Figure 65).

- **Load-crack opening**: This plot shows the crack-opening behavior of the pile splice corresponding to the average of readings from Gauges #9 and #13 (Level 1), #10 and #14 (Level 2), #11 and #15 (Level 3), and #12 and #16 (Level 4).

5.1.1 Specimen 1

In Specimen 1, a crack was observed in the splice section prior to the test setup. In this test, the first new flexural crack was observed at the splice section at Step 1, load $\leq$ 5 kips. Moreover, the first splitting crack (near-horizontal crack) was detected at Step 2

(load ≤10 kips) at the level of the lowest set of strands. As the load increased, more splitting cracks developed on both sides of the splice section at the level of the lowest strand and midsection. These cracks extended farther until the specimen reached its maximum load at 28.09 kips with concrete crushing at the top of the section in the female segment, 2 ft from the splice section. This is in the proximity of the end of the dowel's length (2ft, 6 in). Prior to the concrete crushing, horizontal and vertical cracks showed large openings consistent with splitting due to bond failure. Figure 71 shows the failure mode and crack pattern for this test specimen. The maximum moment capacity was calculated for this specimen to be 178.13 k-ft, taking into account the moment from the self-weight of the specimen and the spreader beam.

Figure 71: Crack propagation and failure mode of Specimen 1

Dissection after testing showed that there is no major misalignment with the holes drilled in the female segment and their corresponding dowels in the male segment (Figure 72).

Figure 72: A photo of the Specimen 1 after test

For Specimen 1, the load-displacement curve, load-deflection profile, crack-opening profile, and load-crack opening curve were plotted, as shown in Figures 73-76, respectively.

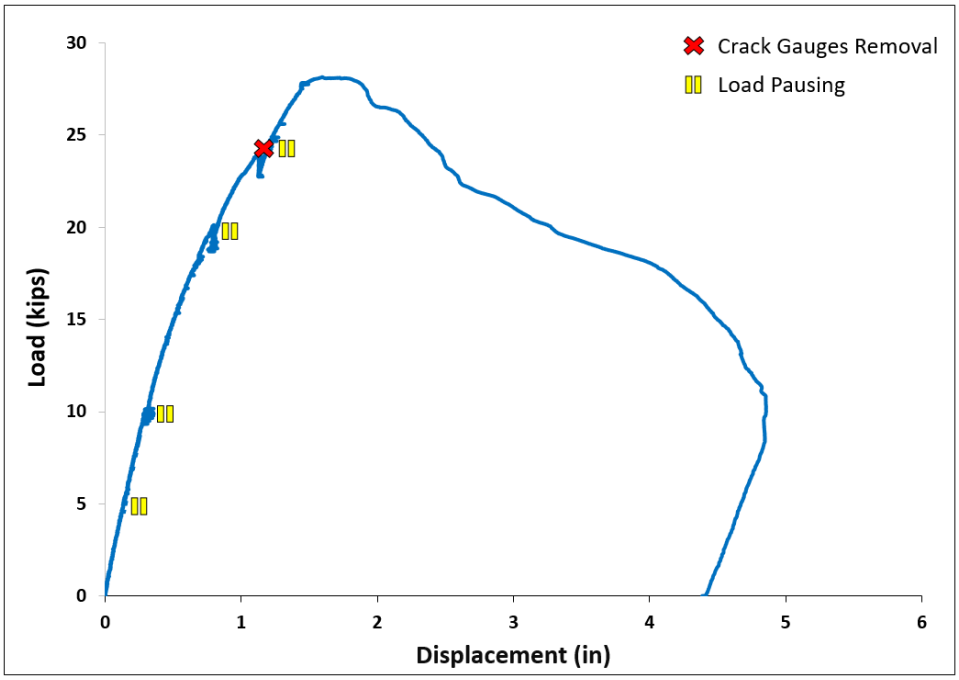

Figure 73: Load-displacement curve for Specimen 1

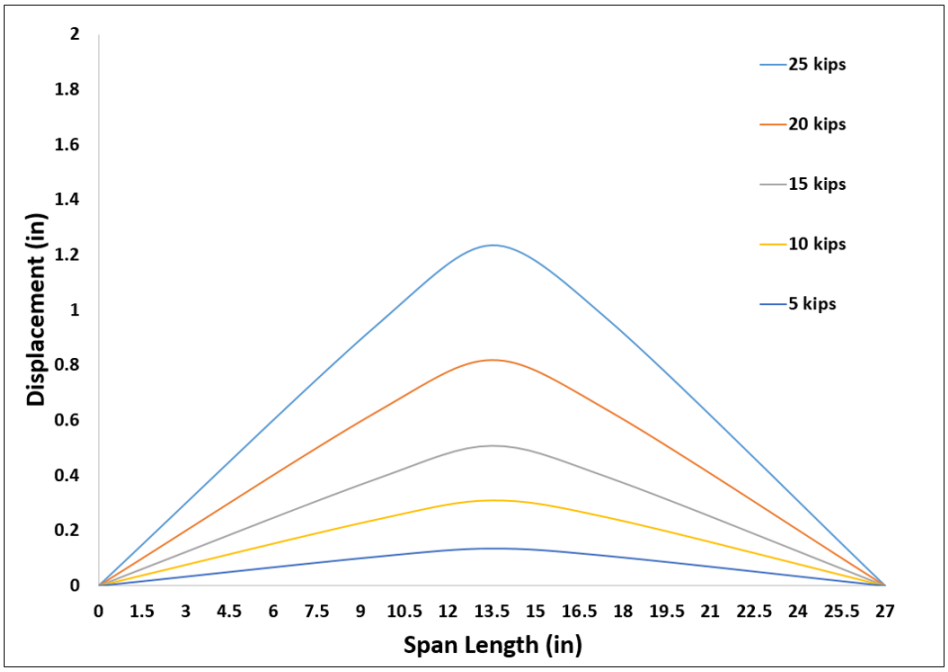

Figure 74: Load-deflection profile for Specimen 1

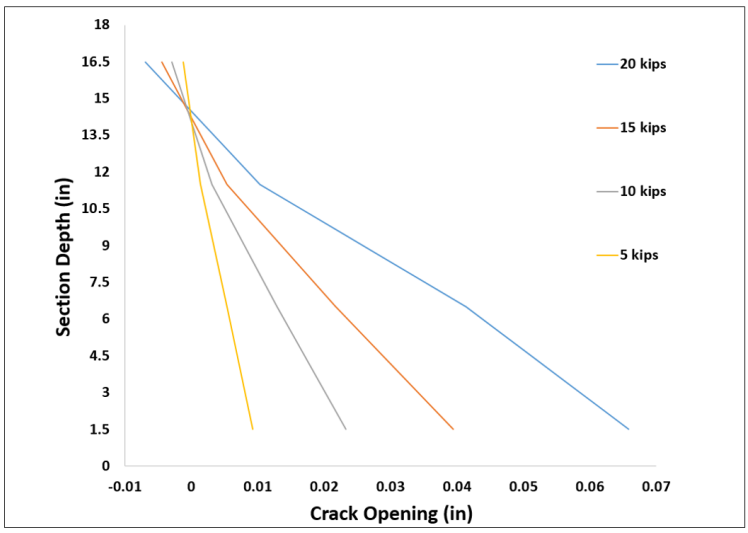

Figure 75: Crack-opening profile for Specimen 1

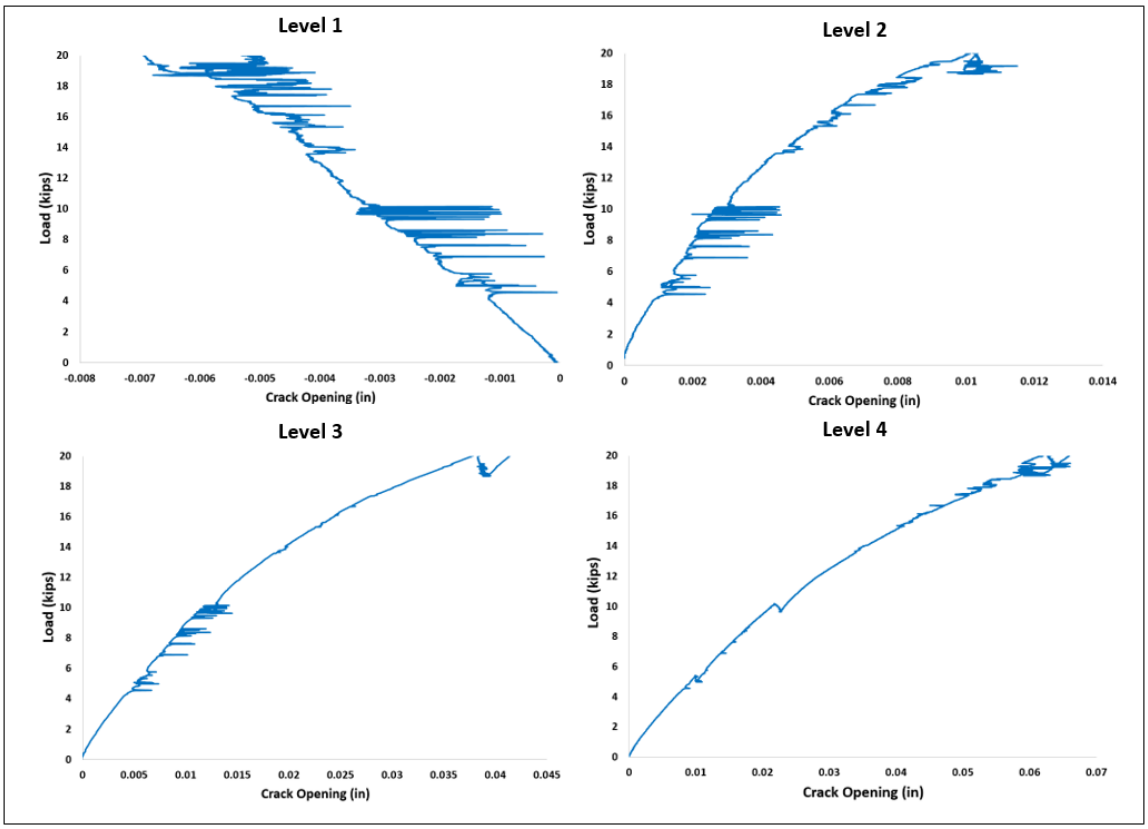

Figure 76: Load-crack opening curves for Specimen 1

5.1.2 Specimen 2

In Specimen 2, a crack was observed in the splice section prior to the test setup. In this test, the first new flexural crack was observed in the splice section at Step 1, load ≤ 5 kips. Moreover, the first splitting crack was detected at Step 2 (load ≤10 kips) at the second level of strands from the top, the second level of strands from the bottom, and at the midsection level. As the load increased, additional splitting cracks developed on both sides of the splice section. These cracks extended farther until the specimen reached its maximum load at 20.53 kips with a large opening consistent with splitting due to bond failure at the bottom of the section in the female segment. Figure 77 shows the failure mode and crack pattern for this test specimen.

Figure 77: Crack propagation and failure mode of Specimen 2

The maximum moment capacity was calculated for this specimen to be 139.38 k-ft, taking into account the moment from the self-weight of the specimen and the spreader beam.

Dissection after testing revealed some issues with the holes drilled in the female segment to receive the dowels. Apparently, secondary drilling was performed to align with the dowels. Figure 78 shows the oversized slanted hole. It is also clear from this figure that the splitting cracks in concrete have bridged the oversized hole, likely resulting in lower over strength for the specimen.

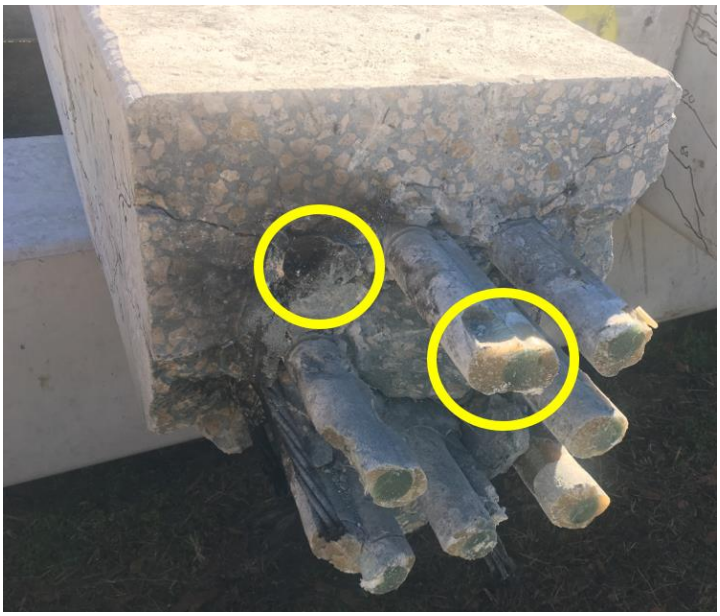

Figure 78: The oversized slanted holes

For Specimen 2, the load-displacement curve, load-deflection profile, crack-opening profile, and load-crack opening curve were plotted, as shown in Figures 79-82, respectively.

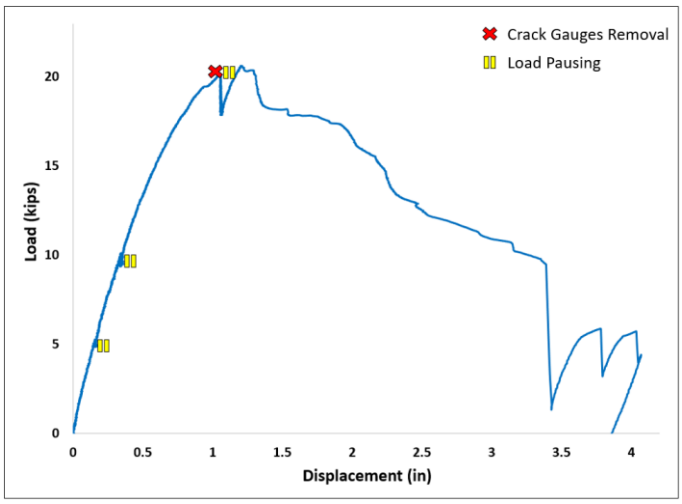

Figure 79: Load-displacement curve for Specimen 2

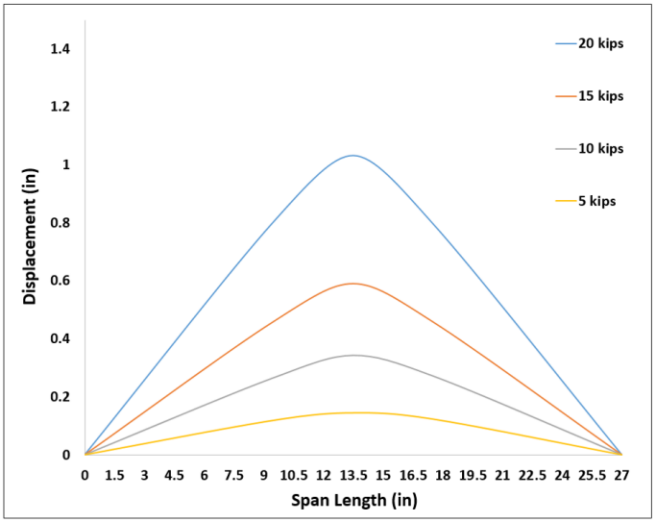

Figure 80: Load-deflection profile for Specimen 2

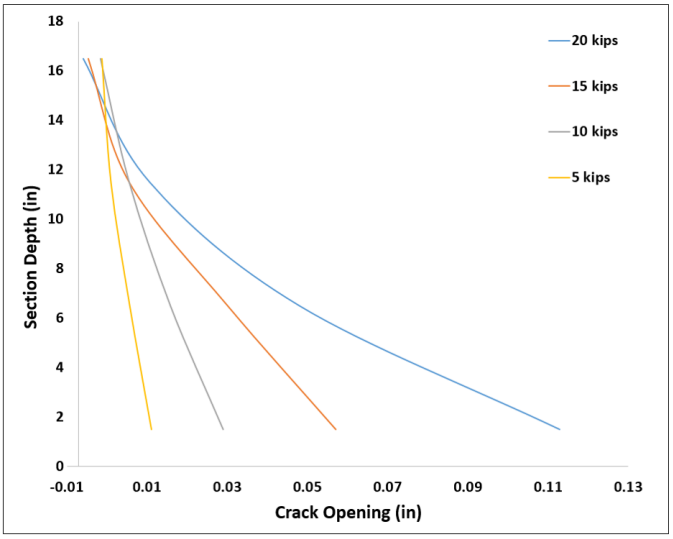

Figure 81: Crack-opening profile for Specimen 2

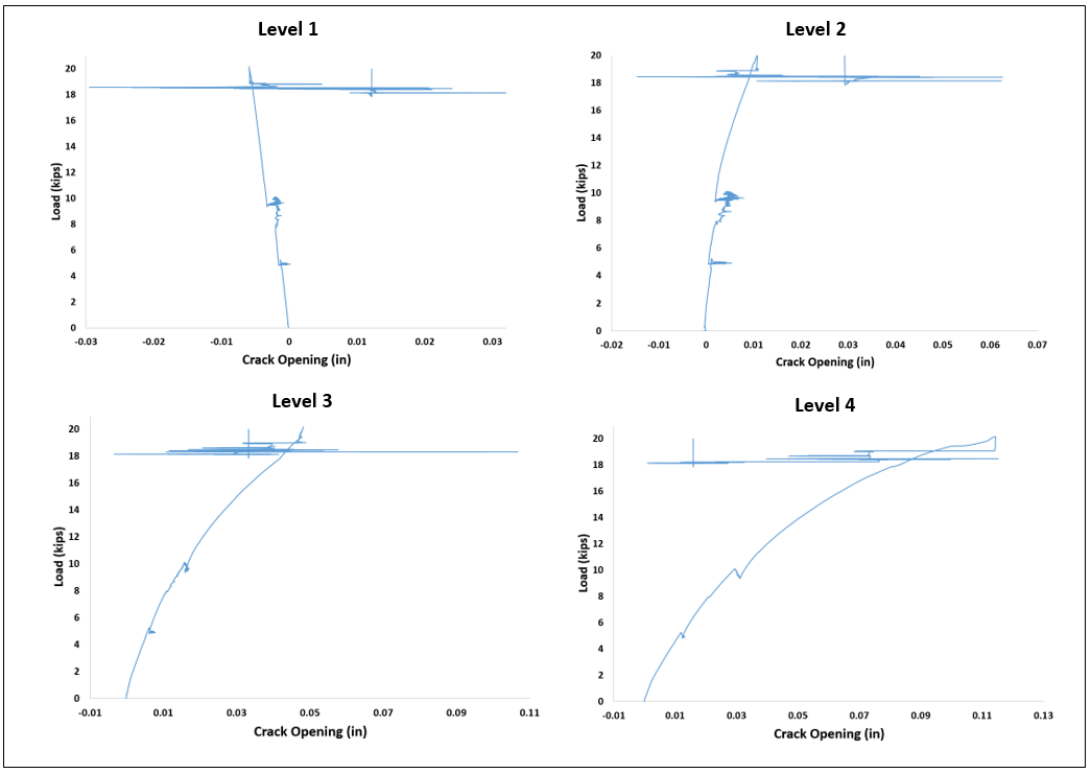

Figure 82: Load-crack opening curves for Specimen 2

5.1.3 Specimen 3

In Specimen 3, a crack was observed in the splice section prior to the test setup. In this test, the first new flexural crack was observed in the splice section at Step 1, load ≤ 5 kips. Moreover, the first splitting crack was detected at Step 2 (load ≤10 kips) at the first and second levels of strands from the bottom of the section. As the load increased, additional splitting cracks developed on both sides of the splice section. These cracks extended farther until the specimen failed at 41.72 kips with concrete crushing at the top of the pile at the splice section. Figure 83 shows the failure mode and crack pattern for this test specimen. The maximum moment capacity was calculated for this specimen to be 247.98 k-ft, taking into account the moment from the self-weight of the specimen and the spreader beam.

Figure 83: Crack propagation and failure mode of Specimen 3

For Specimen 3, the load-displacement curve, load-deflection profile, crack-opening profile, and load-crack opening curve were plotted, as shown in Figures 84-87, respectively.

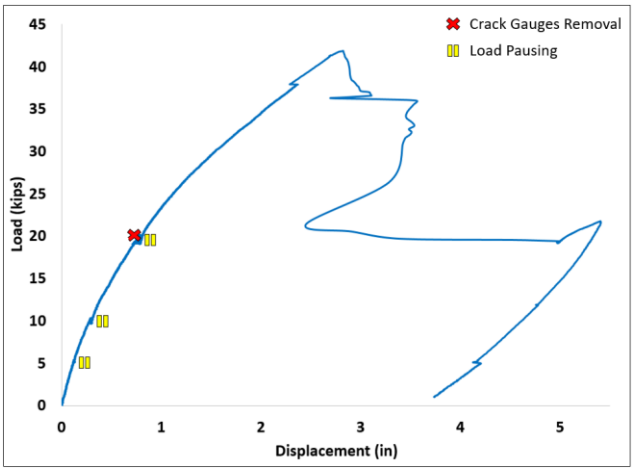

Figure 84: Load-displacement curve for Specimen 3

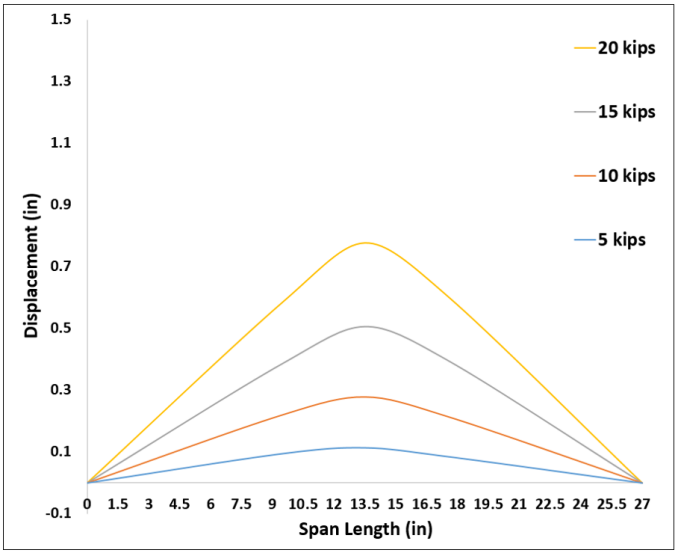

Figure 85: Load-deflection profile for Specimen 3

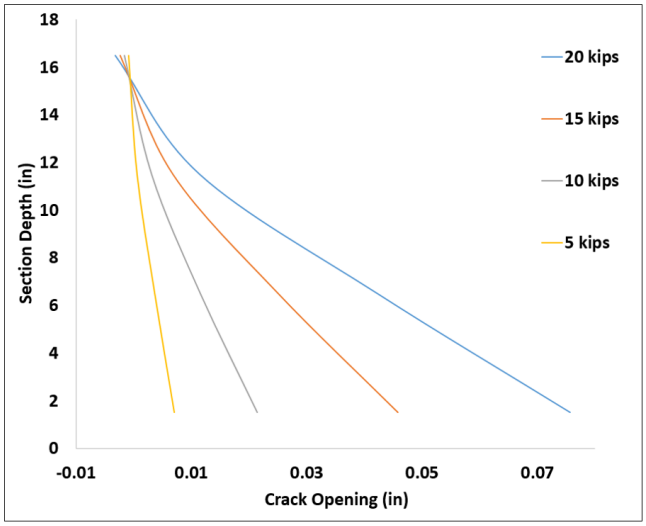

Figure 86: Crack-opening profile for Specimen 3

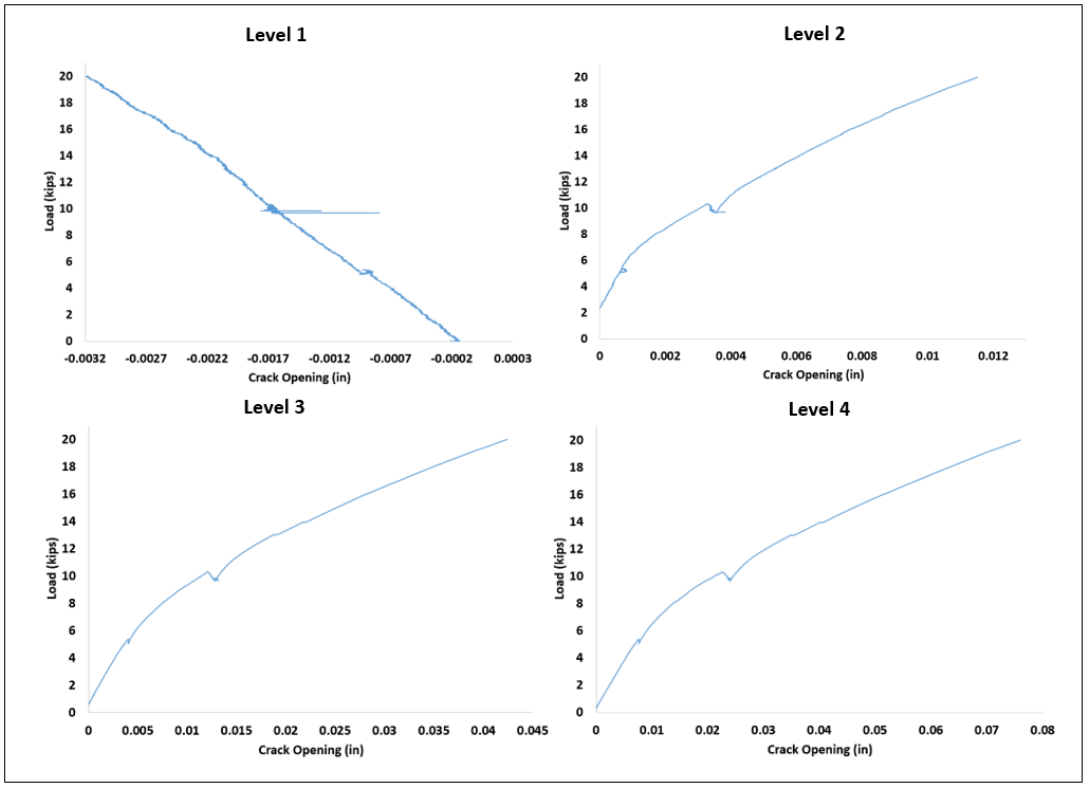

Figure 87: Load-crack opening curves for Specimen 3

5.1.4 Specimen 4

In this specimen, a crack was observed in the splice section prior to the test setup. In this test, the first new flexural crack was observed in the splice section at Step 1, load ≤ 5 kips. Moreover, the first splitting crack was detected at Step 2 (load ≤10 kips) at the second level of strands from the bottom of the section. As the load increased, additional splitting cracks developed on both sides of the splice section. These cracks extended farther until the specimen failed at 41.26 kips with concrete crushing at the top of the pile at the splice section. Figure 88 shows the failure mode and crack pattern for this test specimen. The maximum moment capacity was calculated for this specimen to be 245.62 k-ft, taking into account the moment from the self-weight of the specimen and the spreader beam.

Figure 88: Crack propagation and failure mode of Specimen 4

For Specimen 4, the load-displacement curve, load-deflection profile, crack-opening profile, and load-crack opening curve were plotted as shown in Figures 89-92, respectively.

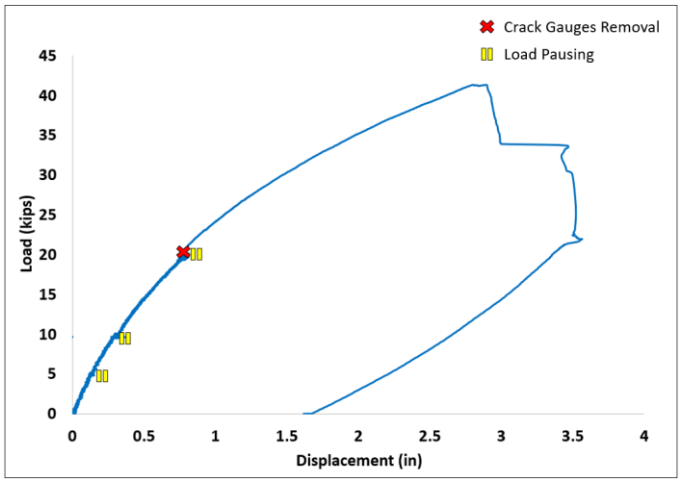

Figure 89: Load-displacement curve for Specimen 4

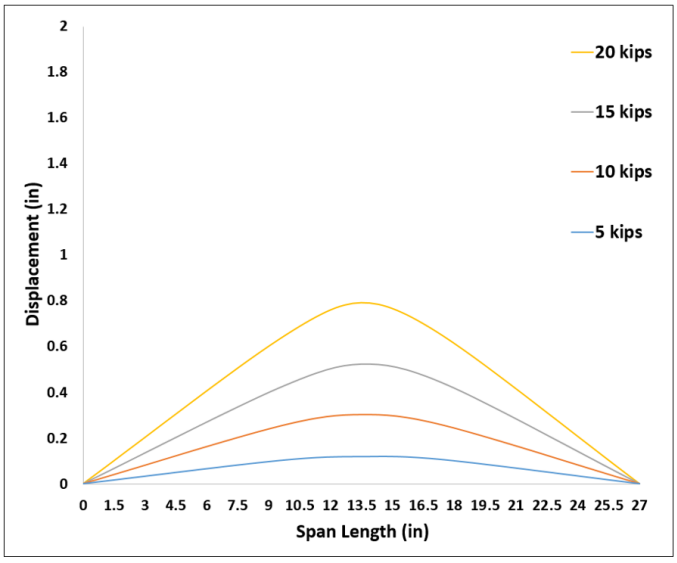

Figure 90: Load-deflection profile for Specimen 4

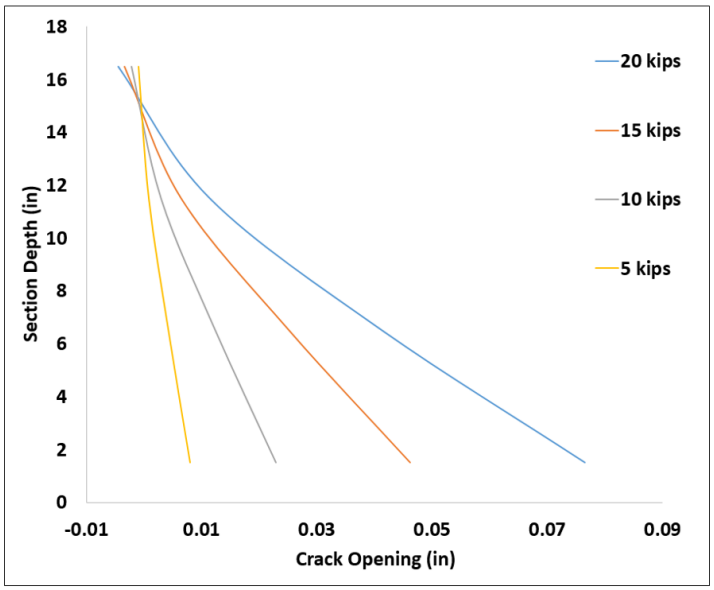

Figure 91: Crack-opening profile for Specimen 4

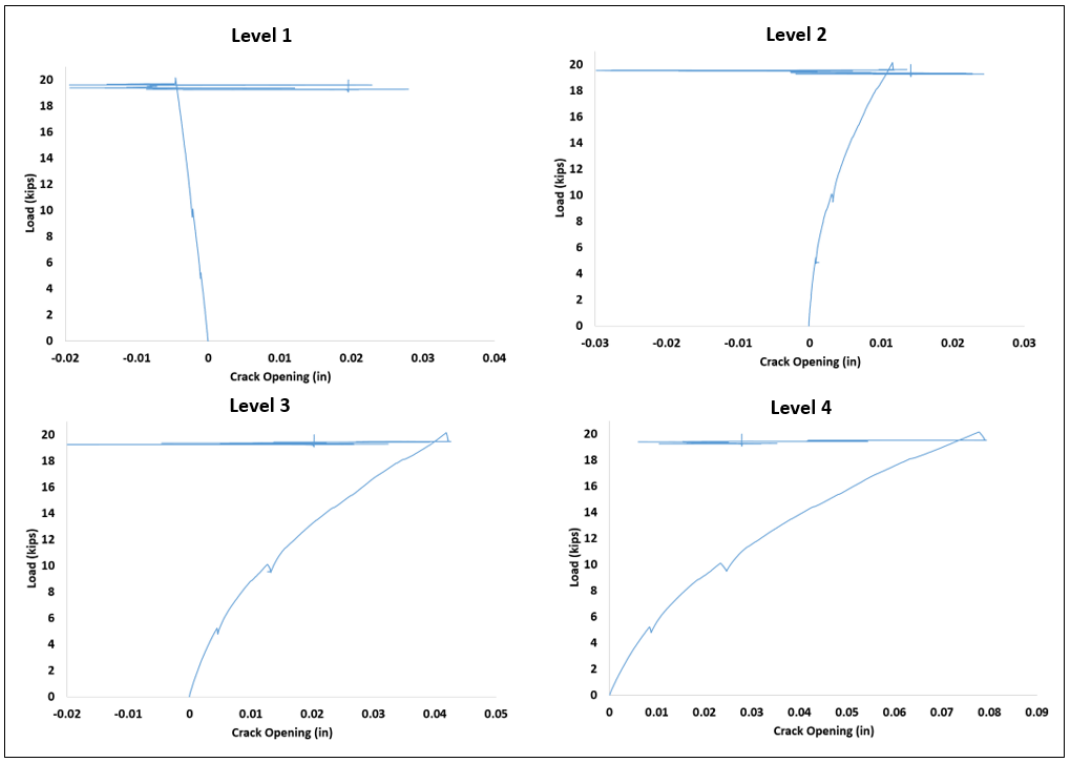

Figure 92: Load-crack opening curves for Specimen 4

5.1.5 Specimen 5

In Specimen 5, a crack was observed in the splice section prior to the test setup. In this test, the first splitting crack was detected at Step 1 (load ≤5 kips) in the midsection. Moreover, the first flexural crack was observed in the splice section at Step 2 (load ≤10 kips). As the load increased, additional splitting cracks developed on both sides of the splice section. These cracks extended farther until the specimen failed at 44.66 kips with a large opening in the male segment, 4ft and 6in from the splice section, which is in the proximity of the end of the dowel's length. The test was continued until the concrete crushed at the top of the section in the male segment at 29.95 kips. Figure 93 shows the failure mode and crack pattern for this test specimen. The maximum moment capacity was calculated for this specimen to be 263.05 k-ft, taking into account the moment from the self-weight of the specimen and the spreader beam.

Figure 93: Crack propagation and failure mode of Specimen 5

For Specimen 5, the load-displacement curve, load-deflection profile, crack-opening profile, and load-crack opening curve were plotted, as shown in Figures 94-97, respectively.

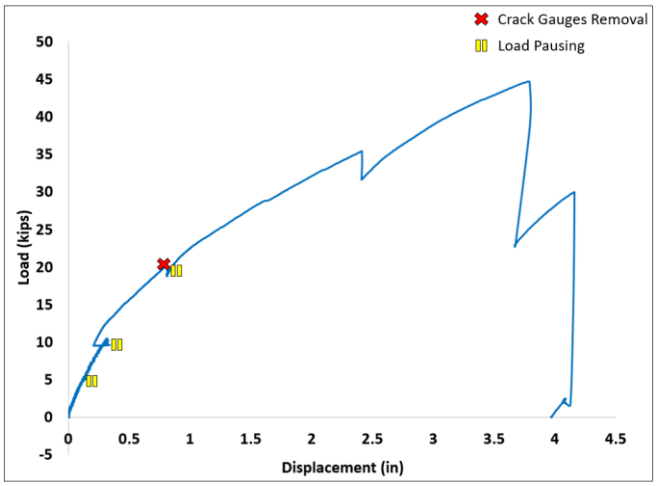

Figure 94: Load-displacement curve for Specimen 5

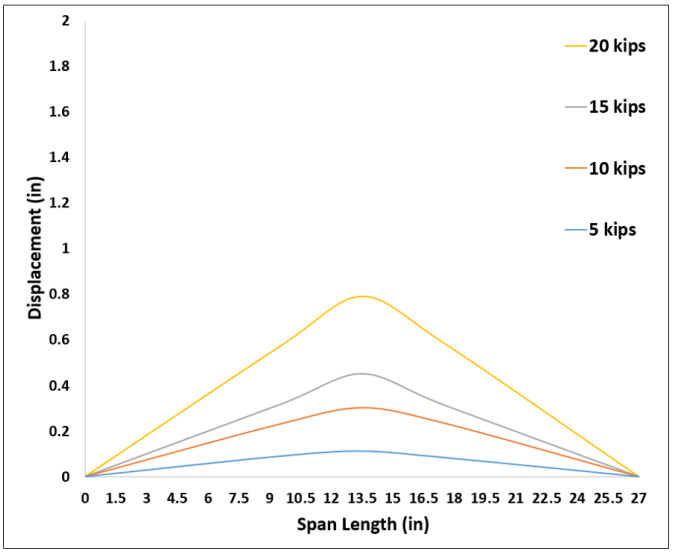

Figure 95: Load-deflection profile for Specimen 5

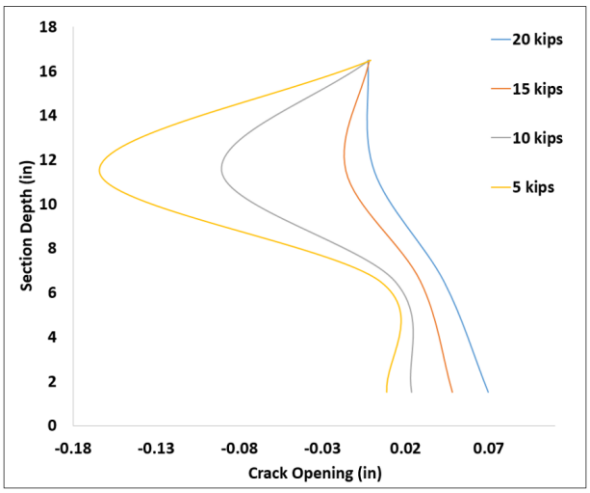

Figure 96: Crack-opening profile for Specimen 5

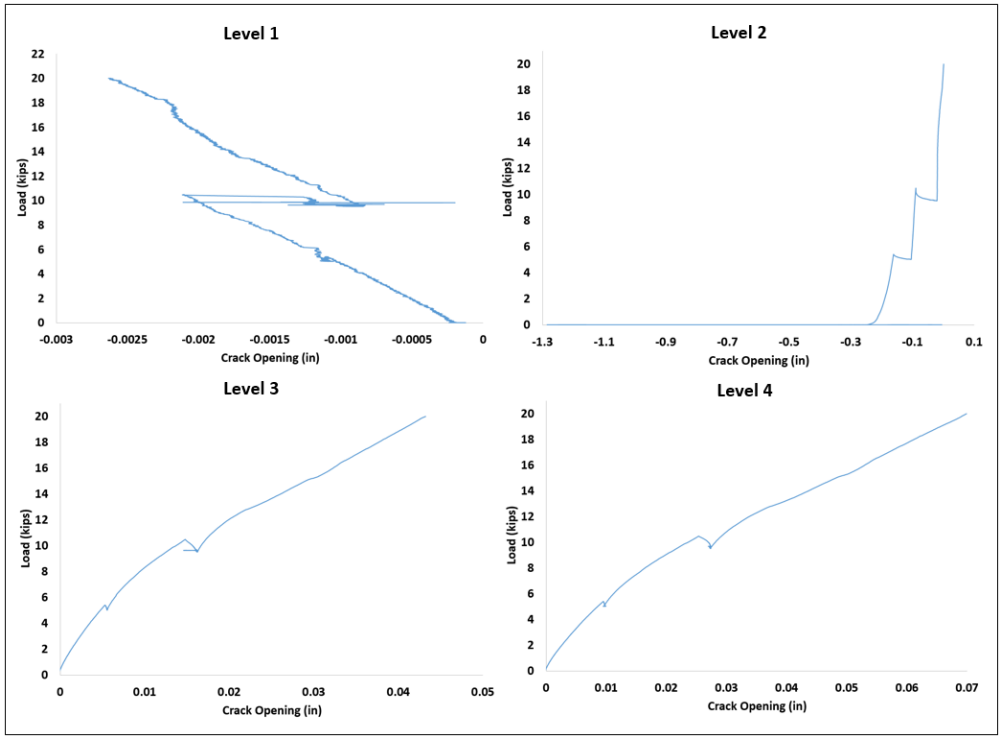

Figure 97: Load-crack opening curves for Specimen 5

5.1.6 Specimen 6

In this specimen, a crack was observed in the splice section prior to the test setup. In this test, the first splitting crack was detected at Step 2 (load ≤10 kips) in the upper level of the dowel and the second level of strands from the top of the section. As the load increased, additional splitting cracks developed on both sides of the splice section. These cracks extended farther until the specimen failed at 43.59 kips with a large opening in the male segment at 4ft and 6in from the splice section, which is in the proximity of the end of the dowel's length. The test was continued until the concrete crushed at the top of the section in the male segment at 30.91 kips. Figure 98 shows the failure mode and crack pattern for this test specimen. The maximum moment capacity was calculated for this specimen to be 257.57 k-ft, taking into account the moment from the self-weight of the specimen and the spreader beam.

For Specimen 6, the load-displacement curve, load-deflection profile, crack-opening profile, and load-crack opening curve were plotted as shown in Figures 99-102, respectively.

Figure 98:Crack propagation and failure mode of Specimen 6

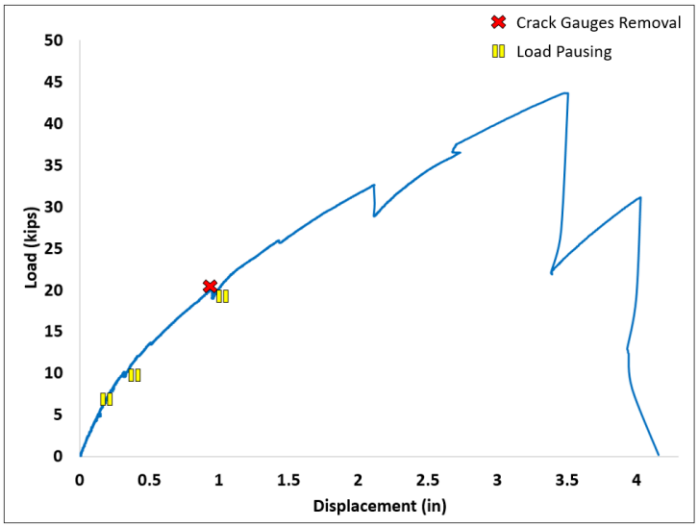

Figure 99: Load-displacement curve for Specimen 6

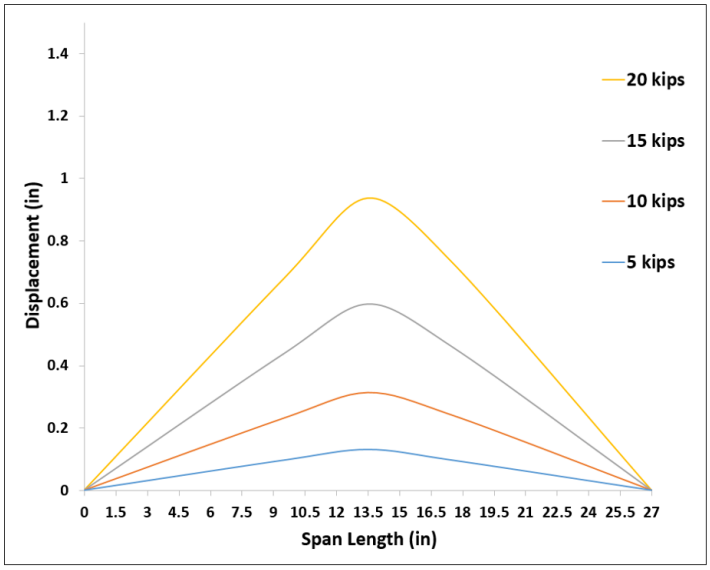

Figure 100: Load-deflection profile for Specimen 6

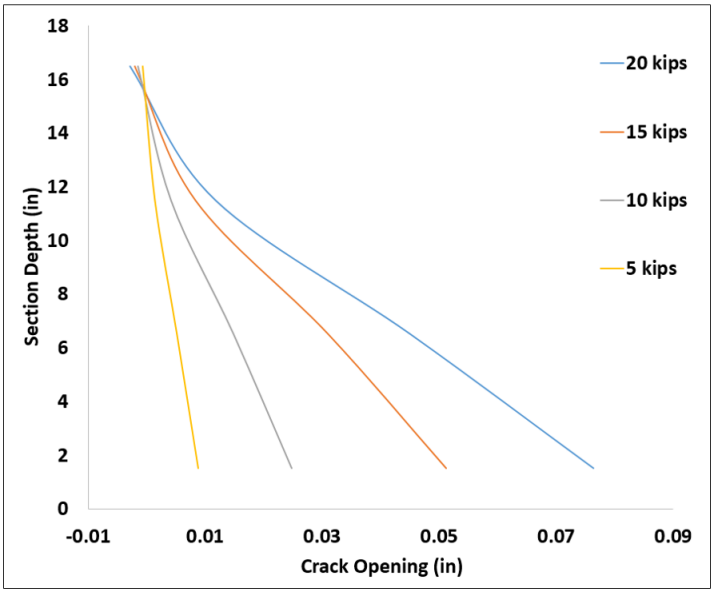

Figure 101: Crack-opening profile for Specimen 6

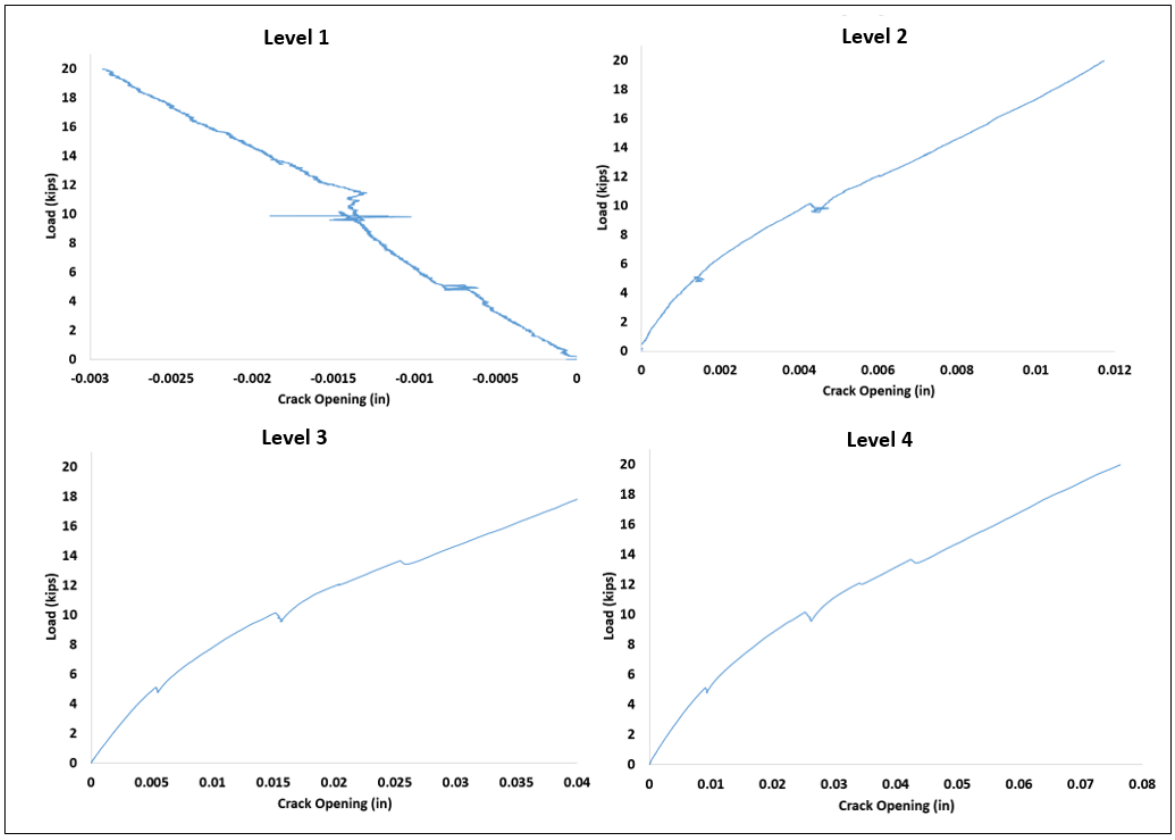

Figure 102: Load-crack opening curves for Specimen 6

5.1.7 Specimen 7

In this specimen, a crack was observed in the splice section prior to the test setup. In this test, the first new flexural crack was observed in the splice section at Step 2 (load ≤10 kips). Moreover, the first splitting crack was detected at Step 3 (load ≤20 kips) at the first and second levels of the strands from the bottom of the section. As the load increased, additional splitting cracks developed on both sides of the splice section. These cracks extended farther until the specimen failed at 61.17 kips with the concrete crushing at the

top of the pile near the splice section. Figure 103 shows the failure mode and crack pattern for this test specimen. The maximum moment capacity was calculated for this specimen to be 347.67 k-ft, taking into account the moment from the self-weight of the specimen and the spreader beam.

For Specimen 7, the load-displacement curve, load-deflection profile, crack-opening profile, and load-crack opening curve were plotted, as shown in Figures 104-107, respectively.

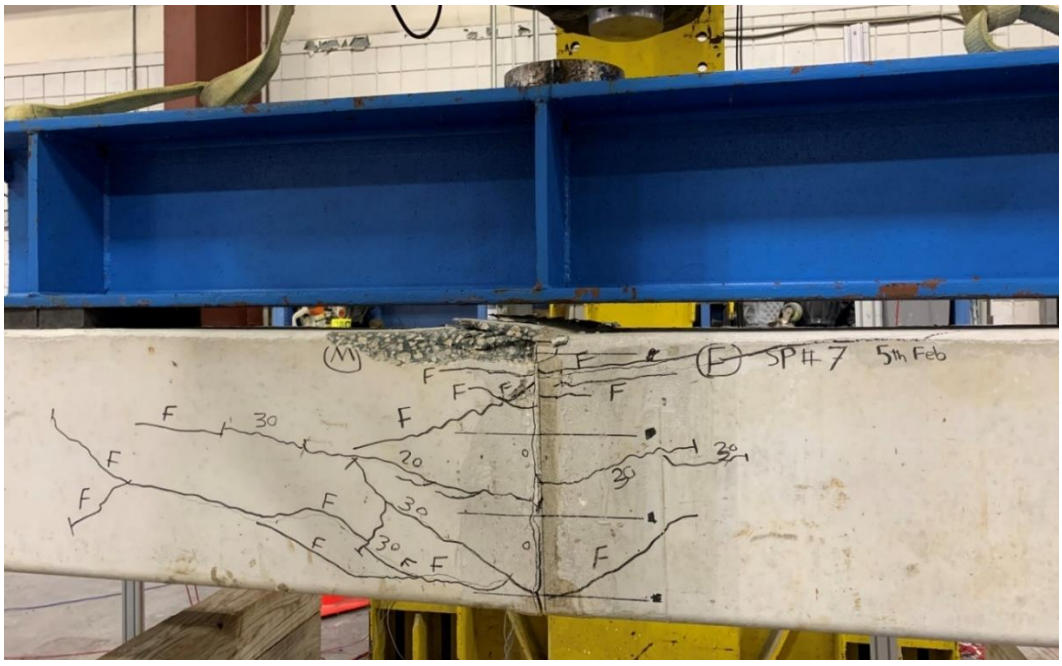

Figure 103: Crack propagation and failure mode of Specimen 7

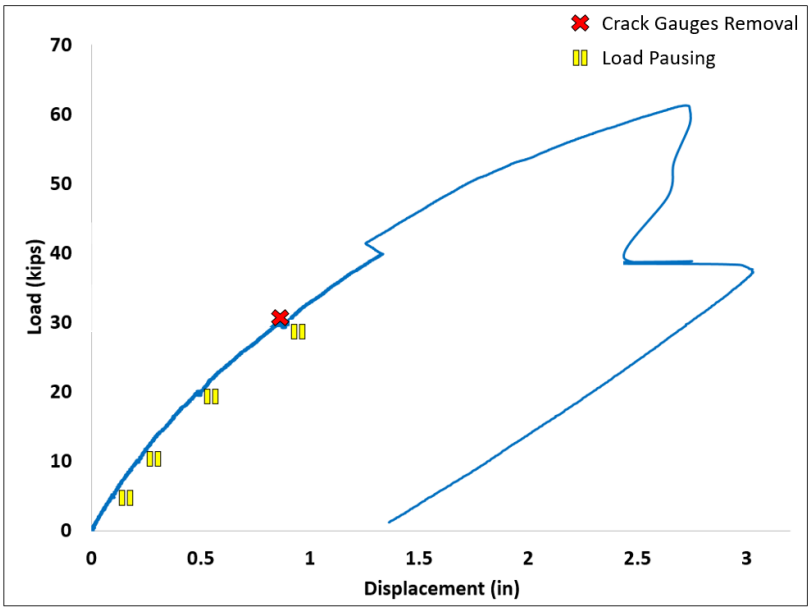

Figure 104: Load-displacement curve for Specimen 7

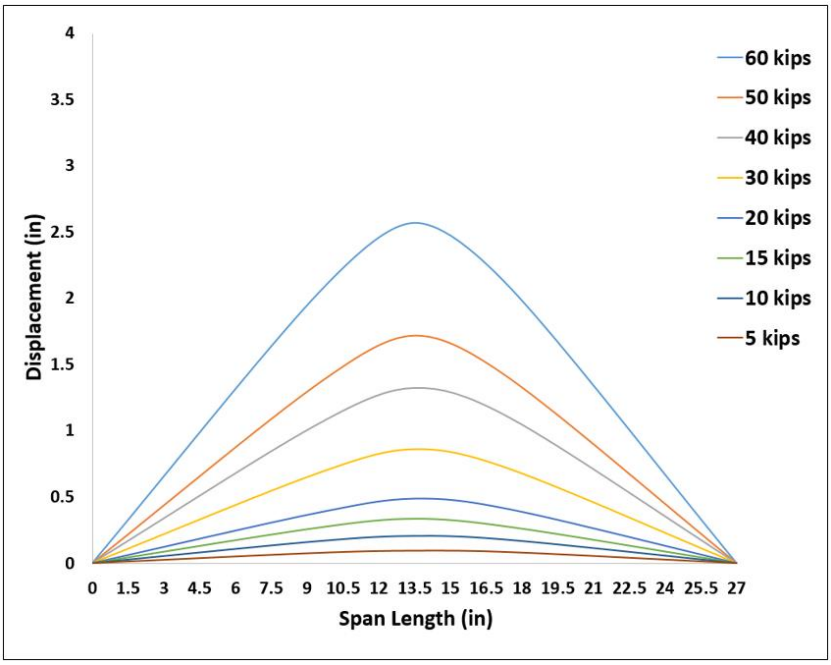

Figure 105: Load-deflection profile for Specimen 7

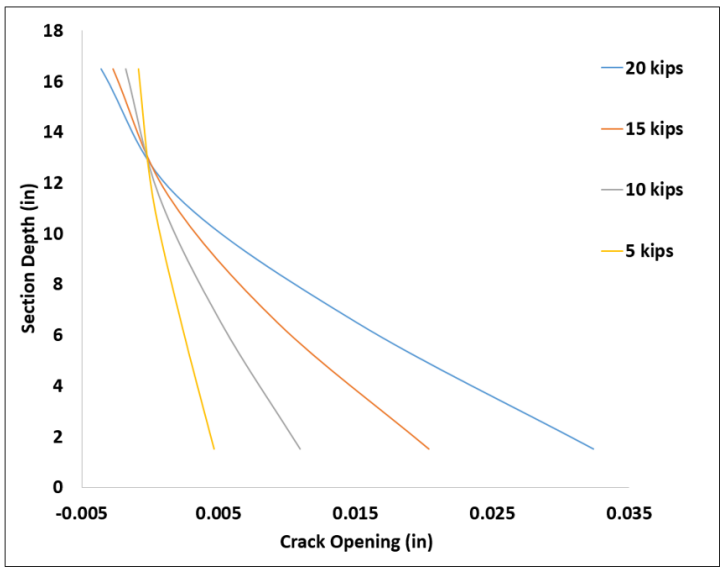

Figure 106: Crack-opening profile for Specimen 7

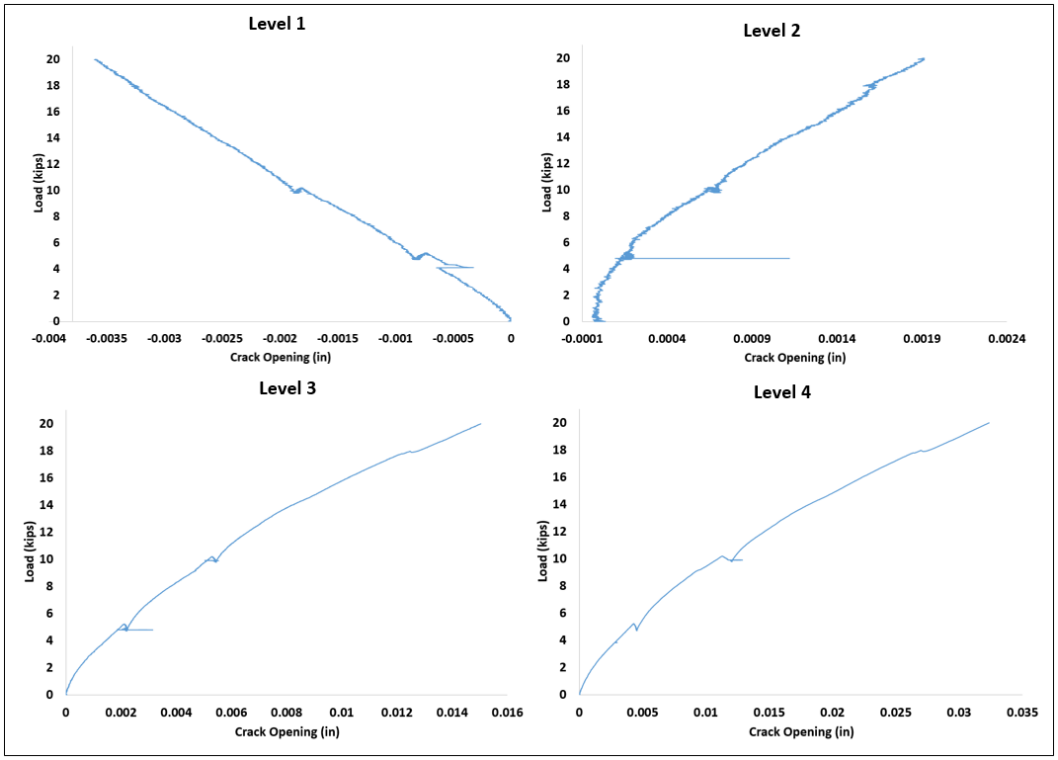

Figure 107: Load-crack opening curves for Specimen 7

5.1.8 Specimen 8

In Specimen 8, a crack was observed in the splice section prior to the test setup. In this test, the first new flexural crack was observed at splice section at Step 1, load ≤ 5 kips. Furthermore, the first splitting crack was detected at Step 2 (load ≤10 kips) at the midsection level. As the load increased, additional splitting cracks developed on both sides of the splice section at the level of the lowest strands and midsection. These cracks extended farther until the specimen failed at 59.82 kips with the concrete crushing at the top of the pile near the splice section. Figure 108 shows the failure mode and crack pattern for this test specimen. The maximum moment capacity was calculated for this specimen to be 340.75 k-ft, taking into account the moment from the self-weight of the specimen and the spreader beam.

Figure 108: Crack propagation and failure mode of Specimen 8

For Specimen 8, the load-displacement curve, load-deflection profile, crack-opening profile, and load-crack opening curve were plotted, as shown in Figures 109-112, respectively.

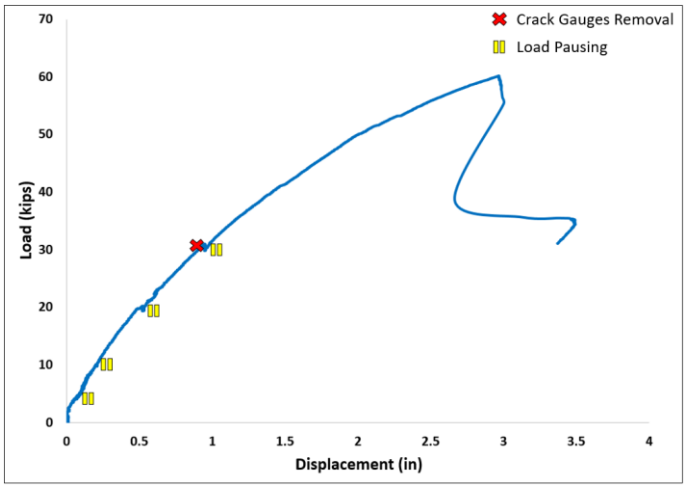

Figure 109: Load-displacement curve for Specimen 8

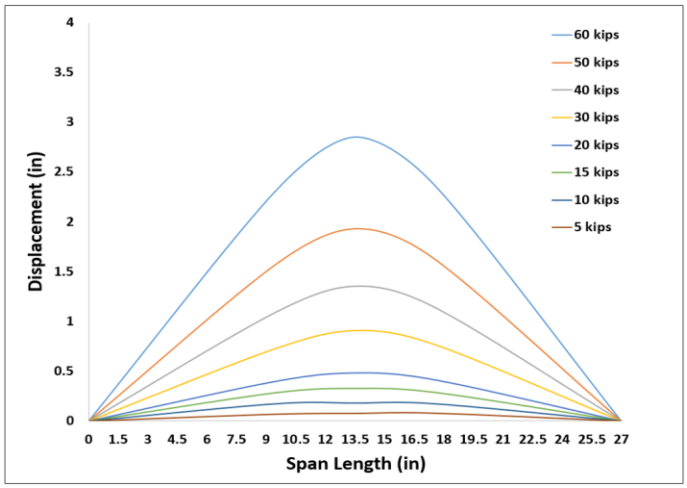

Figure 110: Load-deflection profile for Specimen 8

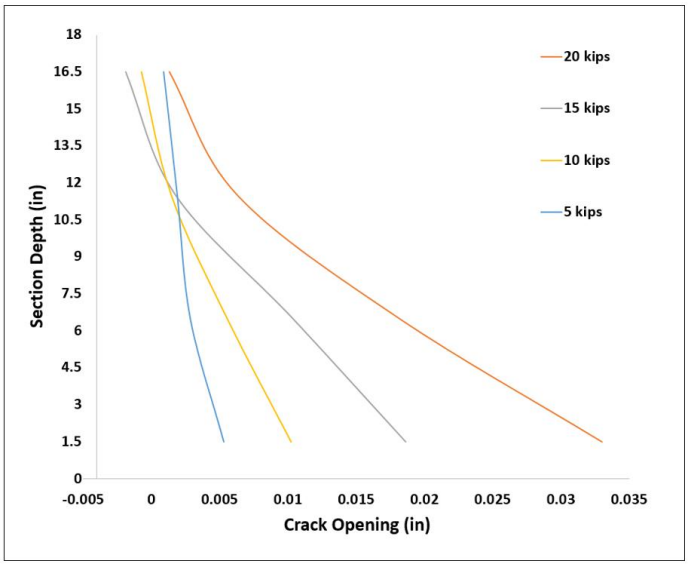

Figure 111: Crack-opening profile for Specimen 8

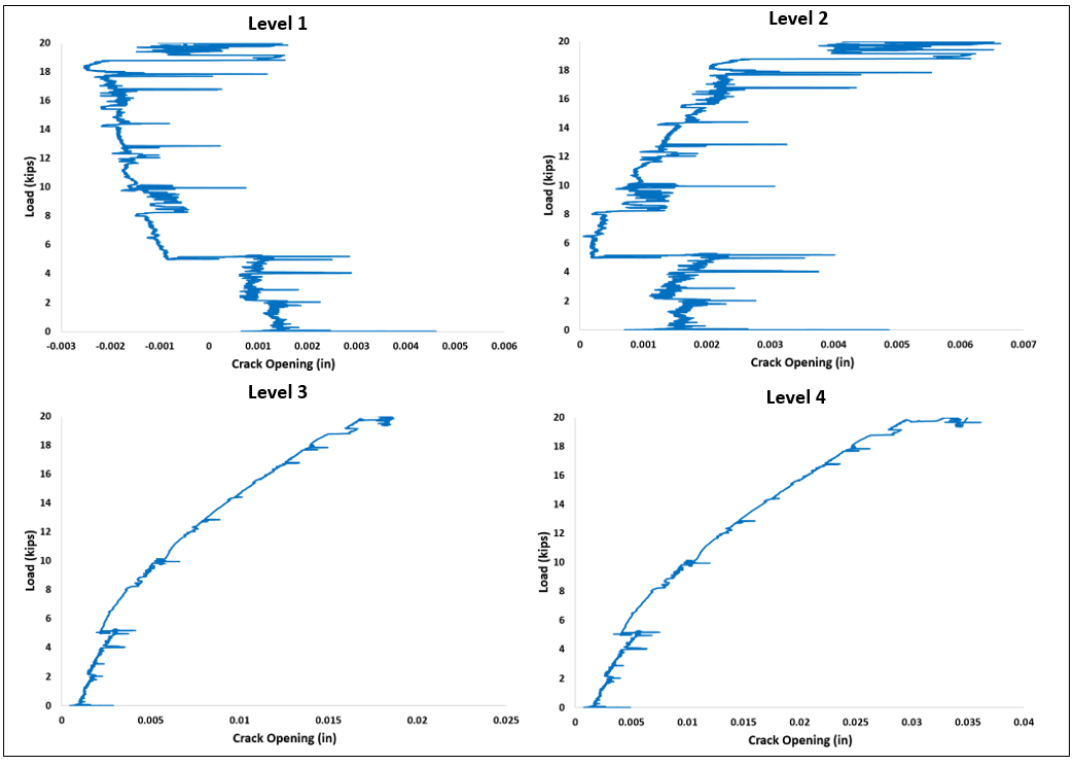

Figure 112: Load-crack opening curves for Specimen 8

5.1.9 Specimen 9

In Specimen 9, a crack was observed in the splice section prior to the test setup. The first splitting crack was detected at Step 2 (load ≤10 kips) at the first and second levels of strands from the top of the section. As the load increased, additional splitting cracks developed on both sides of the splice section. These cracks extended farther until the specimen failed at 36.95 kips with the concrete crushing at the top of the pile at the splice section. Figure 113 shows the failure mode and crack pattern for this test specimen. The maximum moment capacity was calculated for this specimen to be 223.54 k-ft, taking into account the moment from the self-weight of the specimen and the spreader beam.

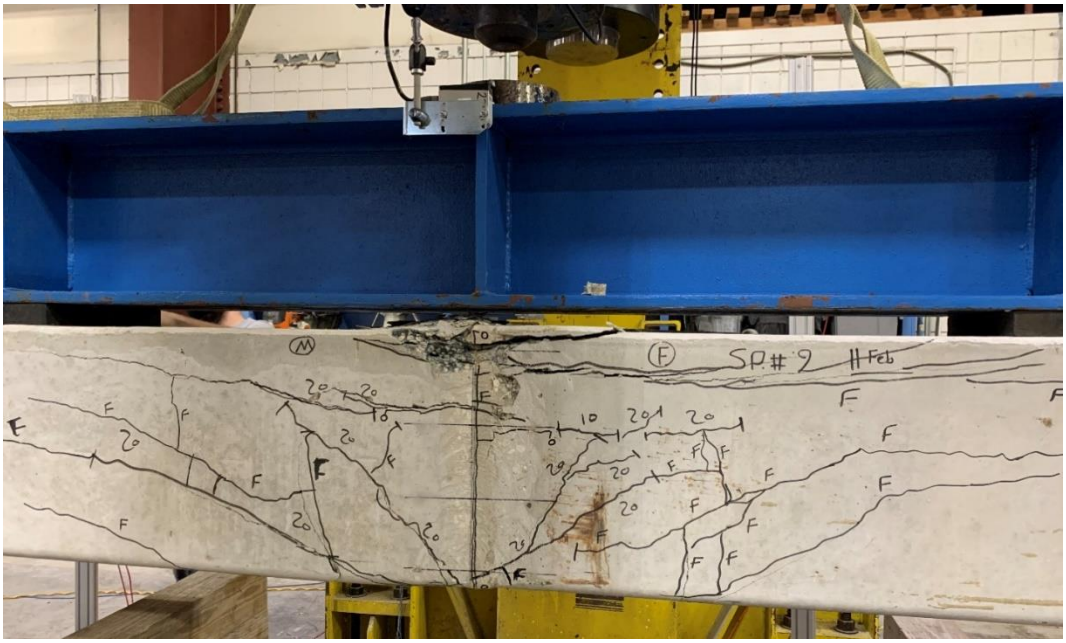

Figure 113: Crack propagation and failure mode of Specimen 9

For Specimen 9, the load-displacement curve, load-deflection profile, crack-opening profile, and load-crack opening curve were plotted, as shown in Figures 114-117, respectively.

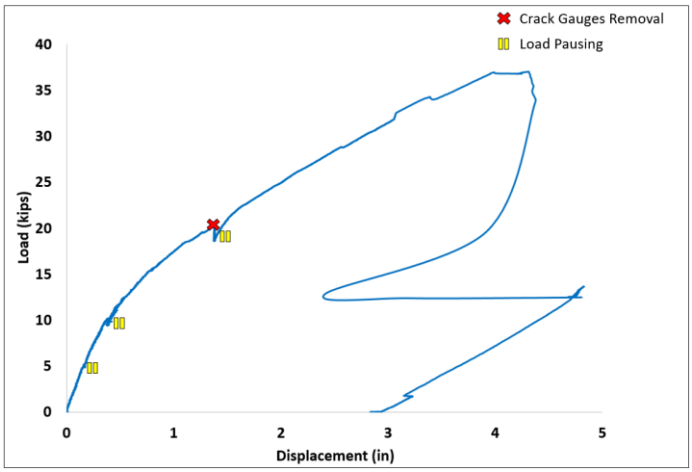

Figure 114: Load-displacement curve for Specimen 9

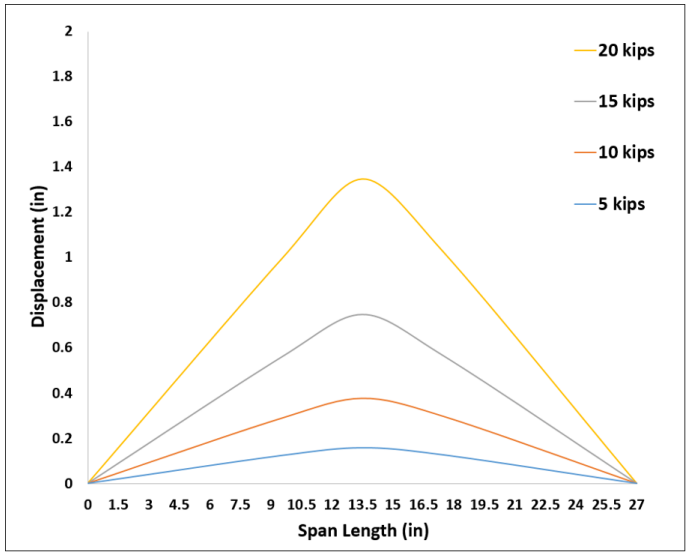

Figure 115: Load-deflection profile for Specimen 9

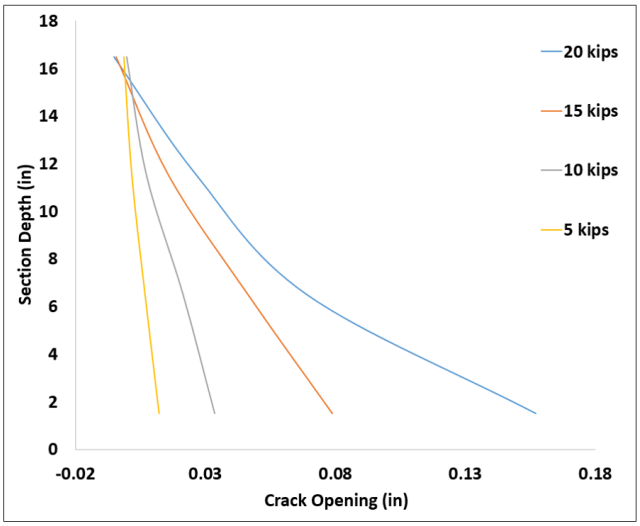

Figure 116: Crack-opening profile for Specimen 9

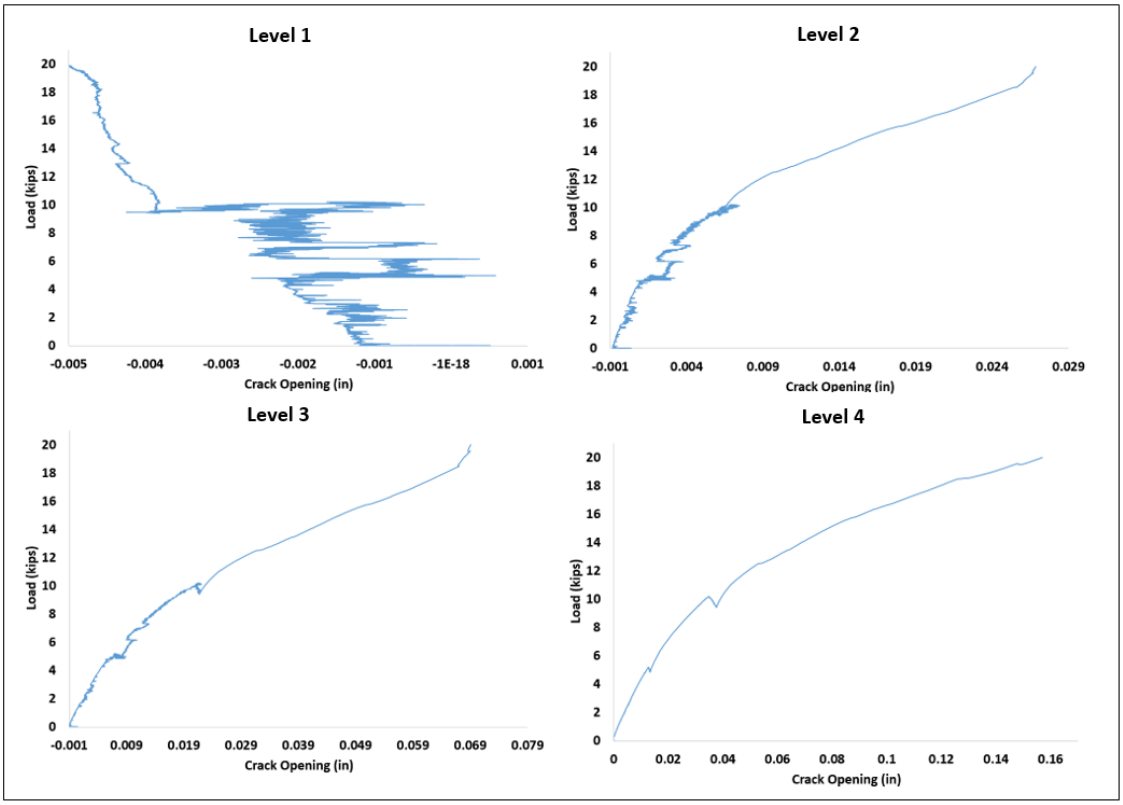

Figure 117: Load-crack opening curves for Specimen 9

5.1.10 Specimen 10

In Specimen 10, a crack was observed in the splice section prior to the test setup. In this test, the first new flexural crack was observed in the splice section at Step 2 (load ≤10 kips). In addition, the first splitting crack was detected at Step 2 (load ≤10 kips) at the second level of strands from the top and midsection. As the load increased, additional splitting cracks developed on both sides of the splice section. These cracks extended farther until the specimen failed at 40.98 kips with the concrete crushing at the top of the pile at the splice section. Prior to the concrete crushing, horizontal and vertical cracks showed large openings consistent with splitting due to bond failure in the male segment. Figure 118 shows the failure mode and crack pattern this test specimen. The maximum moment capacity was calculated for this specimen to be 244.19 k-ft, taking into account the moment from the self-weight of the specimen and the spreader beam.

For Specimen 10, the load-displacement curve, load-deflection profile, crack-opening profile, and load-crack opening curve were plotted. as shown in Figures 119-122, respectively.

Figure 118: Crack propagation and failure mode of Specimen 10

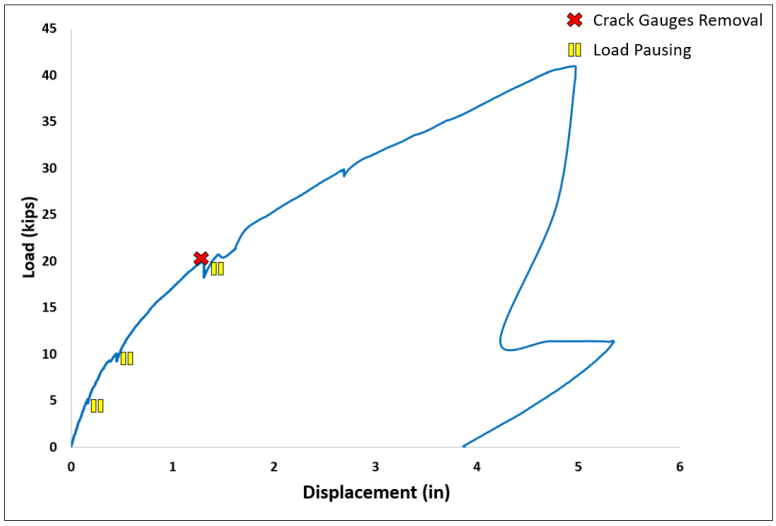

Figure 119: Load-displacement curve for Specimen 10

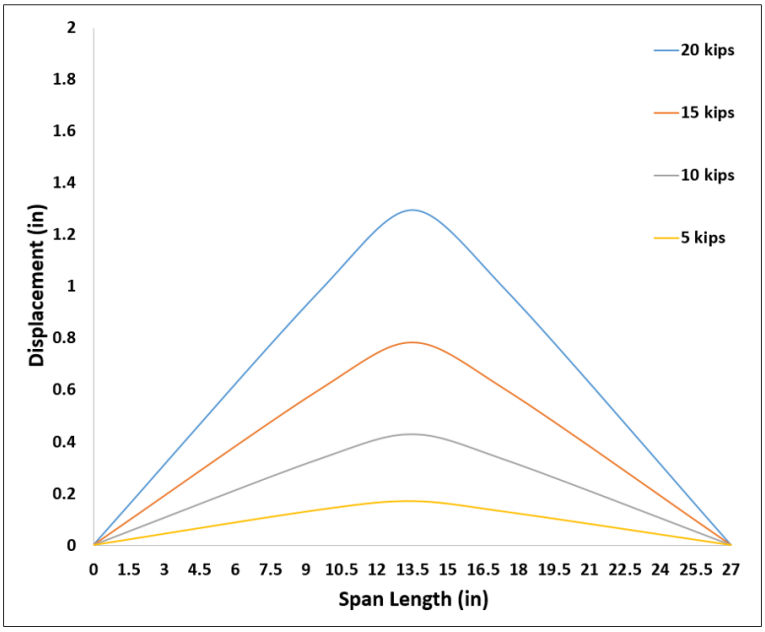

Figure 120: Load-deflection profile for Specimen 10

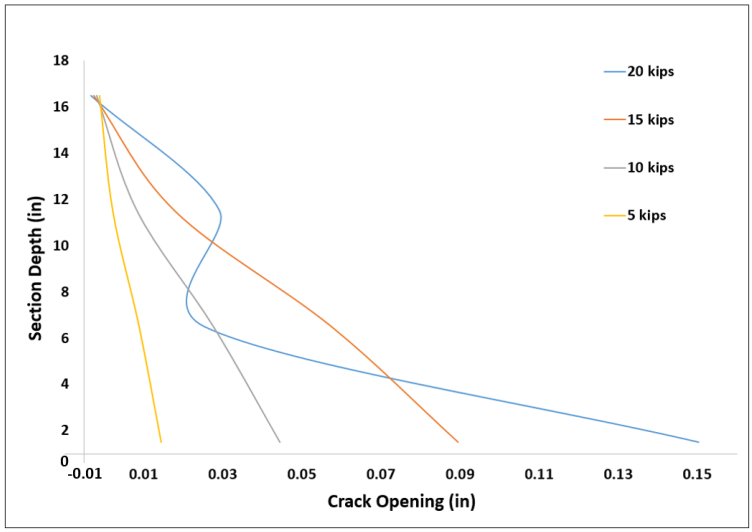

Figure 121: Crack-opening profile for Specimen 10

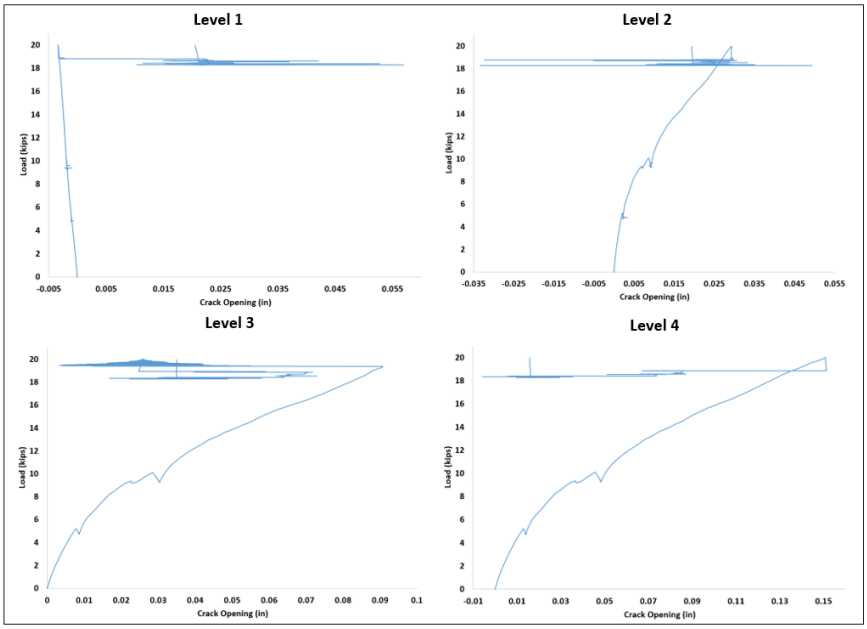

Figure 122: Load-crack opening curves for Specimen 10

5.2 Summary of test results

Figure 123 illustrates four distinctive behaviors for unforeseen specimens (Specimens 1 and 2), preplanned specimens with GFRP dowels (Specimens 3-6), preplanned specimens with CFRP dowels (Specimens 9 and 10), and preplanned specimens with steel dowels (Specimens 7-8). The specimens with steel dowels (Specimens 7 and 8) showed the highest flexural resistance with an average of 344 k-ft. The calculations showed that for pile splices that use steel reinforcement, the steel dowels in the farthest layer from compression zone reaches yielding before concrete crushing. However, the strain at the steel layer does not extend significantly beyond yielding at the concrete crushing. Specimens 5 and 6 with GFRP dowels and CFRP strands demonstrate a better performance in strength among all FRP combinations for preplanned PPCP specimens, with an average flexural resistance of 260 k-ft. Specimens with CFRP dowels (Specimens

9 and 10) show larger deflections, with an average deformation of about 4.5 in at mid-span at their maximum strength. Since FRP dowels in any of these cases do not reach yielding (according to section analysis), the deformation is likely caused by the bond slip of the dowels. Furthermore, for the case of unforeseen PPCP specimens, as it was expected, the test capacities were lower than estimated because of the shorter than required dowel lengths and lack of auxiliary bars.

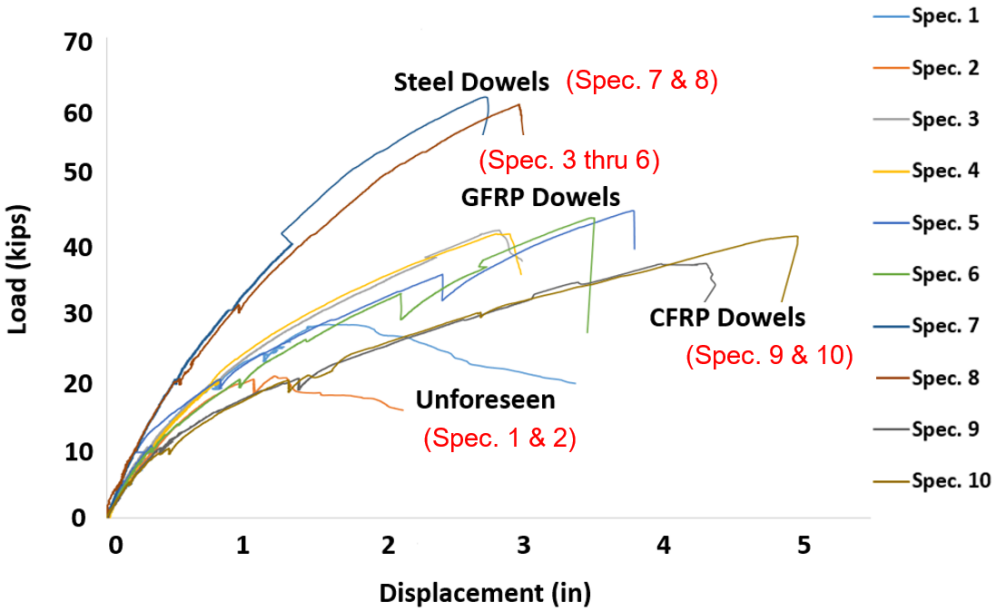

Figure 123: Load-displacement curve for all specimens

Table 26 summarizes the test results for all specimens and compares the moment capacity obtained from the test to the estimated nominal moment capacity using the analytical procedure developed in Chapter 3. With the exception of unforeseen specimens (Specimens 1 and 2), the estimated nominal moment capacities are in very good agreement with the test results. More importantly, the nominal moment capacity estimation is conservative for all preplanned specimens. For the case of unforeseen

specimens, it was expected that the test capacities would be lower than estimated because of the shorter than required dowel lengths and missing auxiliary bars.

Table 26: Moment capacity for all test specimens

Specimen Number	Estimated Nominal Moment Capacity		Moment Capacity from Test	Percentage Difference	
	Concrete Strength			Concrete Strength	
	6.5 ksi	7.3 ksi		6.5 ksi	7.3 ksi
1	222.74 k-ft	233.26 k-ft	178.13 k-ft	-20.03	-23.63
2	222.74 k-ft	233.26 k-ft	139.39 k-ft	-37.42	-40.24
3	222.74 k-ft	233.26 k-ft	247.98 k-ft	11.334	6.3127
4	222.74 k-ft	233.26 k-ft	245.63 k-ft	10.275	5.302
5	222.74 k-ft	233.26 k-ft	263.05 k-ft	18.098	12.772
6	222.74 k-ft	233.26 k-ft	257.57 k-ft	15.637	10.421
7	305.1 k-ft	323.4 k-ft	347.67 k-ft	13.952	7.5035
8	305.1 k-ft	323.4 k-ft	340.75 k-ft	11.684	5.3641
9	198.02 k-ft	207.2 k-ft	223.59 k-ft	12.887	7.8855
10	198.02 k-ft	207.2 k-ft	244.19 k-ft	23.317	17.854

5.3 Observation unforeseen specimens

To accommodate drilling of 1-3/4 – in holes for unforeseen specimens, the precast plant embedded 1-1/2- in PVC pipes to enlarge later with drilling. They stated that the trajectory was difficult to observe once the head of the bit passed the face of the concrete

pile. The 3-ft long drill bit used to perform the holes was warping due to heating and pressure. To correct the warping, they were changing the bit as often as possible to give it time to cool off. Since the holes were performed horizontally, the pressure applied was different from person to person. Also the difference in height of the personnel who performed the holes was substantial, therefore applying pressure upward or downward based on their height. Since the opening of the hole at the splice face had the required size and shape, they were not able to verify the final shape of the hole inside the body of the pile. Consequently, misalignment was introduced for the holes drilled in unforeseen segments. Dissection of unforeseen specimens tested showed no major misalignment for Specimen 1 (see Fig. 27), but indicated noticeable misalignment for Specimen 2 (see Fig. 33). Accordingly, the authors believe that the lower capacity obtained in Specimen 2 is a consequence of applied misalignment affecting the development and progression of splitting cracks and debonding.

5.4 Failure mode observations

Mode of failure is referred to the mechanism developed at or near maximum load and resulting in significant drop in capacity from its maximum. As shown in Table 27, three modes of failure were observed for the test specimens, as follows:

1- Classical flexural failure with crushing of concrete in the compression zone at splice section,
2- Flexural cracking/debonding in the male segment near the end of dowel,
3- Splitting and bond failure for the dowels in the female segment.

Table 27: Loading details for test specimens using GFRP and CFRP Dowels (Specimens 1, 2, 3, 4, 5, 6, 9 and 10)

Failure Mode	Specimens	Test Specimens
Mode 1: Flexural failure at splice section	3, 4, 7, 8, 9 and 10	
Mode 2: Flexural cracking and debonding beyond dowel embedment	5 and 6	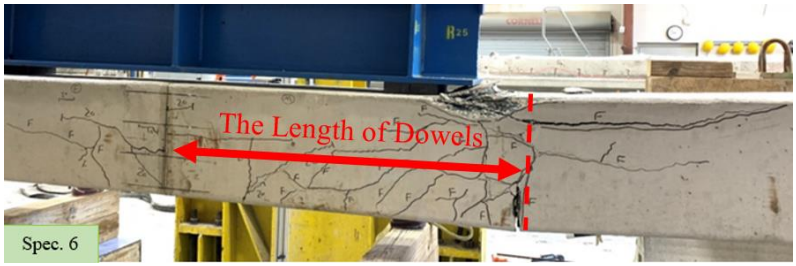
Mode 3: Splitting and bond failure of short dowels	1 and 2	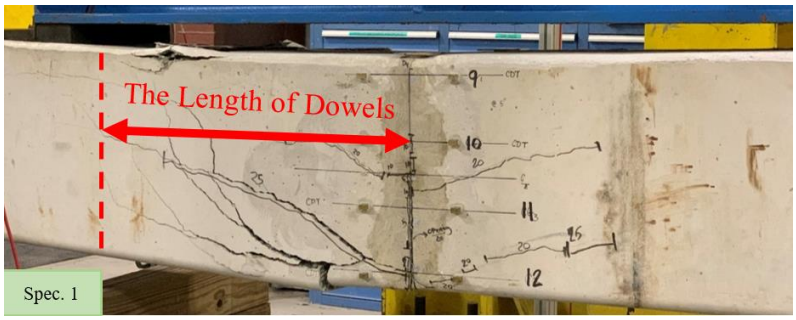

5.4.1 Classical flexural failure:

For Specimens 3, 4, 7, 8, 9 and 10, the failure mode followed the classical flexural failure mechanism with crushing of concrete. This is an indication that development lengths for

dowels and auxiliary bars (if any) were adequate to allow this mode to occur. Figure 88 shows an example of this type of failure mode. Although, splitting cracks were developed and propagated, the confinement seems to have been adequate to keep the dowels engaged until the failure.

5.4.2 Flexural cracking/debonding in the male segment:

For Specimens 5 and 6, the failure mechanism was initiated by flexural cracking and concrete spalling in the male segment at the section near the end of the dowel bar. This failure mode could be an indication of inadequate bond length for CFRP strands. The load resistance dropped significantly with this cracking indicating potential debonding of strands at the cracked section which can also be attributed to lack of adequate confinement at this location (closely-spaced spirals were implemented only in the female segments for the first 4 ft from the splice section). Figure 93 shows an example of this type of failure mode. Concrete crushing shown in the figure above the cracked section occurred after continuing the test beyond maximum at much lower loads. Apparently Specimens 9 and 10 with identical dowel length but CFRP dowels instead of GFRP did not failed similarly, likely for the fact that the splice section with CFRP failed earlier with classical flexural mode.

5.4.3 Splitting and bond failure in the female segment:

For unforeseen test specimens, Specimens 1 and 2, the failure occurred with splitting of concrete cover, bond failure of dowels in female segment, and horizontal and vertical

crack opening at the section near the end of dowel. Figure 77 shows an example of this type of failure mode.

Splitting crack from bond action were observed for all tested specimens. Figure 124, shows cross section of a dissected specimen after the test. Splitting cracks are visible mostly at the level of strands. In some cases, as the example in this figure, enlargement of the splitting cracks likely because of inadequate confinement, resulted in debonding of the strands or dowels.

Figure 124: Dissection of Specimen 5

5.5 Validation of Design Procedure using Experimental Results

In order to validate the adopted design procedure and investigate the effectiveness of GFRP reinforcing bars as bonded dowels for a pile splice design, ten full-scale PPCP specimens of 18×18 in cross-sections with a total length of 28 feet were designed, fabricated, and tested at the Florida Department of Transportation (FDOT) Structures Research Center. In these specimens, three different materials for dowels, which are

GFRP reinforcing bars, Carbon Fiber Reinforced Polymer (CFRP) strand, and traditional carbon-steel reinforcing bars, were used in combination with CFRP and steel prestressing strands for PPCPs for both unforeseen and preplanned drivable splicing cases.

Table 28 summarizes the test results for all specimens and compares their flexural resistance obtained from the test to their estimated nominal flexural resistance using the analytical procedure. The concrete strengths (f'_c) of 6.5 ksi were considered as the nominal concrete strength. As shown in Table 28, the nominal flexural resistance estimation is conservative for all preplanned specimens. Furthermore, the estimated nominal moment capacities are in very good agreement with the test results, with the exception of the unforeseen specimens (Specimens 1 and 2).

For Specimens 3 and 4, GFRP dowels and steel strands, the test results are on average 10% higher than the nominal moment capacity calculated with the design procedure. This level of conservatism is adequate when considering the flexural failure mode of these specimens dominated by concrete crushing.

For Specimens 5 and 6, GFRP dowels and CFRP strands, the test results are on average 15% higher than the nominal moment capacity calculated with the design procedure. Because the failure mode of these specimens is involved with potential bond failure, a slightly higher conservatism is justified.

For Specimens 7 and 8, steel dowels and steel strands, the test results are on average 11% higher than the nominal moment capacity calculated with the design procedure. This

level of conservatism is adequate when considering the flexural failure mode of these specimens dominated by concrete crush.

Table 28: Flexural resistance of experimental and analytical studies for all test specimens

Specimen Number	Nominal Flexural Resistance (k-ft)	Design Moment Capacity (k-ft)	Average Flexural Resistance (k-ft) from Test	Percentage Difference for Test to Nominal	Percentage Difference for Test to Design
1 & 2	*148.3	111.2	158.8	7%	30%
3 & 4	222.7	167.1	246.8	10 %	32%
5 & 6	222.7	167.1	260.3	15%	36%
7 & 8	305.1	256.3	344.2	11%	26%
9 & 10	198.0	148.5	233.9	15%	37%
* Calculation details are explained in Section 3.1					

For Specimens 9 and 10, CFRP dowels and CFRP strands, the test results are on average 15% higher than the nominal moment capacity calculated with the design procedure. A higher conservatism is also justified here due to a large difference between the results of the two tests. This validates the analytical process used for the design of preplanned splices using GFRP and other types of dowels. The use of nominal concrete compressive

strength provides a more reasonable basis for comparison because of the laboratory setup and high level of quality control associated with the experiment.

5.5.1 Nominal Moment Reduction Factor for Unforeseen cases

To account for lower than expected test results for unforeseen cases due to the lower than required dowel length, a reduction factor of 0.67, $\varphi'_{unforseen}$, is proposed to be used to calculate the nominal moment capacity for the unforeseen. Eq. (90) shows the application of the reduction factor.

$\varphi'_{unforseen}$(reduction factor for unforeseen cases) = 0.67 (90)

(Nominal Moment for unforeseen= $\varphi'_{unforseen}$ × Nominal Moment from design procedure)

For calculating the design moment capacity for unforeseen cases, the nominal moment capacity will be multiplied by a strength reduction factor of 0.75, ∅, as it is for the pre-planned cases. This reduction factor provides the level of conservatism similar to that for the preplanned cases. The results shown for Specimens 1 and 2 reflects the use of reduction factor for unforeseen and strength reduction factor.

5.5.2 Comparing Design Moment Capacity with FDOT Requirement

The design moment capacities based on the analytical results using the nominal concrete compressive strength used in test program were calculated with the corresponding strength reduction factors and are shown in Table 29. The concrete strength (f'_c) of 6.5 ksi was considered the nominal concrete strength. The design moment capacities are also

compared to the FDOT mechanical pile splice flexural strength requirement (245 k-ft) in this table.

Table 29: Flexural resistance of experimental study for all test specimens and FDOT requirement

Specimen Number	FDOT Required Flexural Strength (k-ft)	Nominal Flexural Resistance (k-ft)	Resistance Factor, ∅	Design Moment Capacity (k-ft)	Ratio of Design to Required Strength
1	245	222.7	0.75 [49]	167.1	68%
2	245	222.7	0.75 [49]	167.1	68%
3	245	222.7	0.75 [49]	167.1	68%
4	245	222.7	0.75 [49]	167.1	68%
5	245	222.7	0.75 [49]	167.1	68%
6	245	222.7	0.75 [49]	167.1	68%
7	245	305.1	0.84 [60]	256.3	105%
8	245	305.1	0.84 [60]	256.3	105%
9	245	198.0	0.75 [50]	148.5	61%
10	245	198.0	0.75 [50]	148.5	61%

The results indicate that while the test results exceeded (with the exception of unforeseen specimens) the FDOT requirement, the design flexural resistance calculated using the proposed procedure develops approximately 68% of the flexural strength requirement of FDOT for preplanned mechanical pile splices for PPCPs. The design flexural resistance of the steel dowel splices is equal to 105% of the requirement, while the CFRP dowel splice can only develop 61% of the required flexural resistance.

CHAPTER 6: DESIGN SOFTWARE DEVELOPMENT

A design procedure was developed in Chapter 3 for all splice reinforcing materials including GFRP, CFRP, HSSS, and Steel. The design procedure was then validated in the experimental program presented in Chapter 4. To allow structural engineers (E.g. FDOT engineers) to design and modify the procedure for any future design alternatives, a practical and user friendly worksheet was programed by using Mathcad tools.

The Mathcad worksheet is easy to use for the design procedures and provides a vector-based section analysis as well as detailing. As shown in Figure 125, the following are the main features of the design procedure:

- Estimating the nominal and design flexural capacities of epoxy dowel pile splices
- Estimating the development length of CFRP, GFRP, Steel, and HSSS dowels of pile splices
- Estimating the lap splice length of CFRP, GFRP, Steel, and HSSS dowels of pile splices
- Estimating the development length of CFRP, GFRP, Steel, and HSSS strands of piles

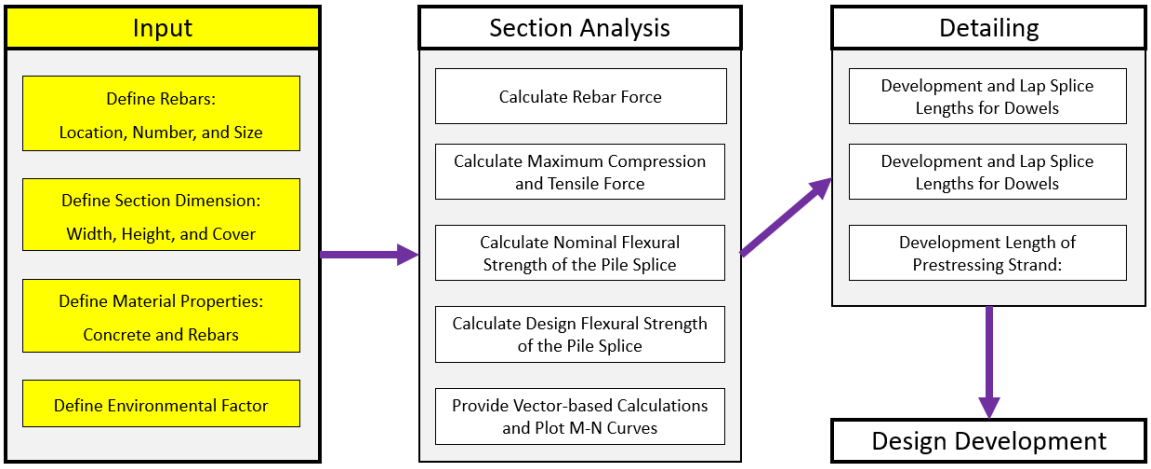

Figure 125: Flowchart of the design procedure developed in the Mathcad worksheet

This design and analysis tools the first customized software for epoxy dowel splices in general and FRP dowel splices in specific. As such, the most recent provisions from codes and guidelines for the design and detailing of FRP-reinforced concrete (ACI-440, AASHTO) were implemented in the design procedure within the software. The procedure developed here was proven to apply to epoxy dowels and was validated by test results.

As an instance, the design procedure programmed for pile splice using an FRP bar and FRP strand are presented below. The other arrangements of FRP Dowel – Steel Strand, Steel Dowel – Steel Strand, and Steel Dowel – FRP Strand are attached as the Appendix C.

Precast Prestressed Concrete Pile Splice Design

Designed by Saman Farhangdoust

This program can be used for **Epoxy Dowel Pile Splice Evaluation - FRP Dowel and FRP Strand**

Grant No.: **BDV29-977-52**
Principal Investigators: **Mehrabi, Armin**
Graduate Research Assistant: **Farhangdoust, Saman**

Sponsered by Florida Department of Transportation (FDOT)
Project Manager: **Nolan, Steven**

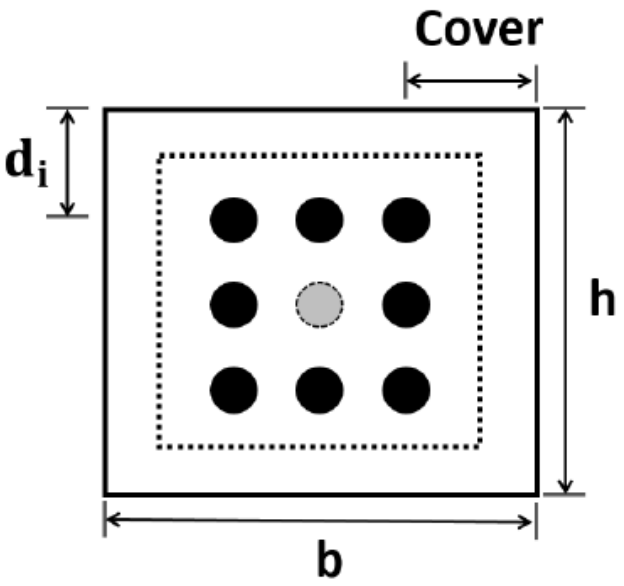

Input

Section Dimension:

b := 18in	Width
h := 18in	Height
Cover := 5.5in	Cover

Rebar:

Input

$d_b := 1.27in$ Nominal Bar Diameter

$n_b := \begin{pmatrix} 1 & 1 & 1 \\ 1 & 0 & 1 \\ 1 & 1 & 1 \end{pmatrix}$ Number and Location

$A_b := \pi \cdot \frac{d_b^{\,2}}{4} = 8.797 \times 10^{-3}\,ft^2$ Area of a rebar

$n_{bl} := \sum_{i=1}^{cols(n_b)} n_b^{\langle i \rangle} = \begin{pmatrix} 3 \\ 2 \\ 3 \end{pmatrix}$ Number of rebars by level

$n_{bl} = \begin{pmatrix} 3 \\ 2 \\ 3 \end{pmatrix}$ Number of bars in each level

$A_{bl} := A_b \cdot n_{bl} = \begin{pmatrix} 0.026 \\ 0.018 \\ 0.026 \end{pmatrix} ft^2$ Area of rebars by level

$A_{bl} = \begin{pmatrix} 3.8 \\ 2.534 \\ 3.8 \end{pmatrix} \cdot in^2$ Area of all bars in each level

$A_{bt} := \sum A_{bl} = 10.134 \cdot in^2$ Area of total bars

$d := \left| \begin{array}{l} d_1 \leftarrow Cover \\ \text{for } i \in 2 .. rows(n_b) \\ \quad \left| \begin{array}{l} \Delta \leftarrow \frac{h - 2 \cdot Cover}{rows(n_b) - 1} \\ d_i \leftarrow d_{i-1} + \Delta \end{array} \right. \\ d \end{array} \right. = \begin{pmatrix} 0.458 \\ 0.75 \\ 1.042 \end{pmatrix} ft$ Level of rebars

Environmental Factor:

Input

$C_E := 0.7$ environmental reduction factor for FRP-bars

FRP-Bar Properties:

$E_f := 6500ksi$ Modulus of Elasticity

$S_{fu} := 98.2 \cdot kip$ Minimum Guaranteed (Nominal) Tensile Load

$f_{fu} := \frac{S_{fu}}{A_b} = 77.52 \cdot ksi$ Guaranteed Tensile Strength

$\varepsilon_{fu} := \frac{f_{fu}}{E_f} = 0.012$ Ultimate Strain

$f_{fd} := C_E \cdot f_{fu} = 54.264 \cdot ksi$ Design Tensile Strength

$\varepsilon_{fd} := \frac{f_{fd}}{E_f} = 8.348 \times 10^{-3}$ Ultimate Design Strain

Concrete properties:

Input

$f'_c := 6ksi$ Compressive Strength

$f'_{ci} := 4ksi$ Compressive Strength at Release

$\varepsilon_{cu} := 0.003$ Maximum Compressive Strain

$$\alpha := \text{if}\left[f'_c \le 10ksi, 0.85, \max\left[0.75, 0.85 - 0.02 \cdot \left(\frac{f'_c}{ksi} - 10\right)\right]\right] = 0.85 \qquad ACI - 318$$

$$\beta_1 := \max\left[0.65, 0.85 - 0.05 \cdot \left(\frac{f'_c}{ksi} - 4\right)\right] = 0.75$$

Ratio of Maximum Flexural Strain at the extreme tension face to the strain at the centroid of the rebar layer nearest to the tension face

FRP Layers Force:

$a := \left| \begin{array}{l} \text{for } j \in 1 .. 60 \\ \quad a_j \leftarrow \frac{h}{60} \cdot j \\ a \end{array} \right. =$ ft

	1
1	0.025
2	0.05
3	0.075
4	0.1
5	0.125
6	0.15
7	0.175
8	0.2
9	0.225
10	0.25
11	0.275
12	0.3
13	0.325
14	0.35
15	0.375
16	...

Range Variable to accomodate an increasing increment

$c := \frac{a}{\beta_1}$

The distance of the concrete block in compression

Tensile Strain in each row

$\varepsilon_f := \left| \begin{array}{l} \text{for } i \in 1 .. \text{rows}(a) \\ \quad \text{for } j \in 1 .. \text{rows}(n_{bl}) \\ \quad\quad \varepsilon_{i,j} \leftarrow \varepsilon_{cu} \cdot \frac{(d_j - c_i)}{c_i} \\ \varepsilon \end{array} \right. =$

	1	2	3
1	0.038	0.065	0.091
2	0.018	0.031	0.044
3	0.011	0.02	0.028
4	$7.312 \cdot 10^{-3}$	0.014	0.02
5	$5.25 \cdot 10^{-3}$	0.011	0.016
6	$3.875 \cdot 10^{-3}$	$8.25 \cdot 10^{-3}$	0.013
7	$2.893 \cdot 10^{-3}$	$6.643 \cdot 10^{-3}$	0.01
8	$2.156 \cdot 10^{-3}$	$5.438 \cdot 10^{-3}$	$8.719 \cdot 10^{-3}$
9	$1.583 \cdot 10^{-3}$	$4.5 \cdot 10^{-3}$	$7.417 \cdot 10^{-3}$
10	$1.125 \cdot 10^{-3}$	$3.75 \cdot 10^{-3}$	$6.375 \cdot 10^{-3}$
11	$7.5 \cdot 10^{-4}$	$3.136 \cdot 10^{-3}$	$5.523 \cdot 10^{-3}$
12	$4.375 \cdot 10^{-4}$	$2.625 \cdot 10^{-3}$	$4.813 \cdot 10^{-3}$

$$f_f := \left| \begin{array}{l} \text{for } i \in 1 .. \text{rows}(a) \\ \quad \text{for } j \in 1 .. \text{rows}(n_{bl}) \\ \quad\quad f_{i,j} \leftarrow \left| \begin{array}{ll} 0 & \text{if } \varepsilon_{f_{i,j}} < 0 \\ \min\left(\varepsilon_{f_{i,j}} \cdot E_f, f_{fd}\right) & \text{otherwise} \end{array} \right. \\ f \end{array} \right.$$

Tensile Stress in each row

$=$ ps

	1	2	3
1	$5.426 \cdot 10^4$	$5.426 \cdot 10^4$	$5.426 \cdot 10^4$
2	$5.426 \cdot 10^4$	$5.426 \cdot 10^4$	$5.426 \cdot 10^4$
3	$5.426 \cdot 10^4$	$5.426 \cdot 10^4$	$5.426 \cdot 10^4$
4	$4.753 \cdot 10^4$	$5.426 \cdot 10^4$	$5.426 \cdot 10^4$
5	$3.412 \cdot 10^4$	$5.426 \cdot 10^4$	$5.426 \cdot 10^4$
6	$2.519 \cdot 10^4$	$5.363 \cdot 10^4$	$5.426 \cdot 10^4$
7	$1.88 \cdot 10^4$	$4.318 \cdot 10^4$	$5.426 \cdot 10^4$
8	$1.402 \cdot 10^4$	$3.534 \cdot 10^4$	$5.426 \cdot 10^4$
9	$1.029 \cdot 10^4$	$2.925 \cdot 10^4$	$4.821 \cdot 10^4$
10	$7.312 \cdot 10^3$	$2.437 \cdot 10^4$	$4.144 \cdot 10^4$
11	$4.875 \cdot 10^3$	$2.039 \cdot 10^4$	$3.59 \cdot 10^4$
12	$2.844 \cdot 10^3$	$1.706 \cdot 10^4$	$3.128 \cdot 10^4$
13	$1.125 \cdot 10^3$	$1.425 \cdot 10^4$	$2.737 \cdot 10^4$
14	0	$1.184 \cdot 10^4$	$2.403 \cdot 10^4$
15	0	$9.75 \cdot 10^3$	$2.112 \cdot 10^4$
16	0	$7.922 \cdot 10^3$	...

$$F_f := \left| \begin{array}{l} \text{for } i \in 1 .. \text{rows}(a) \\ \quad \text{for } j \in 1 .. \text{rows}(n_{bl}) \\ \quad\quad F_{i,j} \leftarrow A_{bl_j} \cdot f_{f_{i,j}} \\ F \end{array} \right.$$

Rebar Force in each row

$=$ lbf

	1	2	3
1	$2.062 \cdot 10^5$	$1.375 \cdot 10^5$	$2.062 \cdot 10^5$
2	$2.062 \cdot 10^5$	$1.375 \cdot 10^5$	$2.062 \cdot 10^5$
3	$2.062 \cdot 10^5$	$1.375 \cdot 10^5$	$2.062 \cdot 10^5$
4	$1.806 \cdot 10^5$	$1.375 \cdot 10^5$	$2.062 \cdot 10^5$
5	$1.297 \cdot 10^5$	$1.375 \cdot 10^5$	$2.062 \cdot 10^5$
6	$9.572 \cdot 10^4$	$1.359 \cdot 10^5$	$2.062 \cdot 10^5$
7	$7.146 \cdot 10^4$	$1.094 \cdot 10^5$	$2.062 \cdot 10^5$
8	$5.326 \cdot 10^4$	$8.954 \cdot 10^4$	$2.062 \cdot 10^5$
9	$3.911 \cdot 10^4$	$7.411 \cdot 10^4$	$1.832 \cdot 10^5$
10	$2.779 \cdot 10^4$	$6.175 \cdot 10^4$	$1.575 \cdot 10^5$
11	$1.853 \cdot 10^4$	$5.165 \cdot 10^4$	$1.364 \cdot 10^5$

Concrete Force:

$F_c := \alpha \cdot f'_c \cdot a \cdot b =$ lbf

	1
1	$2.754 \cdot 10^4$
2	$5.508 \cdot 10^4$
3	$8.262 \cdot 10^4$
4	$1.102 \cdot 10^5$
5	$1.377 \cdot 10^5$
6	$1.652 \cdot 10^5$
7	$1.928 \cdot 10^5$
8	$2.203 \cdot 10^5$
9	$2.479 \cdot 10^5$
10	$2.754 \cdot 10^5$
11	$3.029 \cdot 10^5$
12	$3.305 \cdot 10^5$
13	$3.58 \cdot 10^5$
14	$3.856 \cdot 10^5$
15	$4.131 \cdot 10^5$
16	...

Max allowable compression load:

[LRFD GFRP 5.6.4.4]

$P_{nmaxC} := \alpha \cdot f'_c \cdot b \cdot h = 1.652 \times 10^3 \cdot kip$ Nominal axial resistance

$\Phi := 0.85$

$P_f := \Phi \cdot P_{nmaxC}$ Factored axial resistance

$\phi P_f := 0.75 \cdot P_f = 1.053 \times 10^3 \cdot kip$ Design axial resistance

Nominal Flexural Strength of GFRP Pile Splice

Nominal Axial Strength

$$P_n := \left| \begin{array}{l} \text{for } i \in 1 .. \text{rows}(a) \\ \quad P_{n_i} \leftarrow \min\left[\left(F_{c_i} - \sum_{j=1}^{\text{rows}(n_b)} F_{f_{i,j}}\right), P_f\right] \\ P_n \end{array} \right| = \text{lbf}$$

	1
1	$-5.224 \cdot 10^5$
2	$-4.948 \cdot 10^5$
3	$-4.673 \cdot 10^5$
4	$-4.142 \cdot 10^5$
5	$-3.357 \cdot 10^5$
6	$-2.726 \cdot 10^5$
7	$-1.943 \cdot 10^5$
8	$-1.287 \cdot 10^5$
9	$-4.856 \cdot 10^4$
10	$2.838 \cdot 10^4$
11	$9.634 \cdot 10^4$
12	$1.576 \cdot 10^5$
13	$2.136 \cdot 10^5$
14	$2.643 \cdot 10^5$
15	$3.081 \cdot 10^5$
16	...

Nominal Moment Strength

$$M_n := \left| \begin{array}{l} \text{for } i \in 1 .. \text{rows}(a) \\ \quad M_{n_i} \leftarrow \left[F_{c_i} \cdot \left(\frac{h}{2} - \frac{a_i}{2}\right) + \sum_{j=1}^{\text{rows}(n_b)} \left[F_{f_{i,j}} \cdot \left(d_j - \frac{h}{2}\right)\right]\right] \\ M_n \end{array} \right| = \frac{\text{lb} \cdot \text{ft}^2}{\text{s}^2}$$

	1
1	$6.535 \cdot 10^5$
2	$1.285 \cdot 10^6$
3	$1.894 \cdot 10^6$
4	$2.721 \cdot 10^6$
5	$3.764 \cdot 10^6$
6	$4.626 \cdot 10^6$
7	$5.374 \cdot 10^6$
8	$6.043 \cdot 10^6$
9	$6.436 \cdot 10^6$
10	$6.755 \cdot 10^6$
11	$7.076 \cdot 10^6$
12	$7.394 \cdot 10^6$
13	$7.704 \cdot 10^6$

$P_n =$ ·kip

	1
1	-522.38
2	-494.84
3	-467.3
4	-414.173
5	-335.685
6	-272.561
7	-194.294
8	-128.708
9	-48.564
10	28.38
11	96.342
12	157.566
13	213.608
14	264.256
15	308.117
16	...

$M_n =$ ·ft·kip

	1
1	20.311
2	39.933
3	58.867
4	84.575
5	116.991
6	143.766
7	167.022
8	187.82
9	200.038
10	209.95
11	219.937
12	229.809
13	239.433
14	248.329
15	255.784
16	...

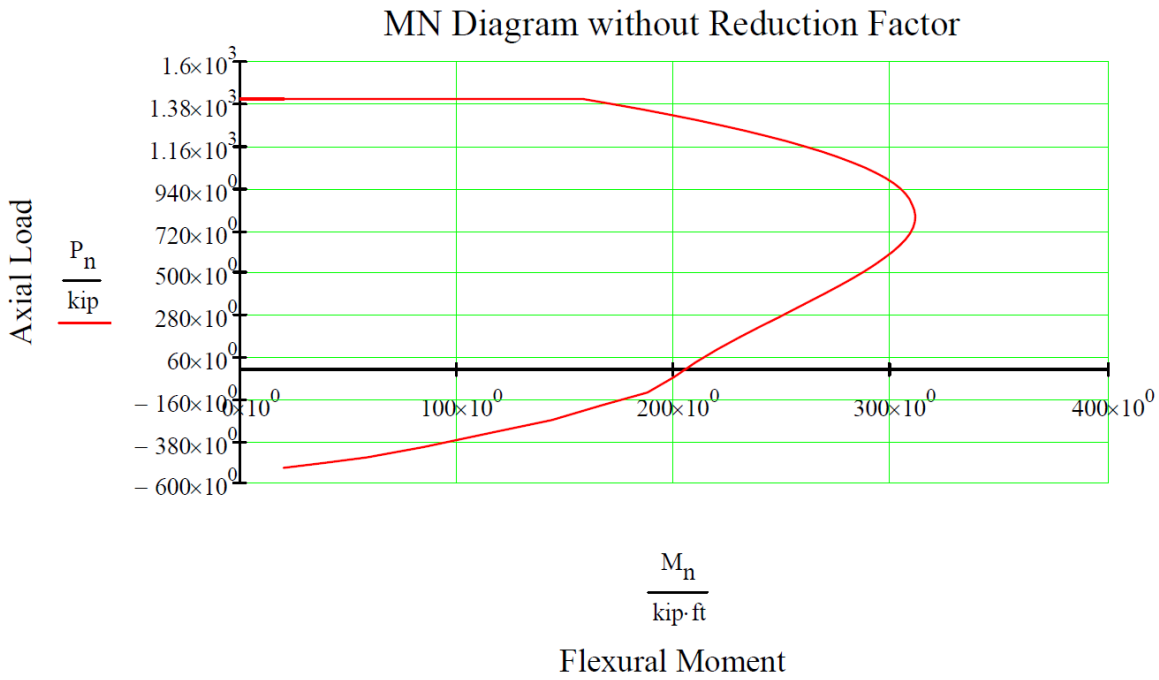

Resistance Factor for Flexural Strength (GFRP) [LRFD GFRP 2.6.3]

$$f_{fr} := \left| \begin{array}{l} m \leftarrow \text{rows}(n_b) \\ d_f \leftarrow d_m \\ A_f \leftarrow A_{bl_m} \\ \rho_f \leftarrow \dfrac{A_f}{b \cdot d_f} \\ f_f \leftarrow 0 \quad \text{if } \rho_f = 0 \\ f_f \leftarrow \sqrt{\left(\dfrac{E_f \cdot \varepsilon_{cu}}{4}\right)^2 + \dfrac{0.85 \cdot \beta_1 \cdot f_c}{\rho_f} \cdot E_f \cdot \varepsilon_{cu}} - 0.5 \cdot E_f \cdot \varepsilon_{cu} \quad \text{otherwise} \\ f_{fr} \leftarrow \min(f_f, f_{fd}) \end{array} \right. = 5.426 \times 10^4 \text{ psi}$$

$$\varepsilon_{ft} := \frac{f_{fr}}{E_f} = 8.348 \times 10^{-3}$$

$$\varepsilon_t := \left| \begin{array}{l} \text{for } i \in 1 .. \text{rows}(a) \\ \quad \varepsilon_{t_i} \leftarrow \varepsilon_{cu} \cdot \dfrac{\left(d_{\text{rows}(n_b)} - c_i\right)}{c_i} \\ \varepsilon_t \end{array} \right. =$$

	1
1	0.091
2	0.044
3	0.028
4	0.02
5	0.016
6	0.013
7	0.01
8	$8.719 \cdot 10^{-3}$
9	$7.417 \cdot 10^{-3}$
10	$6.375 \cdot 10^{-3}$
11	$5.523 \cdot 10^{-3}$
12	$4.813 \cdot 10^{-3}$
13	$4.212 \cdot 10^{-3}$
14	$3.696 \cdot 10^{-3}$

$$\phi_f := \left| \begin{array}{l} \text{for } i \in 1 .. \text{rows}(a) \\ \quad \phi_{f_i} \leftarrow \begin{cases} 0.75 & \text{if } \varepsilon_{t_i} \le 0.80 \cdot \varepsilon_{fd} \\ \left(1.55 - \dfrac{\varepsilon_{t_i}}{\varepsilon_{fd}}\right) & \text{if } 0.80 \cdot \varepsilon_{fd} < \varepsilon_{t_i} < \varepsilon_{fd} \\ 0.55 & \text{otherwise} \end{cases} \\ \phi_f \end{array} \right| =$$

	1
1	0.55
2	0.55
3	0.55
4	0.55
5	0.55
6	0.55
7	0.55
8	0.55
9	0.662
10	0.75
11	0.75
12	0.75

Design Flexural Strength of GFRP Pile Splice

$$P_u := \left| \begin{array}{l} \text{for } i \in 1 .. \text{rows}(a) \\ \quad P_{u_i} \leftarrow \phi_{f_i} \cdot \min\left[\left(F_{c_i} - \sum_{j=1}^{\text{rows}(n_b)} F_{f_{i,j}}\right), P_f\right] \\ P_u \end{array} \right| = \text{lbf}$$

	1
1	$-2.873 \cdot 10^5$
2	$-2.722 \cdot 10^5$
3	$-2.57 \cdot 10^5$
4	$-2.278 \cdot 10^5$
5	$-1.846 \cdot 10^5$
6	$-1.499 \cdot 10^5$
7	$-1.069 \cdot 10^5$
8	$-7.079 \cdot 10^4$
9	$-3.213 \cdot 10^4$
10	$2.129 \cdot 10^4$
11	$7.226 \cdot 10^4$
12	$1.182 \cdot 10^5$
13	$1.602 \cdot 10^5$
14	$1.982 \cdot 10^5$
15	$2.311 \cdot 10^5$
16	...

$$M_u := \left| \begin{array}{l} \text{for } i \in 1 .. \text{rows}(a) \\ \quad M_{u_i} \leftarrow \phi_{f_i} \cdot \left[F_{c_i} \cdot \left(\frac{h}{2} - \frac{a_i}{2} \right) + \sum_{j=1}^{\text{rows}(n_b)} \left[F_{f_{i,j}} \cdot \left(d_j - \frac{h}{2} \right) \right] \right] \\ M_u \end{array} \right. = \quad \frac{lb \cdot ft^2}{s^2}$$

	1
1	$3.594 \cdot 10^5$
2	$7.066 \cdot 10^5$
3	$1.042 \cdot 10^6$
4	$1.497 \cdot 10^6$
5	$2.07 \cdot 10^6$
6	$2.544 \cdot 10^6$
7	$2.956 \cdot 10^6$
8	$3.324 \cdot 10^6$
9	$4.258 \cdot 10^6$
10	$5.066 \cdot 10^6$
11	$5.307 \cdot 10^6$
12	$5.545 \cdot 10^6$
13	$5.778 \cdot 10^6$
14	$5.992 \cdot 10^6$
15	$6.172 \cdot 10^6$
16	...

P_u = ·kip

	1
1	-287.309
2	-272.162
3	-257.015
4	-227.795
5	-184.627
6	-149.909
7	-106.862
8	-70.79
9	-32.13
10	21.285
11	72.256
12	118.175
13	160.206
14	198.192
15	231.087
16	...

M_u = ·ft·kip

	1
1	11.171
2	21.963
3	32.377
4	46.516
5	64.345
6	79.071
7	91.862
8	103.301
9	132.345
10	157.462
11	164.953
12	172.357
13	179.575
14	186.247
15	191.838
16	...

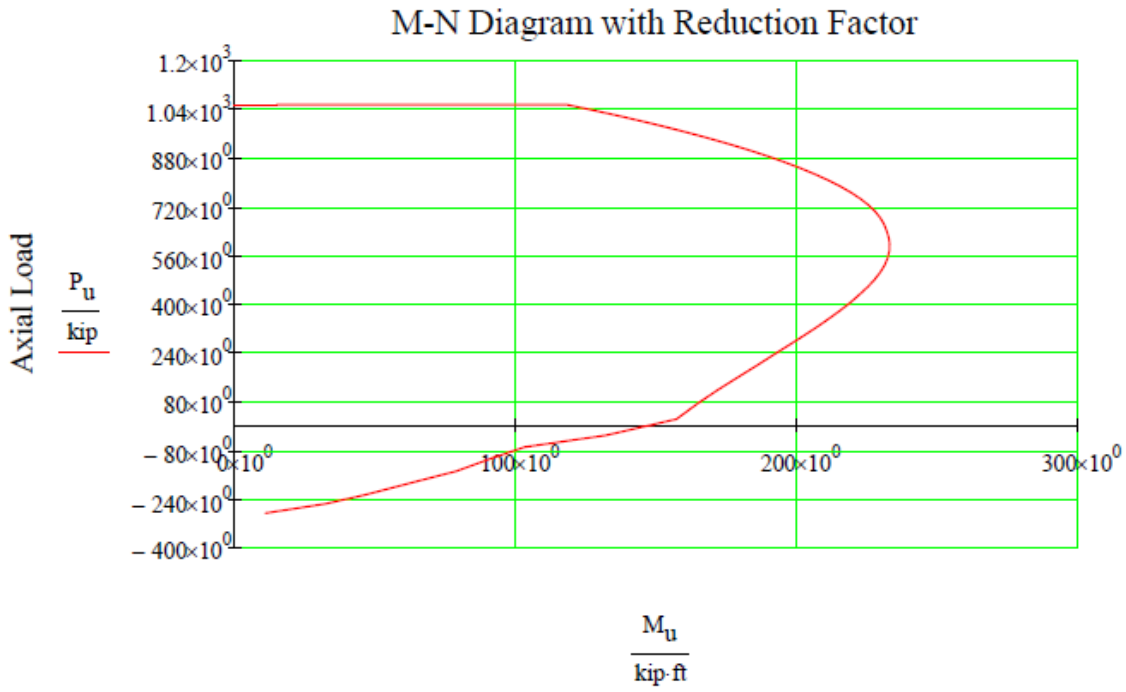

Development and Lap Splice Lengths for FRP Dowels

$$HalfCtC := 0.5\cdot\left(d_3 - d_2\right) = 1.75\cdot in$$

$$L_{dDowe} := \max\left[\left[\frac{31.6\frac{\left(\frac{f_{fr}}{ksi}\right)}{\sqrt{\left(\frac{f'_c}{ksi}\right)}} - 340}{13.6 + \frac{HalfCtC}{d_b}}\cdot d_b\right], \left(20\cdot d_b\right)\right] = 30.528\cdot in$$

ection 2.9.7.4.1-1 of the AASHTO

$$Lap := \max\left(1.3\cdot L_{dDowe}, 12in\right) = 39.687\cdot in$$

Section 2.9.7.6 of the AASHTO-GFRP2

$$L_D := Lap = 39.687\cdot in$$

The Length of Projected Dowels

$$L_H := L_D + 2in = 41.687\cdot in$$

The length of the Holes for Dowels

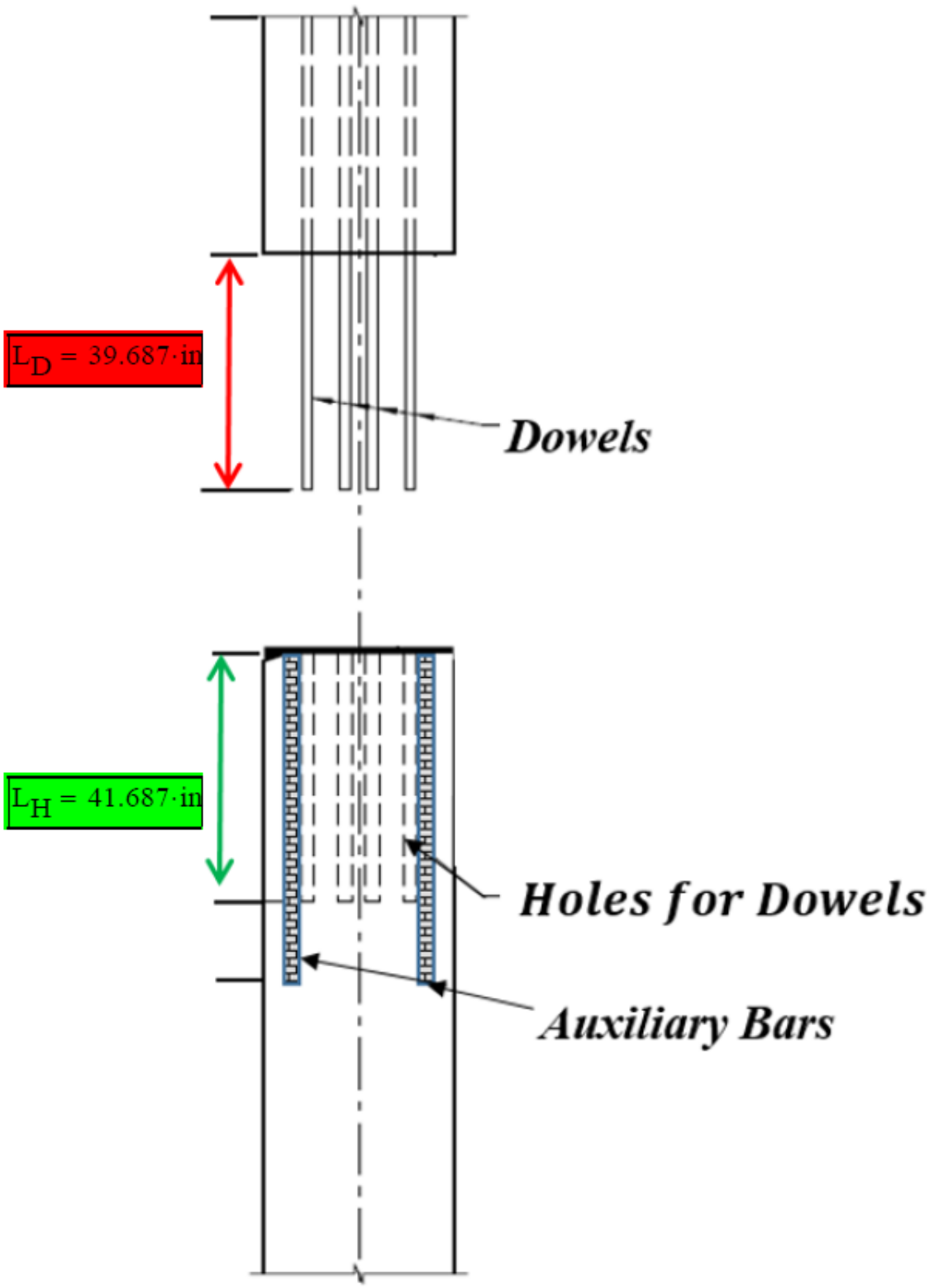
$L_D = 39.687 \cdot in$
Dowels
$L_H = 41.687 \cdot in$
Holes for Dowels
Auxiliary Bars

Section 933 of the FDOT Standard Specification for Road and Bridge Construction

Input

Group #	Strand Types	Diameter	Effective Cross Sectional Area	Nominal Ultimate Load
1	("Single Strand-5.0mm Ø")	0.2	0.025	9.1
2	("7-Strand-7.9mm Ø")	0.31	0.048	17.8
3	("7-Strand-10.8mm Ø")	0.43	0.090	33.1
4	("Single Strand-9.5mm Ø")	0.38	0.110	35.0
5	("7-Strand-12.5mm Ø")	0.49	0.117	43.3
6	("Single Strand-12.7 mm Ø")	0.50	0.196	59.0
7	("7-Strand-15.2mm Ø")	0.60	0.179	66.2
8	("7-Strand-17.2mm Ø")	0.68	0.234	86.6
9	("7-Strand-19.3mm Ø")	0.76	0.289	106.9

$dia :=$ in $A_{ps} :=$ in^2 $P_u :=$ kip

$C_{Es} := 1$ Environmental Reduction Factor for CFRP Strand

$n_{ps} := 1$ Set number of Strand or Total number of strands

$A_{ps.total} := n_{ps} \cdot A_{ps} =$ $\cdot in^2$

	1
1	0.025
2	0.048
3	0.09
4	0.11
5	0.117
6	0.196
7	0.179
8	0.234
9	0.289

Total strand area for each

$$C_{Es} \cdot \frac{P_u}{A_{ps}}$$

$$f_{pu} := C_{Es} \cdot \frac{P_u}{A_{ps}} = \text{·ksi}$$

	1
1	364
2	370.833
3	367.778
4	318.182
5	370.085
6	301.02
7	369.832
8	370.085
9	369.896

Ultimate Tensile Trength of the CFCC

Input

$P_j := 34kip$

Jacking force

$$f_{pi} := \frac{P_j \cdot n_{ps}}{A_{ps.total}} = \text{·ksi}$$

	1
1	1360
2	708.3
3	377.8
4	309.1
5	290.6
6	173.5
7	189.9
8	145.3
9	117.6

Input

Loss := 0.15

Loss Percentage

$f_{Loss} := Loss \cdot f_{pi} =$ ksi

Initial strand losses

	1
1	204
2	106.25
3	56.667
4	46.364
5	43.59
6	26.02
7	28.492
8	21.795
9	17.647

$f_{pe} := f_{pi} - (f_{Loss}) =$ ksi

Effective Prestresstressing Stres

	1
1	$1.156 \cdot 10^3$
2	602.083
3	321.111
4	262.727
5	247.009
6	147.449
7	161.453
8	123.504
9	100

Input

$\alpha_t := 1.1$ in·kip

AASHTO - CFRP-1

$\alpha_d := 1.48$ in·lb

AASHTO - CFRP-1

$f_{pbt} := f_{pi}$

Stress Prior to Transfer

Development Length
for FRP strand

$$L_{dStrand} := \left| \begin{array}{l} \text{for } i \in 1 .. \text{rows}(dia) \\ L_{dStrand_i} \leftarrow \dfrac{\dfrac{f_{pbt_i}}{ksi} \cdot dia_i}{\alpha_t \cdot \left(\dfrac{f'_{ci}}{ksi}\right)^{0.67}} + \dfrac{\left(\dfrac{f_{pu_i}}{ksi} - \dfrac{f_{pe_i}}{ksi}\right) \cdot dia_i}{\alpha_d \cdot \left(\dfrac{f'_c}{ksi}\right)^{0.67}} \\ L_{dStrand} \end{array} \right| = \text{ft}$$

	1
1	5.455
2	5.356
3	5.201
4	3.872
5	5.284
6	3.897
7	5.53
8	5.799
9	6.153

$L'_D := L_{dStrand} =$ in

Length of the Embedded
part of the Dowel

	1
1	65.457
2	64.272
3	62.417
4	46.466
5	63.402
6	46.766
7	66.359
8	69.588
9	73.833

Length of the Auxiliary Bar

$L_A := L_{dStrand} =$ in

	1
1	65.457
2	64.272
3	62.417
4	46.466
5	63.402
6	46.766
7	66.359
8	69.588
9	73.833

The Actual Developement Length considered in Design may Vary from the Length Calculated here. Please See the Relevant Report and Final Design Drawings.

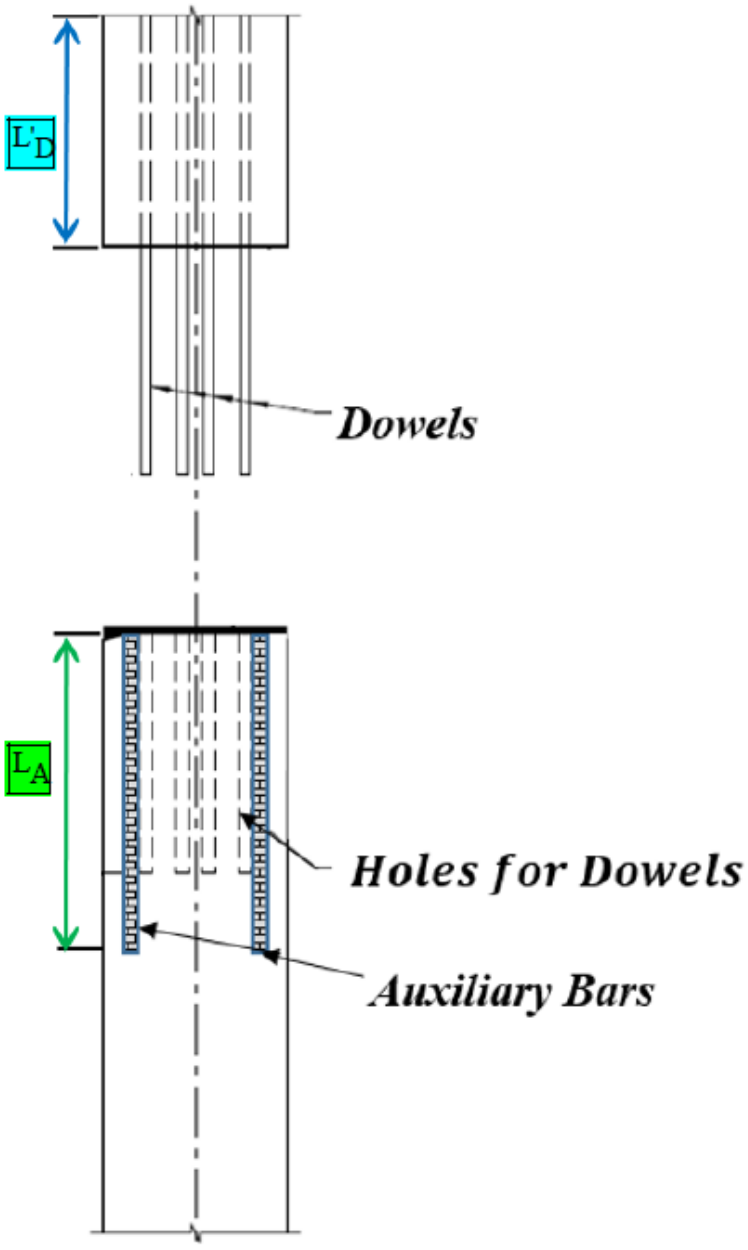

Auxiliary Bar Size = One Size Smaller than the Size of Dowel

Auxiliary Bar Number = Number of Dowel Bars on Perimeter

CHAPTER 7: SUMMARY AND CONCLUSION

7.1 Summary and Conclusions

The GFRP dowel option promises for a more economical option when compared to the use of other corrosion-resistant material (SS or CFRP) for dowels. The dissertation investigated the feasibility and effectiveness of epoxy dowel splice connecting PPCP segments using GFRP bars as dowels. To achieve the objective of this research, a design procedure was developed for an 18×18 in cross section PPCP with GFRP dowel bars. The design procedure followed the respective AASHTO and ACI standards and the provisions of FDOT design specifications. The focus of this study was on the flexural performance at the splice. Ten test specimens, each consisting of two 14 ft pile segments spliced to a total length of 28 ft were fabricated. The specimens contained GFRP, CFRP and Steel bars as dowels, and steel and CFRP strands for prestressing. These specimens were tested in flexure to compare the effectiveness of the new splice system designed using GFRP bars to systems currently available that use other materials for dowels. The results proved the feasibility of the use of GFRP dowels and their constructability. Their installation proved easier than steel bars or CFRP strand-dowels based on observations and discussion with the fabricator.

Three distinctive failure types were observed in experimental tests:

- Unforeseen splice specimens failed by splitting and bond failure in the female segments due to short dowel lengths. This failure resulted in lower strengths than predicted analytically and required by the specifications.

- Specimens for which GFRP dowel was used in combination with piles using CFRP prestressing strands failed by flexural cracking and debonding in the male segment near the end of the GFRP dowel. This failure mode could be an indication of inadequate bond length for CFRP strands.
- The remaining specimens failed in classical flexural mode with the concrete crushing in the compression zone at splice section.

The desired failure mode for pile splices is the Classical Flexural Failure at the splice. In FRP-reinforced concrete sections, concrete crushing before FRP rupture is more desirable because the failure of FRP dowels would result in brittle failure. Accordingly, for those cases where failure was with debonding and split cracking, overall direction of the refinement of the existing design should be to change the failure mode to the desirable classical flexural mode.

The laboratory tests validated the analytical procedure used for designing this new splicing system. The proposed design procedure underestimated the nominal moment capacities for GFRP dowel splices by an average of approximately 14% when compared to the test results. The experimental results showed the ability of the proposed epoxy bonded GFRP dowel pile splice to develop flexural resistance slightly lower than but comparable to that required by FDOT specifications for a preplanned PPCP. Design flexural resistance estimated for GFRP dowels using the design procedure and current AASHTO resistance/reduction factors are 32% lower than the FDOT required strength for mechanical pile splices, but 5% higher for steel dowel splices. Splices using CFRP

dowels showed in average flexural resistance lower than other preplanned splices. As expected, it was observed that the GFRP dowel splice cannot provide the equivalent strength for unforeseen splices because of dowel embedment shorter than the development length. Difficulties in drilling holes for unforeseen splices also affect the strength negatively. The design procedure was successfully implemented in Mathcad for pile splices according to available codes and analytical models. This tool can be used for design of splices of all material types and pile sizes of up to 30x30 in cross section. The research has a strong practical impact by development of new splice design and drawings for FRP dowel splices, and proposing refinement to the existing designs for CFRP and Steel dowel splices, all to be added to the FDOT Standard Plans (Index 455 Series) and Construction Specifications.

7.2 Main Contributions

The research performed for this dissertation has contributed to the body of the knowledge in several aspects:

- As an economic and corrosion-resistant alternative, the effectiveness of GFRP dowels for use in both unforeseen and preplanned PPCP splices was studied through analytical and experimental investigation.
- This research compares GFRP dowel splice performance to that of CFRP strand and conventional carbon steel bar dowels, and provides a better understanding of the performance of spliced bearing.

- A design procedure was developed for pile splices using three different materials for dowels; GFRP reinforcing bars, CFRP strand, and traditional carbon-steel reinforcing bars.
- In order to validate the design procedure, 10 full-scale PPCP specimens of 18×18 in cross-section with a total length of 28 ft were designed, fabricated, assembled and tested at the Florida Department of Transportation (FDOT) Structures Research Center. The results were used to validate the design procedure. Test results also contribute to the body of knowledge by providing researchers the much needed data on the behavior of epoxy dowel pile splices.
- Using numerical approaches and vector-based calculations, a practical design tool was developed in Mathcad software to allow engineers to design pile splices up to 30×30 in cross section.
- This research has developed new splice design and drawings for FRP dowel splices as part of the FDOT standard drawings (Index 455 series) and construction specifications, and proposed refinement to the existing designs for CFRP and Steel dowel splices.

7.3 Recommendation for Future Study

In this study, a design procedure for epoxy dowel pile splice with different materials, including CFRP, GFRP, and Steel, was analytically developed and experimentally validated. Mathcad software was then used to develop a user-friendly design tool for

engineers to be able to design dowel pile splices with a variety of materials, sizes, and configurations. Future studies to complement this study can include the following:

- The focus of this study was on the flexural performance at the splice. Although the tension and compression capacities were also checked in Chapter3 of this dissertation, investigation on shear behavior of the GFRP and CFRP pile splices can be a topic for future investigations.
- As another future research, a detailed finite element model can be developed for parametric study on factors such as different shapes for PPCP cross-section (e.g. Circle sections), varying bonding material, and other arrangements for number and size of dowels as well as their placement. The experimental results reported in this dissertation can be accordingly used for calibration of this model.
- The effect of other parameters such as spacing of stirrups for a better confinement, extending the development length of FRP strands, and replacing the CFRP strands with CFRP bars for dowels can also be a subject for future studies.
- To address the concerns about the behavior of the epoxy GFRP pile splices under driving conditions, it is also recommended to have spliced piles driven with actual field conditions. Using a pile driving analyzer (PDA) to monitor driving stresses while piles are driven will provide valuable information on the behavior of pile and the splice during driving operation. The driven piles can then be extracted from the soil, and subjected to flexural testing to demonstrate their effectiveness in actual field and operation conditions.

REFERENCES

[1] Farhangdoust, S., Mehrabi, A., & Nolan, S. (2021). Analytical Investigation of Prestressed Precast Pile Splice Using Glass Fiber Reinforced Polymer (GFRP) Dowels. The Transportation Research Board (TRB) 100st Annual Meeting.

[2] Farhangdoust S, Mehrabi A. (2020). Non-Destructive Evaluation of Closure Joints in Accelerated Bridge Construction using a Damage Etiology Approach. Applied Sciences. 10(4):1457.

[3] Farhangdoust, S., & Mehrabi, A. (2019, April). NDT inspection of critical ABC details to assure life cycle performance and avoid future unforeseen excessive repairs. In Structures Congress 2019: Bridges, Nonbuilding and Special Structures, and Nonstructural Components (pp. 231-242). Reston, VA: American Society of Civil Engineers.

[4] Mehrabi, A., & Farhangdoust, S. (2019). NDT Methods Applicable to Health Monitoring of ABC Closure Joints (No. ABC-UTC-2013-C3-FIU04). Accelerated Bridge Construction University Transportation Center (ABC-UTC).

[5] Farhangdoust, S., Mehrabi, A., & Mosawi, S. S. (2018). NDT methods applicable to health monitoring of ABC closure joints. In 27th ASNT Research Symposium (pp. 75-87).

[6] Taeby, M., & Mehrabi, A. (2019). Decision Support Framework for Inspection and Maintenance; A focus on Bridges using Post-Tensioning Tendons. Current Trends in Civil & Structural Engineering 3 (5).

[7] Cadenazzi, T., Dotelli, G., Rossini, M., Nolan, S., & Nanni, A. (2019). Life-cycle cost and life-cycle assessment analysis at the design stage of a fiber-reinforced polymer-reinforced concrete bridge in Florida. Advances in Civil Engineering Materials, 8(2), 128-151.

[8] Farhangdoust, S., & Mehrabi, A. (2019). Health monitoring of closure joints in accelerated bridge construction: a review of non-destructive testing application. Journal of Advanced Concrete Technology, 17(7), 381-404.

[9] Lampo, R., Maher, A., Busel, J., & Odello, R. (1997). Design and development of FRP composite piling systems. Plastics in Building Construction, 21(12), 9.

[10] Farhangdoust, S., & Mehrabi, A. (2019, April).ABC-UTC Guideline for: SELECTION OF NDT METHODS APPLICABLE TO HEALTH MONITORING OF ABC CLOSURE JOINTS. Accelerated Bridge Construction University Transportation Center.

[13] Mehrabi, A. B., & Farhangdoust, S. (2018). A laser-based noncontact vibration technique for health monitoring of structural cables: background, success, and new developments. Advances in Acoustics and Vibration, 2018.

[14] Rossini, M., & Nanni, A. (2019). Composite strands for prestressed concrete: State-of-the-practice and experimental investigation into mild prestressing with GFRP. Construction and Building Materials, 205, 486-498.

[15] Clark, J. D. (2020). Florida Department of Transportation Bridge Inventory Annual Report, July 2020

[16] Iskander, M. Recent Developments in Fiber-Reinforced Polymer Composite Piling Practice. Presented at the 81st Annual Meeting of the Transportation Research Board, Washington, D.C., 2002.

[17] Fleming, K., Weltman, A., Randolph, M., & Elson, K. (2008). Piling engineering. CRC press.

[18] Heinz, R. (1993). Plastic piling. Civil Engineering, 63(4), 63.

[19] Horeczko, G. (1995). Marine application of recycled plastics. In Restructuring: America and Beyond (pp. 834-837). ASCE.

[20] Pando, M. A., Ealy, C. D., Filz, G. M., Lesko, J. J., & Hoppe, E. J. (2006). A laboratory and field study of composite piles for bridge substructures (No. FHWA-HRT-04-043). United States. Federal Highway Administration. Office of Infrastructure Research and Development.

[21] Lampo, R., T. Nosker, D. Barno, J. Busel, A. Maher, P. Dutta, and R. Odello. "Development and demonstration of FRP composite fender, loadbearing, and sheet piling systems." USACERL TR-98/123, U.S. Army Corps of Engineers (CERL), 1998.

[22] Sen, R., Iyer, S., Issa, M., & Shahawy, M. (1991). Fiberglass pretensioned piles for marine environment. In Advanced composites materials in civil engineering structures (pp. 348-359). ASCE.

[23] Han, J., Frost, J. D., & Brown, V. L. (2003). Design of fiber-reinforced polymer composite piles under vertical and lateral loads. Transportation research record, 1849(1), 71-80.

[24] Rambo-Roddenberry, M., Joshi, K., Fallaha, S., Herrera, R., Kampmann, R., Chipperfield, J. and Mtenga, P., 2016. Construction, strength, and driving performance of carbon-fiber-reinforced polymer prestressed concrete piles. PCI Journal.

[25] Lampo, R., Maher, A., Busel, J., & Odello, R. (1997). Design and development of FRP composite piling systems. Plastics in Building Construction, 21(12), 9.

[26] Mullins, G., Sen, R., Sagüés, A., Winters, D., Morton, C., Fernandez, J., Johnson, K., DePianta, V., Vomacka, J. and Mitchell, E., 2014. Design and construction of precast piles with stainless reinforcing steel (No. BDK-84-977-07). Florida. Dept. of Transportation.

[27] Belarbi, A., Dawood, M., Bowman, M. and Mirmiran, A., 2017. Synthesis of concrete bridge piles prestressed with CFRP systems (No. FHWA/TX-17/0-6917-1). Texas. Dept. of Transportation. Research and Technology Implementation Office.

[28] Grace, N., 2007. 5-years monitoring of first CFRP prestressed concrete 3-span highway bridge in USA. In Proceedings of the 12th International Conference on Structural Faults & Repair-2008.

[29] Roddenberry, M., Mtenga, P. and Joshi, K., 2014. Investigation of carbon fiber composite cables (CFCC) in prestressed concrete piles (No. BDK83-977-17). Florida. Dept. of Transportation.

[30] Wu, Y., & Nürnberger, U. (2009). Corrosion - technical properties of high - strength stainless steels for the application in prestressed concrete structures. Materials and corrosion, 60(10), 771-780.

[31] FDOT Standard Drawings Index Series 455, (2018) Florida Department of Transportation, Tallahassee, FL.

[32] Nürnberger, U. (2001). Nichtrostende Betonstähle in der Bautechnik-Teil 1: Korrosionsbeständigkeit als Kriterium für innovative Anwendungen. Beton- und Stahlbetonbau, 96(8), 561-570.

[33] Paul, A., Kahn, L.F. and Kurtis, K., 2015. Corrosion-free precast prestressed concrete piles made with stainless steel reinforcement: construction, test and evaluation (No. FHWA-GA-15-1134). Georgia. Department of Transportation. Office of Research.

[34] Cook, R.A. and McVay, M.C., 2003. Alternatives for Precast Pile Splices. University of Florida.

[35] Bruce Jr, R. N., & Hebert, D. C. (1974). Splicing of Precast Prestressed Concrete Piles: Part 1—Review and Performance of Splices. PCI JOURNAL, 19(5), 70-97.

[36] Bruce Jr, R. N., & Hebert, D. C. (1974). Splicing of Precast Prestressed Concrete Piles: Part 2—Tests and Analysis of Cement-Dowel Splice. PCI JOURNAL, 19(6), 40-66.

[37] Liu TC-Y. Prestressed Concrete Piling-Contemporary Design Practice and Recommendations. J. Proc., vol. 67, 1970, p. 201–220.

[38] Alley EW. Long prestressed piles. Civ Eng 1970;40:50.

[39] Gerwick Jr BC. General Report—Prestressed Concrete Piles. Proceedings, 1968, p. 1–30.

[40] Econfina River Bridge in Taylor County F. Epoxy Dowel splice 2015. https://www.youtube.com/watch?v=pyh58qG_w0E.

[41] Navaratnarajah, V. (1981). Flexural tests on epoxy-jointed precast prestressed concrete piles. International Journal of Adhesion and Adhesives, 1(5), 265-270.

[42] Transport Roads and Maritime Services of New South Wales drawing, No. B120, Issue 1 March 2012.

[43] Canner, I. W. (2005). Field Testing of Prestressed Concrete Piles Spliced with Steel Pipes (Doctoral dissertation, University of Florida).

[44] Seal bond Chemicals Co., Access 7/24/2019, Online: http://sealbondchemicals.com/product-item/sealbond-458-pe/

[45] EPIWELD® 580, Eoxy Products, Lambert Corporation, September 2011, Online Access: https://www.buildsite.com/pdf/lambert/EPIWELD-580-Product-Data-1398577.pdf.

[46] Structures Manual. Florida Department of Transportation, Tallahassee, January, 2021.

[47] Standard Specifications for Road and Bridge Construction. Florida Department of Transportation, Tallahassee, January, 2020.

[48] Standard Plans – Index Series 455. Florida Department of Transportation, Tallahassee, 2020-2021.

[49] AASHTO (American Association of State Highway and Transportation Officials). 2018. AASHTO LRFD Bridge Design Guide Specifications for GFRP-Reinforced Concrete Bridges, 2nd Edition, Washington, DC: AASHTO.

[50] AASHTO (American Association of State Highway and Transportation Officials). 2018. Guide Specifications for the Design of Concrete Bridge Beams Prestressed with Carbon Fiber-Reinforced Polymer (CFRP) Systems, 1st Edition, Washington, DC: AASHTO.

[51] Farhangdoust, S., Mehrabi, A., & Nolan, S. (2021). Design of prestressed precast pile splice using glass fiber reinforced polymer (GFRP) dowels. Engineering Structures, 244, 112806.

[52] Dolati, S. S. K., & Mehrabi, A. (2021, April). Review of available systems and materials for splicing prestressed-precast concrete piles. In Structures (Vol. 30, pp. 850-865). Elsevier.

[53] Khedmatgozar Dolati, S. S., & Mehrabi, A. (2021). Alternative Systems and Materials for Splicing Prestressed-Precast Concrete Piles. Transportation Research Record, 03611981211052949.

[54] Farhangdoust, S., Mehrabi, A., & Nolan, S. (2022). GFRP Composite Bars for Splicing Prestressed Precast Concrete Piles: Design and Experimental Investigation. Engineering Structures.

[55] Dolati, S. S. K., & Mehrabi, A. Review of Mechanical Bar Couplers for Splicing Precast Concrete Members.

[56] Tashakori, S., Baghalian, A., Senyurek, V. Y., Farhangdoust, S., McDaniel, D., & Tansel, I. N. (2018). Composites bond inspection using heterodyne effect and SuRE methods. Shock and Vibration, 2018.

[57] Farhangdoust, S., Tashakori, S., Baghalian, A., Mehrabi, A., & Tansel, I. N. (2019, March). Prediction of damage location in composite plates using artificial neural network modeling. In Sensors and Smart Structures Technologies for Civil, Mechanical, and Aerospace Systems 2019 (Vol. 10970, p. 109700I). International Society for Optics and Photonics.

[58] ACI (American Concrete Institute) Committee 440. 2015. Guide for the Design and Construction of Concrete Reinforced with FRP Bars. American Concrete Institute. ACI 440.1R-15.

[59] ACI Committee 318. 2014. Building Code Requirements for Structural Concrete (ACI 318-14) and Commentary (ACI 318R-14). Farmington Hills, MI: ACI.

[60] AASHTO (American Association of State Highway and Transportation Officials). 2017. AASHTO LRFD Bridge Design Specifications, 8th Edition, Washington, DC: AASHTO.

[61] Young, V., and Wan, G.,(2018) "CFRP and HSSS Strands in Prestressed Concrete Design," FDOT Transportation Symposium, June 2018, Orlando FL.

[62] Specification of CFCC, Florida Department of Transportation, 2020.

[63] ACI (American Concrete Institute) Committee 440. 2004. Prestressing Concrete Structures with FRP Tendons. American Concrete Institute. ACI 440.4R-04.

[64] Proposed Specification: 9330100 PRESTRESSING STRAND AND BAR, State Specifications Engineer, Florida Department of Transportation, 2021.

[65] Paul, A., Kahn, L.F. and Kurtis, K., (2015). Corrosion-free precast prestressed concrete piles made with stainless steel reinforcement: construction, test and evaluation (No. FHWA-GA-15-1134). Georgia Department of Transportation, Office of Research.

[66] Mullins, G., Sen, R., Sagüés, A., Winters, D., Morton, C., Fernandez, J., Johnson, K., DePianta, V., Vomacka, J. and Mitchell, E., (2014). Design and construction of precast piles with stainless reinforcing steel (Report No. BDK84 977-07). Florida Deptartment of Transportation.

[67] Tokyo Rope (2012). Technical Data on CFCC.

[68] Mahmoud, Z. I. and Rizkalla, S. H. (1996). "Bond properties of CFRP prestressing reinforcement." Proceedings of the First Middle East Workshop on Structural Composites for Infrastructure Applications, Egypt.

[69] Grace, N. (2000). "Transfer length of CFRP/CFCC strands for double-t girders." PCI Journal, 45(5), 110–126.

APPENDICES

APPENDIX A – SHOP DRAWINGS

PRESTRESSED CONCRETE PILE NOTES

GENERAL SPECIFICATIONS:
The Florida Department of Transportation "Standard Specifications for Road and Bridge Construction".

DESIGN SPECIFICATIONS:
Florida Department of Transportation (FDOT) "Structures Design Guidelines", current edition.

American Association of State Highway and Transportation Officials (AASHTO) "LRFD Bridge Design Specifications", current edition.

DESIGN PARAMETERS:
Square Prestressed Concrete Section: Designed for 1,000 psi uniform compression after prestress losses with out loads.

Pick–up, Storage, and Transportation: 0.0 psi tension w/1.5 times pile self weight.

SPIRAL WIRE:
Each wrap of spirals shall be tied to at least two corner strands. One full turn required for spiral splices.
Carbon Steel spirals shall be tied using steel ties.
CFRP spirals shall be tied using CFRP ties.

CONCRETE CLASS:
Concrete for all piles shall be Class V SLAG, Mix 01 1234, 6,500 psi.

CONCRETE STRENGTH:
The pile cylinder strength shall be 6,000 psi minimum at 28 days and 4,000 psi minimum at time of transfer of the Prestressing Force.

PICK–UP POINTS:
Piles shall be marked at the pick–up points to indicate proper points for attaching handling lines.

PRESTRESSING MATERIALS:
Prestressing carbon steel shall be seven–wire strand, Grade 270.
L.R.S. = Low–Relaxation 0.6" Carbon Steel Strand and shall meet the requirements of FDOT Standard Specifications Section 933.
Prestressing CFRP 7–strand shall meet the requirements of FDOT Standard Specifications Section 933.

REINFORCING MATERIALS (DOWELS):
All reinforcing carbon steel dowels shall meet the requirements of FDOT Standard Specifications Section 415.
All CFRP and GFRP dowels and bars shall meet the requirements of ASTM D7957–17 and FDOT Standard Specifications for Road and Bridge Construction [January 2020] Section 932.
However, the exact material for GFRP and CFRP will be selected in consultation with the precast contractor and communication with FDOT project manager. CFRP Spiral Ties are 0.2"Ø strand spiral tie and shall meet FDOT Standard Specifications Section 933.

SPLICES:
7–strand 19.3 mm Ø CFRP dowel bars are used for piles splices using CFRP dowels according to Drawings Sheets 3,4,5 and 6.
#10 CFRP dowel bars are used for piles splices using GFRP dowels according to Drawings Sheets 3,4,5 and 6.
#10 steel dowel bars are used for piles splices using steel dowels according to Drawings Sheets 3,4,5 and 6

EPOXY
Type AB Epoxy (Pilgrim EM 5–2) shall be used for assembling the test specimens.
Type AB Epoxy grout shall be approved by the FDOT Project Manager before the assembly of test specimens.

SPECIMEN PREPARATION
Holes will be cast using 2" corrugated galvanized steel duct for the preplanned specimens 3–8 and 1 1/2" for specimens 9&10.
For Specimns 3 to 10 the 1" spiral tie pitch shall be continued to 4' below the head of the pile where the dowel holes are utilized.
Unforseen specimen will be cast with 1 1/4" PVC pipe that will be drilled to 1 3/4" hole to simulate field conditions.
Stay–in–place corrugated galvanized steel duct shall meet the requirements of ASTM A653, Coating Designation G90, 26 gauge. Ducts shall be 1 1/2" Ø for CFRP bars, and 2" Ø for steel and GFRP bars with a minimum corrugation (rib) height of 0.12".
ASTM A653, Coating Designation G90, 26 gauge, 2" diameter and a minimum corrugation of 0.12".

MATERIAL SAMPLING AND TESTING:
In addition to the usual amount of testing cylinders collected, 9 cylindrical specimens shall be collected from each batch used for fabrication of pile segments for further testing.
Strands –at least five 6 feet strand for each size and type (steel and CFRP) will be collected from the coils used for fabrication of pile segments.
Rebars –at least five 6 feet bars for each size and type of bars (steel and CFRP, and GFRP) will be collected for further tension testing.
Epoxy samples will be taken for bond testing with concrete, or manufacturer's specifications will be used to determine the mechanical properties of the epoxy material.
Instructions and specifications for mixing, setting and curing time provided by the epoxy manufacturer will be used during assembly of the test specimens.

THE SUBMITTAL OF THESE DRAWINGS DOES NOT CONSTITUE A REVIEW OF THE PRESTRESS DESIGN. IT IS THE RESPONSIBILITY OF THE DESIGN ENGINEER TO REVIEW AND DETERMINE THAT THIS SUBMITTAL AND ITS APPLICATION IS CORRECT. THE PURPOSE AND INTENT OF THIS SUBMITTAL IS TO ILLUSTRATE AND OUTLINE DETAILS NECCESSARY TO MANUFACTURE SAID PRODUCT AS DESIGN BY SELECT STRUCTURAL

SHEET NO.	SS Job NO.	REVISIONS DATE	REVISIONS DESCRIPTION	DRAWN BY		GC	PROJECT	SHEET CONTENTS
1	20079	10/30/20	Modified Splices paragraph	BG APPROVED BY DATE 09/29/20	S & S PRECAST, INC. P.O. BOX 366098 BONITA SPRINGS, FL 34136 (239) 992–8685 FAX: (239) 992–9226	Florida International University 10555 West Flagler Street Miami, FL 33174	18' Test Piles	General Information

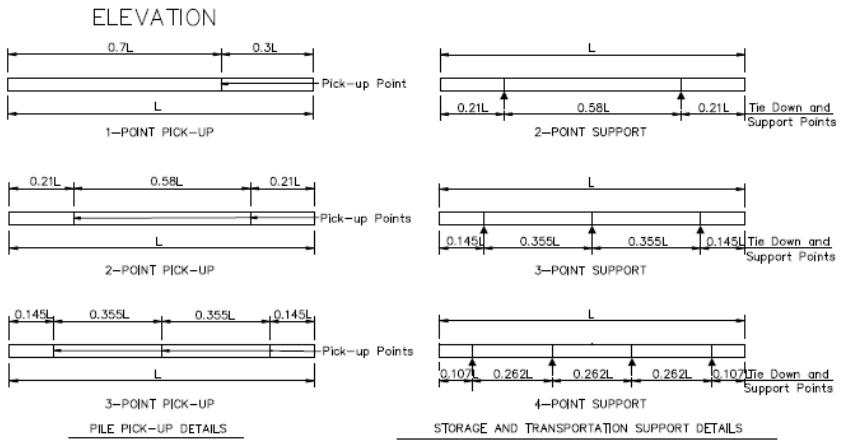

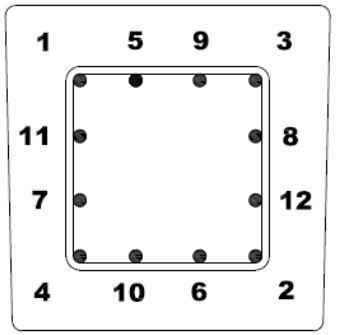

DETENSIONING SCHEDULE
SINGLE RUN

TABLE OF MAXIMUM PILE PICK-UP AND SUPPORT LENGTHS								
	Square Pile Size (Inches)						Required Storage and Transportation Detail	Pick-Up Detail
	12	14	18	20	24	30		
Maximum Pile Length (Feet)	48	52	59	62	68	87	2, 3, or 4 point	1 Point
	69	75	85	89	98	124	2, 3, or 4 point	2 Point
	99	107	121	128	140	178	3 or 4 point	3 Point

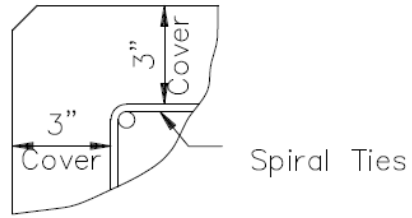

DETAIL SHOWING
TYPICAL COVER

SHEET NO.	SS Job NO.	REVISIONS DATE	REVISIONS DESCRIPTION	DRAWN BY	S & S PRECAST, INC.	GC	PROJECT	SHEET CONTENTS
2	20079			BG APPROVED BY DATE 09/29/20	P.O. BOX 366098 BONITA SPRINGS, FL 34136 (239) 992-8685 FAX: (239) 992-9226	Florida International University 10555 West Flagler Street Miami, FL 33174	18" Test Piles	Detentioning schedule Pick-up, storage and transportation details

ELEVATION VIEW OF FEMALE PILE SEGMENT (PREPLANNED – SPECIMENS 3 THROUGH 10)

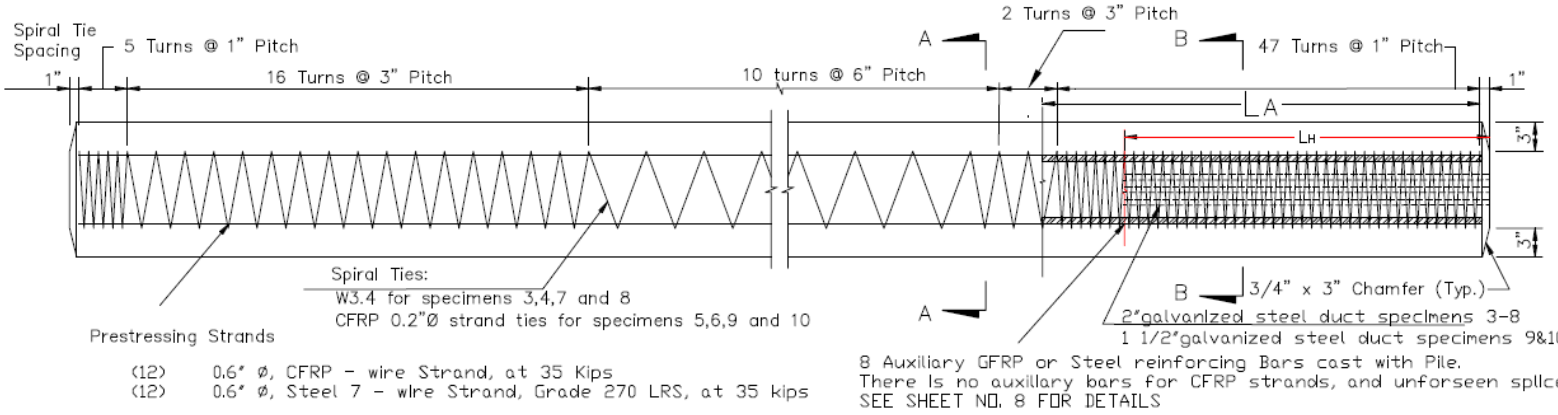

(12) 0.6" Ø, CFRP – wire Strand, at 35 Kips
(12) 0.6" Ø, Steel 7 – wire Strand, Grade 270 LRS, at 35 kips

ELEVATION VIEW OF FEMALE PILE SEGMENT (UNFORSEEN – SPECIMENS 1 AND 2)

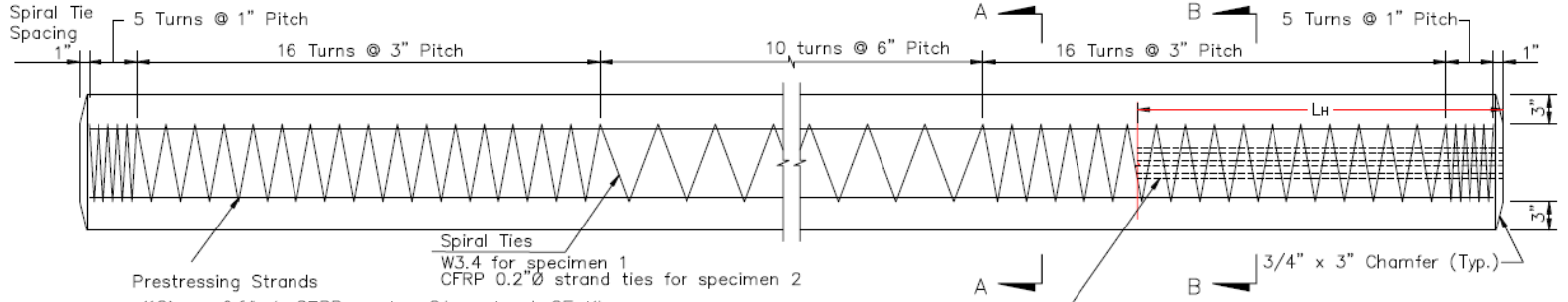

(12) 0.6" Ø, CFRP – wire Strand, at 35 Kips
(12) 0.6" Ø, Steel 7 – wire Strand, Grade 270 LRS, at 35 kips
SEE SHEET NO. 8 FOR DETAILS

SHEET NO.	SS Job NO.	REVISIONS DATE	REVISIONS DESCRIPTION	DRAWN BY	S & S PRECAST, INC.	GC:	PROJECT	SHEET CONTENTS
3	20079	10/12/20	Corrugated steel duct modified from 2" to 1 1/2" For specimens 9 and 10	BG	P.O. BOX 366098 BONITA SPRINGS, FL 34136	Florida International University 10555 West Flagler Street Miami, FL 33174	18" Test Piles	Elevation View
		11/01/20	Type of tie added For each specimen Changed force from 34 kips to 35 kips for CFRP	APPROVED BY	(239) 992-8685 FAX: (239) 992-9226			
				DATE 09/29/20				

ELEVATION VIEW OF MALE PILE SEGMENT (1 THROUGH 10)

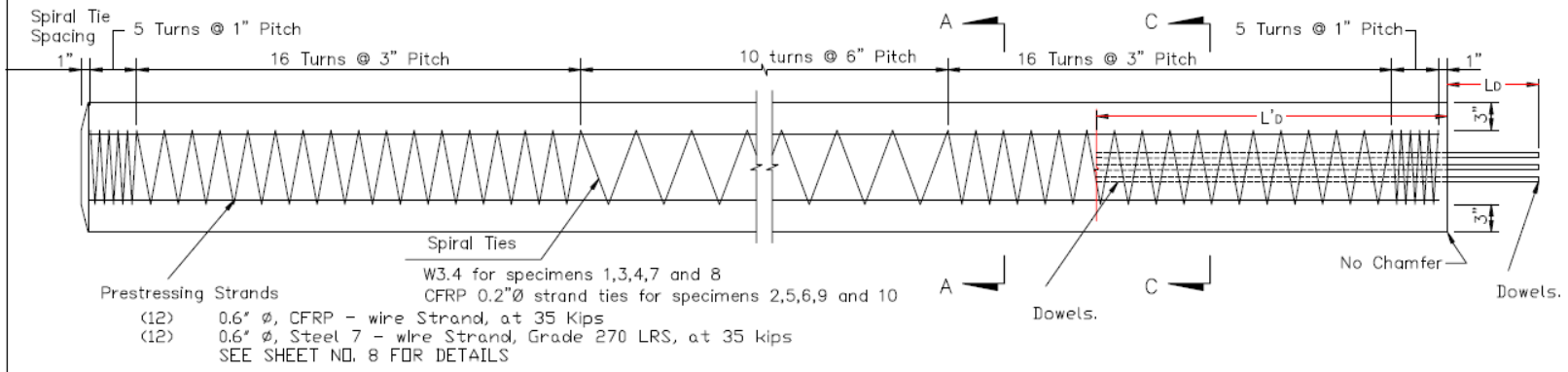

DETAILS				
SPECIMEN #	L_A	L_D	L_H	L'_D
1	0'-0"	2'-6"	2'-8"	8'-3"
2	0'-0"	2'-6"	2'-8"	4'-6"
3&4	8'-3"	3'-4"	3'-6"	8'-3"
5&6	0'-0"	4'-6"	4'-8"	4'-6"
7&8	10'-6"	4'-0"	4'-2"	10'-6"
9&10	0'-0"	4'-6"	4'-8"	4'-6"

SHEET NO.	SS Job NO.	REVISIONS DATE	REVISIONS DESCRIPTION	DRAWN BY	S & S PRECAST, INC.	GC	PROJECT	SHEET CONTENTS
4	20079	10/12/20	Type of tie added for each specimen	BG	P.O. BOX 366098 BONITA SPRINGS, FL 34136	Florida International University 10555 West Flagler Street Miami, FL 33174	18" Test Piles	Elevation View Dimension Details
		11/01/20	Changed force from 34 kips to 35 kips for CFRP	APPROVED BY	(239) 992-8685 FAX: (239) 992-9226			
				DATE 9/29/20				

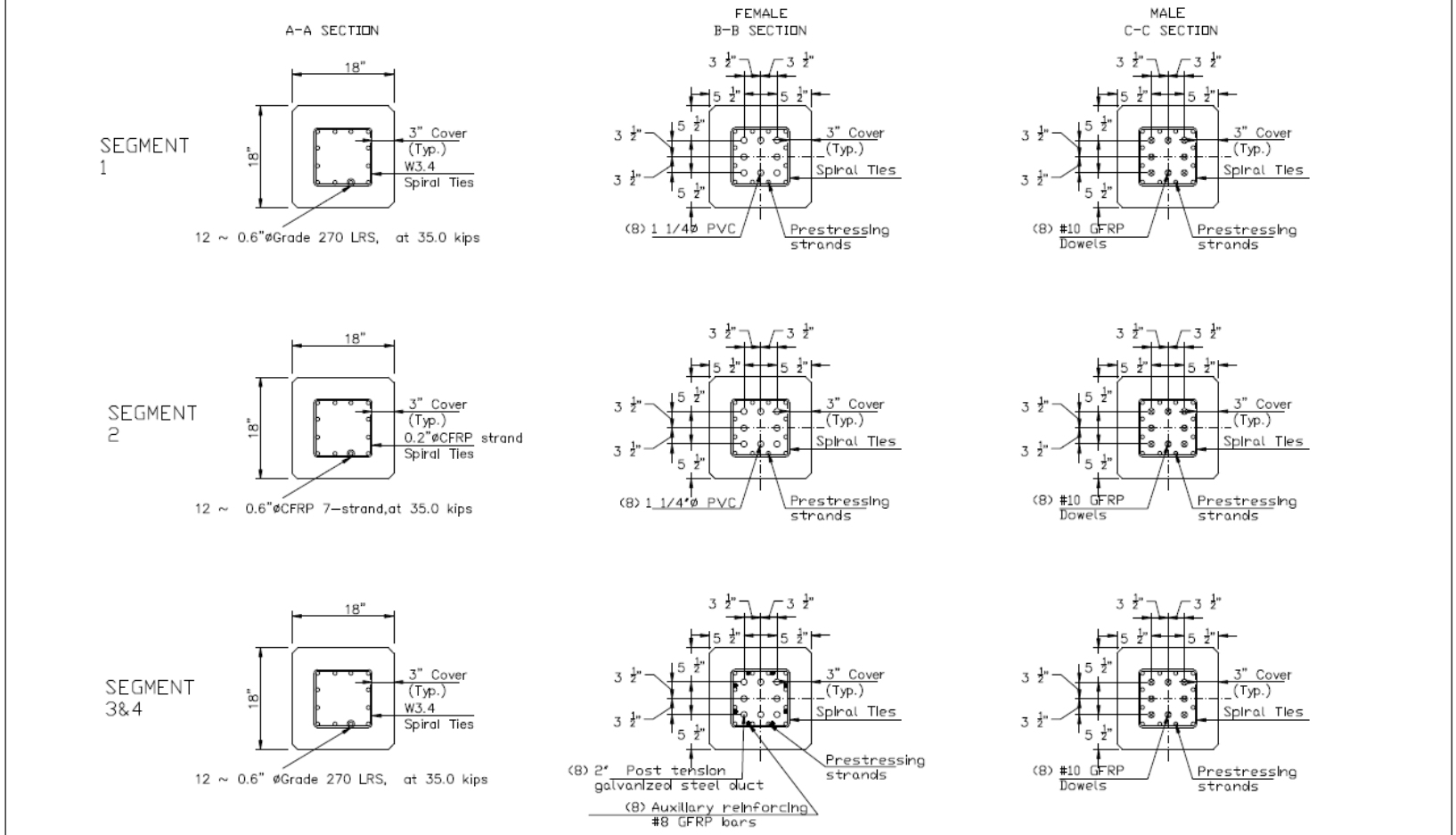

SHEET NO.	SS Job NO.	REVISIONS DATE	REVISIONS DESCRIPTION	DRAWN BY	S & S PRECAST, INC.	GC	PROJECT	SHEET CONTENTS
5	20079	11/01/20	Changed force from 34 kips to 35 kips for CFRP	BG	P.O. BOX 366098 BONITA SPRINGS, FL 34136	Florida International University	18' Test Piles	Section View Segment 1-4
				APPROVED BY	(239) 992-8685 FAX: (239) 992-9226	10555 West Flagler Street		
				DATE 09/29/20		Miami, FL 33174		

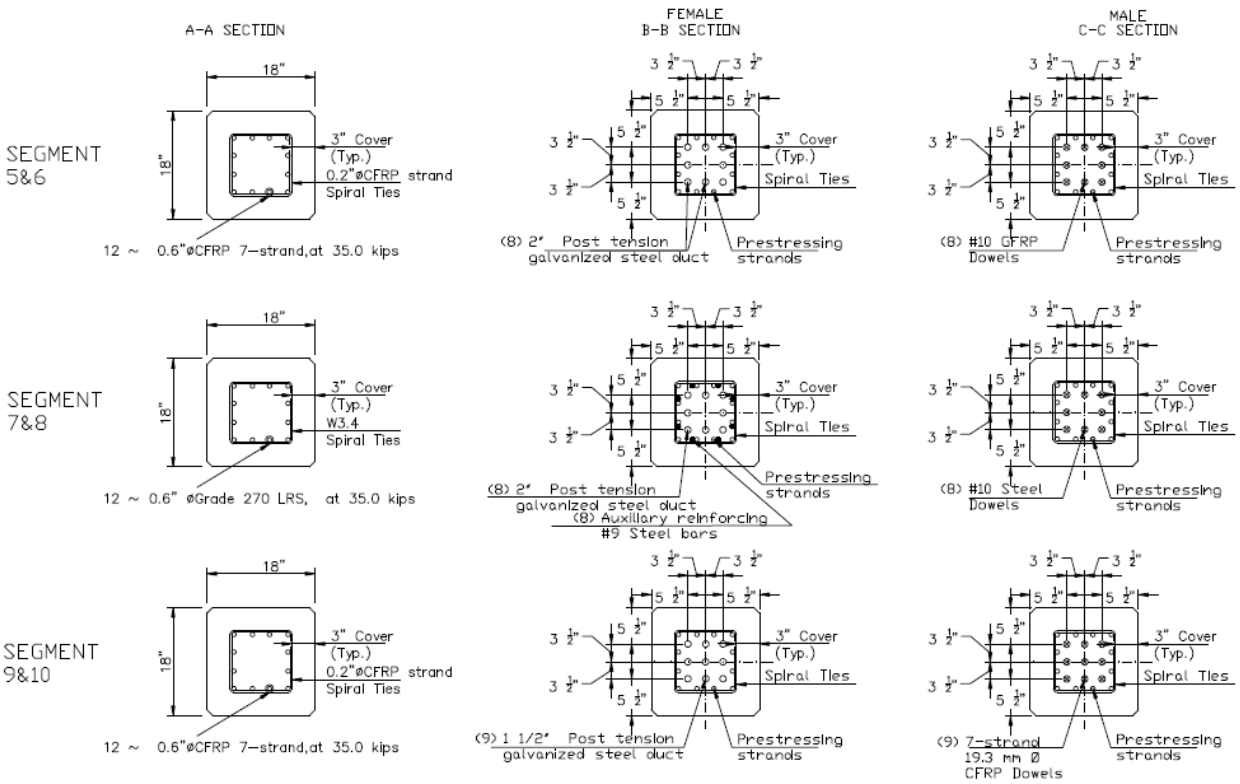

SHEET NO.	SS Job NO.	REVISIONS		DRAWN BY	S & S PRECAST, INC.	GC	PROJECT	SHEET CONTENTS
		DATE	DESCRIPTION	BG	P.O. BOX 366098 BONITA SPRINGS, FL 34136	Florida International University	18" Test Piles	Section View Segment 5-10
6	20079	10/12/20	Corrugated steel duct modified from 2" to 1 1/2" for specimens 9 and 10	APPROVED BY	(239) 992-8685 FAX: (239) 992-9226	10555 West Flagler Street Miami, FL 33174		
		11/01/20	Modified CFRP dowel from #8 to 19.3 mm for specimens 9&10 Changed force from 34 kips to 35 kips for CFRP	DATE 09/29/20				

Detail A

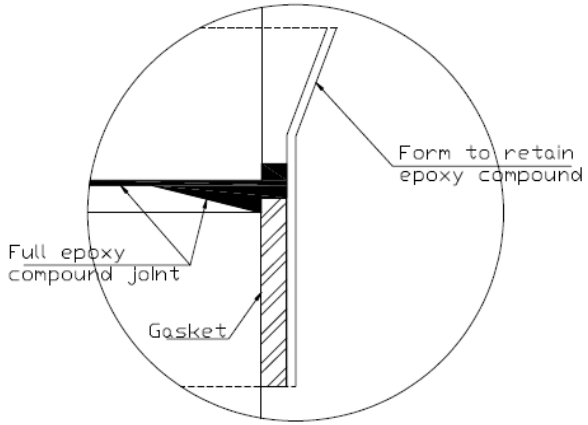

NOTE:
For Specimens 3 and 5: $\frac{3}{8}$" (applied) $\frac{1}{4}$" (final thickness)
For the rest of Specimens: $\frac{3}{8}$" (applied) $\frac{1}{4}$" (final thickness)

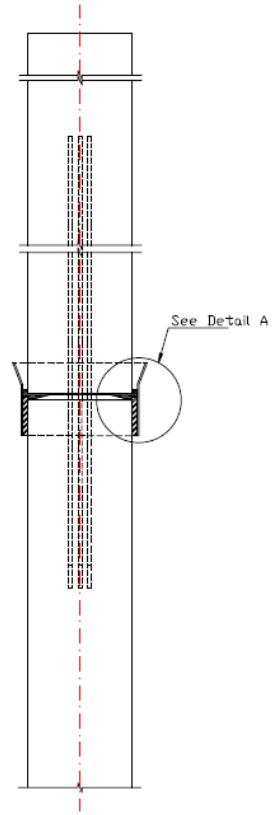

UNFORESEEN PILE
SPLICE DETAIL

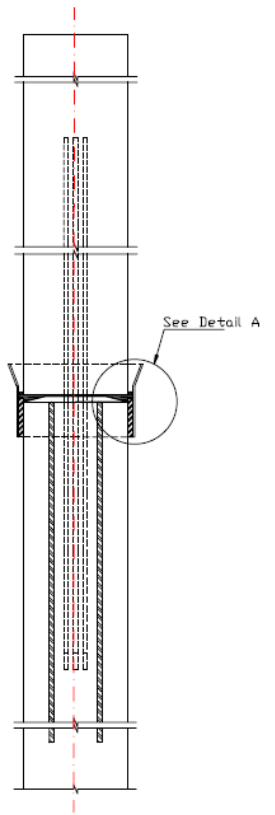

PREPLANNED PILE
SPLICE DETAIL

SHEET NO.	SS Job NO.	REVISIONS DATE	REVISIONS DESCRIPTION	DRAWN BY		GC:	PROJECT	SHEET CONTENTS
7	20079	10/12/20	Expoxy thickness from 5/8" to 3/8" applied Expoxy final thickness from 1/2" to 1/4"	BG APPROVED BY DATE 09/29/20	S & S PRECAST, INC. P.O. BOX 366098 BONITA SPRINGS, FL 34136 (239) 992-8685 FAX: (239) 992-9226	Florida International University 10555 West Flagler Street Miami, FL 33174	18" Test Piles	Epoxy Pile Spice Detail

SPECIMEN 1 (UNFORESEEN)

	LENGTH	SPIRAL		DOWEL			DOWEL HOLE			COMMENT	AUXILIARY BARS			CYDS	WT	PRESTRESSED STRAND
		MATERIAL	# OF TURNS	MATERIAL	QTY.	LENGTH	MATERIAL	QTY.	LENGTH		MATERIAL	QTY.	LENGTH			MATERIAL
FEMALE	14'-0"	W3.4	52	-	-	-	1 ½" PVC	8	2'-8"	SEE DWG	-	-	-	1.17	4725	0.6" Grade 270
MALE	14'-0"	W3.4	52	#10 GFRP	8	10'-9"	-	-	-	SEE DWG	-	-	-	1.17	4725	0.6" Grade 270

SPECIMEN 2 (UNFORESEEN)

	LENGTH	SPIRAL		DOWEL			DOWEL HOLE			COMMENT	AUXILIARY BARS			CYDS	WT	PRESTRESSED STRAND
		MATERIAL	# OF TURNS	MATERIAL	QTY.	LENGTH	MATERIAL	QTY.	LENGTH		MATERIAL	QTY.	LENGTH			
FEMALE	14'-0"	0.2" CFRP	52	-	-	-	1 ½" PVC	8	2'-8"	SEE DWG	-	-	-	1.17	4725	0.6" CFRP 7-strand
MALE	14'-0"	0.2" CFRP	52	#10 GFRP	8	7'-0"	-	-	-	SEE DWG	-	-	-	1.17	4725	0.6" CFRP 7-strand

SPECIMEN 3&4 (PREPLANNED)

	LENGTH	SPIRAL		DOWEL			DOWEL HOLE			COMMENT	AUXILIARY BARS			CYDS	WT	PRESTRESSED STRAND
		MATERIAL	# OF TURNS	MATERIAL	QTY.	LENGTH	MATERIAL	QTY.	LENGTH		MATERIAL	QTY.	LENGTH			
FEMALE	14'-0"	W3.4	80	-	-	-	2"CORRUGATED STEEL DUCT	8	3'-6"	SEE DWG	#8 GFRP	8	8'-3"	1.17	4725	0.6" Grade 270
MALE	14'-0"	W3.4	52	#10 GFRP	8	11'-7"	-	-	-	SEE DWG	-	-	-	1.17	4725	0.6" Grade 270

SPECIMEN 5&6 (PREPLANNED)

	LENGTH	SPIRAL		DOWEL			DOWEL HOLE			COMMENT	AUXILIARY BARS			CYDS	WT	PRESTRESSED STRAND
		MATERIAL	# OF TURNS	MATERIAL	QTY.	LENGTH	MATERIAL	QTY.	LENGTH		MATERIAL	QTY.	LENGTH			
FEMALE	14'-0"	0.2" CFRP	80	-	-	-	2"CORRUGATED STEEL DUCT	8	4'-8"	SEE DWG	-	-	-	1.17	4725	0.6" CFRP 7-strand
MALE	14'-0"	0.2" CFRP	52	#10 GFRP	8	9'-0"	-	-	-	SEE DWG	-	-	-	1.17	4725	0.6" CFRP 7-strand

SPECIMEN 7&8 (PREPLANNED)

	LENGTH	SPIRAL		DOWEL			DOWEL HOLE			COMMENT	AUXILIARY BARS			CYDS	WT	PRESTRESSED STRAND
		MATERIAL	# OF TURNS	MATERIAL	QTY.	LENGTH	MATERIAL	QTY.	LENGTH		MATERIAL	QTY.	LENGTH			
FEMALE	14'-0"	W3.4	80	-	-	-	2"CORRUGATED STEEL DUCT	8	4'-2"	SEE DWG	#9 STEEL	8	10'-6"	1.17	4725	0.6" Grade 270
MALE	14'-0"	W3.4	52	#10 STEEL	8	14'-6"	-	-	-	SEE DWG	-	-	-	1.17	4725	0.6" Grade 270

SPECIMEN 9&10 (PREPLANNED)

	LENGTH	SPIRAL		DOWEL			DOWEL HOLE			COMMENT	AUXILIARY BARS			CYDS	WT	PRESTRESSED STRAND
		MATERIAL	# OF TURNS	MATERIAL	QTY.	LENGTH	MATERIAL	QTY.	LENGTH		MATERIAL	QTY.	LENGTH			
FEMALE	14'-0"	0.2" CFRP	80	-	-	-	1 1/2"CORRUGATED STEEL DUCT	9	4'-8"	SEE DWG	-	-	-	1.17	4725	0.6" CFRP 7-strand
MALE	14'-0"	0.2" CFRP	52	7-strand 19.3 mm CFRP	9	9'-0"	-	-	-	SEE DWG	-	-	-	1.17	4725	0.6" CFRP 7-strand

NOTE: CFRP spiral will be tied using CFRP ties, Steel spiral will be tied using steel ties.
NOTE: CYDS = cubic yards of concrete per specimen
WT = weight of specimen

SHEET NO.	SS Job NO.	REVISIONS DATE	REVISIONS DESCRIPTION	DRAWN BY		GC	PROJECT	SHEET CONTENTS
8	20079	10/12/20	Corrugated steel duct modified from 2" to 1 1/2" for specimens 9 and 10 Dowel type changed for specimens 9 and 10 Note for CYDS. and WT.	BG	S & S PRECAST, INC. P.O. BOX 366098 BONITA SPRINGS, FL 34136 (239) 992-8685 FAX: (239) 992-9226	Florida International University 10555 West Flagler Street Miami, FL 33174	18" Test Piles	Rebar Schedule
				APPROVED BY				
				DATE 09/29/20				

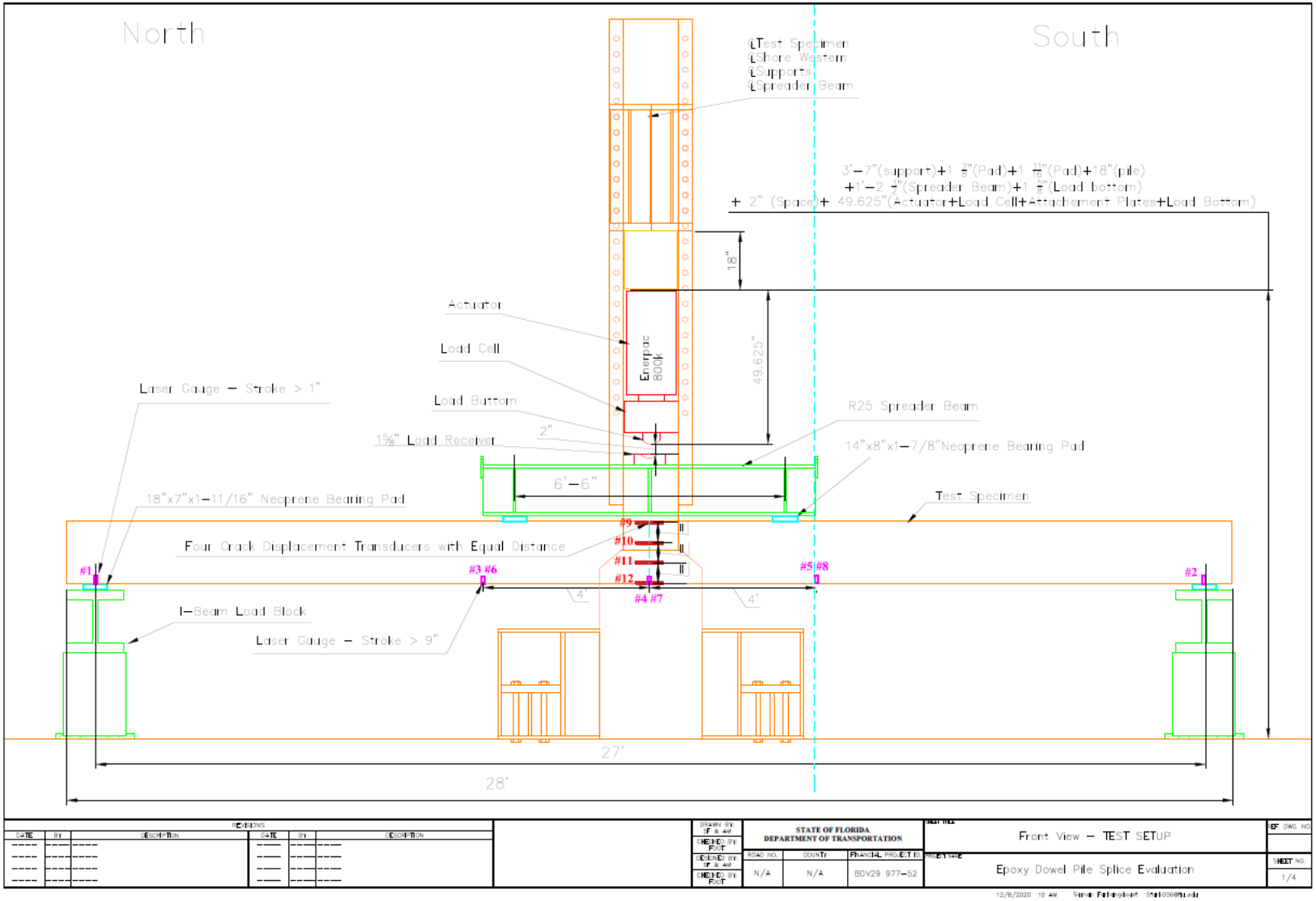
North
South
LTest Specimen
LShore Western
LSupports
LSpreader Beam
3'-7"(support)+1 7/8"(Pad)+1 11/16"(Pad)+18"(pile)
+1'-2 1/2"(Spreader Beam)+1 3/4"(Load bottom)
+ 2" (Space)+ 49.625"(Actuator+Load Cell+Attachement Plates+Load Bottom)
18"
49.625"
Actuator
Load Cell
Load Buttom
15/8" Load Receiver
2"
Enerpac
800k
Laser Gauge - Stroke > 1"
R25 Spreader Beam
14"x8"x1-7/8"Neoprene Bearing Pad
6'-6"
18"x7"x1-11/16" Neoprene Bearing Pad
Test Specimen
Four Crack Displacement Transducers with Equal Distance
#9
#10
#11
#12
#1
#3 #6
#5 #8
#2
#4 #7
4'
4'
I-Beam Load Block
Laser Gauge - Stroke > 9"
27'
28'
REVISIONS
DATE
BY
DESCRIPTION
DRAWN BY: OF & AM
CHECKED BY: PJM
DESIGNED BY: OF & AM
CHECKED BY: PJM
STATE OF FLORIDA
DEPARTMENT OF TRANSPORTATION
ROAD NO.
COUNTY
FINANCIAL PROJECT ID
N/A
N/A
BDV29 977-52
SHEET TITLE
Front View - TEST SETUP
PROJECT NAME
Epoxy Dowel Pile Splice Evaluation
SHEET NO.
1/4

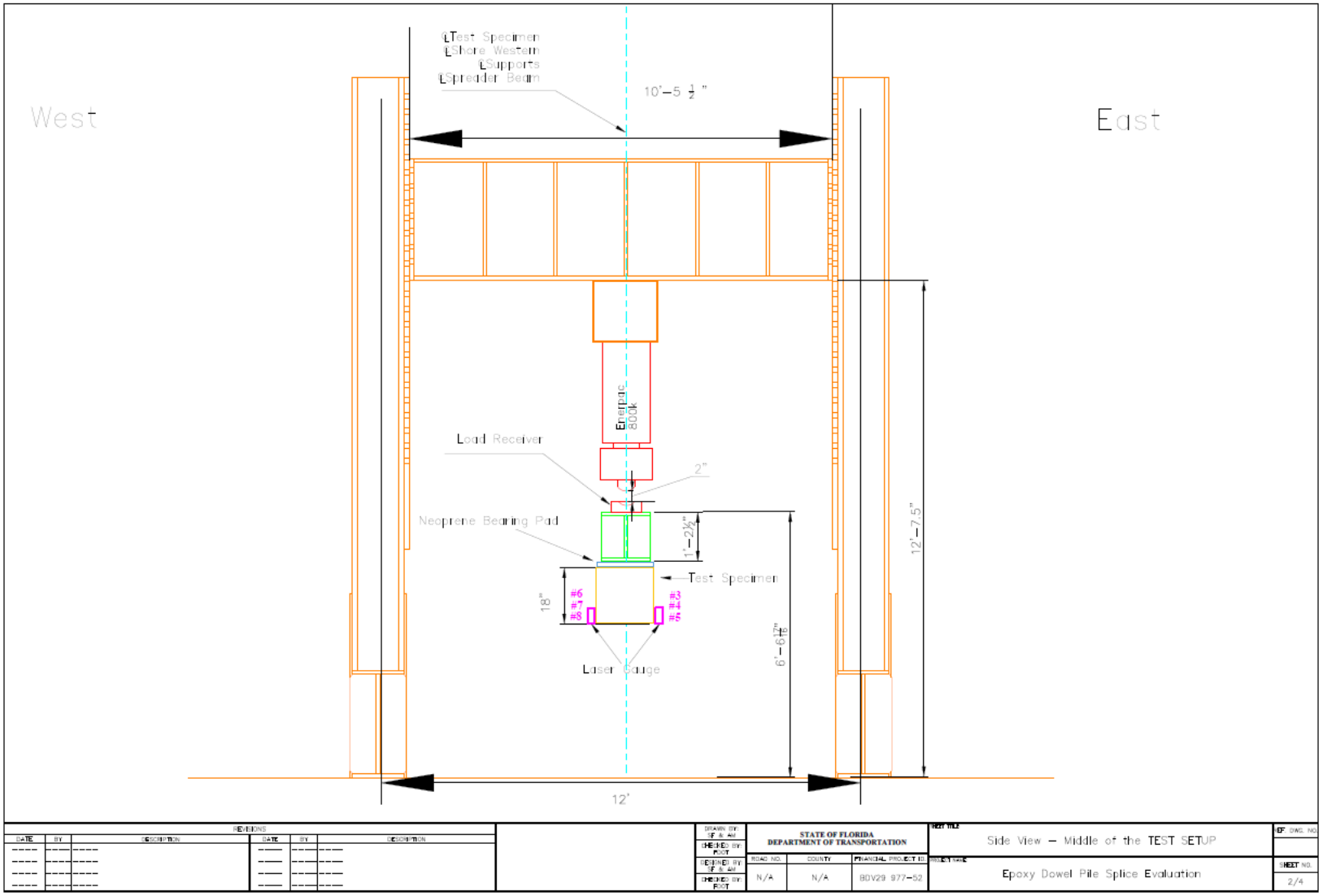
℄Test Specimen
℄Shore Western
℄Supports
℄Spreader Beam
10'–5 ½ "
West
East
Enerpac
800k
Load Receiver
2"
Neoprene Bearing Pad
1'–2½"
Test Specimen
18"
#6
#7
#8
#3
#4
#5
Laser Gauge
6'–6⅞"
12'–7.5"
12'
REVISIONS
DATE
BY
DESCRIPTION
STATE OF FLORIDA
DEPARTMENT OF TRANSPORTATION
ROAD NO.
COUNTY
FINANCIAL PROJECT ID.
N/A
N/A
BDV29 977–52
Side View – Middle of the TEST SETUP
Epoxy Dowel Pile Splice Evaluation
SHEET NO.
2/4

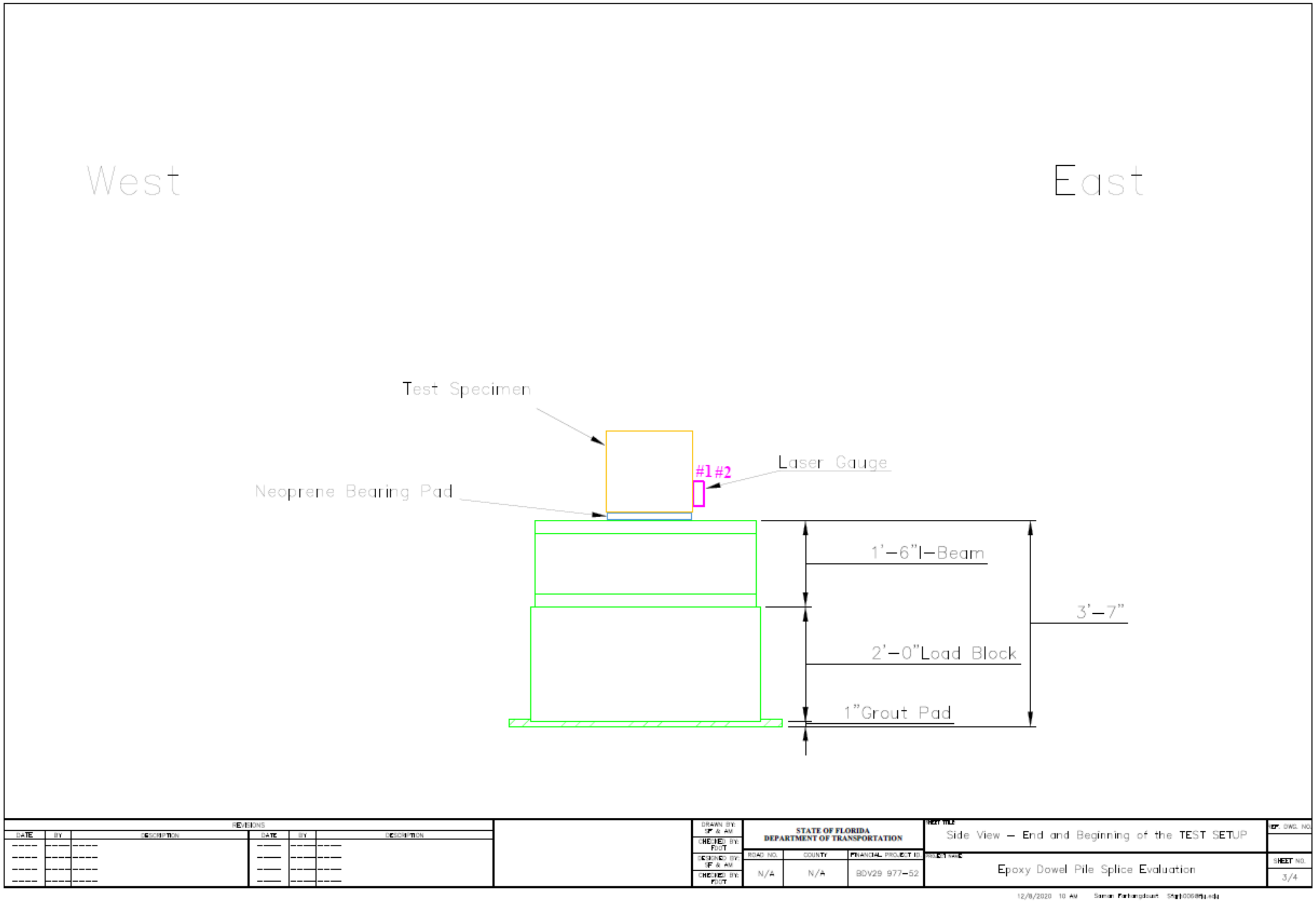
West
East
Test Specimen
#1 #2
Laser Gauge
Neoprene Bearing Pad
1'–6"I–Beam
3'–7"
2'–0"Load Block
1"Grout Pad
REVISIONS
DATE
BY
DESCRIPTION
DATE
BY
DESCRIPTION
DRAWN BY: SF & AM
CHECKED BY: FDOT
DESIGNED BY: SF & AM
CHECKED BY: FDOT
STATE OF FLORIDA
DEPARTMENT OF TRANSPORTATION
ROAD NO.
COUNTY
FINANCIAL PROJECT ID.
N/A
N/A
BDV29 977–52
SHEET TITLE
Side View – End and Beginning of the TEST SETUP
PROJECT NAME
Epoxy Dowel Pile Splice Evaluation
REF. DWG. NO.
SHEET NO.
3/4
12/8/2020 10 AM

Precast Prestressed Concrete Pile Splice Design

Designed by Saman Farhangdoust

This program can be used for Epoxy Dowel Pile Splice Evaluation - FRP Dowel and Steel Strand

Grant No.: BDV29-977-52
Principal Investigators: Mehrabi, Armin
Graduate Research Assistant: Farhangdoust, Saman

Sponsered by Florida Department of Transportation (FDOT)
Project Manager: Nolan, Steven

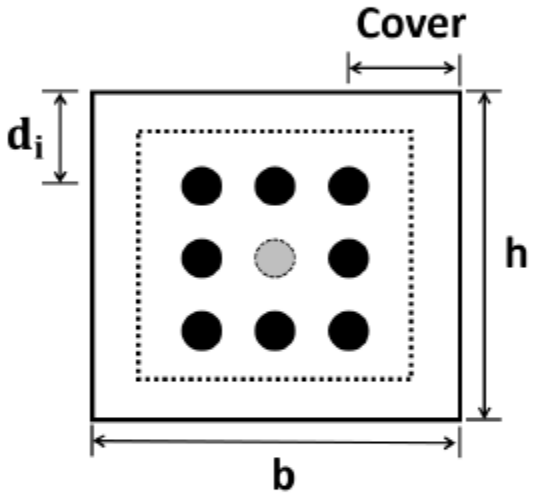

Section Dimension:

b := 18in	Width
h := 18in	Height
Cover := 5.5in	Cover

Rebar:

$d_b := 1.27in$ — Nominal Bar Diameter

$n_b := \begin{pmatrix} 1 & 1 & 1 \\ 1 & 0 & 1 \\ 1 & 1 & 1 \end{pmatrix}$ — Number and Location

$A_b := \pi \cdot \frac{d_b^{\,2}}{4}$ — Area of a rebar

$n_{bl} := \sum_{i=1}^{cols(n_b)} n_b^{\langle i \rangle}$ — Number of rebars by level

$n_{bl} = \begin{pmatrix} 3 \\ 2 \\ 3 \end{pmatrix}$ — Number of bars in each level

$A_{bl} := A_b \cdot n_{bl}$ — Area of rebars by level

$A_{bl} = \begin{pmatrix} 3.8 \\ 2.534 \\ 3.8 \end{pmatrix} \cdot in^2$ — Area of all bars in each level

$A_{bt} := \sum A_{bl} = 10.134 \cdot in^2$ — Area of total bars

Level of rebars

$d :=$ $d_1 \leftarrow Cover$

for $i \in 2 .. rows(n_b)$

$\Delta \leftarrow \frac{h - 2 \cdot Cover}{rows(n_b) - 1}$

$d_i \leftarrow d_{i-1} + \Delta$

d

Environmental Factor:

$C_E := 0.7$ environmental reduction factor for FRP-bars

FRP-Bar Properties:

$E_f := 6500\text{ksi}$ Modulus of Elasticity

$S_{fu} := 98.2\cdot\text{kip}$ Minimum Guaranteed (Nominal) Tensile Load

$f_{fu} := \frac{S_{fu}}{A_b} = 77.52\cdot\text{ksi}$ Guaranteed Tensile Strength

$\varepsilon_{fu} := \frac{f_{fu}}{E_f} = 0.012$ Ultimate Strain

$f_{fd} := C_E\cdot f_{fu} = 54.264\cdot\text{ksi}$ Design Tensile Strength

$\varepsilon_{fd} := \frac{f_{fd}}{E_f} = 8.348\times 10^{-3}$ Ultimate Design Strain

Concrete properties:

$f'_c := 6\text{ksi}$ Compressive Strength

$\varepsilon_{cu} := 0.003$ Maximum Compressive Strain

$\alpha := \text{if}\left[f'_c \le 10\text{ksi}, 0.85, \max\left[0.75, 0.85 - 0.02\cdot\left(\frac{f'_c}{\text{ksi}} - 10\right)\right]\right]$ ACI – 318

$\beta_1 := \max\left[0.65, 0.85 - 0.05\cdot\left(\frac{f'_c}{\text{ksi}} - 4\right)\right]$ Ratio of Maximum Flexural Strain at the extreme tension face to the strain at the centroid of the rebar layer nearest to the tension face

FRP Layers Force:

$$a := \left| \begin{array}{l} \text{for } j \in 1 .. 60 \\ \quad a_j \leftarrow \frac{h}{60} \cdot j \\ a \end{array} \right.$$

Range Variable to accomodate an increasing increment

$$c := \frac{a}{\beta_1}$$

The distance of the concrete block in compression

$$\varepsilon_f := \left| \begin{array}{l} \text{for } i \in 1 .. \text{rows}(a) \\ \quad \text{for } j \in 1 .. \text{rows}(n_{bl}) \\ \quad\quad \varepsilon_{i,j} \leftarrow \varepsilon_{cu} \cdot \frac{(d_j - c_i)}{c_i} \\ \varepsilon \end{array} \right.$$

Tensile Strain in each row

$$f_f := \left| \begin{array}{l} \text{for } i \in 1 .. \text{rows}(a) \\ \quad \text{for } j \in 1 .. \text{rows}(n_{bl}) \\ \quad\quad f_{i,j} \leftarrow \left| \begin{array}{ll} 0 & \text{if } \varepsilon_{f_{i,j}} < 0 \\ \min\left(\varepsilon_{f_{i,j}} \cdot E_f, f_{fd}\right) & \text{otherwise} \end{array} \right. \\ f \end{array} \right.$$

Tensile Stress in each row

$$F_f := \left| \begin{array}{l} \text{for } i \in 1 .. \text{rows}(a) \\ \quad \text{for } j \in 1 .. \text{rows}(n_{bl}) \\ \quad\quad F_{i,j} \leftarrow A_{bl_j} \cdot f_{f_{i,j}} \\ F \end{array} \right.$$

Rebar Force in each row

Concrete Force:

$F_c := \alpha \cdot f'_c \cdot a \cdot b$

Max allowable compression load:

[LRFD GFRP 5.6.4.4]

$P_{nmaxC} := \alpha \cdot f'_c \cdot b \cdot h = 1.652 \times 10^3 \cdot kip$ Nominal axial resistance

$\Phi := 0.85$

$P_f := \Phi \cdot P_{nmaxC}$ Factored axial resistance

$\phi P_f := 0.75 \cdot P_f = 1.053 \times 10^3 \cdot kip$ Design axial resistance

Nominal Flexural Strength of GFRP Pile Splice

$$P_n := \left| \begin{array}{l} \text{for } i \in 1 .. \text{rows}(a) \\ \quad P_{n_i} \leftarrow \min\left[\left(F_{c_i} - \sum_{j=1}^{\text{rows}(n_b)} F_{f_{i,j}}\right), P_f\right] \\ P_n \end{array} \right.$$

Nominal Axial Strength

$$M_n := \left| \begin{array}{l} \text{for } i \in 1 .. \text{rows}(a) \\ \quad M_{n_i} \leftarrow \left[F_{c_i} \cdot \left(\frac{h}{2} - \frac{a_i}{2}\right) + \sum_{j=1}^{\text{rows}(n_b)} \left[F_{f_{i,j}} \cdot \left(d_j - \frac{h}{2}\right)\right]\right] \\ M_n \end{array} \right.$$

Nominal Moment Strength

$P_n =$ kip

	1
1	-522.38
2	-494.84
3	-467.3
4	-414.173
5	-335.685
6	-272.561
7	-194.294
8	-128.708
9	-48.564
10	28.38
11	96.342
12	157.566
13	213.608
14	264.256
15	308.117
16	...

$M_n =$ ft·kip

	1
1	20.311
2	39.933
3	58.867
4	84.575
5	116.991
6	143.766
7	167.022
8	187.82
9	200.038
10	209.95
11	219.937
12	229.809
13	239.433
14	248.329
15	255.784
16	...

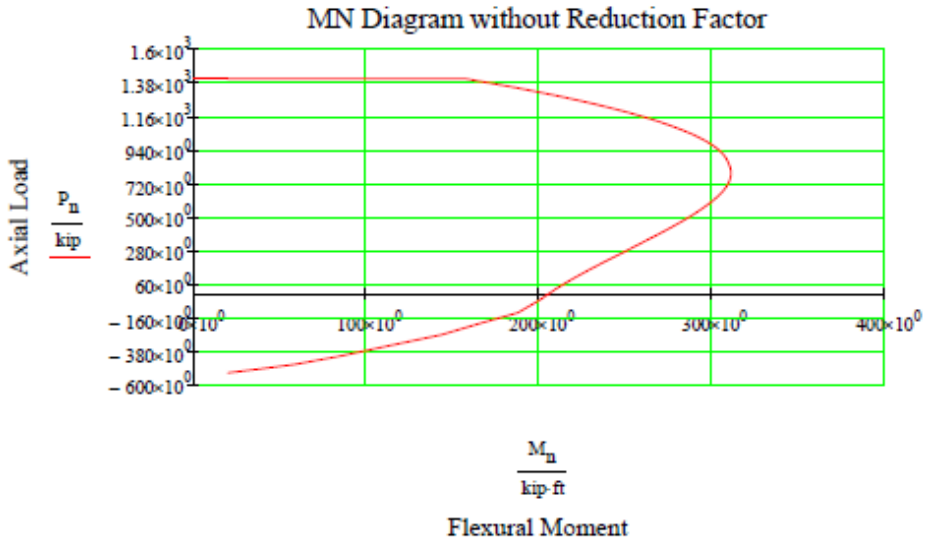

Resistance Factor for Flexural Strength (GFRP) [LRFD GFRP 2.6.3]

$$f_{fr} := \begin{| m \leftarrow \text{rows}(n_b) \\ d_f \leftarrow d_m \\ A_f \leftarrow A_{bl_m} \\ \rho_f \leftarrow \frac{A_f}{b \cdot d_f} \\ f_f \leftarrow 0 \text{ if } \rho_f = 0 \\ f_f \leftarrow \sqrt{\frac{(E_f \cdot \varepsilon_{cu})^2}{4} + \frac{0.85 \cdot \beta_1 \cdot f'_c}{\rho_f} \cdot E_f \cdot \varepsilon_{cu}} - 0.5 \cdot E_f \cdot \varepsilon_{cu} \text{ otherwise} \\ f_{fr} \leftarrow \min(f_f, f_{fd})$$

$$\varepsilon_{fr} := \frac{f_{fr}}{E_f} = 8.348 \times 10^{-3}$$

$$\varepsilon_t := \begin{| \text{for } i \in 1 .. \text{rows}(a) \\ \quad \varepsilon_{t_i} \leftarrow \varepsilon_{cu} \cdot \frac{\left(d_{\text{rows}(n_b)} - c_i\right)}{c_i} \\ \varepsilon_t$$

$$\phi_f := \begin{| \text{for } i \in 1 .. \text{rows}(a) \\ \quad \phi_{f_i} \leftarrow \begin{| 0.75 \text{ if } \varepsilon_{t_i} \le 0.80 \cdot \varepsilon_{fd} \\ \left(1.55 - \frac{\varepsilon_{t_i}}{\varepsilon_{fd}}\right) \text{ if } 0.80 \cdot \varepsilon_{fd} < \varepsilon_{t_i} < \varepsilon_{fd} \\ 0.55 \text{ otherwise} \\ \phi_f$$

Design Flexural Strength of GFRP Pile Splice

$$P_u := \left| \begin{array}{l} \text{for } i \in 1 .. \text{rows}(a) \\ \quad P_{u_i} \leftarrow \phi_{f_i} \cdot \min\left[\left(F_{c_i} - \sum_{j=1}^{\text{rows}(n_b)} F_{f_{i,j}}\right), P_f\right] \\ P_u \end{array} \right.$$

$$M_u := \left| \begin{array}{l} \text{for } i \in 1 .. \text{rows}(a) \\ \quad M_{u_i} \leftarrow \phi_{f_i} \cdot \left[F_{c_i} \cdot \left(\frac{h}{2} - \frac{a_i}{2}\right) + \sum_{j=1}^{\text{rows}(n_b)} \left[F_{f_{i,j}} \cdot \left(d_j - \frac{h}{2}\right)\right]\right] \\ M_u \end{array} \right.$$

$P_u =$ ·kip

	1
1	-287.309
2	-272.162
3	-257.015
4	-227.795
5	-184.627
6	-149.909
7	-106.862
8	-70.79
9	-32.13
10	21.285
11	72.256
12	118.175
13	160.206
14	198.192
15	231.087
16	...

$M_u =$ ·ft·kip

	1
1	11.171
2	21.963
3	32.377
4	46.516
5	64.345
6	79.071
7	91.862
8	103.301
9	132.345
10	157.462
11	164.953
12	172.357
13	179.575
14	186.247
15	191.838
16	...

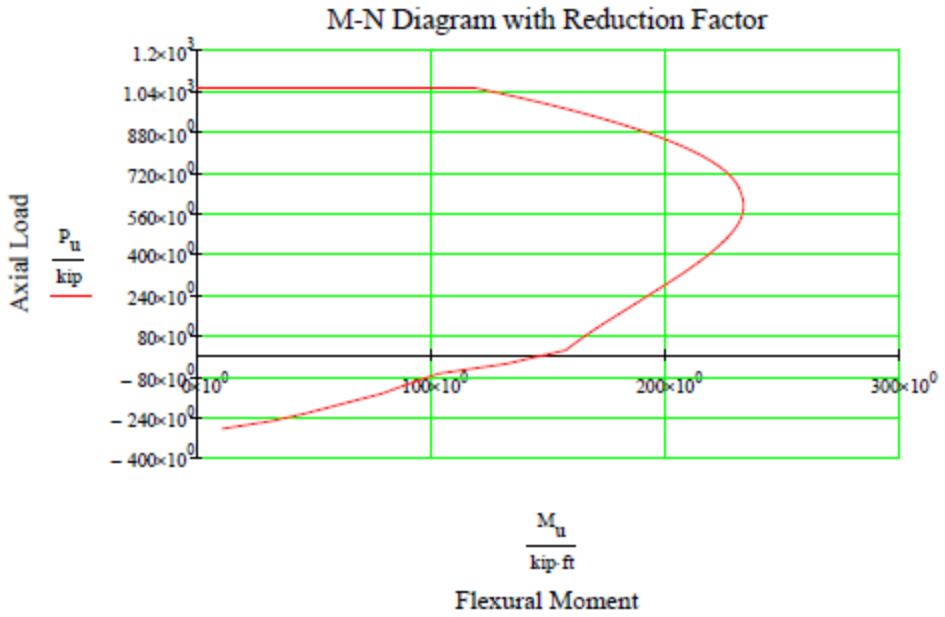
M-N Diagram with Reduction Factor
1.2×10^3
1.04×10^3
880×10^0
720×10^0
560×10^0
400×10^0
240×10^0
80×10^0
– 80×10^0
– 240×10^0
– 400×10^0
0×10^0
100×10^0
200×10^0
300×10^0
Axial Load
p_u / kip
M_u / kip·ft
Flexural Moment

Development and Lap Splice Lengths for FRP Dowels

$$HalfCtC := 0.5 \cdot \left(d_3 - d_2\right) = 1.75 \cdot in$$

$$L_{dDowe} := \max\left[\left[\frac{31.6 \frac{\left(\frac{f_{fr}}{ksi}\right)}{\sqrt{\left(\frac{f'_c}{ksi}\right)}} - 340}{13.6 + \frac{HalfCtC}{d_b}} \cdot d_b\right], \left(20 \cdot d_b\right)\right] = 30.528 \cdot in$$

ection 2.9.7.4.1-1 of the AASHTO

$$Lap := \max\left(1.3 \cdot L_{dDowe}, 12in\right) = 39.687 \cdot in$$

Section 2.9.7.6 of the AASHTO-GFRP2

$$L_D := Lap = 39.687 \cdot in$$

The Length of Projected Dowels

$$L_H := L_D + 2in = 41.687 \cdot in$$

The length of the Holes for Dowels

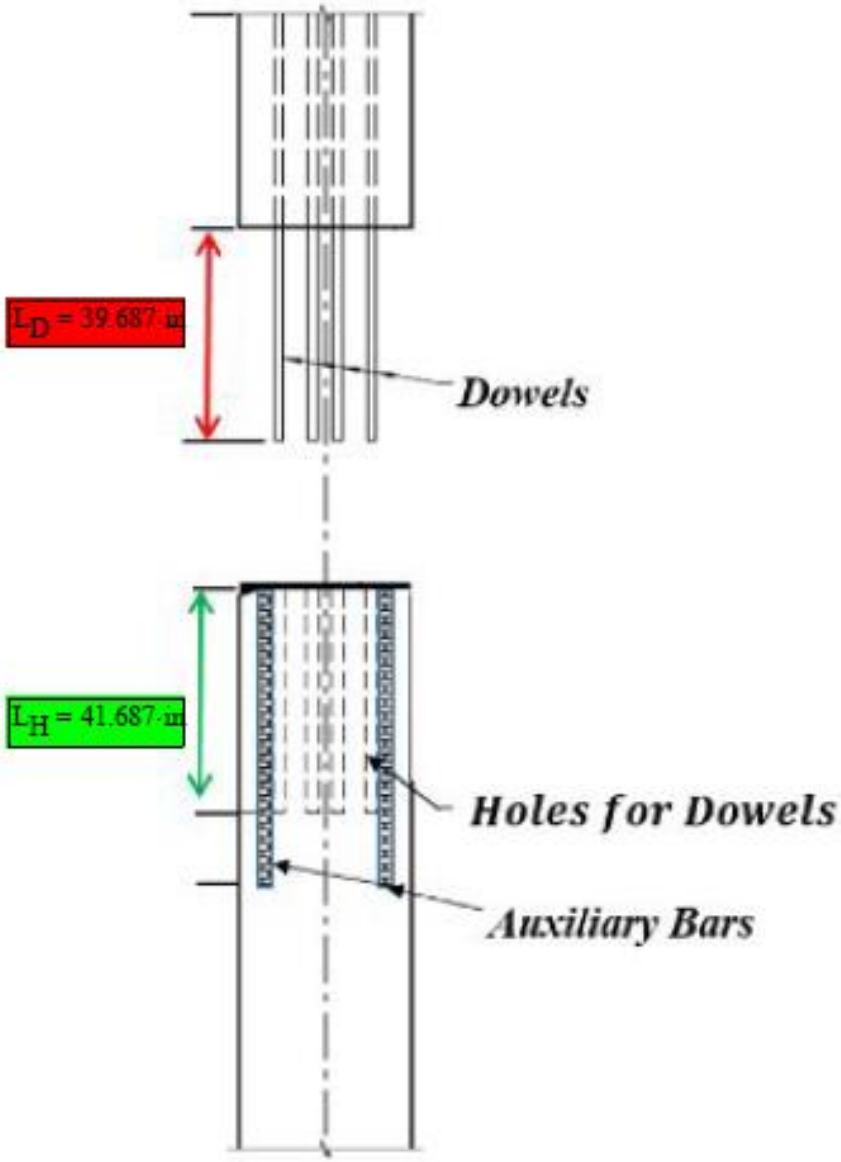
L_D = 39.687 in
Dowels
L_H = 41.687 in
Holes for Dowels
Auxiliary Bars

Development Length of Prestressing Steel/HSSS Strand:

Section 933 of the FDOT Standard Specification for Road and Bridge Construction

$dia_{st} := 0.6in$ Steel Strand Nominal Diameter

$f_{pu} := 270ksi$ Minimum guaranteed ultimate strength

$A_{ps} := 0.217in^2$ Effective Cross Sectional Area of a 0.6in dia Steel Strand

$A_{ps.total} := 4 \cdot A_{ps}$

$dia_w := 0.2in$ WireSpiral Diameter

$\gamma_p := 0.28$ Typical low relaxation strand

$ClearCover := 3in$ Clear Cover

$d_p := h - ClearCover - dia_w - \left(\frac{dia_{st}}{2}\right) = 14.5 \cdot in$ Distance from extreme compression fiber to centroid of prestressing reinforcement

$\rho_p := \frac{A_{ps.total}}{h \cdot d_p}$ Reinforcement Ratio

$$f_{ps} := f_{pu}\left(1 - \frac{\gamma_p \cdot \rho_p \cdot f_{pu}}{\beta_1 \cdot f'_c}\right) = 254.915 \cdot ksi$$

Approximated Stress in strand at flexural failure of beam

$P_j := 35kip$

Jacking force

$$f_{pi} := \frac{P_j}{A_{ps}} = 161.3 \cdot ksi$$

Initial Stress

$Loss := 0.15$

Loss Percentage

$f_{Loss} := Loss \cdot f_{pi} = 24.194 \cdot ksi$

Initial strand losses

$f_{pe} := f_{pi} - (f_{Loss}) = 137.097 \cdot ksi$

Effective Prestresstressing Stress

[AASHTO LRFD 8th Edition 5.9.4.3.2]

$k := 1$

For piling with a depth smaller than 24

$$L_{dStrand} := k \cdot \left[\left(\frac{f_{ps}}{1000 \cdot psi}\right) - \left(\frac{2}{3} \cdot \frac{f_{pe}}{1000 \cdot psi}\right)\right] \cdot dia_{st}$$

Strand Developement Length

$L'_D := L_{dStrand} = 98.11 \cdot in$

The Length of Embedded Dowels

$L_A := L_{dStrand} = 98.11 \cdot in$

The Length of Auxiliary Bars

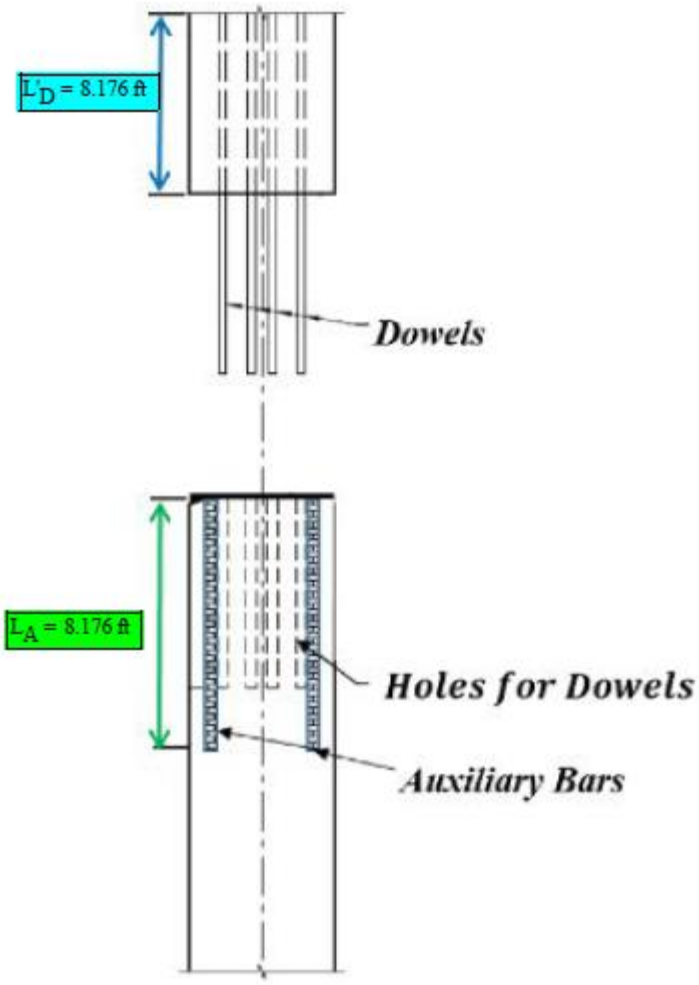

Auxiliary Bar Size and Number as per FDOT Standartd Plans Index 455

Precast Prestressed Concrete Pile Splice Design

Designed by Saman Farhangdoust

This program can be used for Epoxy Dowel Pile Splice Evaluation - Steel Dowel and Strand

Grant No.: BDV29-977-52
Principal Investigators: Mehrabi, Armin
Graduate Research Assistant: Farhangdoust, Saman

Sponsered by Florida Department of Transportation (FDOT)
Project Manager: Nolan, Steven

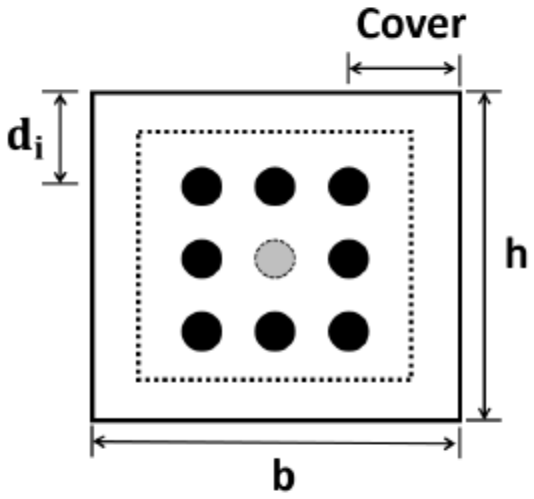

Section Dimension:

b := 18in	Width
h := 18in	Height
Cover := 5.5in	Cover

Rebar:

$d_b := 1.27in$ — Nominal Bar Diameter

$n_b := \begin{pmatrix} 1 & 1 & 1 \\ 1 & 0 & 1 \\ 1 & 1 & 1 \end{pmatrix}$ — Number and Location

$A_b := \pi \cdot \frac{d_b^2}{4}$ — Area of a rebar

$n_{bl} := \sum_{i=1}^{cols(n_b)} n_b^{\langle i \rangle}$ — Number of rebars by level

$n_{bl} = \begin{pmatrix} 3 \\ 2 \\ 3 \end{pmatrix}$ — Number of bars in each level

$A_{bl} := A_b \cdot n_{bl}$ — Area of rebars by level

$A_{bl} = \begin{pmatrix} 3.8 \\ 2.534 \\ 3.8 \end{pmatrix} \cdot in^2$ — Area of all bars in each level

$A_{bt} := \sum A_{bl} = 10.134 \cdot in^2$ — Area of total bars

Level of rebars

$d := \left| \begin{array}{l} d_1 \leftarrow Cover \\ \text{for } i \in 2 .. rows(n_b) \\ \quad \left| \begin{array}{l} \Delta \leftarrow \frac{h - 2 \cdot Cover}{rows(n_b) - 1} \\ d_i \leftarrow d_{i-1} + \Delta \end{array} \right. \\ d \end{array} \right.$

Steel rebar Properties:

$E_s := 29000\text{ksi}$ Steel Modulus of Elasticity

$f_y := 60\text{ksi}$ Steel Yield Strength

Concrete properties:

$f'_c := 6\text{ksi}$ Compressive Strength

$\varepsilon_{cu} := 0.003$ Maximum Compressive Strain

$$\alpha := \text{if}\left[f'_c \le 10\text{ksi}, 0.85, \max\left[0.75, 0.85 - 0.02\cdot\left(\frac{f'_c}{\text{ksi}} - 10\right)\right]\right]$$ ACI – 318

$$\beta_1 := \max\left[0.65, 0.85 - 0.05\cdot\left(\frac{f'_c}{\text{ksi}} - 4\right)\right]$$ Ratio of Maximum Flexural Strain at the extreme tension face to the strain at the centroid of the rebar layer nearest to the tension face

Steel Layers Force:

$$a := \left| \begin{array}{l} \text{for } j \in 1 .. 60 \\ \quad a_j \leftarrow \frac{h}{60} \cdot j \\ a \end{array} \right.$$

Range Variable to accomodate an increasing increment

$$c := \frac{a}{\beta_1}$$

The distance of the concrete block in compression

$$\varepsilon_s := \left| \begin{array}{l} \text{for } i \in 1 .. \text{rows}(a) \\ \quad \text{for } j \in 1 .. \text{rows}(n_{bl}) \\ \quad\quad \varepsilon_{s_{i,j}} \leftarrow \varepsilon_{cu} \cdot \frac{(d_j - c_i)}{c_i} \\ \varepsilon_s \end{array} \right.$$

Tensile Strain in each row

$$f_s := \left| \begin{array}{l} \text{for } i \in 1 .. \text{rows}(a) \\ \quad \text{for } j \in 1 .. \text{rows}(n_{bl}) \\ \quad\quad f_{s_{i,j}} \leftarrow \text{sign}(\varepsilon_{s_{i,j}}) \cdot \min(|\varepsilon_{s_{i,j}}| \cdot E_s, f_y) \\ f_s \end{array} \right.$$

Tensile Stress in each row

$$F_s := \left| \begin{array}{l} \text{for } i \in 1 .. \text{rows}(a) \\ \quad \text{for } j \in 1 .. \text{rows}(n_{bl}) \\ \quad\quad F_{s_{i,j}} \leftarrow A_{bl_j} \cdot f_{s_{i,j}} \\ F_s \end{array} \right.$$

Rebar Force in each row

Concrete Force:

$F_c := \alpha \cdot f'_c \cdot a \cdot b$

Max allowable compression load:

[AASHTO LRFD]

$P_{nmaxC} := \alpha \cdot f'_c \cdot b \cdot h = 1.652 \times 10^3 \cdot kip$ Nominal axial resistance

$\Phi := 0.85$

$P_f := \Phi \cdot P_{nmaxC}$ Factored axial resistance

$\phi P_f := 0.75 \cdot P_f = 1.053 \times 10^3 \cdot kip$ Design axial resistance

Nominal Flexural Strength of Steel Pile Splice

$$P_n := \left| \begin{array}{l} \text{for } i \in 1 .. \text{rows}(a) \\ \quad P_{n_i} \leftarrow \min\left[\left(F_{c_i} - \sum_{j=1}^{\text{rows}(n_b)} F_{s_{i,j}}\right), P_f\right] \\ P_n \end{array} \right.$$ Nominal Axial Strength

$$M_n := \left| \begin{array}{l} \text{for } i \in 1 .. \text{rows}(a) \\ \quad M_{n_i} \leftarrow \left[F_{c_i} \cdot \left(\frac{h}{2} - \frac{a_i}{2}\right) + \sum_{j=1}^{\text{rows}(n_b)} \left[F_{s_{i,j}} \cdot \left(d_j - \frac{h}{2}\right)\right]\right] \\ M_n \end{array} \right.$$ Nominal Moment Strength

$P_n =$ ·kip

	1
1	-580.509
2	-552.969
3	-525.429
4	-497.889
5	-470.349
6	-442.809
7	-415.269
8	-387.729
9	-306.668
10	-228.616
11	-159.747
12	-97.767
13	-41.085
14	29.621
15	102.425
16	...

$M_n =$ ·ft·kip

	1
1	20.311
2	39.933
3	58.867
4	77.112
5	94.669
6	111.537
7	127.717
8	143.208
9	173.621
10	202.468
11	227.948
12	250.73
13	271.279
14	289.924
15	306.91
16	...

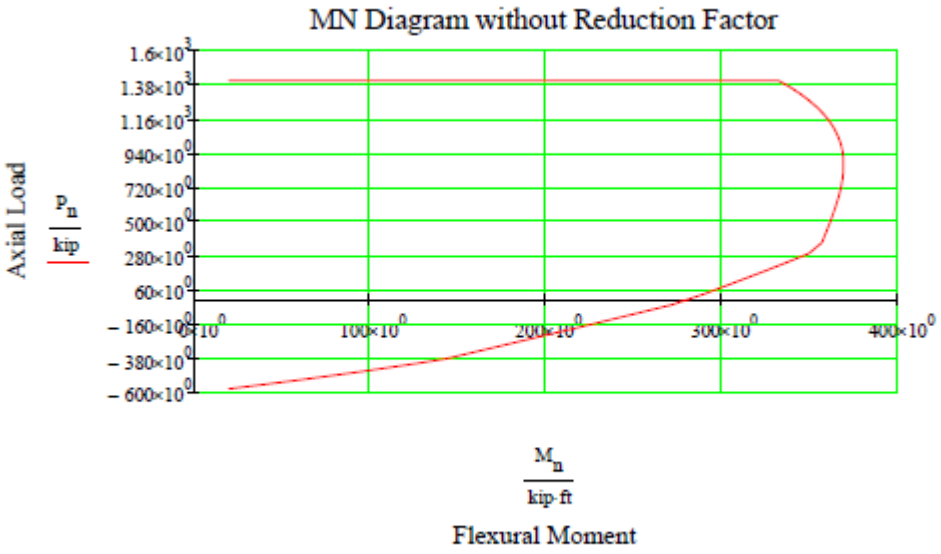

Resistance Factor for Flexural Strength (Steel)

$$\varepsilon_t := \left| \begin{array}{l} \text{for } i \in 1..\text{rows}(a) \\ \quad \varepsilon_{t_i} \leftarrow \varepsilon_{cu} \cdot \dfrac{\left(d_{\text{rows}(n_b)} - c_i\right)}{c_i} \\ \varepsilon_t \end{array} \right.$$

$$\phi_f := \left| \begin{array}{l} \text{for } i \in 1..\text{rows}(a) \\ \quad \phi_{f_i} \leftarrow \left| \begin{array}{ll} 0.9 & \text{if } \varepsilon_{t_i} \geq 0.005 \\ 0.75 + \left[\dfrac{0.15\left(\varepsilon_{t_i} - 0.0020\right)}{0.0030}\right] & \text{if } 0.002 < \varepsilon_{t_i} < 0.005 \\ 0.75 & \text{otherwise} \end{array} \right. \\ \phi_f \end{array} \right.$$

Design Flexural Strength of Steel Pile Splice

$$P_u := \left| \begin{array}{l} \text{for } i \in 1..\text{rows}(a) \\ \quad P_{u_i} \leftarrow \phi_{f_i} \cdot \min\left[\left(F_{c_i} - \sum_{j=1}^{\text{rows}(n_b)} F_{s_{i,j}}\right), P_f\right] \\ P_u \end{array} \right.$$

$$M_u := \left| \begin{array}{l} \text{for } i \in 1..\text{rows}(a) \\ \quad M_{u_i} \leftarrow \phi_{f_i} \cdot \left[F_{c_i} \cdot \left(\dfrac{h}{2} - \dfrac{a_i}{2}\right) + \sum_{j=1}^{\text{rows}(n_b)} \left[F_{s_{i,j}} \cdot \left(d_j - \dfrac{h}{2}\right)\right]\right] \\ M_u \end{array} \right.$$

$P_u =$ ·kip

	1
1	-522.458
2	-497.672
3	-472.886
4	-448.1
5	-423.314
6	-398.528
7	-373.742
8	-348.956
9	-276.001
10	-205.754
11	-143.773
12	-87.074
13	-35.357
14	24.728
15	83.22
16	...

$M_u =$ ·ft·kip

	1
1	18.28
2	35.94
3	52.98
4	69.401
5	85.202
6	100.383
7	114.945
8	128.887
9	156.259
10	182.221
11	205.153
12	223.307
13	233.456
14	242.035
15	249.365
16	...

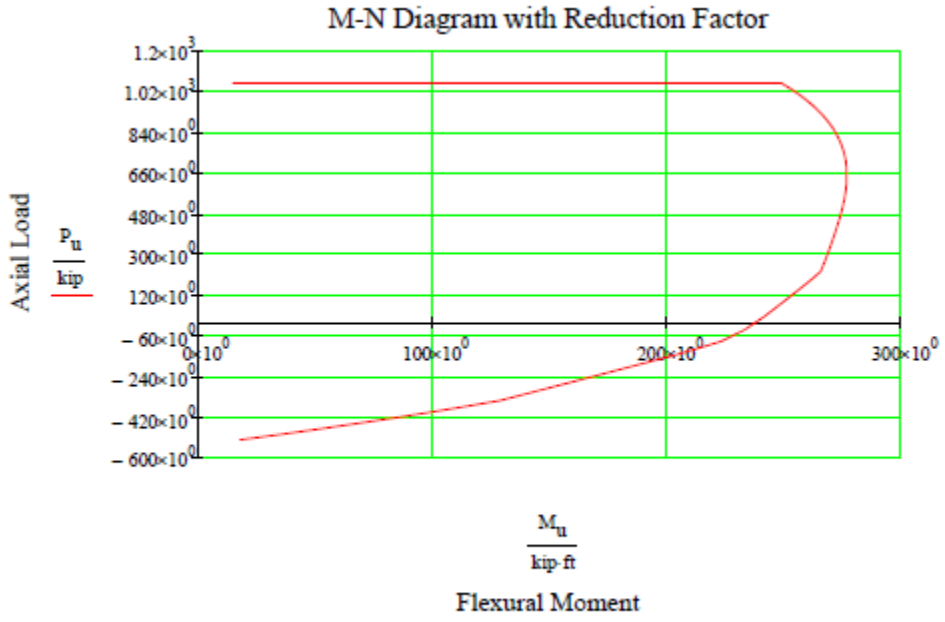

Development and Lap Splice Lengths for Steel Dowels

$\lambda_{rl} := 1$ Reinforcement Location Factor

$\lambda := 1$ Concrete Density Modification Factor

$\lambda_{cf} := 1$ Coating Factor

$\lambda_{cr} := 1$ Excess Reinforcement Factor

$d_{tie} := 0.207in$ Tie Nominal Diameter

$$A_{tr} := \pi \cdot \frac{(d_{tie})^2}{4} = 0.034 \cdot in^2$$

$n := 1$ Number of bars developed along plane of splitting

$S := 3in$ Maximum center-to-center spacing of transverse reinforcement within ld(in)

$$k_{tr} := 40 \cdot \frac{A_{tr}}{S \cdot n} = 0.449 \cdot in$$ Reinforcent confinement factor

$$HalfCtC := 0.5 \cdot (d_3 - d_2) = 1.75 \cdot in$$ Half of spacing

$$\lambda_{rc} := \frac{d_b}{HalfCtC + k_{tr}} = 0.578$$ Reinforcement Confinement Factor

AASHTO 5.10.8.2

$$L_{dDowel} := 2.4 \cdot d_b \cdot \frac{\frac{f_y}{ksi}}{\sqrt{\frac{f'_c}{ksi}}} \cdot \left[\frac{(\lambda_{rl} \cdot \lambda_{cf} \cdot \lambda_{rc} \cdot \lambda_{cr})}{\lambda} \right] = 43.125 \cdot in$$

Dowel Developement Length

$L_{ap} := 1.3 \cdot L_{dDowel} = 56.062 \cdot in$

Dowel LapSplice Length

$L_D := L_{ap} = 56.062 \cdot in$

The Length of Dowels

$L_H := L_D + 2in = 58.062 \cdot in$

The Length of Holes for the Dowels

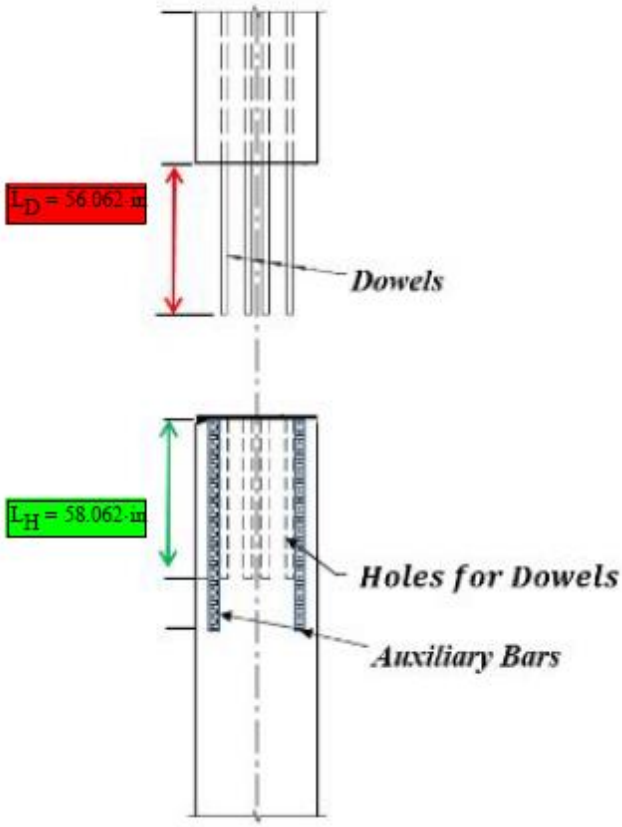

Development Length of Prestressing Steel/HSSS Strand:

Section 933 of the FDOT Standard Specification for Road and Bridge Construction

$dia_{st} := 0.6in$ Steel Strand Nominal Diameter

$f_{pu} := 270ksi$ Minimum guaranteed ultimate strength

$A_{ps} := 0.217in^2$ Effective Cross Sectional Area of a 0.6in dia Steel Strand

$A_{ps.total} := 4 \cdot A_{ps}$

$dia_w := 0.2in$ WireSpiral Diameter

$\gamma_p := 0.28$ Typical low relaxation strand

$ClearCover := 3in$ Clear Cover

$d_p := h - ClearCover - dia_w - \left(\frac{dia_{st}}{2}\right) = 14.5 \cdot in$ Distance from extreme compression fiber to centroid of prestressing reinforcement

$\rho_p := \frac{A_{ps.total}}{h \cdot d_p}$ Reinforcement Ratio

$$f_{ps} := f_{pu}\left(1 - \frac{\gamma_p \cdot \rho_p \cdot f_{pu}}{\beta_1 \cdot f'_c}\right) = 254.915 \cdot ksi$$

Approximated Stress in strand at flexural failure of beam

$P_j := 35kip$

Jacking force

$$f_{pi} := \frac{P_j}{A_{ps}} = 161.3 \cdot ksi$$

Initial Stress

$Loss := 0.15$

Loss Percentage

$f_{Loss} := Loss \cdot f_{pi} = 24.194 \cdot ksi$

Initial strand losses

$f_{pe} := f_{pi} - (f_{Loss}) = 137.097 \cdot ksi$

Effective Prestresstressing Stress

[AASHTO LRFD 8th Edition 5.9.4.3.2]

$k := 1$

For piling with a depth smaller than 24

$$L_{dStrand} := k \cdot \left[\left(\frac{f_{ps}}{1000 \cdot psi}\right) - \left(\frac{2}{3} \cdot \frac{f_{pe}}{1000 \cdot psi}\right)\right] \cdot dia_{st}$$

Strand Developement Length

$L'_D := L_{dStrand} = 98.11 \cdot in$

The Length of Embedded Dowels

$L_A := L_{dStrand} = 98.11 \cdot in$

The Length of Auxiliary Bars

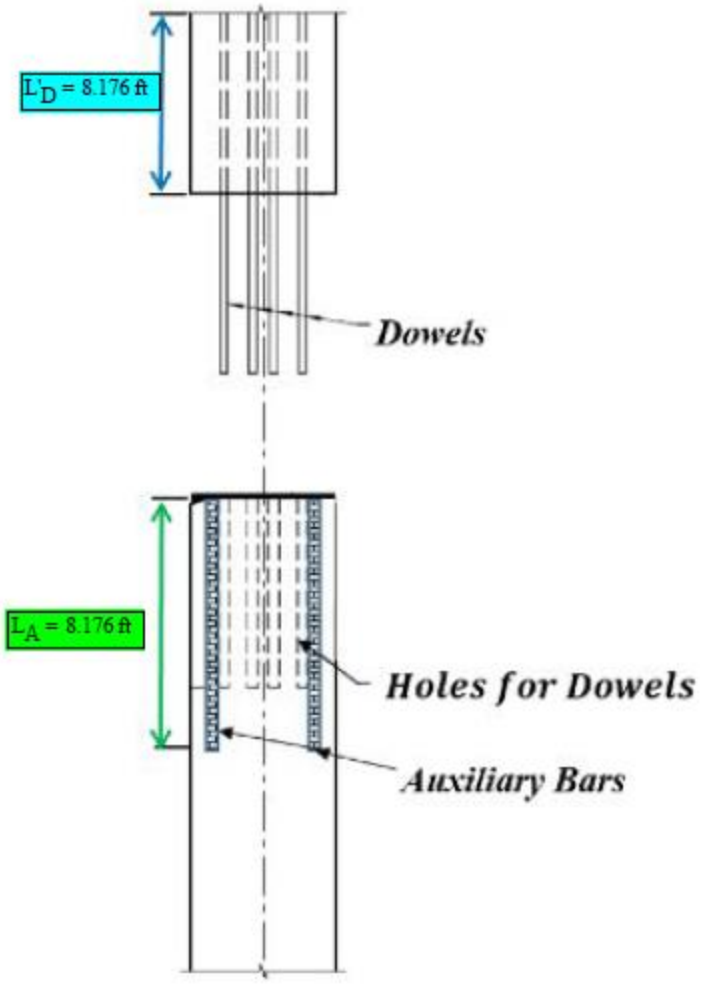

Auxiliary Bar Size and Number as per FDOT Standartd Plans Index 455

Precast Prestressed Concrete Pile Splice Design

Designed by Saman Farhangdoust

This program can be used for Epoxy Dowel Pile Splice Evaluation - Steel Dowel and FRP Strand

Grant No.: BDV29-977-52
Principal Investigators: Mehrabi, Armin
Graduate Research Assistant: Farhangdoust, Saman

Sponsered by Florida Department of Transportation (FDOT)
Project Manager: Nolan, Steven

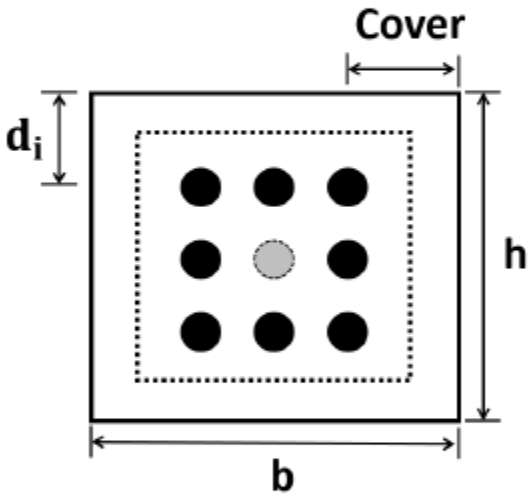

Section Dimension:

b := 18in	Width
h := 18in	Height
Cover := 5.5in	Cover

Rebar:

$d_b := 1.27in$ Nominal Bar Diameter

$n_b := \begin{pmatrix} 1 & 1 & 1 \\ 1 & 0 & 1 \\ 1 & 1 & 1 \end{pmatrix}$ Number and Location

$A_b := \pi \cdot \frac{d_b^2}{4}$ Area of a rebar

$n_{bl} := \sum_{i=1}^{cols(n_b)} n_b^{\langle i \rangle}$ Number of rebars by level

$n_{bl} = \begin{pmatrix} 3 \\ 2 \\ 3 \end{pmatrix}$ Number of bars in each level

$A_{bl} := A_b \cdot n_{bl}$ Area of rebars by level

$A_{bl} = \begin{pmatrix} 3.8 \\ 2.534 \\ 3.8 \end{pmatrix} \cdot in^2$ Area of all bars in each level

$A_{bt} := \sum A_{bl} = 10.134 \cdot in^2$ Area of total bars

$d :=$ Level of rebars

$d_1 \leftarrow Cover$

for $i \in 2 .. rows(n_b)$

$\Delta \leftarrow \frac{h - 2 \cdot Cover}{rows(n_b) - 1}$

$d_i \leftarrow d_{i-1} + \Delta$

d

Steel rebar Properties:

$E_s := 29000ksi$ Steel Modulus of Elasticity

$f_y := 60ksi$ Steel Yield Strength

Concrete properties:

$f'_c := 6ksi$ Compressive Strength

$f'_{ci} := 4ksi$ Compressive Strength at Release

$\varepsilon_{cu} := 0.003$ Maximum Compressive Strain

$$\alpha := \text{if}\left[f'_c \le 10ksi, 0.85, \max\left[0.75, 0.85 - 0.02\cdot\left(\frac{f'_c}{ksi} - 10\right)\right]\right]$$ ACI – 318

$$\beta_1 := \max\left[0.65, 0.85 - 0.05\cdot\left(\frac{f'_c}{ksi} - 4\right)\right]$$ Ratio of Maximum Flexural Strain at the extreme tension face to the strain at the centroid of the rebar layer nearest to the tension face

Steel Layers Force:

$$a := \left| \begin{array}{l} \text{for } j \in 1 .. 60 \\ \quad a_j \leftarrow \frac{h}{60} \cdot j \\ a \end{array} \right.$$

Range Variable to accomodate an increasing increment

$$c := \frac{a}{\beta_1}$$

The distance of the concrete block in compression

$$\varepsilon_s := \left| \begin{array}{l} \text{for } i \in 1 .. \text{rows}(a) \\ \quad \text{for } j \in 1 .. \text{rows}(n_{bl}) \\ \quad\quad \varepsilon_{s_{i,j}} \leftarrow \varepsilon_{cu} \cdot \frac{(d_j - c_i)}{c_i} \\ \varepsilon_s \end{array} \right.$$

Tensile Strain in each row

$$f_s := \left| \begin{array}{l} \text{for } i \in 1 .. \text{rows}(a) \\ \quad \text{for } j \in 1 .. \text{rows}(n_{bl}) \\ \quad\quad f_{s_{i,j}} \leftarrow \text{sign}\left(\varepsilon_{s_{i,j}}\right) \cdot \min\left(\left|\varepsilon_{s_{i,j}}\right| \cdot E_s, f_y\right) \\ f_s \end{array} \right.$$

Tensile Stress in each row

$$F_s := \left| \begin{array}{l} \text{for } i \in 1 .. \text{rows}(a) \\ \quad \text{for } j \in 1 .. \text{rows}(n_{bl}) \\ \quad\quad F_{s_{i,j}} \leftarrow A_{bl_j} \cdot f_{s_{i,j}} \\ F_s \end{array} \right.$$

Rebar Force in each row

Concrete Force:

$F_c := \alpha \cdot f'_c \cdot a \cdot b$

Max allowable compression load:

[LRFD GFRP 5.6.4.4]

$P_{nmaxC} := \alpha \cdot f'_c \cdot b \cdot h = 1.652 \times 10^3 \cdot kip$ Nominal axial resistance

$\Phi := 0.85$

$P_f := \Phi \cdot P_{nmaxC}$ Factored axial resistance

$\phi P_f := 0.75 \cdot P_f = 1.053 \times 10^3 \cdot kip$ Design axial resistance

Nominal Flexural Strength of Steel Pile Splice

$$P_n := \left| \begin{array}{l} \text{for } i \in 1 .. \text{rows}(a) \\ \quad P_{n_i} \leftarrow \min\left[\left(F_{c_i} - \sum_{j=1}^{\text{rows}(n_b)} F_{s_{i,j}}\right), P_f\right] \\ P_n \end{array} \right.$$

Nominal Axial Strength

$$M_n := \left| \begin{array}{l} \text{for } i \in 1 .. \text{rows}(a) \\ \quad M_{n_i} \leftarrow \left[F_{c_i} \cdot \left(\frac{h}{2} - \frac{a_i}{2}\right) + \sum_{j=1}^{\text{rows}(n_b)} \left[F_{s_{i,j}} \cdot \left(d_j - \frac{h}{2}\right)\right]\right] \\ M_n \end{array} \right.$$

Nominal Moment Strength

$P_n =$ ·kip

	1
1	-580.509
2	-552.969
3	-525.429
4	-497.889
5	-470.349
6	-442.809
7	-415.269
8	-387.729
9	-306.668
10	-228.616
11	-159.747
12	-97.767
13	-41.085
14	29.621
15	102.425
16	...

$M_n =$ ·ft·kip

	1
1	20.311
2	39.933
3	58.867
4	77.112
5	94.669
6	111.537
7	127.717
8	143.208
9	173.621
10	202.468
11	227.948
12	250.73
13	271.279
14	289.924
15	306.91
16	...

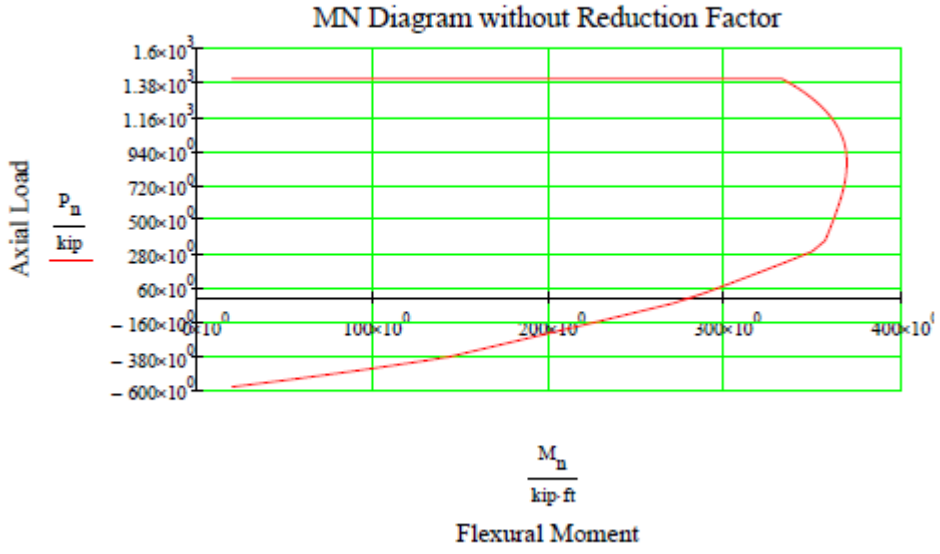

Resistance Factor for Flexural Strength (Steel) [ACI 318-14]

$$\varepsilon_t := \left| \begin{array}{l} \text{for } i \in 1 .. \text{rows}(a) \\ \quad \varepsilon_{t_i} \leftarrow \varepsilon_{cu} \cdot \dfrac{\left(d_{\text{rows}(n_b)} - c_i\right)}{c_i} \\ \varepsilon_t \end{array} \right.$$

$$\phi_f := \left| \begin{array}{l} \text{for } i \in 1 .. \text{rows}(a) \\ \quad \phi_{f_i} \leftarrow \left| \begin{array}{ll} 0.9 & \text{if } \varepsilon_{t_i} \geq 0.005 \\ 0.75 + \left[\dfrac{0.15\left(\varepsilon_{t_i} - 0.0020\right)}{0.0030}\right] & \text{if } 0.002 < \varepsilon_{t_i} < 0.005 \\ 0.75 & \text{otherwise} \end{array} \right. \\ \phi_f \end{array} \right.$$

Design Flexural Strength of Steel Pile Splice

$$P_u := \left| \begin{array}{l} \text{for } i \in 1 .. \text{rows}(a) \\ \quad P_{u_i} \leftarrow \phi_{f_i} \cdot \min\left[\left(F_{c_i} - \sum_{j=1}^{\text{rows}(n_b)} F_{s_{i,j}}\right), P_f\right] \\ P_u \end{array} \right.$$

$$M_u := \left| \begin{array}{l} \text{for } i \in 1 .. \text{rows}(a) \\ \quad M_{u_i} \leftarrow \phi_{f_i} \cdot \left[F_{c_i} \cdot \left(\dfrac{h}{2} - \dfrac{a_i}{2}\right) + \sum_{j=1}^{\text{rows}(n_b)} \left[F_{s_{i,j}} \cdot \left(d_j - \dfrac{h}{2}\right)\right]\right] \\ M_u \end{array} \right.$$

P_u = ·kip

	1
1	-522.458
2	-497.672
3	-472.886
4	-448.1
5	-423.314
6	-398.528
7	-373.742
8	-348.956
9	-276.001
10	-205.754
11	-143.773
12	-87.074
13	-35.357
14	24.728
15	83.22
16	...

M_u = ·ft·kip

	1
1	18.28
2	35.94
3	52.98
4	69.401
5	85.202
6	100.383
7	114.945
8	128.887
9	156.259
10	182.221
11	205.153
12	223.307
13	233.456
14	242.035
15	249.365
16	...

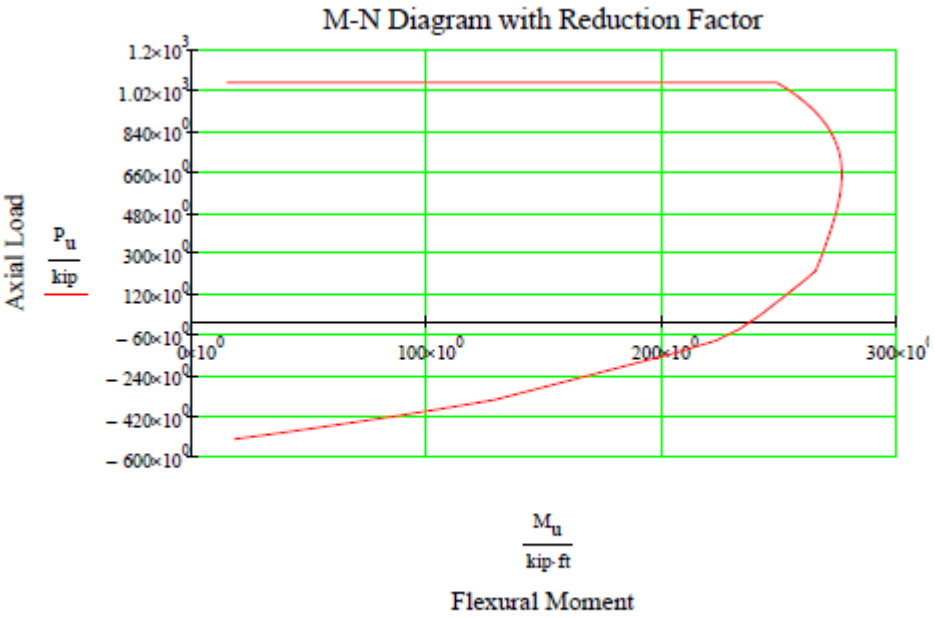

Development and Lap Splice Lengths for Steel Dowels

$\lambda_{rl} := 1$ Reinforcement Location Factor

$\lambda := 1$ Concrete Density Modification Factor

$\lambda_{cf} := 1$ Coating Factor

$\lambda_{cr} := 1$ Excess Reinforcement Factor

$d_{tie} := 0.207in$ Tie Nominal Diameter

$A_{tr} := \pi \cdot \frac{(d_{tie})^2}{4} = 0.034 \cdot in^2$

$n := 1$ Number of bars developed along plane of splitting

$S_c := 3in$ Maximum center-to-center spacing of transverse reinforcement within ld(in)

$k_{tr} := 40 \cdot \frac{A_{tr}}{S \cdot n} = 0.449 \cdot in$ Reinforcent confinement factor

$HalfCtC := 0.5 \cdot (d_3 - d_2) = 1.75 \cdot in$ Half of spacing

$\lambda_{rc} := \frac{d_b}{HalfCtC + k_{tr}} = 0.578$ Reinforcement Confinement Factor

AASHTO 5.10.8.2

$$L_{dDowel} := 2.4 \cdot d_b \cdot \frac{\frac{f_y}{ksi}}{\sqrt{\frac{f'_c}{ksi}}} \cdot \left[\frac{(\lambda_{rl} \cdot \lambda_{cf} \cdot \lambda_{rc} \cdot \lambda_{cr})}{\lambda}\right] = 43.125 \cdot in$$

Dowel Developement Length

$L_{ap} := 1.3 \cdot L_{dDowel} = 56.062 \cdot in$

Dowel LapSplice Length

$L_D := L_{ap} = 56.062 \cdot in$

The Length of Dowels

$L_H := L_D + 2in = 58.062 \cdot in$

The Length of Holes for the Dowels

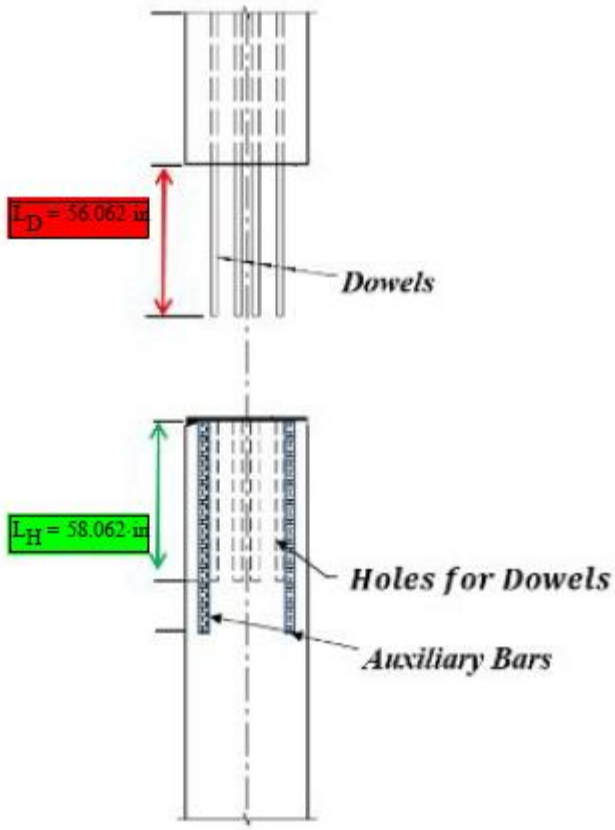

Development Length of Prestressing FRP Strand:

Section 933 of the FDOT Standard Specification for Road and Bridge Construction

Group #	Strand Types	Diameter	Effective Cross Sectional Area	Nominal Ultimate Load
1	("Single Strand-5.0mm ø")	0.2	0.025	9.1
2	("7-Strand-7.9mm ø")	0.31	0.048	17.8
3	("7-Strand-10.8mm ø")	0.43	0.090	33.1
4	("Single Strand-9.5mm ø")	0.38	0.110	35.0
5	("7-Strand-12.5mm ø")	dia := 0.49 in	A_{ps} := 0.117 in^2	P_u := 43.3 kip
6	("Single Strand-12.7 mm ø")	0.50	0.196	59.0
7	("7-Strand-15.2mm ø")	0.60	0.179	66.2
8	("7-Strand-17.2mm ø")	0.68	0.234	86.6
9	("7-Strand-19.3mm ø")	0.76	0.289	106.9

C_{Es} := 1 Environmental Reduction Factor for CFRP Strand

n_{ps} := 1 Set number of Strand or Total number of strands

$A_{ps.total} := n_{ps} \cdot A_{ps} =$

	1
1	0.025
2	0.048
3	0.09
4	0.11
5	0.117
6	0.196
7	0.179
8	0.234
9	0.289

$\cdot in^2$ Total strand area for each

$$f_{pu} := C_{Es} \cdot \frac{P_u}{A_{ps}} =$$

	1
1	364
2	370.833
3	367.778
4	318.182
5	370.085
6	301.02
7	369.832
8	370.085
9	369.896

$\cdot ksi$ Ultimate Tensile Trength of the CFCC

$P_j := 34kip$ Jacking force

$$f_{pi} := \frac{P_j \cdot n_{ps}}{A_{ps.total}} =$$

	1
1	1360
2	708.3
3	377.8
4	309.1
5	290.6
6	173.5
7	189.9
8	145.3
9	117.6

$\cdot ksi$

$Loss := 0.15$ Loss Percentage

$f_{Loss} := Loss \cdot f_{pi} =$

	1
1	204
2	106.25
3	56.667
4	46.364
5	43.59
6	26.02
7	28.492
8	21.795
9	17.647

ksi

Initial strand losses

$f_{pe} := f_{pi} - (f_{Loss}) =$

	1
1	$1.156 \cdot 10^3$
2	602.083
3	321.111
4	262.727
5	247.009
6	147.449
7	161.453
8	123.504
9	100

ksi

Effective Prestresstressing Stress

$\alpha_t := 1.1$ in·kip

AASHTO - CFRP-1

$\alpha_d := 1.48$ in·lb

AASHTO - CFRP-1

$f_{pbt} := f_{pi}$

Stress Prior to Transfer

AASHTO-CFRP1

$$L_{dStrand} := \left| \begin{array}{l} \text{for } i \in 1 .. \text{rows}(dia) \\ L_{dStrand_i} \leftarrow \dfrac{\dfrac{f_{pbt_i}}{ksi} \cdot dia_i}{\alpha_t \cdot \left(\dfrac{f_{ci}}{ksi}\right)^{0.67}} + \dfrac{\left(\dfrac{f_{pu_i}}{ksi} - \dfrac{f_{pe_i}}{ksi}\right) \cdot dia_i}{\alpha_d \cdot \left(\dfrac{f_c}{ksi}\right)^{0.67}} \\ L_{dStrand} \end{array} \right.$$

Development Length for FRP strand

$L_{dStrand} =$

	1
1	65.457
2	64.272
3	62.417
4	46.466
5	63.402
6	46.766
7	66.359
8	69.588
9	73.833

in

Length of the Embedded part of the Dowel

$L_{dStrand} =$

	1
1	65.457
2	64.272
3	62.417
4	46.466
5	63.402
6	46.766
7	66.359
8	69.588
9	73.833

in

Length of the Auxiliary Bar

The Actual Developement Length considered in Design may Vary from the Length Calculated here. Please See the Relevant Report and Final Design Drawings.

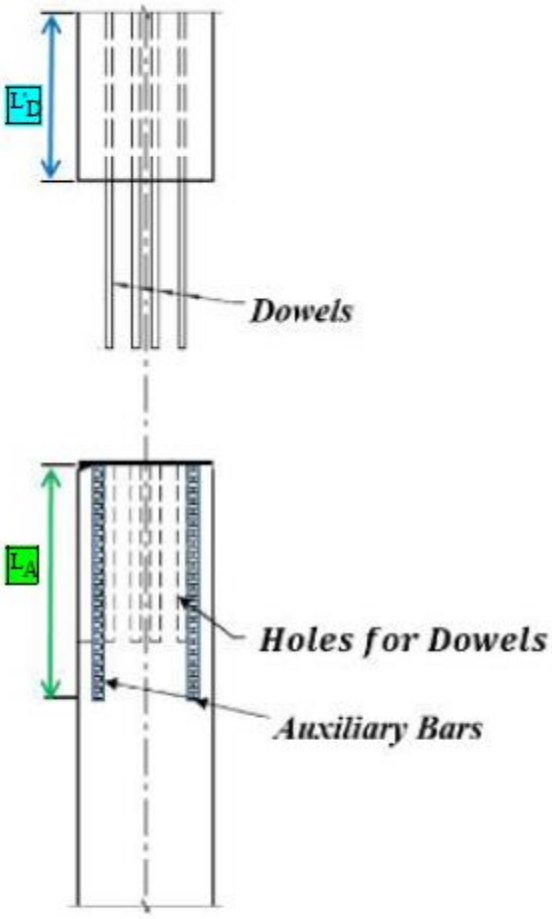

Auxiliary Bar Size = One Size Smaller than the Size of Dowel

Auxiliary Bar Number = Number of Dowel Bars on Perimeter

VITA

SAMAN FARHANGDOUST

2008-2011	B.Sc., Mechanical Engineering – Solid Mechanics major Mashhad, Iran
2012-2014	M.S., Mechanical Engineering – Rolling Stock Engineering major Iran University of Science and Technology Tehran, Iran
2016-2017	Polytechnic University of Catalonia - Barcelona, Spain
2017-2020	M.S., Civil Engineering Florida International University Miami, Florida, USA
2017-2021	Ph.D., Civil Engineering – Structural Engineering major Florida International University Miami, Florida, USA

PUBLICATIONS AND PRESENTATIONS

1. Farhangdoust, S., Mehrabi, A. and Nolan, S., 2021. Design of prestressed precast pile splice using glass fiber reinforced polymer (GFRP) dowels. Engineering Structures, 244, p.112806. DOI: https://doi.org/10.1016/j.engstruct.2021.112806
2. Tashakori S, Farhangdoust S, Baghalian A, McDaniel D, Tansel I.N., Mehrabi A. (2020). Damage Detection of 3D Printed Mold Using the Surface Response to Excitation Method. Structural Engineering and Mechanics, vol. 75, no. 3. DOI: https://doi.org/10.12989/sem.2020.75.3.369.
3. Eghbali, P., Younesian, D., & Farhangdoust, S. (2020). Enhancement of the low-frequency acoustic energy harvesting with auxetic resonators. Applied Energy. 270, 115217. DOI: https://doi.org/10.1016/j.apenergy.2020.115217.
4. Farhangdoust, S., Georgeson, G. E., Ihn, J.B., and Chang, F. K. (2021). Kirigami Auxetic Structure for High Efficiency Power Harvesting in Self-powered and Wireless Structural Health Monitoring Systems. Smart Materials and Structures. DOI: https://doi.org/10.1088/1361-665X/abcaaf
5. Farhangdoust, S., Georgeson, G. E., Ihn, J.B., and Mehrabi, A. (2021). Embedded Metamaterial Subframe Patch for Increased Power Output of Piezoelectric Energy Harvesters. Journal of Nondestructive Evaluation, Diagnostics and Prognostics of Engineering Systems.
6. Aghaei, S. M., Aasi, A., Farhangdoust, S., & Panchapakesan, B. (2020). Graphene-like BC6N nanosheets are potential candidates for detection of volatile organic

compounds (VOCs) in human breath: A DFT study. Applied Surface Science, 147756. DOI: https://doi.org/10.1016/j.apsusc.2020.147756.
7. Farhangdoust S, Mehrabi A. (2020). Non-Destructive Evaluation of Closure Joints in Accelerated Bridge Construction using a Damage Etiology Approach. Applied Sciences. 10(4):1457. DOI: https://doi.org/10.3390/app10041457.
8. Eghbali P, Younesian D, Farhandoust S. (2020). Enhancement of piezoelectric vibration energy harvesting with auxetic boosters. International Journal of Energy Research. 44:1179–1190. DOI: https://doi.org/10.1002/er.5010.
9. Farhangdoust S, Eghbali P, and Younesian D. (2020). Bistable tuned mass damper for suppressing the vortex induced vibrations in suspension bridges. Earthquakes and Structures, 18, no. 3: 313. DOI: https://doi.org/10.12989/eas.2020.18.3.313.
10. Hosseinkhani, A., Younesian, D., Shakeri, R., & Farhangdoust, S. (2019). Vibro-acoustic response analysis of fractional railpads in frequency domain. Mechanics Based Design of Structures and Machines. 1-18. DOI: https://doi.org/10.1080/15397734.2019.1688169.
11. Farhangdoust, S. & Mehrabi, A. B. (2019). Health Monitoring of Accelerated Bridge Construction Closure Joints – Review of Non-destructive Testing Methods. Journal of Advanced Concrete Technology. 17(7). 381-404. DOI: https://doi.org/10.3151/jact.17.381.
12. Tashakori, S., Baghalian, A., Senyurek, V. Y., Farhangdoust, S., McDaniel, D., & Tansel, I. N. (2018). Composites Bond Inspection Using Heterodyne Effect and SuRE Methods. Shock and Vibration. DOI: https://doi.org/10.1155/2018/1361932.
13. Hosseinkhani, A., Younesian, D., & Farhangdoust, S. (2018). Dynamic analysis of a plate on the generalized foundation with fractional damping subjected to random excitation. Mathematical Problems in Engineering. DOI: https://doi.org/10.1155/2018/3908371.
14. Mehrabi, A. B., & Farhangdoust, S. (2018). A Laser-Based Noncontact Vibration Technique for Health Monitoring of Structural Cables: Background, Success, and New Developments. Advances in Acoustics and Vibration, 2018. DOI: https://doi.org/10.1155/2018/8640674
15. Farhangdoust, S., Mehrabi, A., and Nolan, S. (2021, January). Analytical Investigation of Prestressed Precast Pile Splice Using Glass Fiber Reinforced Polymer (GFRP) Dowels. Transportation Research Board 100th Annual Meeting. Transportation Research Board. Advances and Innovation in Structural Design Materials and Bridge Designs session, USA.
16. Farhangdoust, S., Moradisizkoohi, H., Georgeson, G., Mehrabi, A., & Soleimani, K. (2021, March). NDE 4.0 for In-motion wheel inspection of a high-speed train via a RF energy harvesting module: an autonomous cyber-physical approach toward the smart city. In NDE 4.0 and Smart Structures for Industry, Smart Cities, Communication, and Energy (Vol. 11594, p. 1159405). International Society for Optics and Photonics.
17. Farhangdoust, S., Georgeson, G., Ihn, J. B., Aghaei, S. M., & Laflamme, S. (2021, March). Bio-inspired metasurface skin to enhance the performance of blue energy harvesting. In Sensors and Smart Structures Technologies for Civil, Mechanical, and